



Polyelectrolyte based  
**NANO-approaches for Cancer therapy or  
diagnostics**

Thesis submitted for the degree of  
“Doctor of Philosophy”

**S.I.S.S.A**  
**Statistical and Biological Physics**

**CANDIDATE**  
Subhra Mandal

**SUPERVISOR**  
Prof. Giacinto Scoles  
Dr. Silke Krol

SISSA - via Bonomea-265, 34136 Trieste - ITALY

---

---

---

---

*Dedicated to-*

**To my family and all my friends**

---

---

## Declaration

The work described in this thesis was carried out at the International School for Advanced Studies, Trieste, between October 2007 and August 2010. All work reported arises from my own experiments and in collaboration with Catinara Hosptal, University of Trieste as well as University of Pavia. This thesis is composed of the following published and unpublished papers.

“Novel generation of non-aggregating targeted functionalized gold nanoparticles and a detailed surface enhanced Raman spectroscopic characterization”.

**Subhra Mandal**, Alois Bonifacio, Francesco Zanuttin, Valter Sergo, Silke Krol, (accepted by **Langmuir**)

“Double strike - Target specific polymeric coacervate nanoparticles inhibit proliferation and induce apoptosis in Cancer cell by integrating anti-sense and gene therapy.”

**Subhra Mandal**, Natalia Rosso, Claudio Tiribelli, Giacinto Scoles, Silke Krol. (manuscript in preparation to be submitted in ACS Nano)

"Selective labeling of cancer cells by Poly-allylamine induces rapid cell death".

**Subhra Mandal**, Natalia Rosso, Francesca Petrera, Serena Bonin, Giorgio Stanta, Fauzia Jabeen, José Luis Toca-Herrera, Marco Möller, Giacinto Scoles, Claudio Tiribelli, Silke Krol. (manuscript in preparation)

Present thesis work has not been handed to any other University for any reward.

---

## Acknowledgements

I would like to express my gratitude to my supervisors Prof. Giacinto Scoles and Dr. Silke Krol, who gave me an opportunity to pursue a PhD degree in Nanotechnology, a completely new field for me. Their constant support, stimulating suggestions and encouragement helped me in both, all the time of research work and the writing of this thesis. I would like to thank Dr. Natalia Rosso and Dr. Francesca Petrera for the long discussions and suggestions that helped me to sort out scientific and technical details of some of my thesis work. I am thankful to Dr. Fauzia Jabeen, with whom I performed the SEM analysis. I am grateful to my friend from India, Mr. Jayadri Sekhar Ghosh, who is in his last year of Ph.D., in ILS, India and Dr. Sailesh Bajpai, in ICGEB, Trieste for helping with their insightful comments, suggestions and constructive criticisms in the molecular biology part of my thesis work. A special thanks to Ms. Diane Latawiec, first for being my great friend, but also for her valuable suggestions and corrections to improving my English writing ability.

I wish to thank Dr. Francesco Zanuttin for his critical criticism and numerous discussions that helped me to improve my work & knowledge in the field. Thanks to my vivid multinational group of Dr. Julian Lopez-Viota Gallardo (Spanish), Dr. Maria Fernanda de Sousa (Portuguese) and Ms. Eleonora Toffoli (Italian) with whom I shared many hard and funny moments of my Ph.D. life. I thank them all for the support they provided me throughout my thesis work.

Many friends have helped me stay sane through these years. I wish to thank Dr. Sailesh Bajpai, Dr. Rajesh Shahapure, again Dr. Fauzia Jabeen, Ms. Irene, Ms. Swathi, Ms. Zyenap and all my Indian friends. I greatly value their friendship. A special thanks to Dr. Asha Nair and Dr. Fouzia Bano, my very good friends in Trieste, for all those wonderful moments with them. They helped me to feel 'at home' in Trieste, far away from my home.

Most importantly, none of this would have been possible without the love and patience of my family. Most importantly, my brother Assistant Prof. Partha Pratim Mondal, because of whom I am able to pursue my Ph.D. thesis here in SISSA. A special thanks to my sister-in-law Dr. Latha Mondal for her constant source of love, concern, support and strength all these years.

---

I would like to thank again Dr. Asha Nair for teaching me so many critical things about data analysis, making good quality figures using various software and many more things which I can't enumerate. A special thanks again to my friend Jayadri Sekhar Ghosh, who listened me calmly and patiently, during all my angry and depressive moments. Thanks for being with me Joy. I am deeply indebted to my parents, even though they are far away, they are a great support for me. To my mom, a very good friend and a nice listener with whom I can talk for hours. Although she didn't always understand my problems , she would always tells me, that at the end everything will be fine and we have to calmly go through the tough moments of life. Her inspirational words have helped to keep my smile throughout my thesis work. A special thanks to my dad who was the only person who believed my ability all through and encouraged me to carry on, although at times I was not sure.

Lastly and most importantly, I would like to thank SISSA, for providing me the opportunity to pursue my Ph.D. and collaborating with CBM to allow me to carryout my thesis work. A special thanks to CBM, for allowing and providing me access to all the facilities required for my thesis work. Thanks to CIPE, for funding all of my thesis projects.

The list to thank people is so long, as all the people I asked for help has helped me by 'going-out of the way'. I would like to thank each and everyone of you. I THANK YOU ALL FROM BOTTOM OF MY HEART. THANKS FOR BEING WITH ME.

---

## Abbreviations

AFM	Atomic Force Microscopy
AuNP	Gold Nanoparticles
AcGFP1	<i>Aequorea coerulea</i> Green Fluorescence Protein
ALL	Acute Lymphoblastic Leukemia
AML	Acute Myeloid Leukemia
ATP	Adenosine triphosphate
BNCT	Boron Neutron Capture Therapy
BSA	Bovine Serum Albumin
CaCl <sub>2</sub>	Calcium Chloride
CAT	Computed Angled Tomography
CHI	Chitosan
CLL	Chronic Lymphoid Leukemia
CLSM	Confocal Laser Scanning Microscope
CPs	Coacervate Particles
CSF	Colony-Stimulating Factor
CT	Computed Tomography
DEPC	Diethylpyrocarbonate
DiA	Dialkylaminostyryl
DLS	Dynamic Light Scattering
DMEM	Dulbecco's Modified Eagle's Medium
DMEM/F12	Dulbecco's Modified Eagle's Medium/Nutrient F-12 Ham
DMEM-hg	Dulbecco's modified Eagle's high glucose medium
DMSO	Dimethylsulfoxide
DNA	Deoxyribonucleic acid
dsRNA	Double-stranded RNA
ECM	Extra-Cellular Matrix
EDS	Energy-dispersive X-ray spectroscopy
EGFR-2	Epidermal Growth Factor Receptor-2
EPR	Enhanced Permeation and Retention
FACS	Fluorescence activated cell scanning
FBS	Foetal Bovine Serum

---

fCPs	Fluorescent labelled CPs
FE-SEM	Field Emission Scanning Electron Microscope
FCS	Fetal Calf Serum
FITC	Fluorescein Isothiocyanate
FITC-PAH	Poly(fluorescein allylamine hydrochloride)
Fo	Folic acid
FPNGs	FITC-PAH/PSS coated Polyelectrolyte coated Nano-Gold particles
FR	Folate receptor
GPI	Glycosylphosphatidylinositol
HER2	Human Epidermal growth factor Receptor 2
hFR $\alpha$	Human Folate receptor alpha
hFR $\beta$	Human Folate receptor beta
hFR- $\gamma$ / $\gamma$ 4)	Human Folate receptor gamma/gamma4
INF	Interferon-alfa
IL-2	Interleukin-2
KCl	Potassium Chloride
LbL	Layer-by-layer
LWM-CHI	Low Molecular Weight Chitosan
MRI	Magnetic Resonance Imaging
MSV	Multi-Stage Vectors system
MTT	3-(4,5-dimethylthiazol-2-yl)-2,5-diphenyl tetrazolium bromide
MW	Molecular Weight
NCI	National Cancer Institute
NGS	Normal Goat Serum
NIR	Near-Infra red therapy
N:P	Amine to Phosphate ratio
ODN	Oligonucleotides
OD	Optical Density
O/N	Overnight
PFA	Paraformaldehyde
PAH	Poly(allylamine hydrochloride)
PCA	Polycyanoacrylate

---

PCL	Polycaprolactone
PDI	Poly Dispersity Index
PDT	Photodynamic therapy
PEI	Poly-ethylenimines
PET	Positron Emission Tomography
PI	Propidium Iodide
PLA-PEG-PLA	Poly(lactide- <i>block</i> -poly(ethyleneglycol)- <i>block</i> -poly(lactide
PLA	Poly(lactic acid
PLGA	Poly(lactic-co-glycolic
PNGP	Polyelectrolyte coated Nano-Gold Particles
PSS	poly(sodium 4-styrenesulfonate)
PE	Polyelectrolyte
PNGs	Polyelectrolyte coated Nano-Gold particles
PPTT	Plasmonic Photothermal therapy
PTT	Photothermal therapy
QD	Quantum Dots
RISC	RNA-induced silencing complex
RT	Room Temperature
RNA	Ribonucleic acid
RNAi	RNA interference
SEM	Scanning Electron Microscopy
SERS	Surface Enhanced Raman Spectroscopy
siRNA	short interfering RNA
TEM	Transmission Electron Microscopy
WEM	Williams E medium
v/v	Volume/volume
WHO	World Health Organisation

---

# Contents

Declaration	i
Acknowledgement	ii
Abbreviations	iv
Summary of the thesis	xiv
<b>Cancer: Introduction</b>	<b>1</b>
1. Abstract	2
2. Cancer: Introduction	2
2.1. Cancer: an overview	2
2.2. Nanomedicine and new drug therapies for Cancer	6
2.2.1. Conventional therapies for cancer	6
2.2.2. Nano therapeutic advances for cancer therapy	13
2.2.3. Nanomedicines and drug delivery system	13
2.3. Nanotechnologies in bioimaging and detection of Cancer	
2.3.1. Conventional Cancer diagnostics	17
2.3.2. Nano-devices in cancer imaging and diagnostic	19
3. References	23
<b>Part-1: The target specific polyion coated nanogold based approach</b>	<b>33</b>
1. A brief overview	34
2. Nanotechnology in cancer applications	35
2.1. Polymeric nanodrugs	35
2.2. Polymer coated nanoparticles in drug delivery	36
2.3. Layer-by-Layer deposition of polyelectrolyte multilayer on gold nanoparticles	37
2.3.1. Interactions between polyelectrolytes in LbL deposition	39

---

2.3.2. The Zone Model for LbL multilayer film growth	40
2.4. Important properties of gold nanoparticles	41
2.4.1. Light absorption by gold nanoparticles	41
2.4.2. Light scattering of gold nanoparticles	46
2.5. Gold nanoparticles in cancer imaging and photothermal therapy	50
2.6. Targeting nano-drugs for cancer specificity	54
2.6.1. Folic acid as cancer cell targeting ligand	54
2.6.2. Folate receptors as cancer cell target	56
3. References	60
Chapter 1: Novel generation of non-aggregating targeted functionalized gold nanoparticles and a detailed surface enhanced Raman spectroscopic characterization.	
1.1 Aim of the present work	77
Chapter 2:	
2.1 Introduction	78
2.2 References	82
Chapter 3: Materials and Methods	
3.1. Materials	86
3.2. Methods	
3.2.1. Gold nanoparticle preparation, coating and functionalisation	86
3.2.2. Particle agglomeration by small ions	90
3.2.3. Surface characterization by SERS and Raman measurements	91
3.2.4. Cellular nanoparticle up-take	92
3.3. References	94
Chapter 4: Results and Discussion	
4.1. Surface characterization by SERS and Raman measurements	95
4.2. Synthesis of non-aggregating polyelectrolyte multilayer PNGs	98
4.3. Stability of aq. PNGs and 0.5M PNGs against aggregation in presence of small ions	100

---

4.4. Electrostatic functionalisation of 0.5M FPNG with folic acid for cancer cell targeting	103
4.5. Target specific internalization of Fo-0.5M FPNGs in cancer cell lines	105
4.6. Non-specific internalization of Fo-0.5M FPNGs in macrophage cell line	107
4.7. Boron conjugation within the layers of Fo-0.5MPNG as probe for BNCT	
4.7.1. Synthesis of Fo- <sup>10</sup> BPNG and its stability in different solutions	108
4.7.2. Interaction of Fo-0.5M <sup>10</sup> BFPNGs with non-cancerous and cancer cells	111
4.8. References	114
Chapter 5:	
5.1. Conclusions	117
5.2. References	120
<b>Part-2: Target specific polymeric coacervate nanoparticle approach</b>	121
1. A brief overview	122
1.1. Oncogenes and tumor suppressor genes	123
1.1.1. Gain-of-Function Mutations Convert Proto-Oncogenes into Oncogenes	123
1.1.1.1. c-Myc oncoprotein and human cancer	124
1.1.1.2. Structure of the c-Myc protein	126
1.1.2. Loss-of-function mutations in tumor-suppressor genes are oncogenic	126
1.1.2.1. p53 and human cancers	128
1.1.2.2. Structure of the p53 protein	128
1.2. Nanomedicine and novel therapeutic strategies	130
1.2.1. Nanotechnology for antisense therapy	131
1.2.2. Nanotechnology for gene therapy	133
1.2.3. Ideal nanoscopic drug delivery system	134
1.2.3.1. Strategies to overcome tumor level resistance	134

---

1.2.2. Target specific drug delivery	136
2. References	137
Chapter 1: Double strike - Target specific polymeric coacervate nanoparticles inhibit proliferation and induce apoptosis in Cancer cell by integrating anti-sense and gene therapy.	
1.2 Aim of the present work	147
Chapter 2:	
2.1. Introduction	148
2.1.1. The core of the system: introducing gene therapy	150
2.1.2. The next layer introducing antisense therapy	150
2.1.3. The outermost layer reduces the uptake in macrophage system (MPS)	151
2.1.4. CP decorated with cancer targeting molecule	152
2.2. References	154
Chapter 3: Materials and Methods	
3.1. Materials	164
3.2. Methods	
3.2.1. Coacervate particle preparation	165
3.2.2. CP stability analysis	168
3.2.3. CPs Internalization and Transfection efficiency determination	168
3.2.4. Protein extraction and Western blot	169
3.2.5. CP induced apoptosis analysis	171
3.2.6. Cell Viability analysis	172
3.2.7. Macrophage recognition	173
3.3. References	174
Chapter 4: Results and Discussions	
4.1. Synthesis and characterization of the multifunctional coacervate particles	175
4.2. CP multi-functionality analysis	180

---

4.2.1.	Folate-receptor mediated uptake efficiency of Fo-fCPs	180
4.2.2.	Transfection efficiency of Fo-CP	182
4.2.3.	CPs identification by the MPS	183
4.2.4.	Targeted antisense and gene therapeutic efficiency of the Fo-P <sup>3</sup> iMCp53 CPs	184
4.2.4.1.	CP induces targeted protein down- or up-regulation	184
4.2.4.2.	CP induced apoptosis in cancer cells	186
4.2.4.3.	CP causes decrease in cell viability	187
4.3.	References	189
 Chapter 5:		
5.1.	Conclusions	192
5.2.	References	195
 <b>Part-3: The Polycationic Approach</b>		
1.	A brief overview	198
1.1.	Differences in the physical properties of cancer and normal cells	198
1.1.1.	Surface charge	198
1.1.2.	Mechanical properties of cell membranes	203
1.1.3.	Modification of Extra-Cellular Matrix (ECM)	204
1.2.	Polycations as cancer treatment	205
1.3.	The polycationic approach for diagnostic and therapy	206
2.	References	207
 Chapter 1: Selective labeling of cancer cells by Poly-allylamine induces rapid cell death.		
1.1.	Aim of the present work	213
 Chapter 2:		
2.1.	Introduction	214
2.2.	References	217



---

4.2.1. PAH reduces cancer cell	238
4.3. PAH-beads Analysis	241
4.3.1. SEM, EDS and immuno-assays of PAH beads	241
4.3.2. PAH-bead toxicity analysis	243
4.3.2.1. FACS analysis	243
4.3.2.2. MTT assay	243
4.4. References	245
 Chapter 5:	
5.3. Conclusions	247
5.4. References	250
 <b>Concluding remarks and Future Outlook</b>	 252
 <b>Epilogue</b>	 255

---

## Summary of the Dissertation

The work presented here has been aimed at exploring a polymer nanoparticle based approach to cancer diagnostics and therapy. Cancer is the second leading cause of death in the world. Nanoparticles and polymer science have opened up a new world of opportunities for the development of efficient medical diagnostic methods and of selective cancer therapy. The different (sometimes hierarchical and/or multilayer) structures, shapes and compositions of nanoparticles provide good potential for their application in the biomedical field. With the development of nanotechnology, various types of uncoated and coated nanoparticles are being developed for cancer diagnostics and therapy.

In an attempt to contribute towards improving cancer therapy three approaches have been explored in the present thesis, all of them exploiting a different characteristic of the cancerous cell / nanoparticle interaction, and all of them containing a certain degree of innovation.

1) The first approach uses target specific, polymer coated gold nanoparticles and is based on the advantages which arise due to their easy preparation, efficient bioconjugation, potential non-cytotoxicity, and their tunable and enhanced absorption and scattering of electromagnetic radiation that provides an opportunity for their use in cancer cell imaging. Furthermore, their strong absorption provides a possibility for them to be used in efficient cancer diagnostics ultimately coupled to selective photo-thermal therapy. This combination of diagnostics and therapeutic ability defines what in the current literature is often called a *THERANOSTIC SYSTEM*. In this part, we will describe and show the development of a new protocol to prepare stable multilayer, polymer coated gold nanoparticles system conjugated with folic acid, which makes them potentially, a viable and efficient cancer cell targeted theranostic system. We also show that in between different layers one can upload drugs or

---

other molecules of interest for diagnoses or therapy or both. This is shown by uploading a Boron 10 ( $^{10}\text{B}$ ) compound in the target specific coated gold nanoparticles, to be developed as a probe for Boron neutron capture therapy (BNCT).

2) The second novel therapeutic approach for cancer developed in this thesis is based on the development of the first combined genomics based delivery of TWO “drugs” to correct at the same time TWO fundamental alteration in the cell cycle check-point and cell signaling pathway in cancer cells. Here too we use multilayer electropolymer deposition technology describing the preparation and characterization of target specific folic acid containing Coacervate Particles (CPs). We show here that these CPs are capable to deliver (therefore allowing for cell death), to three vey different cancer cell lines, siRNA against the oncogenic mRNA (e.g. c-myc) to stop cancer cell proliferation and a plasmid bearing a wild-type tumor suppressor gene (e.g. the *p53* gene) which are capable of inducing apoptosis and are mutated away in at least 50% of all cancer types.

3) The third part of this thesis, will describe a simple pure polyelectrolyte approach. To a rapid diagnosis of the presence of cancer cells which has possible ramifications also for cancer therapy. In contrast to the two previous methods that were receptor based targeted systems, this approach exploits the physical characteristic differences between normal and cancer cells e.g. low membrane rigidity, low membrane integrity and higher concentration of negative surface charge in many cancerous cells compared to normal healthy cells.

The unifying theme of the present thesis that has been the hallmark of the work of one of my two supervisors (Dr. Silke Krol) in recent years is the systematic exploitation of the electrostatic interactions between nanoparticles and polymers as well as between cells and polymers and between polymers themselves. These interactions (that are the same as those followed by nature, sometimes more specifically through hydrogen bonding) give to our

---

approach, maximum flexibility to introduce new or to integrate different systems to develop multi-functional and/or multi-drug systems. Whilst the approaches used were specifically applied, to cancer, it should be possible to develop them for application to other diseases for better diagnostics and improved therapeutics.

---

---

# **Cancer: Introduction**

**1. Abstract**

Cancer is the second leading cause of death in the world only after coronary diseases. It is estimated that within the next 30 years, it will become the main reason for death. This bothersome statistic result not from an increase in incidences of cancer, but because deaths from heart disease could be reduced to nearly half, while the number of cancer-related deaths remains about the same. This emphasizes the need for new and more effective therapies.

In this section, the importance of nano-diagnostic and therapeutic aspects of nanotechnology will be assessed as a new weapon in the arsenal to fight cancer, exploring the advances in areas such as improved drug delivery, new therapies, and bio-imaging.

**2. 1. Cancer: an overview**

According to the World Cancer Report 2008 by WHO, the global cancer burden has

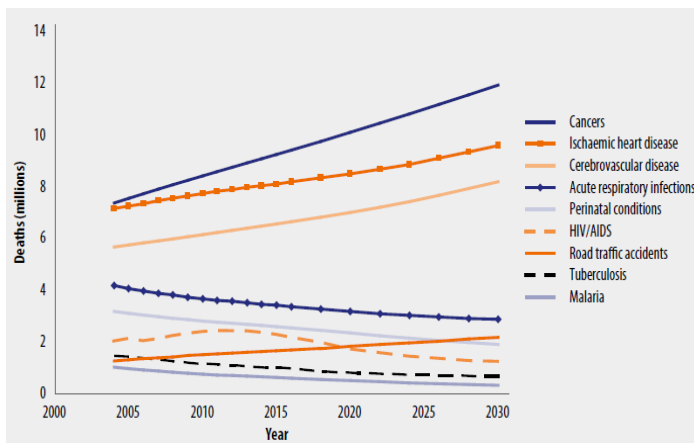


Fig. 1-1. Predicted global deaths for selected cause from 2004-2030 [1].

doubled in the last thirty years of the twentieth century, and it is estimated that it will double again, between 2000 and 2020 and almost triple by 2030 (fig.1-1) [1].

Cancer, which was once considered to be a disease of the westernized, industrialized

countries, has now become a common disease of low- and medium-resource countries (table 1-1) [2].

*Table 1.1. Summary of cancer (excluding non-melanoma skin cancer) incidences and mortality worldwide in 2008 (GLOBOCAN 2008, WHO) [2].*

Estimated numbers (thousands)	Men		Women		Both sexes	
	Cases	Deaths	Cases	Deaths	Cases	Deaths
World	6629	4225	6038	3345	12667	7570
More developed regions	2975	1528	2584	1223	5559	2751
Less developed regions	3653	2697	3453	2122	7106	4819
WHO Africa region (AFRO)	253	209	318	226	571	435
WHO Americas region (PAHO)	1276	611	1233	568	2509	1179
WHO East Mediterranean region (EMRO)	214	169	214	144	428	313
WHO Europe region (EURO)	1823	1044	1604	823	3427	1867
WHO South-East Asia region (SEARO)	742	566	909	564	1651	1130
WHO Western Pacific region (WPRO)	2316	1621	1755	1016	4071	2637
IARC membership (21 countries)	3081	1613	2811	1351	5892	2964
United States of America	745	294	692	271	1437	565
China	1622	1222	1194	736	2816	1958
India	430	321	518	312	948	633
European Union (EU-27)	1332	693	1114	539	2446	1232

In Italy (2001), cancer accounted for 31% of all deaths (table 1-2a) [3]. In comparison with the Eur-A (according to World Health Organisation (WHO), those european countries with *very low child and very low adult mortality* where categorized as Eur-A) average males (<24 years old) showed about 17% excess mortality due to cancer, whereas females showed 15% excess mortality due to cancer (table 1-2b) [3]. Mortality due to cancer of the lymphoid and haematopoietic tissue for children (0–14 years old) in Italy was found to be the sixth highest in the 2001 as compared to Eur-A. Furthermore, people between the ages of 15–29 years old, revealed the death rate due to these types of cancer was the second highest in Eur-A, and equal with Luxembourg (table 1-2c) [3].

The “war against cancer” is now in its fourth decade since the declaration of the National Cancer Act was passed in 1971. To control, conquer, and eliminate cancer, we need to understand cancer as acquirably as possible [4].

Cancer is a disease where abnormal cells divide without control and during metastasis they are able to invade through the blood and lymph systems, other tissues. Thus, cancer could spread all over the body [5].

Table 1.2. Selected mortality in Italy compared with Eur-A averages (a). Selected mortality data for the group aged (b) 1–14 years and (c) 15–24 years by sex in Italy and Eur-A: SDR per 100 000 of population and percentage changes from 1995 to latest available year [3].

Condition	SDR per 100 000		Excess mortality in Italy (%)	Total deaths in Italy (%)	Total deaths in Eur-A (%)
	Italy (2001)	Eur-A average (2001)			
<b>Selected noncommunicable conditions</b>	467.0	519.5	- 10.1	81.0	79.9
<i>Cardiovascular diseases</i>	221.5	246.3	- 10.0	38.4	37.9
Ischaemic heart disease	70.9	97.3	- 27.1	12.3	15.0
Cerebrovascular disease	59.4	62.0	- 4.2	10.3	9.5
Diseases of pulmonary circulation and other heart disease	58.7	57.0	3.0	10.2	8.8
<i>Malignant neoplasms</i>	178.1	181.8	- 2.1	30.9	28.0
Trachea/bronchus/lung	37.4	37.0	1.2	6.5	5.7
Female breast	25.5	27.1	- 5.9	4.4	4.2
Colon/rectal/anal	18.4	20.7	- 11.1	3.2	3.2
Prostate	17.9	25.0	- 28.6	3.1	3.8
<i>Respiratory diseases</i>	31.3	47.7	- 34.5	5.4	7.3
Chronic lower respiratory diseases	15.9	20.0	- 20.7	2.8	3.1
Pneumonia	7.6	16.5	- 53.9	1.3	2.5
<i>Digestive diseases</i>	27.0	30.7	- 12.1	4.7	4.7
Chronic liver disease and cirrhosis	13.6	12.8	6.8	2.4	2.0
<i>Neuropsychiatric disorders</i>	9.2	13.0	- 29.4	1.6	2.0
<b>Selected communicable conditions</b>	4.2	8.1	- 48.2	0.7	1.2
HIV/AIDS	0.0	0.9	- 100.0	- 0.0	0.1
<b>External causes</b>	34.3	39.5	- 13.1	6.0	6.1
<i>Selected unintentional causes</i>	21.4	16.1	33.2	3.7	2.5
Motor vehicle traffic injuries	11.8	10.0	18.2	2.0	1.5
Falls	9.6	6.1	57.8	1.7	0.9
<i>Selected intentional causes</i>	6.8	11.4	- 40.1	1.2	1.8
Self-inflicted (suicide)	5.9	10.5	- 43.3	1.0	1.6
Violence (homicide)	0.9	1.0	- 5.2	0.2	0.1
<b>Ill-defined conditions</b>	7.2	21.3	- 66.4	1.2	3.3
<b>All causes</b>	576.3	650.1	- 11.3	100.0	100.0

Causes of death	Sex	Italy (2001)		Eur-A (2001)			
		Rate	Change (%)	Average	Change (%)	Minimum	Maximum
<b>All causes</b>	Both	15.2	- 30.1	17.0	- 20.4	12.9	28.2
	M	17.4	- 29.0	19.2	- 20.3	12.6	32.2
	F	12.9	- 31.7	14.8	- 20.4	4.9	24.1
<i>Cardiovascular diseases</i>	M	1.6	- 31.9	0.9	- 26.0		1.8
	F	1.6	- 49.7	1.0	- 21.8		1.6
Ischaemic heart disease	M				- 75.0		0.6
	F				- 66.7		0.2
Cerebrovascular disease	M	0.1	- 77.4	0.2	- 44.4		0.4
	F	0.3	- 66.3	0.2	- 39.4		0.7
<i>Malignant neoplasms</i>	M	3.9	- 24.9	3.3	- 15.4		5.1
	F	2.8	- 19.2	2.7	- 10.4		4.9
Lung cancer	M				- 80.0		0.2
	F						0.3
Breast cancer	F				- 100.0		0.1
<i>Respiratory diseases</i>	M	0.9	- 28.9	0.8	- 13.7		3.0
	F	0.6	- 41.1	0.7	- 11.9		2.4
<i>Digestive diseases</i>	M	0.2	- 61.4	0.3	- 21.6		0.7
	F	0.2	- 51.1	0.2	- 25.0		2.6
<i>External causes</i>	M	5.0	- 33.6	6.4	- 30.7	3.5	20.3
	F	2.7	- 22.9	4.0	- 24.3		7.0
Motor vehicle traffic injuries	M	2.7	- 36.8	2.7	- 30.3		8.0
	F	1.5	- 14.5	1.8	- 29.3		4.1
Suicide	M	0.3	- 21.2	0.4	- 11.9		0.7
	F	0.1		0.1	0.0		0.6

Causes of death	Sex	Italy (2001)		Eur-A (2001)			
		Rate	Change (%)	Average	Change (%)	Minimum	Maximum
<b>All causes</b>	All	50.7	- 14.0	53.1	- 13.2	37.4	69.7
	M	75.8	- 15.4	77.8	- 13.0	59.4	110.2
	F	24.6	- 9.5	27.7	- 13.2	13.9	34.8
<i>Cardiovascular diseases</i>	M	4.0	- 20.6	3.3	- 12.1		5.7
	F	1.9	- 1.5	1.8	- 13.1		2.9
Ischaemic heart disease	M	0.3	3.2	0.3	- 15.0		1.6
	F	0.1	- 52.6	0.1	- 7.7		0.7
Cerebrovascular disease	M	0.6	- 35.5	0.7	- 13.6		1.4
	F	0.4	- 30.5	0.4	- 24.1		1.4
<i>Malignant neoplasms</i>	M	6.3	- 13.4	5.4	- 7.9		15.5
	F	4.3	- 4.7	3.7	- 7.9		7.0
Lung cancer	M	0.1	- 14.3	0.1	- 50.0		0.3
	F			0.0	- 33.3		0.3
Breast cancer	F			0.1	- 16.7		0.3
<i>Respiratory diseases</i>	M	0.8	- 44.9	1.1	- 25.7		4.5
	F	0.5	- 22.9	0.8	- 18.8		2.0
<i>Digestive diseases</i>	M	0.4	- 57.6	0.5	- 28.8		1.2
	F	0.3	- 41.7	0.3	- 30.4		1.1
<i>External causes</i>	M	53.2	- 9.4	54.9	- 12.0	33.0	96.5
	F	12.4	- 8.7	14.3	- 14.8	6.9	23.5
Motor vehicle traffic injuries	M	35.7	- 7.6	30.2	- 9.3	14.9	71.1
	F	8.7	- 2.9	8.1	- 10.7	2.6	14.3
Suicide	M	6.4	- 8.5	11.2	- 11.5		36.7
	F	1.3	- 17.0	2.5	- 24.3		7.5

NA = not applicable. Blank = rate < 0.1

Anatomically, tumors are highly heterogeneous, showing elevated proliferation along with necrosis or hemorrhages in the core [6]. The tumor-induced blood vessels are highly permeable enhancing macromolecular transport due to the presence of open gaps (inter-endothelial junctions & trans-endothelial channels), vesicular vascular organelles and fenestrations [7]. In vivo fluorescence microscopic studies suggest that the cutoff and the size of these pores are around 400nm [8]. However, the transport of anticancer drugs in/across interstitium was opposed by physiological (i.e., interstitial pressure) properties of the tumor or physic-chemical properties of the drug molecule (e.g. size, configuration, charge, hydrophobicity) [8].

Moreover cancer is caused by abnormalities in the genetic material of the transformed cells [9]. These abnormalities are due to mutations in the DNA of a normal cell, changing them to transformed cells or “mutants”. Mutations are mainly caused by exposure to carcinogens; such as tobacco smoke, radiation, chemicals, or infectious agents [10]. Other cancer-enhancing genetic abnormalities may occur randomly due to errors in DNA replication, or are inherited [11]. The heritability of cancers is usually affected by complex interactions between carcinogens and the host's genome with cancer-enhancing genetic abnormalities present in cells from birth. Although much progress has been made in cataloging the environmental causes and cellular and molecular biological basis for this dreaded disease, we still do not have a precise understanding of the differences between a cancer cell and its normal counterpart.

Cancer development occurs when cells in a part of the body begin an ‘out-of-control’ growth of abnormal cells, and instead of dying, they outlive normal cells and continue to form new abnormal cells. Hanahan and Weinberg [5] have highlighted six hallmarks of most cancer, if not all (fig. 1-2). Cancer cells acquire autonomy from growth signals, evasion of

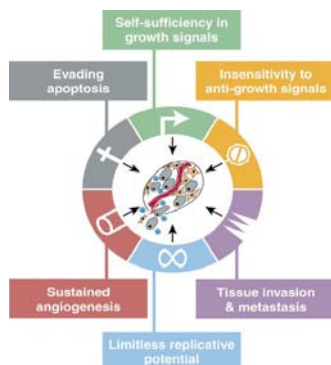


Fig. 1-2. The Six hallmarks of cancer [5].

growth inhibitor signals, evasion of apoptotic cell death, unlimited replication potential, angiogenesis, and invasion and metastasis, of which all are essential for carcinogenesis.

With the completion of the human genome sequencing in 2001 [10, 13] and subsequent improvements in the sequence data [14], we are now closer to being able to fully characterize the differences between normal and tumor cells. At about the

same time that the human genome was sequenced, a new, novel focus of research evolved from the convergence and coalescence of many diverse scientific disciplines. This new era of research called “nanotechnology” introduced the creation, manipulation, and application of structures in the nanometer range.

As described by Heath and Davis [15], nanoparticles have four unique properties that distinguish them from other cancer therapeutics: (1) the nanoparticle, which by itself can have therapeutic or diagnostic properties and which can carry a complex and highly concentrated therapeutic “payload”; (2) nanoparticles can be attached to multivalent targeting ligands which yield high affinity and specificity for target cells; (3) nanoparticles can accommodate multiple drug molecules that allow combinatorial cancer therapy, either simultaneously or serial; and (4) nanoparticles can bypass multiple drug resistance mechanisms typical for traditional chemotherapeutics.

## **2.2. Nanomedicine and new drug therapies for Cancer**

### **2.2.1. Conventional therapies for cancer**

The traditional strategies for cancer treatment, includes surgery, radiation, and chemotherapy or combined strategies of these treatments. These are supplemented by some

more specialized therapies such as immunotherapy or hormone therapy which can be applied only some tumor types [16].

The oldest form of cancer treatment is surgery. It renders the greatest chance of cure, mainly for solid tumors; especially those which have not yet metastasized to other parts of the body. It is and will remain in future one of the most important weapons against cancer.

Radiotherapy is the second major weapon against cancer. Radiation therapy involves use of high-energy particle beams or waves (radiation), such as X-rays, gamma rays, neutrons or pions for treating cancer [17]. Radiotherapists often implant radioisotopes into tumors [18]. The radioactive material transfers its energy into highly energetic electrons which ionize the matter they hit, such as water and/or proteins or other molecules of the cell cytoplasm, or RNA and DNA. This ionization changes the molecules and hence leads to variations or inactivation in their biological properties; e.g causing cell death or inhibits cell division. Radiation is more harmful for cancerous cells than for normal cells because cancerous cells are more unstable in all respects and thus more vulnerable to the damaging radiations. However, the cellular repair mechanism is also not prominently active in the highly dividing cells like cancer cells. However, due to proper functionally active cellular repair mechanism normal cells can recover from the effects of radiation more easily. One of the major drawbacks of radiotherapy is that that it is impossible to treat only tumor cells, without affecting the surrounding healthy cells.

Chemotherapy uses chemicals to treat cancer, especially suitable for those cancers that have been spread out (metastasized) and can not be treated any longer by localized methods such as surgery and radiation. One common characteristic of most cancer cells is their rapid rate of cell division. Anticancer drugs like taxol (interferes with the depolarization of microtubules and hyperstabilizes their structure), doxo- (is thought to intercalates in DNA) or

daunorubicin (intercalates, with its daunosamine residue directed toward the minor groove), all adversely affects the process of cell division. Thus are aimed to destroy aggressive cancers. Nevertheless, chemotherapeutics have the same disadvantage like radio-therapeutics. They are unspecific and therefore do not distinguish between healthy and cancerous cell and hence damage also healthy cells as well.

Some more specialized therapies which are only applicable in specific tumor types are hormone, immune or photodynamic therapy (PDT). Hormone therapy which is also known as androgen deprivation therapy or androgen suppression therapy changes the internal environment and prevents the growth of cancers that are hormone-dependent, such as some cases of breast or prostate cancers [19, 20]. Hormone therapy lowers androgen levels (either by surgery or drugs such as pituitary down-regulators and anti-androgens) and slows down the tumor growth or reduces the tumor volume.

PDT which is a very local and highly tumor specific treatment has greatly reduced the side-effects as the photosensitizer is accumulating mainly (intravenous or intratumoral injection) in the tumor tissue and then becomes activated by a local application of non-toxic infrared light. This irradiation produces highly toxic singlet oxygen which irreversibly damages the cancer cells so they undergo apoptosis or necrosis [21-24]. Unfortunately this technique can be used exclusively for superficial tumors such as melanomas, head and neck cancer, tumors of the bladder because of the limited light penetration of the tissue and accessibility by a light source.

Immunotherapy (also known as biologic therapy) has emerged as a more specific cancer treatment method for cancers that affect the immune system, like leukemia (cancer of the leukocytes) and lymphoma (cancer of the lymphatic tissues). These cancers weaken the immune system and make it harder for the body to fight off disease. Immunotherapy has

proven to be a new cancer treatment that stimulates a patient's immune system so it is better able to fight disease by administration of cytokines or monoclonal antibodies [25]. Cytokines bind to cancer cells, making them easily recognizable and more susceptible to the action of other immune cells. Other cytokines enhance the killing action of immune cells and help the natural ability of the body to repair cells damaged by radiation or chemotherapy [26, 27]. Interferon-alfa (INF- $\alpha$ ), interleukin-2 (IL-2) and colony-stimulating factor (CSFs) have shown promise as cancer therapies. INF- $\alpha$  slows the growth of cancer cells, and promotes more normal cell activity and stimulates the body's natural immune system to fight cancer cells, according to the National Cancer Institute (NCI). Monoclonal antibodies specifically target cancer cells and then block their activation (therapeutic antibodies) or inhibit tumor growth by delivering covalently bound radioactive chemicals (targeting antibodies) [28]. A few of these monoclonal antibodies are currently in clinical trials. Moreover, the Food and Drug Administration (FDA) has approved some of them for certain types of cancer treatment (see Table1-3, respectively) [29, 30]. Compared to the side effects of standard chemotherapy, the side effects of naked mAbs are often "allergic" reactions which rarely can be life-threatening but often prevents a second treatment [31].

Table 1.3. (a) List of Monoclonal antibodies till 2008, includes approved and investigational drugs as well as drugs that have been withdrawn from market; consequently (the column Use does not necessarily indicate clinical usage). (b) FDA approved therapeutic monoclonal antibodies [29].

**a**

Name	Trade name	Type	Source	Target	Use
Abagovomab		mab	mouse	CA-125 (imitation)	ovarian cancer
Adecatumumab		mab	human	EpCAM	prostate and breast cancer
Afutuzumab		mab	humanized	CD20	lymphoma
Alacizumab pegol		F(ab') <sub>2</sub>	humanized	VEGFR2	cancer
Altumomab pentetate	Hybri-ceaker	mab	mouse	CEA	colorectal cancer (diagnosis)
Anatumomab mafenatox		Fab	mouse	TAG-72	non-small cell lung carcinoma
Apolizumab		mab	humanized	HLA-DR ?	hematological cancers
Bavituximab		mab	chimeric	phosphatidylserine	cancer, viral infections
Bectumomab	LymphoScan	Fab'	mouse	CD22	non-Hodgkin's lymphoma (detection)
Belimumab	Benlysta, LymphoStat-B	mab	human	BAFF	non-Hodgkin lymphoma etc.
Besilesomab	Scintimun	mab	mouse	CEA-related antigen	inflammatory lesions and metastases (detection)
Bevacizumab	Avastin	mab	humanized	VEGF-A	metastatic cancer
Bivatuzumab mertansine		mab	humanized	CD44 v6	squamous cell carcinoma
Blinatumomab		BITE	mouse	CD19	cancer
Brentuximab vedotin		mab	chimeric	CD30 (TNFRSF8)	hematologic cancers
Cantuzumab mertansine		mab	humanized	mucin CanAg	colorectal cancer etc.
Capromab pendetide	Prostascint	mab	mouse	prostatic carcinoma cells	prostate cancer (detection)
Catumaxomab	Removab	3funct	rat/mouse hybrid	EpCAM, CD3	ovarian cancer, malignant ascites, gastric cancer
CC49		mab	mouse	TAG-72	tumor detection
Cetuximab	Erbix	mab	chimeric	EGFR	metastatic colorectal cancer and head and neck cancer
Citatumumab bogatox		Fab	humanized	EpCAM	ovarian cancer and other solid tumors
Cixutumumab		mab	human	IGF-1 receptor	solid tumors
Clivatuzumab tetraxetan		mab	humanized	MUC1	pancreatic cancer
Conatumumab		mab	human	TRAIL-R2	cancer
Dacetuzumab		mab	humanized	CD40	hematologic cancers
Denosumab	Prolia	mab	human	RANKL	osteoporosis, bone metastases etc.
Detumomab		mab	mouse	B-lymphoma cell	lymphoma
Ecromeximab		mab	chimeric	GD3 ganglioside	malignant melanoma
Edrecolomab	Panorex	mab	mouse	EpCAM	colorectal carcinoma
Elotuzumab		mab	humanized	SLAMF7	multiple myeloma
Epratuzumab		mab	humanized	CD22	cancer, SLE
Ertumaxomab	Rexomun	3funct	rat/mouse hybrid	HER2/neu, CD3	breast cancer etc.
Etaracizumab	Abegrin	mab	humanized	integrin $\alpha_v\beta_3$	melanoma, prostate cancer, ovarian cancer etc.

Table 1-3. (a) List of Monoclonal antibodies till 2008 (continuation.....)

Name	Trade name	Type	Source	Target	Use
Farletuzumab		mab	humanized	folate receptor 1	ovarian cancer
Figitumumab		mab	human	IGF-1 receptor	adrenocortical carcinoma, non-small cell lung carcinoma etc.
Galiximab		mab	chimeric	CD80	B-cell lymphoma
Gemtuzumab ozogamicin	Mylotarg	mab	humanized	CD33	acute myelogenous leukemia
Glembatumumab vedotin		mab	human	GPVMB	melanoma, breast cancer
Ibritumomab tiuxetan	Zevalin	mab	mouse	CD20	non-Hodgkin's lymphoma
Igovomab	Indimacis-125	F(ab') <sub>2</sub>	mouse	CA-125	ovarian cancer (diagnosis)
Imciromab	Myoscint	mab	mouse	cardiac myosin	cardiac imaging
Intetumumab		mab	human	CD51	solid tumors (prostate cancer, melanoma)
Inotuzumab ozogamicin		mab	humanized	CD22	cancer
Iplimumab		mab	human	CD152	melanoma
Iratumumab		mab	human	CD30 (TNFRSF8)	Hodgkin's lymphoma
Labetuzumab	CEA-Cide	mab	humanized	CEA	colorectal cancer
Lintuzumab		mab	humanized	CD33	cancer
Lucatumumab		mab	human	CD40	multiple myeloma, non-Hodgkin's lymphoma, Hodgkin's lymphoma
Lumiliximab		mab	chimeric	CD23 (IgE receptor)	chronic lymphocytic leukemia
Mapatumumab		mab	human	TRAIL-R1	cancer
Matuzumab		mab	humanized	EGFR	colorectal, lung and stomach cancer
Milatumumab		mab	humanized	CD74	multiple myeloma and other hematological malignancies
Mitumomab		mab	mouse	GD3 ganglioside	small cell lung carcinoma
Nacolomab tafentox		Fab	mouse	C242 antigen	colorectal cancer
Naptumomab estafenatox		Fab	mouse	5T4	non-small cell lung carcinoma, renal cell carcinoma
Necitumumab		mab	human	EGFR	non-small cell lung carcinoma
Nimotuzumab	Theracim, Theraloc	mab	humanized	EGFR	squamous cell carcinoma, head and neck cancer, nasopharyngeal cancer, glioma
Nofetumomab merpentan	Verluma	Fab	mouse	?	cancer (diagnosis)
Ofatumumab	Arzerra	mab	human	CD20	chronic lymphocytic leukemia etc.
Olaratumab		mab	human	PDGF-R $\alpha$	cancer
Oportuzumab monatox		scFv	humanized	EpCAM	cancer
Oregovomab	OvaRex	mab	mouse	CA-125	ovarian cancer
Panitumumab	Vectibix	mab	human	EGFR	colorectal cancer
Pemtumomab	Theragyn	?	mouse	MUC1	cancer
Pertuzumab	Omnitarg	mab	humanized	HER2/neu	cancer
Pintumomab		mab	mouse	adenocarcinoma antigen	adenocarcinoma (imaging)
Pritumumab		mab	human	vimentin	brain cancer
Ramucirumab		mab	human	VEGFR2	solid tumors
Rilotumumab		mab	human	HGF	solid tumors
Rituximab	MabThera, Rituxan	mab	chimeric	CD20	lymphomas, leukemias, some autoimmune disorders

*Table 1-3. (a) List of Monoclonal antibodies till 2008 (continuation.....)*

Name	Trade name	Type	Source	Target	Use
Satumomab pentetide		mab	mouse	TAG-72	cancer (diagnosis)
Sibrotuzumab		mab	humanized	FAP	cancer
Tacatumab tetraxetan	AFP-Cide	mab	humanized	alpha-fetoprotein	cancer
Taplitumomab paptox		mab	mouse	CD19	cancer
Tenatumomab		mab	mouse	tenascin C	cancer
TGN1412		?	humanized	CD28	chronic lymphocytic leukemia, rheumatoid arthritis
Ticilimumab (= tremelimumab)		mab	human	CTLA-4	cancer
Tigatumab <sup>[4]</sup>		mab	humanized	TRAIL-R2	cancer
TNX-650		?	humanized	IL-13	Hodgkin's lymphoma
Tositumomab	Bexxar	?	mouse	CD20	follicular lymphoma
Trastuzumab	Herceptin	mab	humanized	HER2/neu	breast cancer
Tremelimumab		mab	human	CTLA-4	cancer
Tucotuzumab celmoleukin <sup>[17][37]</sup>		mab	humanized	EpCAM	cancer
Veltuzumab <sup>[4]</sup>		mab	humanized	CD20	non-Hodgkin's lymphoma
Volociximab <sup>[10]</sup>		mab	chimeric	integrin $\alpha_5\beta_1$	solid tumors
Votumumab	HumaSPECT	mab	human	tumor antigen CTAA16.88	colorectal tumors
Zalutumumab <sup>[10]</sup>	HuMax-EGFr	mab	human	EGFR	squamous cell carcinoma of the head and neck
Zanolimumab <sup>[2]</sup>	HuMax-CD4	mab	human	CD4	rheumatoid arthritis, psoriasis, T-cell lymphoma

*Table 1-3. (b) FDA approved therapeutic monoclonal.*

Antibody	Brand name	Approval date	Type	Target	Indication (What it's approved to treat)
Alemtuzumab	Campath	2001	humanized	CD52	Chronic lymphocytic leukemia
Bevacizumab	Avastin	2004	humanized	Vascular endothelial growth factor (VEGF)	Colorectal cancer, Age related macular degeneration
Cetuximab	Erbix	2004	chimeric	epidermal growth factor receptor	Colorectal cancer, Head and neck cancer
Gemtuzumab	Mylotarg	2000	humanized	CD33	Acute myelogenous leukemia (with calicheamicin)
Ibritumomab tixetan	Zevalin	2002	murine	CD20	Non-Hodgkin lymphoma (with yttrium-90 or indium-111)
Panitumumab	Vectibix	2006	human	epidermal growth factor receptor	Colorectal cancer
Ranibizumab	Lucentis	2006	humanized	Vascular endothelial growth factor A (VEGF-A)	Macular degeneration
Rituximab	Rituxan, Mabthera	1997	chimeric	CD20	Non-Hodgkin lymphoma
Tositumomab	Bexxar	2003	murine	CD20	Non-Hodgkin lymphoma
Trastuzumab	Herceptin	1998	humanized	ErbB2	Breast cancer

### **2.2.2. Nano therapeutic advances for cancer therapy**

Conceivably, the greatest immediate impact of nanotechnologies in cancer therapy is in the realm of drug delivery. The therapeutic index of nearly all drugs currently being used could be improved if they were more efficiently delivered to their biological targets through appropriate application of nanotechnological tools [32, 33]. On the other hand, those drugs that have previously failed clinical trials because of toxicity concerns may be re-examined using nanoparticulated preparations [34].

An effective and safe cancer drug or drug deliver system should fulfill the following requirements: a) it must have an adequate drug concentration which allows an effective dose at the tumor cells, b) it must be targeted to tumor cells, and prevent uptake by normal cells, c) should have high biocompatibility, d) should have a long half-life in blood circulation, and being stable and keep the drug until they reach their target.

### **2.2.3. Nanomedicines and drug delivery system**

Nowadays nanomaterials system focus on development of target specific, slow but controlled drugs release system. A major milestone was achieved in drug delivery systems with the development of technologies that can mask the nano carriers from the immune system. This has significantly increased the nano-drug or drug delivery systems blood half-life. The introduction of synthetic lipid derivatives of polyethyleneglycol (PEG) confers 'stealth' capability on nanocarrier system, due to the hydrophilicity of the PEG chains. This PEG stealth avoids opsination and reduces fast blood clearance by immune recognition. Hence helps in passive accumulation in tumors via an enhanced permeation and retention (EPR) effect [35-37].

The first generation of nano drug delivery systems was nanometric liposomes delivering their chemotherapy payloads to the tumour reducing the overall toxicity to the body [38]. PEG coating have improved the circulation of these liposomal drugs in blood. Liposomal formulations of doxorubicin are approved for use in Kaposi sarcoma, breast cancer and refractory ovarian cancer.

The next generation was polyplexes, polymeric nanoparticles precipitated with drug molecules and surface functionalized prevent the immune recognition and nowadays even having targeting moieties in form of antibodies or folic acid [39, 40].

For therapeutic applications, selective or preferential delivery of nanomaterials to sites of cancer has to be optimal. The targeting of nanoparticles can be achieved by the conjugation of a tumor-specific ligand(s) to nanoparticles for delivery of nanoparticles to tumor sites [41, 42]. Targeting moieties that have been investigated includes antibodies, peptides, cell surface ligands, and aptamers [43, 44]. Targets on tumor cells include tumor antigens, cell surface receptors that are internalized (e.g. folate receptors (FR) [45], transferrin receptors [46], and tumor vasculature [47]). Active targeting has been extensively studied in preclinical models but has not been effectively translated into current clinical applications [48]. In preclinical models, targeting has invariably led to an increased accumulation of nanocarriers in tumors [48, 49]. In many instances, though targeting has enhanced cancer cell uptake at in-vitro level but at tumor level overall tumor accumulation of nanoparticles was not significant (table 1-4) [48-51]. One potent outcome of this technology has been the development of nucleic acid ligands, called aptamers, which mimic antibodies and act as potential replacements because they can be designed to bind practically against any antigen. Moreover they are preventing the problem with immunogenicity of antibodies [52]. Aptamers have a high affinity for the targeted antigens and have been investigated successfully to direct PEG-coated nanoparticles

to prostate-specific membrane antigen for prostate cancer [53]. There are numerous other examples of aptamer-guided targeting of nanoparticles [54-58]. This area of research promises to provide an important new weapon in the arsenal to improve cancer treatment outcome.

*Table 1.4. Various nanoparticles as Drug Delivery Carriers [48].*

Nanoparticle	Size (nm)	Carried therapeutic agent	Examples of potential targeted therapeutic application	Advantage
Polymeric biodegradable nanoparticles	10-1,000	Plasmid DNA, proteins, peptides, low molecular weight compounds	Brain tumor therapy [Olivier et al., [1999]]; Kreuter et al., [2003], bone healing [Labhasetwar et al., [1999]], vaccine adjuvant [Raghuvanshi et al., [2001]], coating gut suture [Cohen et al., [2000]], restenosis [Guzman et al., [1996]]; Panyam et al., [2002], inflamed colonic mucosa [Lamprecht et al., [2001]], diabetes therapy [Al Khouri et al., [1986]]; Watnasirichailkul et al., [2000]]	Sustain localized drug therapeutic agent for weeks
Silica nanoparticles	<100	Proteins, DNA, anticancer therapeutic agents, high molecular weight compounds	Photodynamic therapy [Roy et al., [2003b]], liver therapy [Roy et al., [2003a]]; Dey, [2005]], diabetes therapy [Cherian et al., [2000]]	Can be easily prepared, water-soluble, and stable in biological environment
Metallic nanoparticles	<50	Anticancer therapeutic agents, proteins, DNA	Cancer therapy [Wang et al., [2004]]; Priyabrata et al., [2005]]	Extremely small size with vast surface area to carry large dose
Polymeric micelles	<100	DNA, anticancer therapeutic agents, proteins	Solid tumors therapy [Yokoyama et al., [1990]]; Kataoka et al., [2001]; Rapoport et al., [2003]], antifungal treatment [Yu et al., [1998]]	Have hydrophobic core, and so they are suitable carriers for water-insoluble drug
Liposomes	50-100	Proteins, DNA, anticancer therapeutic agents	Tumors therapy [Goren et al., [1996]]; Vershuis et al., [1998]; Lasic et al., [1999]], HIV therapy [Slepishkin et al., [1996]], vaccine delivery [Rao and Alving, [2000]]	Effective in reducing system toxicity and can stay longer in targeted tissue
Dendrimers	<10	DNA, anticancer therapeutic agents, antibacterial therapeutic agents, antiviral therapeutic agents, high molecular weight compounds	Tumors therapy [Kobayashi et al., [2001]]; Quintana et al., [2002]; Latallo et al., [2005]], bacterial infection treatment [Chen and Cooper, [2002]]; Boas and Heegaard, [2004]], HIV therapy [Witvrouw et al., [2000]]; Rojo and Delgado, [2004]]	Can be modified to carry hydrophobic or hydrophilic drug

Finally, the success of nanotechnology in the future will depend on toxicologic issues associated with understanding of the fate of nanocarriers in the body, as well as the elimination of the risk metabolic products. In this respect, the possibility of using drug carriers made from natural polymers (e.g., chitosan, alginate, polypeptides) represents an attractive prospect [59-62].

The unique properties of nanoparticles and the possibilities to redesign according to one's need have opened the door to new, noninvasive strategies for cancer therapy, previously not possible. This includes photothermal therapy (PTT), nanoparticle enhanced radiotherapy, targeted combinatorial cancer therapy, and nanoparticle-enhanced radiofrequency cancer therapy.

PTT relies on unique properties of nanoparticles which have high absorption in the red or near infrared (NIR) region. Nanoshells have been most extensively characterized as nanoscale mediators of photothermal ablation. O'Neal et al. [63] first demonstrated thermal ablation of tumors in a mouse model following systemic injection of particles and exposure of tumors to NIR light. Other nanostructures such as nanorods and carbon nanotubes which also strongly absorb in the NIR region have also been utilized.

Gold is an excellent absorber of X-rays. The tumor loaded with nanogold, has lead to an enhanced effect in the cancerous tissue compared with the dose received by normal tissue during a radiotherapy treatment [64]. Gold nanoparticles have been demonstrated to enhance the effect of radiotherapy on tumors in vitro [65] and in mouse models of cancer such as melanoma [63-66]. This phenomenon suggests that the specific delivery of gold nanoparticles to cancer has the potential to enhance the efficacy of radiation therapy on cancer, allowing dose reduction with reduced toxicity to surrounding normal tissues.

Nanotechnology clearly holds immense potential for targeting cancer. These approaches will encompass the desired goals of early detection, tumor regression with limited collateral damages, and efficient monitoring of response to chemotherapy. The exciting milestones made in these areas need to be paralleled with safety evaluations of the platforms before they are translated to the clinics. Nevertheless, we believe that the next few years are likely to see an increasing number of nanotechnology-based therapeutics and diagnostics reaching the clinic.

Recently, Multi-Stage Vectors (MSV) have been introduced which are designed to attach to the blood vessel walls in a tumor (fig. 1-3, above left). Nanoparticles released by the MSVs (fig. 1-3, above right) then seek cancerous cells and inject material designed to kill that particular cancer (fig. 1-3, bottom) [67].

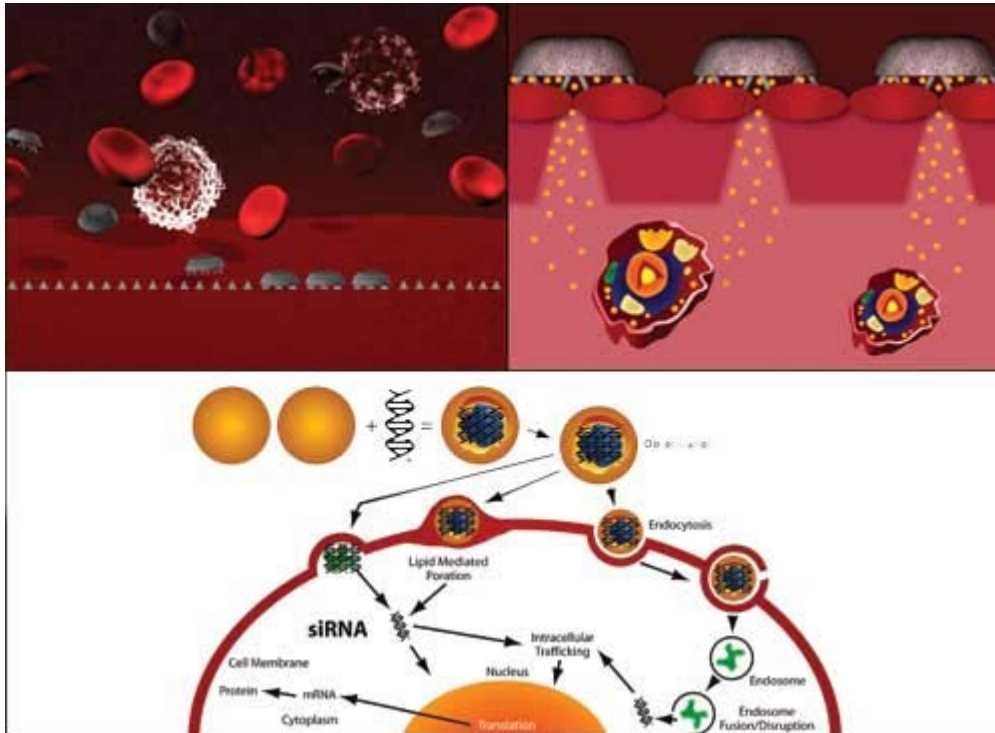


Fig.1-3. A Multi-Stage Vectors system (MSV), presenting an implanted drug release system in blood vessels [67].

## 2. 3. Nanotechnologies in bioimaging and detection of Cancer

### 2.3.1. Conventional Cancer diagnostics

Conventional primary cancer diagnostics are based on tissue pathology, such as biopsy, endoscopy, and imaging which all looked at the cell appearance under the microscope [68, 69]. Until now biopsy is the only definitive prove for the presence of cancer cells. During a biopsy, the doctor removes a sample of the tissue from the abnormal area or removes the whole tumor and then the pathologist examines the tissue visually.

In order to use more non-invasive technologies and visualize also metastasis, imaging was developed examining the body by X-ray, or computed tomography (CT), ultrasonography and MRI (magnetic resonance imaging). It usually uses a contrast agent to increase the imaging contrast for certain organs. One can distinguish two different types of images,

functional (MRI, contrast comes from biological active substances (water)) and anatomical (contrast comes from e.g. bones).

X-ray imaging is the most common way to visualize tumors. In this case a radiotracer is administered intravenously or orally and passively accumulates in the tumor. CT, sometimes called CAT (computed angled tomography) scan, uses special x-ray equipment to obtain image data from different angles and then uses computer processing to show a 3-dimensional cross-section of body.

Recently, an improved imaging system was developed by positron emission tomography (PET) often used with CT X-ray scan. PET is a nuclear medicine imaging technique which produces functional 3-D or 4-D (where 4<sup>th</sup> dimension is time) image. PET is used heavily in clinical oncology (medical imaging of tumors and the search for metastases) [70]. Ultrasonography uses high-frequency sound waves to enter the body and the reflected echoes to produce a sonogram. But the main problem is the low contrast because usually it is used without contrast agents. One improvement is now the usage of coated or uncoated gas bubbles to improve contrast [71, 72].

Magnetic resonance imaging (MRI) uses radiofrequency waves and a strong magnetic field to provide remarkably clear and detailed pictures of internal organs and soft tissues. The technique has proven very valuable for the diagnosis of a broad range of pathologic conditions in all parts of the body including cancer, heart and vascular disease, stroke, spinal and joint problems. Moreover it can be used not only for anatomical images but also for functional.

The advanced development of cancer molecular biology in the last decade has made enormous progress in understanding the molecular events that accompany malignant transformation and progression by genomics and proteomics [73]. Molecular diagnostics

determines the molecular markers such as genes and proteins typical for cancer cells and the signatures interacting patterns of cancer cells (i.e. the genetic changes disrupt the cell's normal communication network, due to altered proteins along many different pathways cause signals to be garbled, intercepted, amplified, or misdirected) [74, 75]. However, with these advances in the conventional methods, no significant improvement in diagnostics and staging of the majority of cancer cells in real time [76]. This led to requirement for more sophisticated methodology for cancer therapy and diagnostics.

### 2.3.2. Nano-devices in cancer imaging and diagnostic

Advances in nanoscience and nanotechnology are augmenting a significant improvement of the above mentioned conventional methods leading to a great progress in cancer diagnostics. One of the challenges of nanotechnology has been the development of multimodal contrast agents (i.e., imaging simultaneously or in succession by more than one imaging modality). This approach offers the potential to integrate the advantages of different techniques while at the same time surmounting the limitations of each other [77, 78]. Multimodal contrast agents offer improvements in patient care, and at the same time

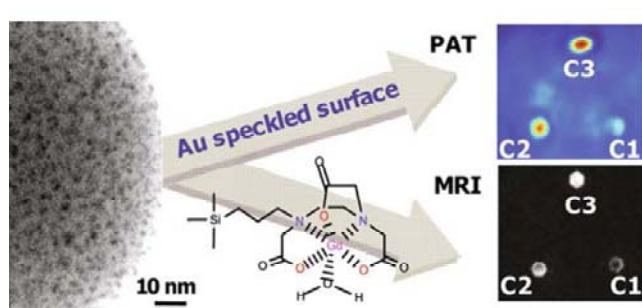


*Figure-1.4. Gold-speckled silica nanoparticles doped with gadolinium shell for dual-mode imaging in PET and MRI. The signal tagged C1, C2, and C3 are increasing concentrations of particles in a tissue-like phantom [78].*

reduce costs and enhance safety, by limiting the number of contrast agent administrations required for imaging purposes. For example, Gd-doped gold-speckled silica nanoparticles were developed as a multimodal contrast agent for MRI and PET

using reversed micelles (fig. 1-4) [79]. Quantum dots, which are generally defined as particles with physical dimensions smaller than the exciton Bohr radius [80], are emerging as powerful optical contrast agents, both for monitoring cellular events and for imaging tumours in vivo. The multimodal quantum dots (Q-dots) with the fluorescence, X-ray contrast, and magnetic properties (fig. 1-5) [81] can contribute greatly in the field of cancer imaging. Unlike Q-dots, a noble-metal nanoparticle exhibits unique optical properties,

depending upon the size and shape of the particles, due to surface plasmon resonance (SPR). For these properties, metal nanoparticles

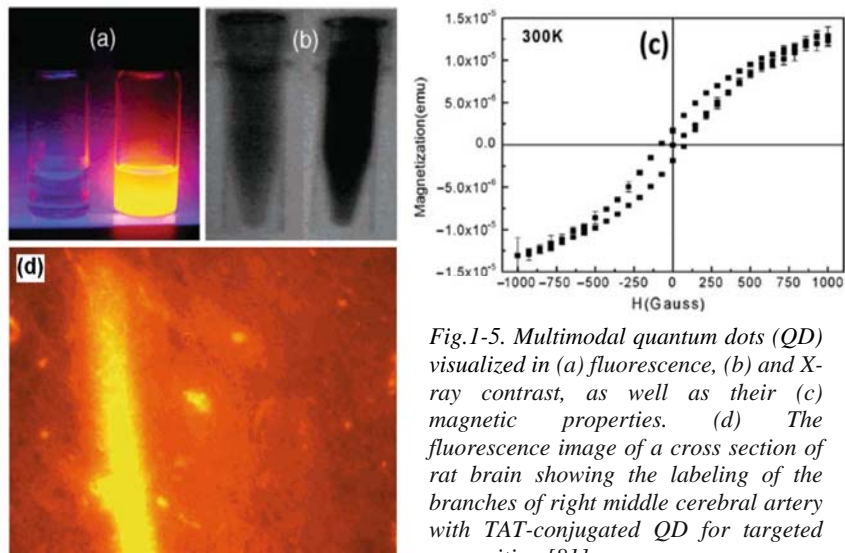


Fig.1-5. Multimodal quantum dots (QD) visualized in (a) fluorescence, (b) and X-ray contrast, as well as their (c) magnetic properties. (d) The fluorescence image of a cross section of rat brain showing the labeling of the branches of right middle cerebral artery with TAT-conjugated QD for targeted recognition [81].

have been used for developing oligonucleotide-functionalized gold nanoparticles based

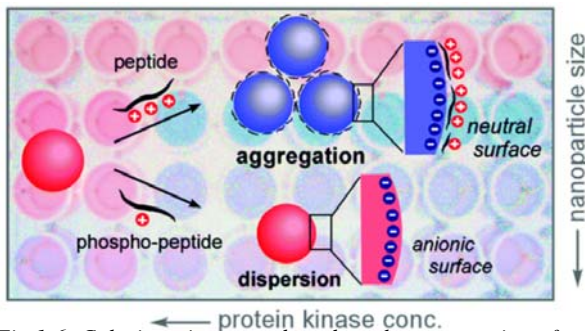
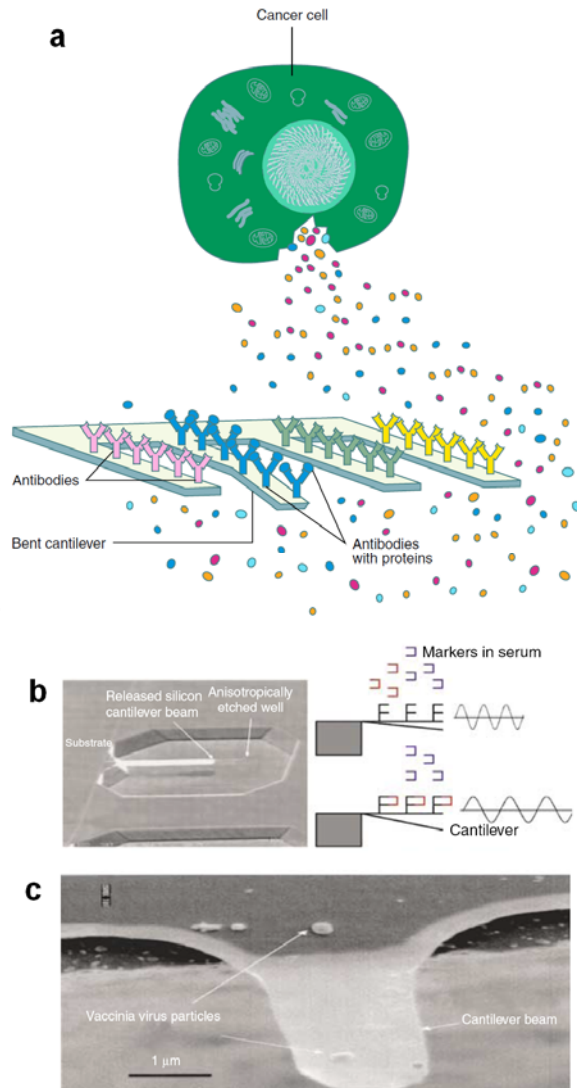


Fig.1-6. Colorimetric assays based on the aggregation of gold nanoparticles (AuNPs). Two categories can be distinguished, cross-linking, and dispersion. The principle is to assay the effect of the AuNP size on the dynamic range of Optical Density (OD) before and after aggregation [82].

commercialized biomedical assays for the ultra-sensitive detection of biomarker in diseases like cancer (fig. 1-6) [82, 83].

Cancer-related nanotechnology research is preceding in another frontier in diagnostics i.e. laboratory-based diagnostics. Nanodevices can

provide rapid and sensitive detection of cancer-related molecules by enabling detection to investigate molecular changes even when they occur only in a small percentage of cells. Nanocantilever is a device capable of detecting masses as small as 1 attogram ( $1 \times 10^{-18}$  g) at ambient temperature and pressure. Conventional devices (e.g. Knudsen cell with Quartz crystal microbalance, detection sensitivity  $>1\text{ng}$  [84]) require high vacuum and low temperature in order to achieve comparable sensitivity. The nanocantilever sensors are tiny cantilevers of a few hundred nanometres across that vibrate like a nano “diving board”. When an object rests on the 'diving board' the frequency at which it vibrates changes in proportion to the added mass (fig. 1-7) [85].



*Fig. 1-7. Nanocantilevers are devices which are coated with antibodies to capture target macromolecules such as proteins, viruses or other biomolecules by the principle of a nanobalance. This can be used for designing a new class of ultra-small highly sensitive sensors for viruses, bacteria and other pathogens or single cell analysis [85].*

Another nanodevice developed in recent years is the nanowire sensors. Nanowire sensor arrays are highly sensitive, label-free, multiplexed electrical detection system developed for

cancer marker detection using silicon-nanowire field-effect devices in which distinct nanowires and surface receptors are incorporated into arrays (fig. 1-8) [86].

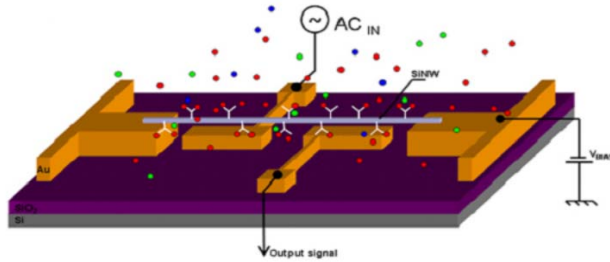
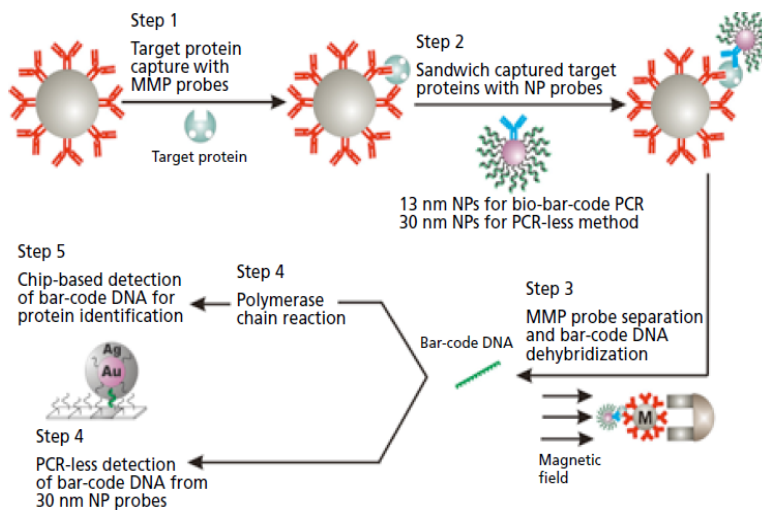


Figure 1-8. The nanowire nanosensor allows for real time cancer marker detection at a very low concentration and with very high selectivity and specificity [86].

The newly developed bio-barcode assay system for detection of nucleic acid or protein targets (without PCR) has been shown to be extraordinary sensitive (attomolar sensitivity) [87]. Two types of particles are used in the assay: (i) a magnetic micro-particle with



recognition elements for the target of interest; and (ii) a gold nanoparticle (AuNP) with a second recognition agent (which can form a sandwich around the target in conjunction with the magnetic particle) and hundreds of thiolated single-

Fig. 1-9. The bio-barcode assay is a sandwich immunoassay system [87].

strand oligonucleotide barcodes (fig. 1-9). After reaction with the analyte, a magnetic field is used to localize and collect the sandwich structures, and then the barcode strands are released. They can be identified on a microarray via scanometric detection or *in situ* if the barcodes carry also a detectable marker [88].

### 3. References

1. [http://www.who.int/healthinfo/global\\_burden\\_disease/GBD\\_report\\_2004update\\_part\\_2.pdf](http://www.who.int/healthinfo/global_burden_disease/GBD_report_2004update_part_2.pdf)
2. <http://globocan.iarc.fr/factsheets/cancers/all.asp>
3. [http://www.euro.who.int/\\_data/assets/pdf\\_file/0012/103215/E88550.pdf](http://www.euro.who.int/_data/assets/pdf_file/0012/103215/E88550.pdf)
4. Kawasaki ES, Player A. Nanotechnology, nanomedicine, and the development of new, effective therapies for cancer. *Nanomedicine* 2005;1(2):101-109.
5. Hanahan D, Weinberg RA. The six hallmarks of cancer. *Cell* 2000;100:57–70.
6. Vaupel P, Kallinowski F, Okunieff P. Blood flow, oxygen and nutrient supply, and metabolic microenvironment of human tumors: a review. *Cancer Res* 1989;49(23):6449-6465.
7. Jain RK. Transport of molecules in the tumor interstitium: a review. *Cancer Res*. 1987;47(12):3039-3051.
8. Unezaki S, Maruyama K, Hosoda JI, Nagae I, Koyanagi Y, Nakata M, *et al.* Direct measurement of the extravasation of polyethyleneglycol-coated liposomes into solid tumor tissue by in vivo fluorescence microscopy. *Int J Pharm* 1996;144(1):11-17.
9. Kinzler KW, Vogelstein B. Introduction. In: Seils A, Noujaim SR, Boyle PJ, editors. *The genetic basis of human cancer*, 2<sup>nd</sup> ed. New York: McGraw-Hill, Medical Pub. Division, 2002, p. 3-6.
10. Boyland E. Different types of carcinogens and their possible modes of action: a review. *Cancer Res*. 1952;12(2):77-84..
11. Stein GS, Pardee AB, editors. *Cell cycle and growth control: biomolecular regulation and cancer*, 2<sup>nd</sup> ed.. Hoboken, New Jersey: John Wiley & Sons Inc, 2004.

12. International Human Genome Sequencing Consortium. Initial sequencing and analysis of the human genome. *Nature* 2001;409:860- 921.
13. Venter JC, Adams MD, Myers EW, Li PW, Mural RJ, Sutton GG, et al. The sequence of the human genome. *Science* 2001;291:1304-51.
14. International Human Genome Sequencing Consortium. Finishing the euchromatic sequence of the human genome. *Nature* 2004;431:931-945.
15. Heath JR, Davis ME. Nanotechnology and cancer. *Annu Rev Med* 2008;59:251-265.
16. Miller AB, Hoogstraten B, Staquet M, Winkler A. Reporting results of cancer treatment. *Cancer* 1981;47(1):207-214.
17. Israel L, editor. *Conquering Cancer*. New York: Random House, 1978.
18. Thorell JI, Larson SM editors. *Radioimmunoassay and Related Techniques. Methodology and Clinical Applications*. Saint Louis, The C. V. Mosby Company, 1978.
19. Vrbanec D, Belev B, Pavlinić-Diminić V, Pezerović D, Dusper B, Plestina S, *et al.* Hormonal therapy with aromatase inhibitor in advanced breast cancer. *Lijec Vjesn* 1998;120(10-11):315-318.
20. Torri V, Floriani I. Cyproterone acetate in the therapy of prostate carcinoma. *Arch Ital Urol Androl* 2005;77(3):157-163.
21. Chen WR, Adams RL, Carubelli R, Nordquist RE. Laser-photosensitizer assisted immunotherapy: a novel modality for cancer treatment. *Cancer Lett* 1997;115(1):25-30.
22. Chen WR, Adams RL, Higgins AK, Bartels KE, Nordquist RE. Photothermal effects on murine mammary tumors using indocyanine green and an 808-nm diode laser: an *in vivo* efficacy study. *Cancer Lett* 1996;98(2):169-173.

23. D'Cruz AK, Robinson MH, Biel MA. mTHPC-mediated photodynamic therapy in patients with advanced, incurable head and neck cancer: a multicenter study of 128 patients. *Head Neck* 2004;26(3):232-240.
24. Dolmans DE, Fukumura D, Jain RK. Photodynamic therapy for cancer. *Nat Rev Cancer* 2003;3(5):380-387.
25. Rosenberg SA. A new era for cancer immunotherapy based on the genes that encode cancer antigens. *Immunity* 1999;10(3):281-287.
26. Dranoff G. Cytokines in cancer pathogenesis and cancer therapy. *Nat Rev Cancer* 2004;4(1):11-22.
27. Kim-Schulze S, Taback B, Kaufman HL. *Surg Oncol Clin N Am* 2007;16(4):793-818, viii.
28. Weiner LM. An overview of monoclonal antibody therapy of cancer. *Semin Oncol* 1999;26(4 Suppl 12):41-50.
29. Harari PM. Epidermal growth factor receptor inhibition strategies in oncology. *Endocr Relat Cancer* 2004;11(4):689-708.
30. Waldmann TA. Immunotherapy: past, present and future. *Nat Med* 2003;9(3):269-277.
31. Gruber R, Holz E, Riethmüller G. Monoclonal antibodies in cancer therapy. Springer *Semin Immunopathol* 1996;18(2):243-251.
32. Sahoo SK, Labhasetwar V. Nanotech approaches to drug delivery and imaging. *Drug Discov Today* 2003;8:1112-1120.
33. Vasir JK, Reddy MK, Labhasetwar V. Nanosystems in drug targeting: opportunities and challenges. *Curr Nanosci* 2005;1:47-64.

34. Kipp JE. The role of solid nanoparticle technology in the parenteral delivery of poorly water-soluble drugs. *Int J Pharm* 2004;284:109-122.
35. Mosqueira VC, Legrand P, Gref R, Heurtault B, Appel M, Barratt G. Interactions between a macrophage cell line (J774A1) and surface-modified poly (D,L-lactide) nanocapsules bearing poly(ethylene glycol). *J Drug Target* 1999;7(1):65-78.
36. Gref R, Domb A, Quellec P, Blunck T, Muller RH, Verbavatz JM, Langer R. The controlled intravenous delivery of drugs using PEG-coated sterically stabilized nanospheres. *Adv Drug Deliv Rev* 1995;16(2):215-233.
37. Gref R, Luck M, Quellec P, Marchand M, Dellacherie E, Harnisch S, *et. al.* 'Stealth' corona-core nanoparticles surface modified by polyethylene glycol (PEG): influences of the corona (PEG chain length and surface density) and of the core composition on phagocytic uptake and plasma protein adsorption. *Colloids Surf. B: Biointerfaces* 2000;18(3-4):301-313.
38. Moghimi SM, Hunter AC, Murray JC (2005) Nanomedicine: current status and future prospects. *FASEB J* 19:311-330.
39. Guo W, Lee RL. Receptor-targeted gene delivery via folate-conjugated polyethylenimine. *AAPS PharmSci* 1999;1(4):E19.
40. van Steenis JH, van Maarseveen EM, Verbaan FJ, Verrijck R, Crommelin DJ, Storm G, *et al.* Preparation and characterization of folate-targeted pPEG-coated pDMAEMA-based polyplexes. *J Control Release* 2003;87(1-3):167-176.
41. Allen TM. Ligand-targeted therapeutics in anticancer therapy. *Nat Rev Cancer* 2002;2(10):750-763.

42. Black KC, Kirkpatrick ND, Troutman TS, Xu L, Vagner J, Gillies RJ, *et al.* Gold nanorods targeted to delta opioid receptor: plasmon-resonant contrast and photothermal agents. *Mol Imaging* 2008;7(1):50-57.
43. Lammers T, Hennink WE, Storm G. Tumour-targeted nanomedicines: principles and practice. *Br J Cancer* 2008;99(3):392-397.
44. Cho K, Wang X, Nie S, Chen ZG, Shin DM. Therapeutic nanoparticles for drug delivery in cancer. *Clin Cancer Res* 2008 Mar 1;14(5):1310-1316.
45. Santra S, Liesenfeld B, Dutta D, Chatel D, Batich CD, Tan W, *et al.* Folate conjugated fluorescent silica nanoparticles for labeling neoplastic cells. *J Nanosci Nanotechnol.* 2005;5(6):899-904.
46. Sahoo SK, Ma W, Labhasetwar V. Efficacy of transferrin-conjugated paclitaxel-loaded nanoparticles in a murine model of prostate cancer. *Int J Cancer* 2004;112(2):335-340.
47. Smith BR, Cheng Z, De A, Koh AL, Sinclair R, Gambhir SS. Real- Time Intravital Imaging of RGD-Quantum Dot Binding to Luminal Endothelium in Mouse Tumor Neovasculature. *Nano Lett* 2008;8(9):2599-2606.
48. Yih TC, Al-Fandi M. Engineered Nanoparticles as Precise Drug Delivery Systems. *J Cell Biochem* 2006;97(6):1184-1190.
49. Kirpotin DB, Drummond DC, Shao Y, Shalaby MR, Hong K, Nielsen UB, *et al.* Antibody targeting of long-circulating lipidic nanoparticles does not increase tumor localization but does increase internalization in animal models. *Cancer Res* 2006;66(13):6732-6740.
50. Park JW, Benz CC, Martin FJ. Future directions of liposome- and immunoliposome-based cancer therapeutics. *Semin Oncol* 2004;31(6 Suppl 13):196-205.

51. Shive MS, Anderson JM. Biodegradation and biocompatibility of PLA and PLGA microspheres. *Adv Drug Deliv Rev.* 1997;28(1):5-24.
52. Wang Y, Khaing ZZ, Li N, Hall B, Schmidt CE, Ellington AD. Aptamer Antagonists of Myelin-Derived Inhibitors Promote Axon Growth. *PLoS One* 2010;5(3):e9726.
53. Farokhzad OC, Jon S, Khademhosseini A, Tran TN, Lavan DA, Langer R. Nanoparticle-aptamer bioconjugates: a new approach for targeting prostate cancer cells. *Cancer Res* 2004;64:7668-72.
54. Vasir JK, Reddy MK, Labhasetwar V. Nanosystems in drug targeting: opportunities and challenges. *Curr Nanosci* 2005;1:47-64.
55. Brannon-Peppas L, Blanchette JO. Nanoparticle and targeted systems for cancer therapy. *Adv Drug Deliv Rev* 2004;56:1649-1659.
56. Cortez-Retamozo V, Backmann N, Senter PD, Wernery U, De Baetselier P, Muyldermans S, *et al.* Efficient cancer therapy with a nanobody-based conjugate. *Cancer Res* 2004;64:2853-2857.
57. Gillies ER, Frechet JM. Dendrimers and dendritic polymers in drug delivery. *Drug Discov Today* 2005;10:35-43.
58. Schiffelers RM, Ansari A, Xu J, Zhou Q, Tang Q, Storm G, *et al.* Cancer siRNA therapy by tumor selective delivery with ligandtargeted sterically stabilized nanoparticle. *Nucleic Acids Res* 2004;32:e149.
59. Illum L, Jabbal-Gill I, Hinchcliffe M, Fisher AN, Davis SS. Chitosan as a novel nasal delivery system for vaccines. *Adv Drug Deliv Rev* 2001;51(1-3):81-96.
60. S. Aiba. Molecular structures and properties of partially *N*-acetylated chitosans. In: Brine CJ, Sandford PA, Zikakis JP, editors. *Advances in Chitin and Chitosan*, London: Elsevier, 1992. p. 137-144.

61. Muzzarelli RAA. Chitosan. In: Belcher R, Freiser H, editors. Natural Chelating Polymers; Alginic acid, Chitin, and Chitosan. Oxford: Pergamon Press, 1973. p. 144–176.
62. Lee M, Lo AC, Cheung PT, Wong D, Chan BP. Drug carrier systems based on collagen-alginate composite structures for improving the performance of GDNF-secreting HEK293 cells. *Biomaterials*. 2009; 30(6):1214-1221.
63. O'Neal DP, Hirsch LR, Halas NJ, Payne JD, West JL. Photo-thermal tumor ablation in mice using near infrared-absorbing nanoparticles. *Cancer Lett* 2004;209(2):171-176.
64. Hainfeld JF, Dilmanian FA, Slatkin DN, Smilowitz HM. Radiotherapy enhancement with gold nanoparticles. *J Pharm Pharmacol* 2008;60(8):977-985.
65. Roa W, Zhang X, Guo L, Shaw A, Hu X, Xiong Y, *et al*. Gold nanoparticle sensitize radiotherapy of prostate cancer cells by regulation of the cell cycle. *Nanotechnology*;20(37):375101.
66. Chang MY, Shiau AL, Chen YH, Chang CJ, Chen HH, Wu CL. Increased apoptotic potential and dose-enhancing effect of gold nanoparticles in combination with single-dose clinical electron beams on tumor-bearing mice. *Cancer Sci*. 2008;99(7):1479-1484.
67. Bair FE, editor. *Cancer Sourcebook: Basic Information on Cancer Types, Symptoms, Diagnostic Methods, and Treatments, Including Statistics on Cancer Occurrences World (Health Reference Series), Vol. 1*, Omnigraphics, 1990.
68. Nakamura RM, Grody WW, Wu JT, Nagle RB, editors. *Cancer diagnostics, current and future trend*, Humana Press, Inc., 2004.

69. Young H, Baum R, Cremerius U, Herholz K, Hoekstra O, Lammertsma AA, *et al.* Measurement of clinical and subclinical tumour response using [18F]-fluorodeoxyglucose and positron emission tomography: review and 1999 EORTC recommendations. *Eur J Cancer* 1999;35(13):1773–1782.
70. Postema M, Schmitz G. Bubble dynamics involved in ultrasonic imaging. *Expert Rev Mol Diagn* 2006;6(3):493-502.
71. Overvelde M, Vos HJ, de Jong N, Versluis M. Ultrasound Contrast Agent Microbubble Dynamics. In: Paradossi G, Pellegretti P, Trucco A, editors. *Ultrasound Contrast Agents: Targeting and Processing Methods for Theranostics*. Milan: Springer-verlag, 2010. pp. 79-97.
72. Roulston JE, John MS, editors. *Molecular Diagnosis of Cancer Methods and Protocols*, 2nd ed. Humana Press, Inc., 2004.
73. Eleftherios, PD. Proteomic Patterns in Biological Fluids: Do They Represent the Future of Cancer Diagnostics? *Clin Chem* 2003;49(8):1272-1275.
74. Balmain A, Gray J, Ponder B. The genetics and genomics of cancer. *Nat Genet* 2003;33 Suppl:238-244.
75. Sokolov K, Aaron J, Hsu B, Nida D, Gillenwater A, Follen M, *et at.* Optical systems for in vivo molecular imaging of cancer. *Technol Cancer Res Treat* 2003;2(6):491-504.
76. Mulder WJ, Griffioen AW, Strijkers GJ, Cormode DP, Nicolay K, Fayad ZA. Magnetic and fluorescent nanoparticles for multimodality imaging. *Nanomedicine (Lond)* 2007;2(3):307-324.

77. Graves EE, Ripoll J, Weissleder R, Ntziachristos V. A submillimeter resolution fluorescence molecular imaging system for small animal imaging *Med Phys* 2003;30(5):901-911.
78. Sharma P, Brown SC, Bengtsson N, Zhang Q, Walter GA, Grobmyer SR, *et al.* Gold-speckled multimodal nanoparticles for noninvasive bioimaging. *Chem Mater* 2008;20(19):6087-6094.
79. Chan WC, Maxwell DJ, Gao X, Bailey RE, Han M, Nie S. Luminescent quantum dots for multiplexed biological detection and imaging. *Curr Opin Biotechnol* 2002;13: 40–46.
80. Santra S, Yang H, Holloway PH, Stanley JT, Mericle RA. Synthesis of water-dispersible fluorescent, radio-opaque, and paramagnetic CdS: Mn/ZnS quantum dots: a multifunctional probe for bioimaging. *J Am Chem Soc* 2005;127(6):1656–1657.
81. Oishi J, Asami Y, Mori T, Kang JH, Niidome T, Katayama Y. Colorimetric enzymatic activity assay based on noncrosslinking aggregation of gold nanoparticles induced by adsorption of substrate peptides. *Biomacromolecules* 2008;9(9):2301-2308.
82. Shim SY, Woo JR, Nam EJ, Hong HJ, Inhee MJ, Kim YH, Nam JM. Stepwise silver-staining-based immunosorbent assay for amyloid- $\beta$  autoantibody detection. *Nanomedicine* 2008;3(4):485-493.
83. Hwang K S, Lee S-M, Kim S K, Lee J H, Kim T S. Micro- and Nanocantilever Devices and Systems for Biomolecule Detection. *Annu Rev Anal Chem (Palo Alto Calif)* 2009;2:77-98.
84. Hunter AC. Application of the quartz crystal microbalance to nanomedicine. *J Biomed Nanotechnol* 2009;5(6):669-675.

85. Zheng G, Patolsky F, Cui Y, Wang WU, Lieber CM. Multiplexed electrical detection of cancer markers with nanowire sensor arrays. *Nat Biotechnol.* 2005;23(10):1294-1301.
86. Nam JM, Stoeva SI, Mirkin CA. Bio-bar-code-based DNA detection with PCR-like sensitivity. *J Am Chem Soc* 2004;126(19):5932-5933.
87. Goluch ED, Nam JM, Georganopoulou DG, Chiesl TN, Shaikh KA, Ryu KS, *et al.* A bio-barcode assay for on-chip attomolar-sensitivity protein detection. *Lab Chip* 2006;6(10):1293-1299.
88. Tanaka T, Mangala LS, Vivas-Mejia PE, Nieves-Alicea R, Mann AP, Mora E, *et al.* Sustained small interfering RNA delivery by mesoporous silicon particles. *Cancer Res* 2010;70(9):3687-3696.

---

**Part 1:**

**The target specific polyion coated  
nanogold based approach**

## **1. A brief overview**

When the size of a material is reduced to the nanometric range the properties change completely with respect to the bulk material or even molecules in an unpredictable way. In metals for example the surface properties become dominant and give nanoparticles some new properties [1, 2]. A nanoparticle is here defined as a sub-microscopic particle with the dimension less than 100nm. The radiative properties of noble metal nanoparticles (like gold, silver and copper) is greatly enhance if interacting with resonant electromagnetic radiation due to the coherent collective oscillation of electrons in the conduction band induces large surface electric fields [3]. This enhances both the absorption and light scattering by orders of magnitude properties as compared to strong absorbing molecules [4] or the fluorescence of fluorophores, respectively [5]. These unique properties of noble metal nanoparticles provide a great potential to be used in applications, such as biochemical sensors [6], biological imaging and medical therapeutics [6-12] as well as catalysts because of their high surface-to-volume ratios [13, 14].

In case of polymeric nanoparticles consisting of drug molecules precipitated by polyelectrolytes or neutral polymers it was observed that they have additional therapeutic capabilities like inhibiting the multi drug resistance in cancer cells. This observation has led to the development of a novel field of science, polymer genomics [15].

In the following sections, the properties of the main compounds (polyelectrolytes as multifunctional tool, nanogold as core and for possible imaging purposes, and targeting moieties to allow guided delivery to cancer cells) for the fabrication of the newly developed nano drugs and delivery systems in the frame of my PhD will be described in more detail.

## **2. Nanotechnology in cancer applications**

Nanoparticles and nanocapsules has opened a new arena in the field of cancer therapy because of its unique properties such as the small size, controlled release of drugs and reduced toxic side-effects [2, 5, 16-24]. Metallic nanostructures demonstrate unique electronic, photonic, catalytic as a consequence of the size reduction from bulk material to the nanoscale [2, 25-29]. These nanoparticles exhibit similar size ranges as many biomolecules, such as proteins and DNA, and thus offer great possibilities for the integration of nanotechnology into biotechnology. Typical applications comprise contrast agents for disease diagnostics and therapies [30-60], developing homogenous and highly sensitive immuno-assay [34-36] and assembling new materials [37, 38].

### **2.1. Polymeric nanodrugs**

The nanotherapeutics has drawn the attention of world from researcher to companies. The first nanodrug to be approved by FDA was Abraxis BioScience's Abraxane, for metastatic breast cancer treatment, in 2005 [39]. From then onward, there is no turning back and now there are several in the list of FDA (table 1-1) [40, 41]. With the introduction of nanodrug, the whole medicinal world is now aging to a new era of drug development. The whole concept of drug formulation from characteristics, bioavailability, pharmacokinetics, stability, drug use, and toxicity has to be reconsidered. It is predicted that better understanding and application of nanotechnology will ensure the effective drug delivery which would ultimately enhance the efficacy of treatment and patient drug use compliance [39].

Table 1-1. FDA approved nano-drug delivery systems in the market [40].

Type of nanostructure	Trade name	Active ingredient	Indication	Company
Polymeric nanoparticles	Adagen	Adenosine deaminase	Adenosine deaminase (ADA) enzyme deficiency	Enzon Pharmaceuticals Inc., Bridgewater, NJ, USA
	Onscaspar	L-asparaginase	Acute lymphoblastic leukaemia	Enzon Pharmaceuticals Inc., NJ, USA
	Copaxone	Glatiramer Acetate	Relapsing-remitting multiple sclerosis	Teva Pharmaceuticals, Tikva, Isreal
	Macugen	Pegaptanib Sodium	All types of neovascular age-related macular degeneration	Nektar Therapeutics, San Carlos, CA, USA; OSI Pharmaceuticals, Melville, NY, USA
	Pegasys	Pegylated interferon alfa-2a	Hepatitis C	Nektar Therapeutics, CA, USA
	Neulasta	Pegfilgrastim	Neutopenia	Nektar Therapeutics, CA, USA; Amgen Inc, Thousand Oaks, CA, USA
	PEG-INTRON	Peginterferon alfa-2b	Hepatitis C	Nektar therapeutics, CA, USA
	Somavert	Pegvisomant	Acromegaly	Nektar therapeutics, CA, USA
	Liposomes	Abelcet	Amphotericin B	Fungal infections
Depocyt		Cytarabine	Lymphomatous meningitis	Enzon Pharmaceuticals Inc., NJ, USA
Liposomes	AmBisome	Amphotericin B	Fungal infections	Gilead Sciences Inc., Foster City, CA, USA
	Daunoxome	Daunorubicin	Kaposi's sarcoma	Gilead Sciences Inc., CA, USA
	Myocet	Doxorubicin	Advanced breast cancer	Zeneus/Cephalon, Inc., Frazer, PA, USA
	Epaxal	Inactivated Hepatitis A virus	Hepatitis A	Berna Biotech, Bern, Switzerland
	Inflexal V	Inactivated influenza surface antigen	Influenza	Berna Biotech, Bern, Switzerland
	DepoDur	Morphine	Analgesia	EKR Therapeutics, Bedminster, NJ, USA
	Visudyne	Verteporfin	Age-related macular degeneration	QLT Inc., Vancouver, British Colombia, Canada; Novartis, Basel, Switzerland
	Doxil	Doxorubicin	Ovarian cancer and Kaposi's sarcoma	Ortho Biotech, Bridgewater, NJ, USA
	Caelyx	Doxorubicin	Ovarian cancer, Kaposi's sarcoma & breast cancer	Schering-Plough, Kenilworth, NJ, USA
	Estrasorb	Estradiol	Menopausal – Hot flushes	Novavax, Rockville, MD, USA
Liposomes	Survanta	Beractant (bovine lung homogenate)	Respiratory distress syndrome	Abbott Laboratories, IL, USA
	Alveofact	Bovactant(bovine lung lavage)	Respiratory distress syndrome	Boehringer Ingelheim GmbH, Ingelheim, Germany
	Curosurf	Poractant alfa (porcine lung homogenate)	Respiratory distress syndrome	Chiesi Farmaceutici SpA, Parma, Italy

## 2.2. Polymer coated nanoparticles in drug delivery

The use of nanoparticles, polymeric or metallic, is an attractive novel vehicle for drug delivery because their small size allows for intravenous administration and the surface makes them suitable for multifunctional coatings. Especially polymer multilayer coating on

nanoparticles has several advantages such as easy incorporation of drugs within the layers on

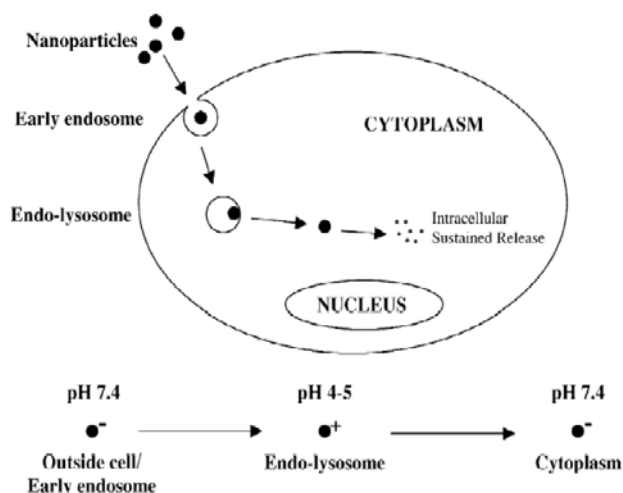


*Fig. 1-1. Intracellular trafficking of nanoparticles. Following their uptake by the cell, nanoparticles were transported through early endosomes to the sorting endosomes. A fraction of nanoparticles recycle back to the cell exterior while another fraction is transported to secondary endosomes/lysosomes from where nanoparticles escape into the cytoplasm. Nanoparticles that escape into the cytoplasm could act as intracellular reservoirs for sustained release of the encapsulated therapeutic agent [44].*

cancer cells when conjugated to targeting molecule and then release the drugs to the cancer [45].

the nanoparticles, the ability to stabilize the drugs in vivo and decreased toxicity of the incorporated drug molecules [42, 43]. Fig 1-1 [44] depicts a common way of the drug delivery into cells and the later releasing to target. Polymer can also be functionalized with cancer marker targeting molecules as other nanoparticles. Accordingly, the polymer can specifically target the

### 2.3. Layer-by-Layer Deposition of Polyelectrolyte multilayer on gold nanoparticles

The Layer-by-layer (LbL) technique basically develops non-covalently bound ultra-thin multilayered capsules of organic compounds such as polyelectrolytes, multilayer films which are formed by the consecutive electrostatic adsorption of oppositely charged polyions [46-49]. Popularity of this technique is due to the ability to create highly tailored polymer thin matrices with a nearly unlimited range of functional groups and to incorporate via electrostatic but also via hydrophobic interaction a drug molecule which facilitates the release compared to covalent binding. Moreover the polymers can explore therapeutic properties by themselves increasing the potency of nanoparticulated polymeric drug systems.

To enhance stability, biocompatibility and affinity of the capsules, a variety of materials such as bio-polymers, proteins, DNA, lipids, synthetic polyelectrolytes, multivalent dyes and magnetic nanoparticles have been used to fabricate and design the shell [50, 51]. A schematic presentation in fig. 1-2, explains the different types of interactions involved in between the polyionic layers within the capsule which determines the final structure of the polyion multilayer thin film [52]. Moreover, other short range forces (like van der Waals force and hydrogen bonding) also play a significant role in determining the film thickness, the final morphology of the film, the surface properties, and in some cases, can determine the stability of multi-layers [52].

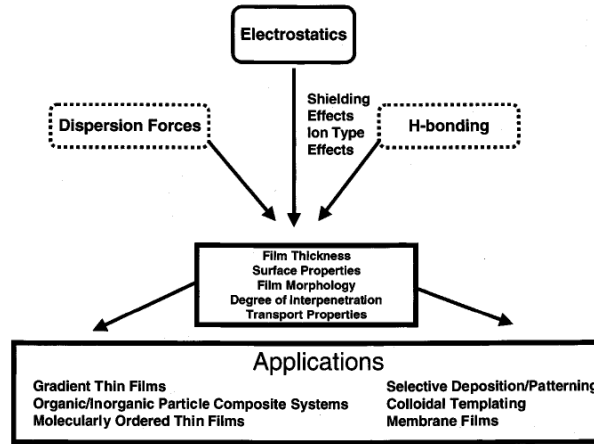


Figure 1-2. A schematic representation of forces involved in layer-by-layer film growth following the applications achieved by controlling or manipulating these interactions with processing [52].

The electrostatic interaction is the key interaction between the polyions. The understanding of these interactions has helped in the development of new ordered systems like 3-dimensional polymer structures and

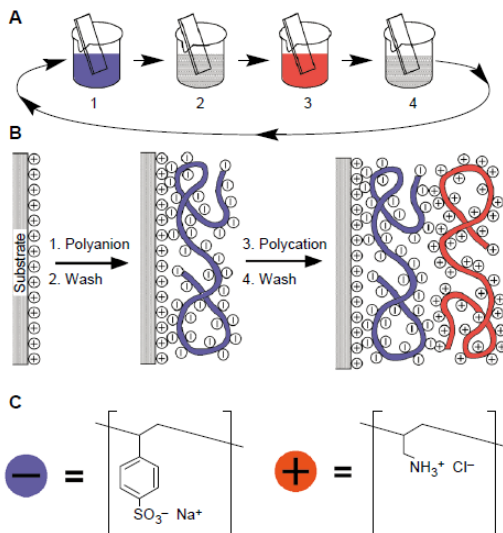
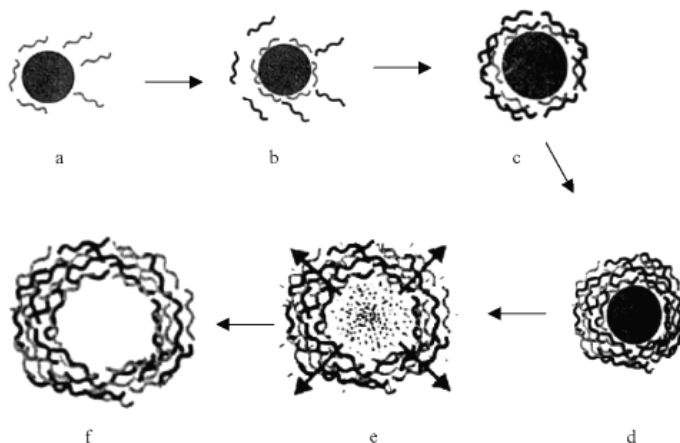


Figure 1-3. (A) Schematic of the film deposition process using slides and beakers. Steps 1 and 3 represent the adsorption of a polyanion and polycation, respectively, and steps 2 and 4 are washing steps. The four steps are the basic buildup sequence for the simplest film architecture, (A/B). The construction of more complex film architectures requires only additional beakers and a different deposition sequence. (B) Simplified molecular picture of the first two adsorption steps, depicting film deposition starting with a positively charged substrate. Counterions are omitted for clarity. The polyion conformation and layer interpenetration are an idealization of the surface charge reversal with each adsorption step. (C) Chemical structures of two typical polyions, the sodium salt of poly(styrene sulfonate) and poly(allylamine hydrochloride) [53].

patterns, selective membranes, and a range of functional organic and organic-inorganic hybrid composite thin films [52]. Fig. 1-3 schematically outlined, the LbL multilayer growth composed of polyions or other charged molecular or colloidal objects (or both) [53]. With the same principle, multilayers are prepared on colloids and on objects with dimensions of several tens of centimetres or

meters (fig 1-4) [54]. The foremost advantages of the LbL adsorption from solution are that many different materials can be integrated in between the multilayer films and that the possible layer architectures could



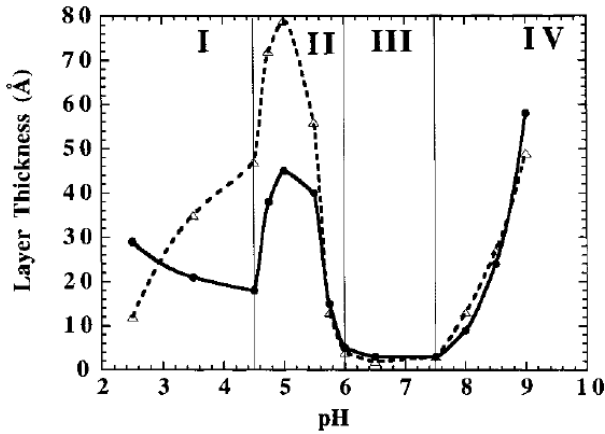
*Fig. 1-4. Schematic illustration of the polyelectrolyte deposition process and of subsequent core decomposition, as a) core attacked by polyelectrolytes; b) coating of charged polyelectrolytes on core; c) coating of alternative charged polyelectrolyte; d) core with well-deposited polyelectrolyte coated layers; e) process of core decomposition and removal from coated polyelectrolyte shells and f) Core removed hollow capsules [54].*

be completely determined in the

deposition sequence. The most remarkable examples of multi-composite shell include proteins [55-56], clay platelets [50, 55, 57-60], virus particles [61], and gold colloids [62, 63].

### 2.3.1. Interactions between polyelectrolytes in LbL deposition

The Influence of small ions on strong polyelectrolytes and their interaction with the oppositely charged polyion is quite limited. However, in case of weak polyelectrolyte, the layer thickness and its stability could be varied by the ionic strength or pH of the polyelectrolyte solution before deposition [64]. This is due to the fact that the varying pH condition affects the charge density on the polyelectrolyte (fig. 1-5) [65]. Accordingly, by



changing the ionic strength of a weak polyelectrolyte solution capsule parameters like layer thickness and permeability can be tuned.

Figure 1-5. The average incremental layer thickness contributed by weak polyelectrolytes (i.e. PAA and PAH) adsorbed layer as function of solution pH, over the pH range 2.5-9.0. Both the polyelectrolyte, dipping solutions in this case were at the same pH. Solid line represents the PAA (polyanion) layer thickness, and the dashed line is the PAH (polycation) layer thickness [65].

### 2.3.2. The Zone Model for LbL multilayer film growth

The multilayer growth of two simple cationic or anionic homopolyelectrolyte can be divided in 3 distinct zones. Zone I, also considered as charged zone, comprise the first one or few layers close to the template. The polyelectrolytes in this zone are highly influenced by the charge of the template; while oppositely charge polyions are attracted the likewise charged polyions are repulsed. Zone II is considered as “bulk” or neutral, in this zone the multilayers are not influenced by the environment due to protection from the zone I and II. Zone III is also charged as zone I. Polyelectrolytes of this zone are influenced by the surrounding medium (i.e. solution or air) to which they present the interface (fig. 1-6) [66]. The zonal distribution pattern illustrates that the Zone II, is the most suitable region for uploading drug or other molecules of interest.

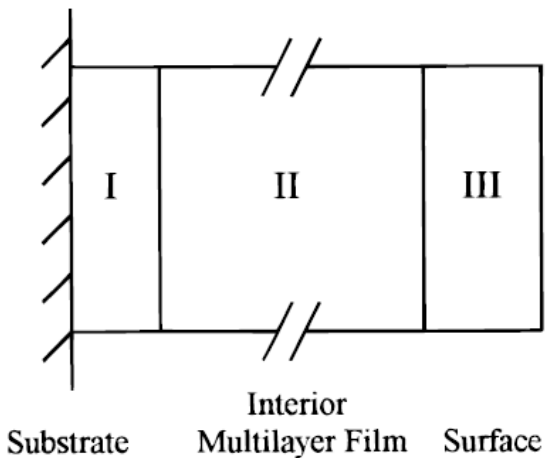


Figure 1-6. Schematic representation of a multilayer. Multilayer films can be subdivided into three regions: I, II, and III. It should be noted that the transitions between regions I and II and between II and III are gradual and not as sharp as schematically depicted here [66].

## 2.4. Important properties of gold nanoparticles

In the present work, gold nanoparticles are used as the core for LbL polymer deposition due to its unique properties which may be eventually utilized for diagnostics as well as therapy for cancer in the future.

### 2.4.1. Light absorption by gold nanoparticles

Gold nanoparticles show a strong absorption band in the visible region due to plasmon

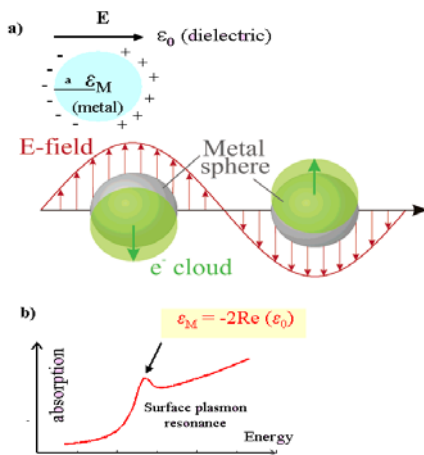


Figure 1-7. a) A scheme of surface plasmon absorption of spherical nanoparticles, showing the displacement of the conduction electron charge cloud relative to the nuclei -dipole surface plasmon oscillation [68]. b) A typical surface plasmon absorption spectrum of spherical nanoparticles.

resonance. Metallic nanoparticles of sub-wavelength size in an oscillating electromagnetic field, leads to field amplification, both inside and in the near-field zone out-side the particle called localized plasmon resonance [67]. As a consequence, nanoparticles exhibit bright colours both in transmitted and reflected light due to resonance enhanced absorption and scattering. The surface plasmon absorption occurs due to the dipole oscillations of the free electrons with respect to the ionic core of the spherical nanoparticles

[25]. A net charge difference is shown on the nanoparticle surface when an interaction with an electric field results in a polarization of the electrons with respect to the ionic core of a nanoparticle (see fig 1-7) [68]. The polarizability  $\alpha$ , of a small metallic sphere of sub-wavelength diameter in electrostatic approximation is given by

$$\alpha = 4\pi a^3 \frac{\epsilon_M - \epsilon_0}{\epsilon_M + 2\epsilon_0} \quad (1.1)$$

Where 'a' is the radius of the particle;  $\epsilon_M$  and  $\epsilon_0$ , are the isotropic and non-absorbing medium's dielectric constant and dielectric response on nanoparticles surface, respectively.

This induces a dipolar oscillation of all the electrons in the same phase. The frequency of the electromagnetic field becomes resonant with the coherent electron motion and is designated as  $\epsilon_M = -2\text{Re}(\epsilon_0)$ . This relationship is called Fröhlich condition and

associated mode (in an oscillating field) is referred to as, the *dipole surface plasmon* of metal nanoparticles. A strong absorption

band of gold nanoparticles at around 520nm in the spectrum of (Fig 1-8), is the source of the observed brilliant red color of gold nanoparticles in solution.

Mie (1908) explained first the surface plasmon resonance behavior of spherical metal nanoparticles [69]. He solved Maxwell's equation for an electromagnetic light wave interacting with a small metallic sphere. His theory found a wide applicability as it allows the calculation of particle extinction spectra, when the material dielectric function is known and the size is smaller than the wavelength of the light [67]. For nanoparticles much smaller than the wavelength of light (<20nm), only the dipole oscillation contributes significantly to the extinction cross section and therefore Mie's theory is reduced to the following equation:

$$C_{ext} = 9 \frac{\omega}{c} V \frac{\epsilon}{[\epsilon_1 + 2\epsilon_0]^2 + \epsilon_2^2} \quad (1.2)$$

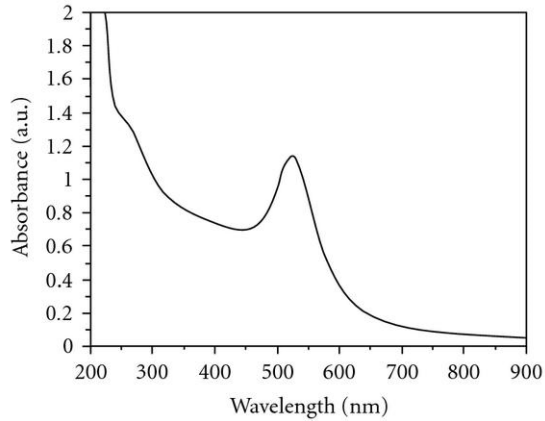


Fig. 1-8. Surface plasmon absorption spectrum of 15nm gold nanoparticles. A strong absorption band, around 520 nm in the spectrum, is the origin of the observed red color of the nanoparticles solution.

Where  $V$  is the particle volume,  $\omega$  is the angular frequency of the exciting light,  $c$  is the speed of light, and  $\epsilon_0$  and  $\epsilon = \epsilon_1 + i \epsilon_2$ , are the dielectric functions of the surrounding medium and the material itself respectively. The resonance condition is fulfilled when  $\epsilon_1(\omega) = -2\epsilon_0$  if  $\epsilon_2$  is small or weakly dependent on  $\omega$  [70]. The plasmon bandwidth mainly depends on  $\epsilon_2(\omega)$ . For bigger nanoparticles, the light is not able to polarize the nanoparticles homogeneously and the retardation effect leads to the excitation of higher-order modes [2]. From equation (1.2), it can be seen that the peak intensity and position of the surface plasmon absorption

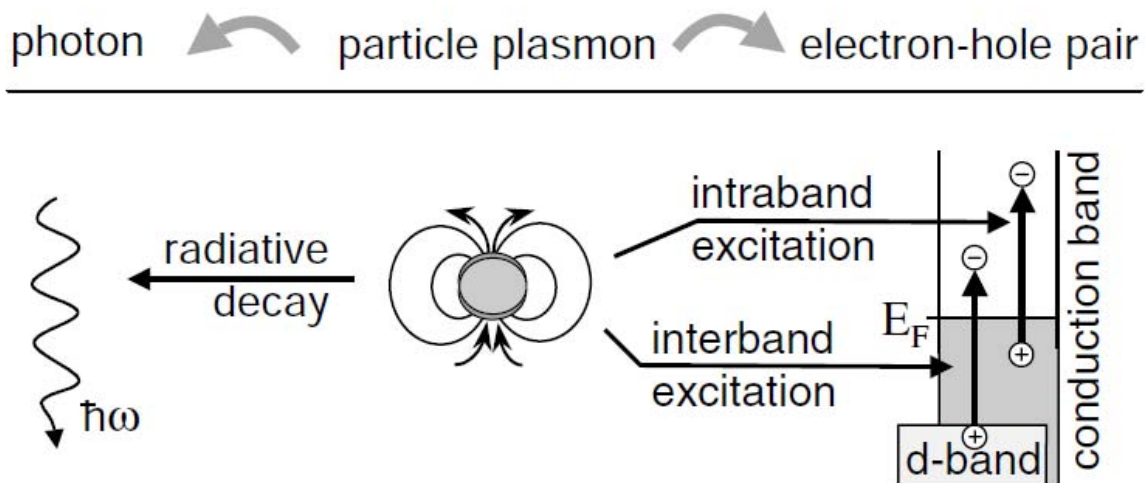


Figure 1-9. Schematic representation of radiative (left) and nonradiative (right) decay of particle plasmons in noble-metal nanoparticles. The nonradiative decay occurs via excitation of electron-hole pairs either within the conduction band (intraband excitation) or between the d band and the conduction band (interband excitation) [71].

band is dependent on the size and shape of the metal nanoparticles as well as the dielectric constant of the metals and the medium surrounding the particles [2]. The plasmon resonance of particles beyond the quasi-static regime ( $a > 10\text{nm}$ ) is damped by two competing processes

(fig. 1-9) [71]: a radiative decay process into photons, dominating for larger particles, and a non-radiative process due to absorption. The non-radiative decay is mainly due to the creation of electron-hole pairs through either intraband excitations within the conduction band or by the interband transitions from lower-lying d-bands to the sp conduction band (for noble metal particles). Due to the above reason, as the size increases, the absorption maximum shows a red shift (See fig. 1-10, part a) [69]. The bandwidth also changes when the

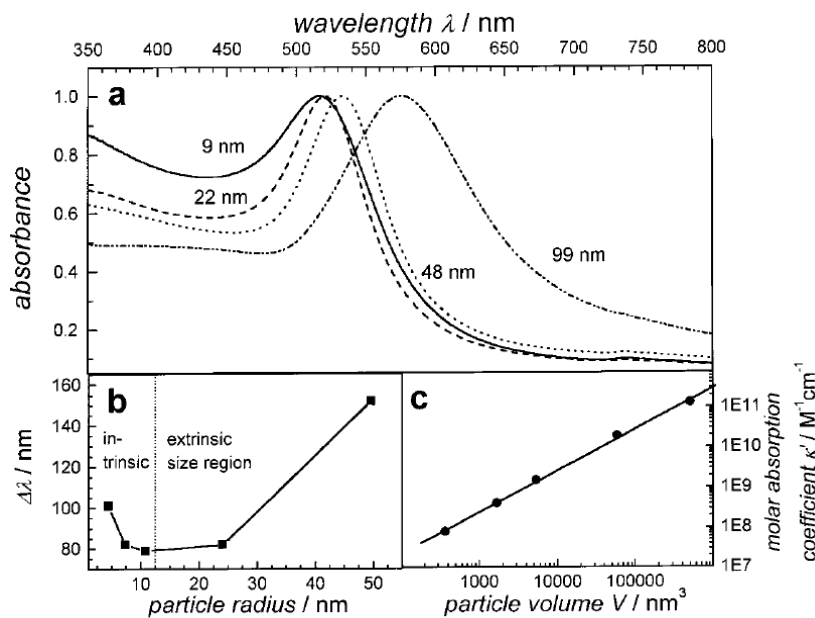


Figure 1-10. Size effects on the surface plasmon absorption of spherical gold nanoparticles. The UV-vis absorption spectra of colloidal solutions of gold nanoparticles with diameters varying between 9 and 99 nm show that the absorption maximum red-shifts with increasing particle size in part a, while the plasmon bandwidth follows the behavior illustrated in part b. The bandwidth increases with decreasing nanoparticle radius in the intrinsic size region and also with increasing radius in the extrinsic size region, as predicted by theory. In part c the extinction coefficients of these gold nanoparticles at their respective plasmon absorption maxima are plotted against their volume on a double logarithmic scale. The solid line is a linear fit of the data points, illustrating that a linear dependence is observed, in agreement with the Mie theory [69].

size changes. Link and El-Sayed [4] have shown that the bandwidth decreases with the increase of the nanoparticle size when the nanoparticles are less than 20nm in diameter (Fig 1-10, part b) and the bandwidth increases with the increase of the nanoparticle size, when the nanoparticles are larger than 20nm.

It has been a well established fact that the bandwidth is inversely proportional to the radius ‘a’ of the particle for sizes smaller than ~20 nm [69]. It has also been observed that the

absorption coefficient is linearly dependent upon the volume of the nanoparticles which is in agreement with the Mie-theory (Fig 1-10, part c) [69].

The strong surface plasmon absorption property of gold nanoparticles offers a great potential in photo-thermal therapeutic applications. It is seen that the strong absorbed radiation is converted efficiently into heat on a picosecond time domain, due to electron-phonon and phonon-phonon processes [72]. Thus, upon the laser irradiation at the surface plasmon absorption band, the nanoparticles absorb photon energy and then immediately transfer into heat energy. If the nanoparticles are incorporated or incubated with biomolecules, cells or tissues, this heat energy will cause the sharp increase on the local temperature around the nanoparticles and thus cause the damage of the surrounding materials. This photo-thermal destructive effect can be used as a therapy for cancer.

The higher optical cross-sections of the gold nanospheres i.e. of 3-4 orders of magnitude as compared to those of conventionally used dyes, has made gold nanoparticles a good candidate for photo-thermal therapy. For instance, El-Sayed *et al.* [73] and Huang *et al.* [74] have successfully used gold nanospheres for laser photo-thermal destruction of cancer cells with molar absorption coefficient  $\epsilon$  of  $7.66 \times 10^9 \text{M}^{-1}\text{cm}^{-1}$ ) at a plasmon resonance wavelength maximum at 528nm. The  $\epsilon$ -value of the nanoparticle is 5 orders of magnitude larger than the molar extinction coefficient for indocyanine green ( $\epsilon = 1.08 \times 10^4 \text{M}^{-1}\text{cm}^{-1}$  at 778nm [2]), a Near-Infrared (NIR) dye commonly used in laser photothermal tumor therapy. For treating cancer, gold nanoparticles provide a novel class of photo-absorber in medical applications. In comparison to the strongly absorbing Eosin Y ( $\epsilon = 1.12 \times 10^5 \text{M}^{-1}\text{cm}^{-1}$  at 524nm [75]) dye, gold nanoparticles absorb about  $10^2$  stronger (for nanospheres of 15nm in diameter,  $\epsilon = 8.1 \times 10^7 \text{M}^{-1}\text{cm}^{-1}$  at 520nm [2]). Thus, strong plasmon resonance properties make gold nanoparticles a strong probe for photo-thermal therapy (PTT).

### 2.4.2. Light scattering of gold nanoparticles

Gold colloidal nanoparticles are responsible for the brilliant red and yellow colors in stained glass windows. Gold nanoparticle suspensions scatter colored light when illuminated by a beam of white light [76].

It is well-known that the plasmon resonance of metal nanoparticles is strongly sensitive to the nanoparticle size, shape, and the dielectric properties of the surrounding medium. The light-scattering gold nanoparticle suspensions

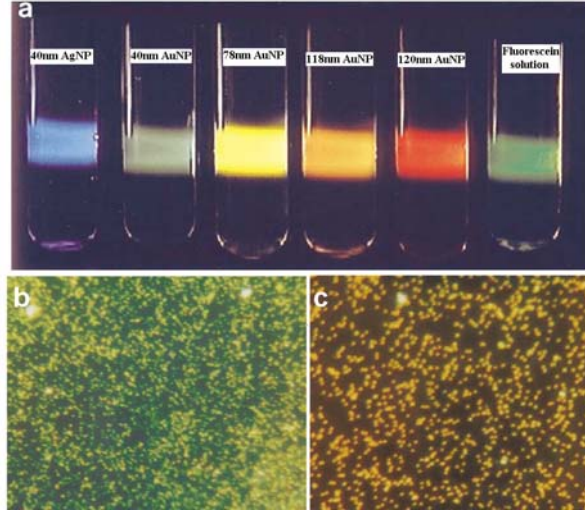


Figure 1-11. (a) Photograph showing the appearance of light-scattering suspensions of silver and gold particles and a solution of fluorescein when illuminated by a narrow beam of white light. Composition, particle diameter, and particle molar concentration are as follows from left to right: silver, 40 nm ( $2 \times 10^{-12}$  M); gold, 40 nm ( $1.3 \times 10^{-11}$  M), 78 nm ( $1.7 \times 10^{-12}$  M), 118 nm ( $5 \times 10^{-13}$  M), and 140 nm ( $3 \times 10^{-13}$  M); Solution of fluorescein ( $2 \times 10^{-6}$  M). Light microscopic image of (b) 58-nm and (c) 78-nm diameter gold particles as seen in under light microscope system and modified for detecting light scattering particles (60 $\times$  objective and  $\times 10$  eyepiece) [5].

have the same appearance as fluorescent solutions as shown in Fig 1-11 [5].

Yguerabide and Yguerabide [5] presented the theory of the light-scattering properties. The light scattering intensity is described by equation (1.3)

$$I = \frac{16 \pi^4 a^6 n_{med}^4 I_0}{r^2 \lambda_0^4} \left| \frac{m^2 - 1}{m^2 + 2} \right|^2 \sin^2(\alpha) \quad (1.3)$$

where spherical nanoparticle with radius ‘a’ is much smaller than the wavelength  $\lambda_0$  of the incident beam is given by the Rayleigh expression, which depends upon the detection

direction of the scattered light [77]. The light-scattering power of the nanoparticle is expressed in terms of the light-scattering cross section defined by the expression (1.4)

$$C_{sca} = \frac{128 \pi^5 a^6 n_{med}^4}{3 \lambda_0^4} \left| \frac{m^2 - 1}{m^2 + 2} \right|^2 \quad (1.4)$$

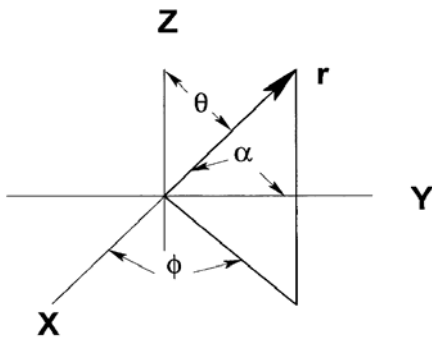


Fig. 1-12. Coordinate systems for describing the geometrical arrangement of the illuminating and detecting systems. A light-scattering suspension is at the origin of the coordinate system. A monochromatic light beam travels along the z axis and is polarized along the y direction. The direction  $r$  for detection of scattered light is described by the spherical coordinates,  $\theta$  and  $\Phi$ .  $\alpha$  is the angle between  $r$  and direction of polarization  $y$  of the incident beam [6]

where ‘ $a$ ’ is the particle radius,  $n_{med}$  is the refractive index of the medium surrounding the particle,  $I_0$  is the intensity of the incident monochromatic light,  $m$  is the relative refractive index of the bulk particle material,  $\alpha$  is the angle between the detection direction  $r$  and the incident beam,  $\lambda_0$  is the wavelength of the incident beam (Fig 1-12) [6].

From equations 1.4 and 1.5, it can be seen that the light scattering power is proportional to the sixth power of the particle radius. Fig 1-13 [6] shows the

normalized light scattering profile of the gold nanospheres in different sizes and Table 1-2 [6]

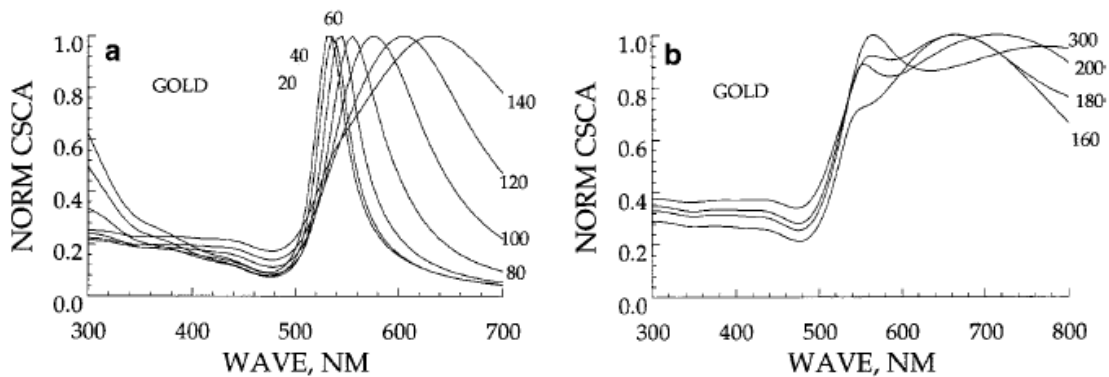


Fig. 1-13. Calculated light scattering cross section vs wavelength for homogeneous, spherical gold particles with different diameters [6].

shows the relative strength of the light scattering of these particles. Therefore, the strength and the light scattering profile can be tuned by changing the size of the nanoparticles.

Table 1-2. Calculated light absorption and scattering properties for gold particles of different Sizes [6].

Dia (nm)	$\lambda_{\text{max}}$ (nm) <sup>a</sup>	$C_{\text{sca}}$ (cm <sup>2</sup> )	$I_{\text{U}}(0)$	$I_{\text{U}}(90)$	$\epsilon$ (M <sup>-1</sup> cm <sup>-1</sup> )	$\varphi_{\text{s}}$	$Q_{\text{sca}}$
20	535	$8.36 \times 10^{-14}$	1.77	0.882	$1.57 \times 10^9$	0.014	0.027
40	535	$6.05 \times 10^{-12}$	129	63.9	$1.63 \times 10^{10}$	0.1	0.482
60	545	$6.33 \times 10^{-11}$	$1.35 \times 10^3$	668	$5.32 \times 10^{10}$	0.313	2.24
80	555	$2.31 \times 10^{-10}$	$4.97 \times 10^3$	$2.44 \times 10^3$	$1.14 \times 10^{11}$	0.546	4.6
100	575	$4.56 \times 10^{-10}$	$9.84 \times 10^3$	$4.83 \times 10^3$	$1.62 \times 10^{11}$	0.739	5.81
120	605	$6.9 \times 10^{-10}$	$1.48 \times 10^4$	$7.32 \times 10^3$	$2.07 \times 10^{11}$	0.876	6.1
140	635 <sup>b</sup>	$8.79 \times 10^{-10}$	$1.89 \times 10^4$	$9.4 \times 10^4$	$2.46 \times 10^{11}$	0.94	5.71
160	665	$1.02 \times 10^{-9}$	$2.22 \times 10^4$	$1.11 \times 10^4$	$2.8 \times 10^{11}$	0.963	5.09
180	560	$1.16 \times 10^{-9}$	$2.5 \times 10^4$	$1.27 \times 10^4$	$3.14 \times 10^{11}$	0.974	4.56
200	565	$1.38 \times 10^{-9}$	$7.53 \times 10^4$	$1.86 \times 10^4$	$4.51 \times 10^{11}$	0.788	4.39
300	565	$2.94 \times 10^{-9}$	$1.7 \times 10^5$	$3.82 \times 10^4$	$7.98 \times 10^{11}$	0.968	4.16

<sup>a</sup> Wavelength of the maximum peak of the scattering cross section vs wavelength graph in the wavelength range 380–700 nm. Entries in all columns of the same row are for the maximum peak wavelength.

<sup>b</sup> For diameters greater than 140 nm, two peaks appear in the light scattering spectrum. Data are tabulated at the wavelength of the most intense peak.

Note.  $C_{\text{sca}}$ , Light-scattering cross section.  $I_{\text{U}}(0)$  and  $I_{\text{U}}(90)$ , Scattered light intensities measured at 0 (forward) and 90° with respect to the direction of an unpolarized incident light beam.  $\epsilon$ (M<sup>-1</sup> cm<sup>-1</sup>), Molar decadic extinction coefficient.  $\varphi_{\text{s}}$ , Light-scattering yield.  $Q_{\text{sca}}$ , Scattering efficiency defined by Eq. [1.4]. Medium refractive index = 1.33.

The light scattering properties of gold nanoparticles offer great potential for their application in biomedical imaging. For example, the light scattered by 60nm gold nanoparticles is 10<sup>5</sup> times more brilliant than the fluorescence emitted by fluorescein molecules. In addition, the scattered light color and intensity can be tuned by changing the size and shapes of the gold. Compared to fluorescent molecules, the use of gold nanoparticles for imaging is simple because they do not photobleach like fluorophores.

From the explanation above, we know that the peak intensity and position of both surface plasmon absorption and scattering bands are dependent upon the size and shape of the metal nanoparticles. For the calculation of the total extinction ( $Q_{\text{abs}}$ ) and scattering ( $Q_{\text{sca}}$ ) efficiency of gold nanospheres, the Mie theory for homogeneous spheres was considered [66]. Since the total extinction efficiency is equal to the sum of scattering and absorption efficiency, the absorption and scattering percentage vary according to size and shape of the nanoparticles, the Mie theory for total  $Q_{\text{ext}}$  and  $Q_{\text{sca}}$  (for a homogeneous sphere) are expressed as infinite series [73]:

$$Q_{ext} = \frac{2}{x^2} \sum_{n=1}^{\infty} (2n+1) \text{Re}[a_n + b_n] \quad (1-7)$$

$$Q_{sca} = \frac{2}{x^2} \sum_{n=1}^{\infty} (2n+1) \text{Re}[a_n^2 + b_n^2] \quad (1-8)$$

$$Q_{abs} = Q_{ext} - Q_{sca} \quad (1-9)$$

$$a_n = \frac{m \psi_n(mx) \psi_n'(x) - \psi_n(x) \psi_n'(mx)}{m \psi_n(mx) \xi_n'(x) - m \xi_n(x) \psi_n'(mx)} \quad (1-10)$$

$$b_n = \frac{\psi_n(mx) \psi_n'(x) - m \psi_n(x) \psi_n'(mx)}{\psi_n(mx) \xi_n'(x) - m \xi_n(x) \psi_n'(mx)} \quad (1.11)$$

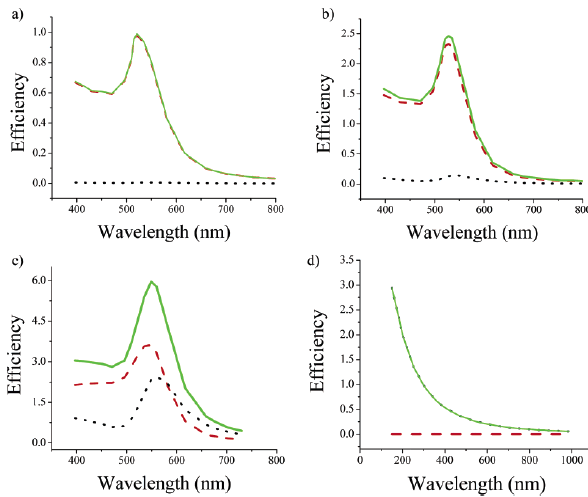


Fig. 1-14. Calculated spectra of the efficiency of absorption  $Q_{abs}$  (red dashed), scattering  $Q_{sca}$  (black dotted), and extinction  $Q_{ext}$  (green solid) for gold nanospheres (a)  $D=20$  nm, (b)  $D=40$  nm, (c)  $D=80$  nm, and polystyrene nanospheres (d)  $D=300$  nm [73].

Fig 1-14 shows the calculated size and shape dependence of the percentage of the absorption and scattering efficiency [73] using Mie theory, separation of variables method and discrete dipole approximation method.

For 40nm nanospheres, the absorption cross section is higher than the light

scattering cross section. However, if the shapes change to a spheroid or nanorod with an aspect ratio of 2, they are equal and when the aspect ratio changes to 3 for the nanorod the scattering cross section dominates [47]. By varying the aspect ratio of nanorods the absorption and scattering efficiency can be tuned. This tunability between the absorption and scattering provides great flexibility for their use in imaging and PTT.

### 2.5. Gold nanoparticles in cancer imaging and PTT

During this decade, a variety of nanostructures with unique optical properties has been

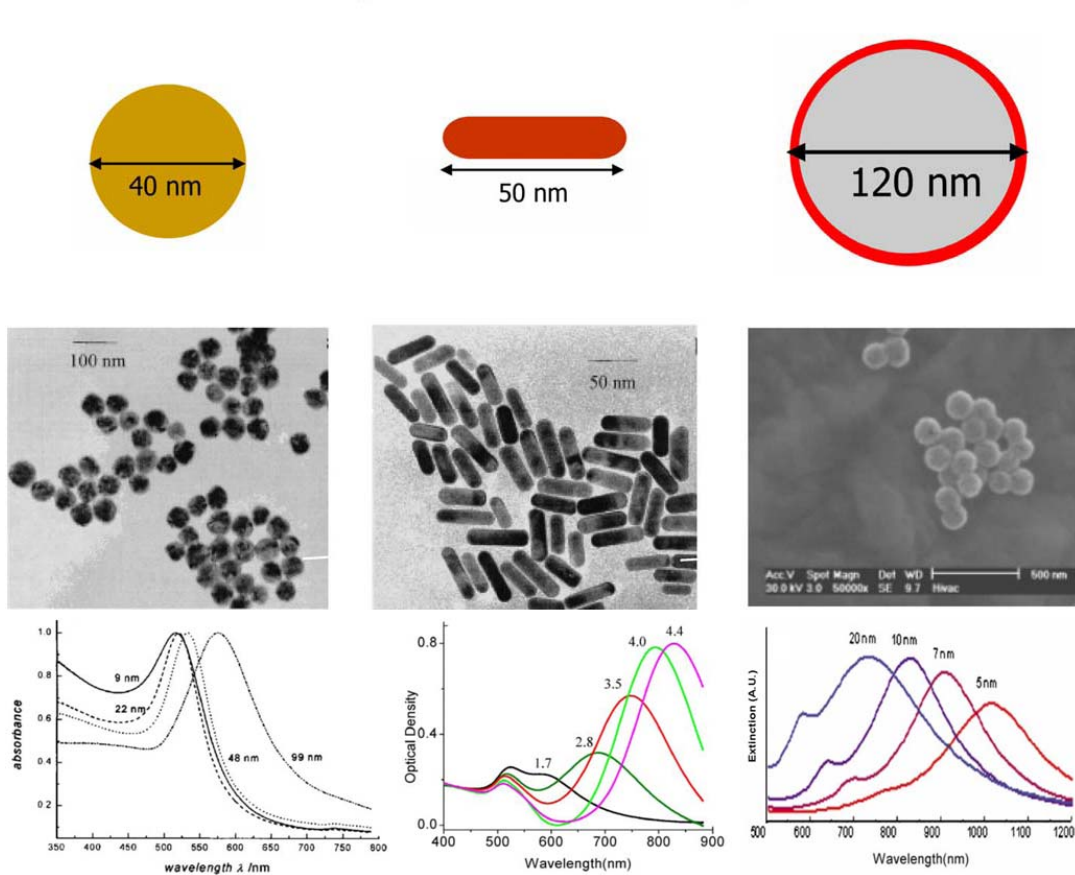


Fig. 1-15. Plasmonic gold nanostructures commonly used for PTT. a) Nanospheres (transmission electron microscopy [TEM] image); b) nanorods (TEM image); c) Nanoshells (TEM image) [80].

characterized that are useful in PTT [3, 30, 78-81]. The plasmonic property of the metallic nanostructures is being utilized for PTT and is thus termed as plasmonic photothermal therapy (PPTT) [79] in order to distinguish it from PTT and PDT. Currently, the chief nanostructures that have been demonstrated in PPTT are gold nanospheres [45, 73, 74, 81, 83–86], gold nanorods [86–89], gold nanoshells [90–93], gold nanocages [94, 95], and carbon nanotubes [96] due to their strongly enhanced absorption in the visible and NIR regions. Of these structures, the first three nanostructures (fig. 1-15) are especially promising, because of their ease of preparation, multi-functionalization, and tunable optical properties [80].

The absorption band of core/shell particles can be tuned by adjusting the ratio of the thickness of the gold shell or the diameter core (Fig 1-15, [80]) and thus enables both strong scattering and absorption efficiency. Therefore, they can be used as dual imaging/therapy contrast agents (see Fig 1-16, [79]). Fig 1-17 [12] shows the PTT using gold nanoshell in *in vivo* experiments.

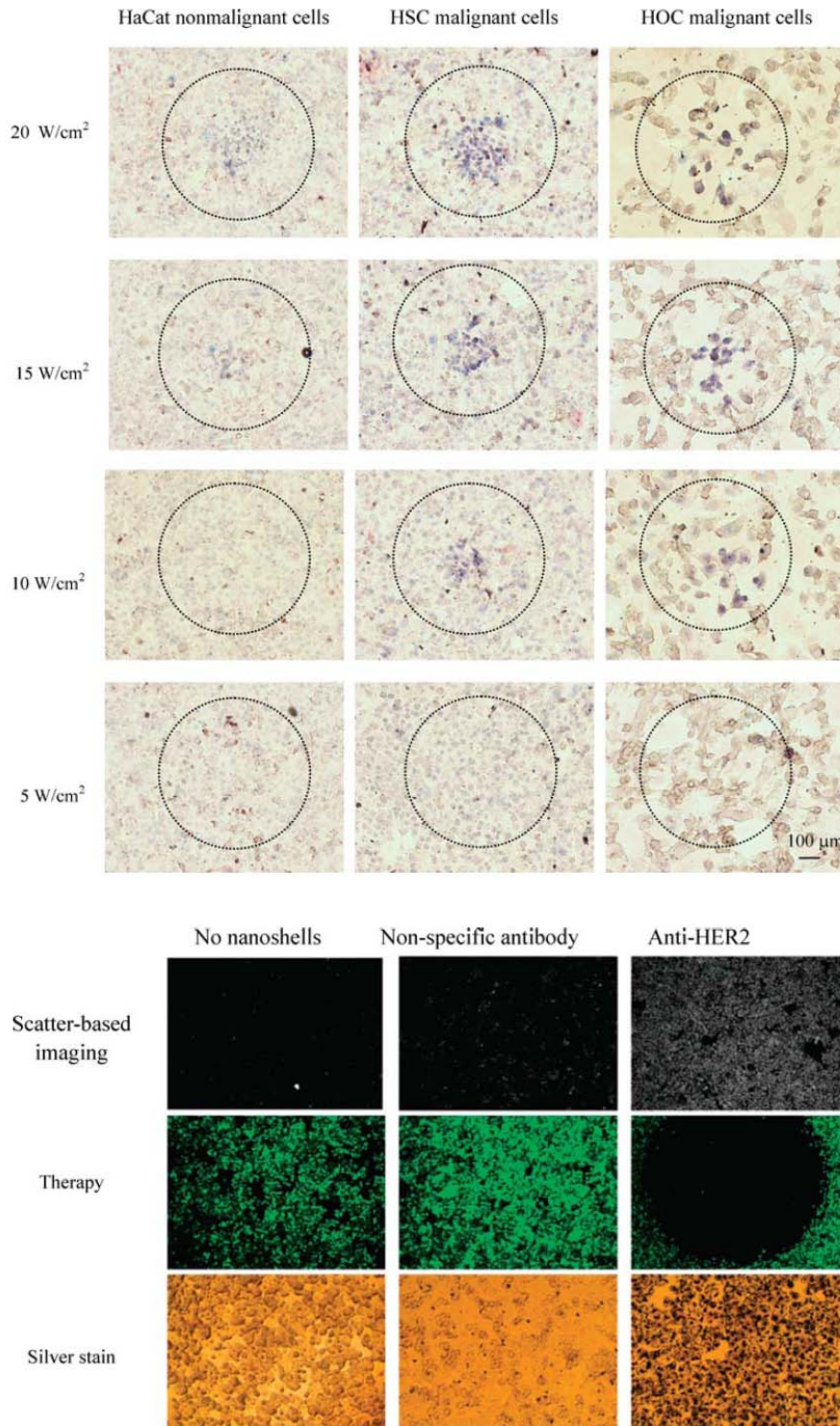


Fig. 1-16. (a) Selective PPTT for cancer cells in the NIR region by using anti-EGFR conjugated gold nanorods [79]. After incubation with anti-EGFR conjugated gold nanorods, HaCat normal cells are destroyed at a laser power threshold of 20 W/cm<sup>2</sup>, while HSC and HOC cancerous cells are destroyed at a much lower threshold of 10 W/cm<sup>2</sup>. The difference reflects the much larger density of gold nanorods on the surface of the cancer cells compared to that on the normal cells (b) Selective PPTT for cancer cells by using anti-Her2 antibody conjugated gold nanoshells. Only the cells incubated with anti-Her2 antibody conjugated gold nanoshells are damaged under NIR irradiation [93].

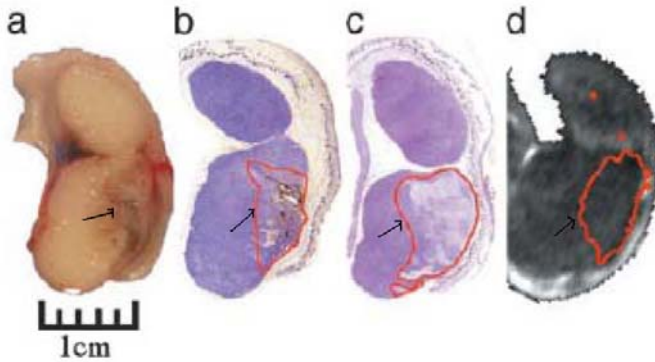


Fig. 1-17. (a) Gross pathology after in vivo cancer treatment with nanoshells and NIR laser reveal hemorrhaging and loss of tissue birefringence beneath the apical tissue surface. (b) Silver staining of a tissue section reveals the region of localized nanoshells (outlined in red). (c) Hematoxylin and eosin staining within the same plane clearly shows tissue damage within the area occupied by nanoshells. (d) Likewise, MRTI calculations reveal an area of thermal damage of similar dimension to a, b, and c [12].

Various preliminary studies have reported that the light scattering properties of gold nanoparticles makes them useful as contrast agents for biomedical imaging e.g. multiphoton plasmon resonance microscopy [9], second harmonic generation microscopy [97],

third-harmonic generation microscopy [11], optical coherence microscopy [10] and confocal scanning optical microscopy [9]. Gold nanoparticles have several advantages as compared to other agents, for imaging application. The nanogold scatters light very strongly, hence is much brighter than chemical fluorophores and can be easily seen in concentrations as low as  $10^{-16}$ M [5, 72]. Moreover it is resistant to photobleaching. Sokolov *et al.* [7, 8] used confocal microscopy to detect the scattering of anti-EGFR/Au nanoparticles

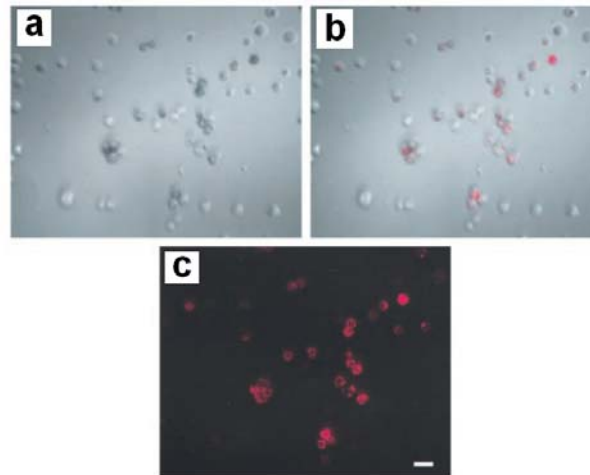
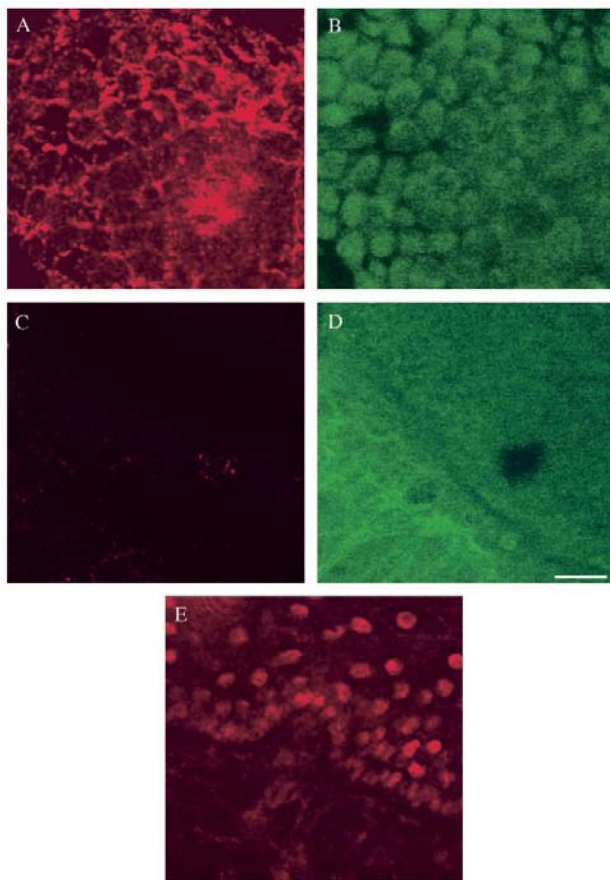


Fig. 1-18. SiHa cells labeled with anti-EGFR gold conjugates in (a) brightfield (b) in brightfield with laser pointer illumination (red patches due to particle internalization). (c) laser-pointer illumination at grazing incidence. The scattering of gold conjugates is false-colored in red. The laser pointer emits light in 630–680nm region with power output less than 5mW. The laser pointer illuminated an area ca. 3–5mm in diameter. The scale bar is ca.  $30\mu\text{m}$  [7].

in cervical cancer (see fig 1-18, 1-19). Irradiation with a laser will only produce single color



*Fig. 1-19. Laser scanning confocal reflectance (A, C, and E) and confocal fluorescence (B and D) images of precancerous (A and B) and normal (C-E) fresh cervical ex vivo tissue labeled with anti-EGFR/gold conjugates. Reflectance images were obtained with 647nm excitation wavelength, and fluorescence images were obtained using 488nm excitation and 515nm long band-pass emission filter. Reflectance images A and C were obtained after labeling with gold conjugates under the same acquisition conditions. Image E was obtained after 6% AA solution was added to the normal cervical biopsy and laser power was increased by ~6-fold. AA is a nonspecific contrast agent that is used in reflectance imaging of epithelium to increase scattering from nuclei (6). Confocal fluorescence images B and D were obtained under the same acquisition conditions. The reflectance images are false colored in red. The scale bar is 20 $\mu$ m [7].*

which is close to the laser wavelength used. When illuminated with a beam of white light, gold nanoparticles scatter light of different colors in dependence of the size and shape. [8]. This color dependent scattering property provides the potential for imaging studies with a simple white light source, which has a low penetration depth during *in vivo* application.

## **2.6. Targeting nano-drugs for cancer specificity**

Most negative side-effects of anticancer drugs stem from the fact that they are widely distributed throughout the body, causing damage of both, tumour and normal cells. Consequently, the efficacy of chemotherapy and, similarly, radiotherapy is often limited due

to this problem, which is normally tackled by the use of small non-antigenic ligands targeted to cancer cells.

### 2.6.1. Folic acid as cancer cell targeting ligand

The Low molecular weight (MW) targeting agents, such as folic acid (Fo), and its counterpart, the FR, have emerged as the most [98-103] promising tool for selective cancer therapy

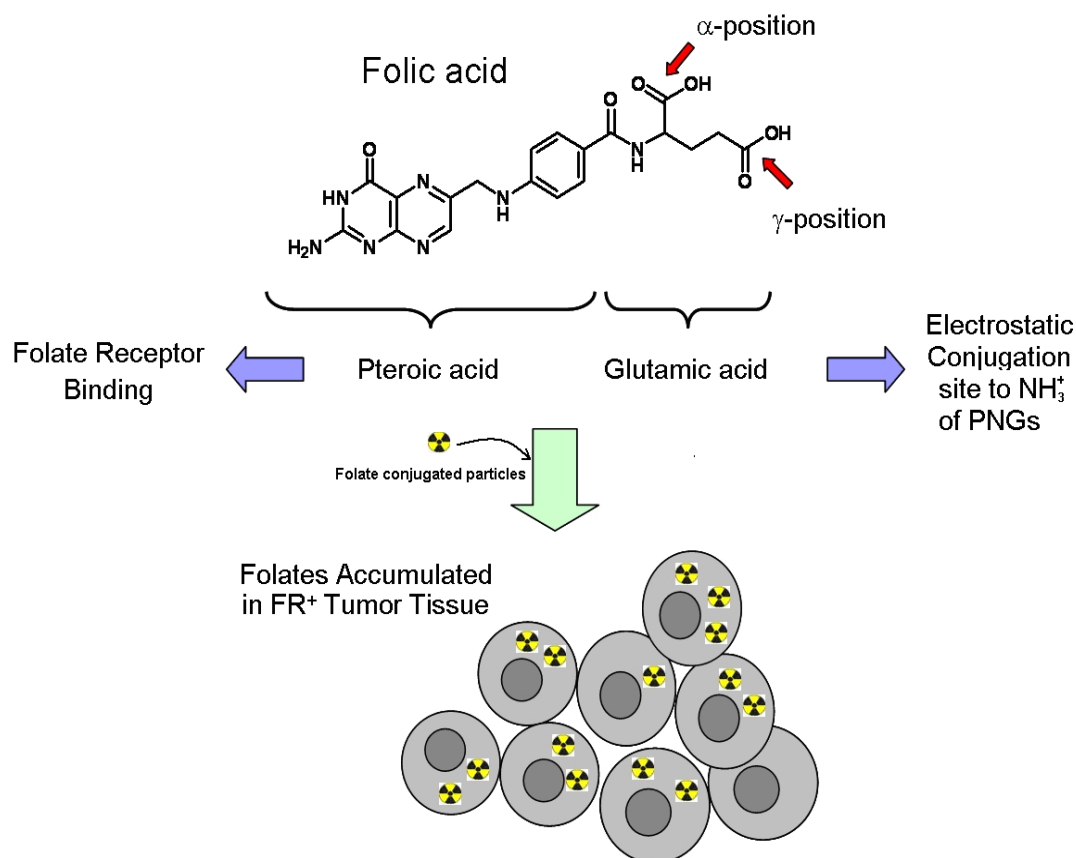


Fig. 1-20. Folic Acid. Conjugation of a chelating-linker system or electrostatic conjugation of a  $\text{NH}_3^+$  group of coated particles is accessible via the  $\alpha$ - or  $\gamma$ -carboxyl group of the glutamate-moiety of folic acid whereas the pterioate part is essential for FR-binding. After receptor binding of the radiofolate the FR/radiofolate complex is internalized via endocytosis leading to radioactivity deposition throughout the tumor cell tissue [140].

(fig. 1-20). It was found that malignant cells overexpress significantly higher number of folate receptors ( $\geq 20$  pmol  $^3\text{H}$ folate/ $10^6$  cells) than normal epithelial cells and fibroblasts ( $\leq 1$  pmol  $^3\text{H}$ folate / $10^6$  cells) [99, 104-108]. This receptor has also been reported as a tumor marker in most cancers [104], but especially in ovarian carcinoma [100, 101]. Moreover folic

acid has a very high affinity for its cell surface receptor ( $K_d \sim 1\text{nM}$ ) [109] and its efficient cell internalization [119-114]. Once the folic acid binds to the folate receptor, it is delivered directly to the nucleus of the cell, because folic acid is required for RNA synthesis [108, 110]. Thus, the advantages of using Fo as targeting agent is that it is stable, non-immunogenic and less expensive as compared to proteins such as monoclonal antibodies. These properties make it a highly recommended molecule for nuclear delivery of anticancer agents [115].

### **2.6.2. Folate receptors as cancer cell target**

The mammalian FR occurs as a family of homologous glycopolypeptides which bind folate compounds and antifolates (a group of compounds commonly used to treat various forms of cancer by produce an intracellular state of folic acid deficiency in turn inhibiting

folate-dependent enzymes along the folate metabolic pathway) with high affinity (fig.1-21) [103]. The cDNAs for isoforms of FR from human (hFR- $\alpha$ , hFR- $\beta$  and hFR- $\gamma/\gamma_4$ ) as well as murine (mFR- $\alpha$ , mFR- $\beta$ ) [116-119] even though illustrates >70% similarity in their deduced amino acid sequences, they display significant differences in their relative affinities and stereospecificities for the reduced



*Fig. 1-21. Structure prediction of folate receptor using sequence information (accession No.:CAG46816.1) in FFAS03 where receptor tyrosine protein kinase Musk (3HKL) covered as template. The ligand binding groove shows the interaction of pterioic acid moiety of folic acid [149].*

folate compounds and antifolate drugs [119, 121]. The hFR- $\alpha$  and hFR- $\beta$  are attached to the cell membrane by a glycosylphosphatidylinositol (GPI) anchor [116, 122–124] and internalize bound folate/antifolate and folate conjugates by an endocytic mechanism [104, 125, 126] whereas hFR- $\gamma$  is a soluble folate binding protein that is constitutively secreted in the absence of an efficient signal for GPI modification [127]. The expressions of hFR isoforms are differentially tissue-specific and its elevated level in several malignancies is also differential [98, 100, 101, 120, 129]. Usually, hFR- $\alpha$  is expressed in certain normal epithelial cells but is immensely elevated in some carcinomas. The hFR- $\beta$  isoform is absent in most normal tissues as well as moderately expressed in placenta, spleen and thymus. However, it is highly overexpressed in certain malignancies of non-epithelial origin including myeloid leukemia. In general, the expression of hFR- $\gamma/\gamma_4$  isoform is restricted to tissues and malignant cells of hematopoietic origin including lymphoid cells [128]. The FR isoforms are, hence, regarded as promising tumor-specific targets for a number of experimental cancer therapies and also has demonstrated to be a potential prognostic and diagnostic serum marker [105, 106, 128-137].

The FR $\alpha$  is generally over-expressed in several epithelial malignancies, including ovarian, renal, lung, and breast cancers [138]. Whilst the proper function of FR $\alpha$  in tumors is not yet established, in the kidney it serves as a high affinity salvage receptor. It retrieves folate from the filtrate and returns it via transcytosis to the blood [139]; in the brain, it probably concentrates folate in the cerebrospinal fluid [140]. The expression of FR $\alpha$  in normal tissues is restricted to the apical surfaces of polarized epithelial cells [141], where it is not exposed to the blood stream. The FR $\alpha$  also regulated the folate

homeostasis, by ubiquitously expressing reduced FRs that conjugated to low molecular weight compounds like proteins, or nanoparticles. These reduced FR conjugates are then internalized by photon-coupled folate transporter [142]. This property has been implicated for targeting of chemotherapeutic drugs, cytotoxic viruses, or imaging agents to FR $\alpha$ -expressing cells. FR $\alpha$  became very popular in the field of targeted biological therapy of ovarian cancer [143, 144]. It has been reported that expression of FR $\alpha$  is at a level 10- to 100-fold higher in majority of non-mucinous epithelial ovarian tumors than in the kidney and on lung and breast epithelial cells [145]. Moreover, FR $\alpha$  is also considered as tumor marker, as 70% of women with ovarian or breast cancer showing measurable immune responses against this protein [146]. The high level of expression of FR $\alpha$ , its tumor specificity and the potential to boost immunogenicity to tumors with FR $\alpha$ -specific approaches, have generated enthusiasm for testing different strategies to target FR $\alpha$  in ovarian cancer patients. For example, MORAb-003, a humanized, high-affinity monoclonal antibody against FR $\alpha$  based, which is at present undergoing phase II testing on ovarian cancer patients after cell-mediated cytotoxicity caused by complement-dependent killing [147]. Additionally, Boiocchi and co-workers have stated that FR $\alpha$  overexpression may be an indicator of platinum resistance in ovarian cancer i.e., higher levels of FR $\alpha$  expression after primary treatment may be a predictor of chemotherapy response failure [148].

The present part of the thesis will describe in detail, the preparation, characterization and application of target specific multilayer coated gold nanoparticles for cancer therapy. This includes the development of a modified layer-by-layer coating protocol in order to improve the stability against aggregation of polyelectrolyte coated nanogold (PNG) system in

presence of small ions; electrostatic conjugation of the cancer targeting molecule as well as the incorporation of Boron ( $^{10}\text{B}$ ) in the PNG system for Boron Neutron Capture Therapy (BNCT) combined with photothermal cancer therapy.

### **3. References**

1. Parak WJ, Manna L, Simmel FC, Gerion D, Alivisatos P. Quantum dots. In. Schmid G. Nanoparticles. Weinheim: Wiley-VCH, 2004. pp. 4-6.
2. Kreibig U, Vollmer M, editors. Optical Properties of Metal Clusters. New York: Springer, 1995.
3. El-Sayed MA. Some interesting properties of metals confined in time and nanometer space of different shapes. *Acc Chem Res* 2001;34(4):257-264.
4. Link S, El-Sayed MA. Spectral properties and relaxation dynamics of surface plasmon electronic oscillations in gold and silver nanodots and nanorods. *J Phys Chem B* 1999;103:8410-8426.
5. Yguerabide J, Yguerabide EE. Light-scattering submicroscopic particles as highly fluorescent analogs and their use as tracer labels in clinical and biological applications. *Anal Biochem* 1998 10;262(2):157-176.
6. Mirkin CA, Letsinger RL, Mucic RC, Storhoff JJ. A DNA-based method for rationally assembling nanoparticles into macroscopic materials. *Nature* 1996 15;382(6592):607-609.
7. Sokolov K, Aaron J, Hsu B, Nida D, Gillenwater A, Follen M, *et al.* Optical systems for in vivo molecular imaging of cancer. *Technol Cancer Res Treat* 2003;2(6):491-504.
8. Sokolov K, Follen M, Aaron J, Pavlova I, Malpica A, Lotan R, *et al.* Real-time vital optical imaging of precancer using anti-epidermal growth factor receptor antibodies conjugated to gold nanoparticles. *Cancer Res* 2003;63(9):1999-2004.
9. Yelin D, Oron D, Thiberge S, Moses E, Silberberg Y. Multiphoton plasmon-resonance microscopy. *Opt Express* 2003;11(12):1385-1391.

10. Raub CB, Orwin EJ, Haskell R. Immunogold labeling to enhance contrast in optical coherence microscopy of tissue engineered corneal constructs. *Conf Proc IEEE Eng Med Biol Soc* 2004;2:1210-1213.
11. Yelin D, Oron D, Korkotian E, Segal M, Silberberg Y. Third-harmonic microscopy with a titanium sapphire laser. *Appl Phys B. Lasers and Optics* 2002;74(1):S97-S101.
12. Hirsch LR, Stafford RJ, Bankson JA, Sershen SR, Rivera B, Price RE, *et al.* Nanoshell-mediated near-infrared thermal therapy of tumors under magnetic resonance guidance. *Proc Natl Acad Sci U S A* 2003;100(23):13549-13554.
13. Freund PL, Spiro M. Colloidal catalysis: the effect of sol size and concentration. *J Phys Chem* 1985;89(7):1074-1077.
14. Freund PL, Spiro M. Catalysis by colloidal gold of the reaction between ferricyanide and thiosulphate ions. *J Chem Soc Faraday Trans 1* 1986;82(7):2277-2282.
15. Kabanov AV. Polymer genomics: an insight into pharmacology and toxicology of nanomedicines. *Adv Drug Deliv Rev* 2006;58(15):1597-1621.
16. Jana, NR, Gearheart L, Murphy CJ. Wet Chemical Synthesis of High Aspect Ratio Cylindrical Gold Nanorods. *J Phys Chem B* 2001;105(19):4065-4067.
17. Jin R, Cao Y, Mirkin CA, Kelly KL, Schatz GC, Zheng JG. Photoinduced conversion of silver nanospheres to nanoprisms. *Science* 2001;294(5548):1901-1903.
18. Sun Y, Xia Y. Shape-controlled synthesis of gold and silver nanoparticles. *Science* 2002;298(5601):2176-2179.
19. Maillard M, Giorgio S, Pileni MP. Silver Nanodisks. *Adv Mater* 2002;14(15):1084-1086.

20. Murray CB, Noms DJ, Bawendi MG. Synthesis and characterization of nearly monodisperse CdE (E = sulfur, selenium, tellurium) semiconductor nanocrystallites. *J Am Chem Soc* 1993;115(19):8706-8715.
21. Dabbousi BO, Rodriguez-Viejo J, Mikulec FV, Heine JR, Mattoussi H, Ober R, *et al.* (CdSe)ZnS Core–Shell Quantum Dots: Synthesis and Characterization of a Size Series of Highly Luminescent Nanocrystallites. *J Phys Chem B* 1997;101(46):9463-9475.
22. Peng X, Schlamp MC, Kadavanich AV, Alivisatos AP. Epitaxial Growth of Highly Luminescent CdSe/CdS Core/Shell Nanocrystals with Photostability and Electronic Accessibility. *J Am Chem Soc* 1997;119(30):7019-7029.
23. Guzelian AA, Katari JEB, Kadavanich AV, Banin U, Hamad KE, Juban A, *et al.* Synthesis of Size-Selected, Surface-Passivated InP Nanocrystals. *J Phys Chem* 1996;100(17):7212-7219.
24. Hines MA, Guyot-Sionnest P. Synthesis and Characterization of Strongly Luminescing ZnS-Capped CdSe Nanocrystals. *J Phys Chem* 1996;100(2):468-471.
25. Link S, El-Sayed MA. Optical properties and ultrafast dynamics of metallic nanocrystals. *Annu Rev Phys Chem* 2003;54:331-366.
26. Schmid G, editor. *Clusters and Colloids: From Theory to Application*. Weinheim: Wiley-VCH, 1994.
27. Kamat PV, Meisel D, editors. *Semiconductor Nanoclusters—Physical, Chemical, and Catalytic Aspects*. Amsterdam: Elsevier, 1997.
28. Edelstein AS, Cammaratra RC, editors. *Nanomaterials: Synthesis, Properties and Applications*. Bristol: Inst Phys 1996.
29. Hagfeldt A, Grätzel M. Molecular photovoltaics. *Acc Chem Res* 2000;33(5):269-277.

30. Niemeyer CM, Ceyhan B. DNA-Directed Functionalization of Colloidal Gold with Proteins *Angew Chem Int Ed Engl* 2001;40(19):3685-3688.
31. Bruchez MJr, Moronne M, Gin P, Weiss S, Alivisatos AP. Semiconductor nanocrystals as fluorescent biological labels. *Science* 1998;281(5385):2013-2016.
32. Chan WC, Nie S. Quantum dot bioconjugates for ultrasensitive nonisotopic detection. *Science* 1998;281(5385):2016-2018.
33. Pathak S, Choi SK, Arnheim N, Thompson ME. Hydroxylated quantum dots as luminescent probes for in situ hybridization. *J Am Chem Soc* 2001;123(17):4103-4104.
34. Elghanian R, Storhoff JJ, Mucic RC, Letsinger RL, Mirkin CA. Selective colorimetric detection of polynucleotides based on the distance-dependent optical properties of gold nanoparticles. *Science* 1997;277(5329):1078-1081.
35. Dubertret B, Calame M, Libchaber AJ. Single-mismatch detection using gold-quenched fluorescent oligonucleotides. *Nat Biotechnol* 2001;19(4):365-370.
36. Reynolds RA III, Mirkin CA, Letsinger RL. Homogeneous, Nanoparticle-Based Quantitative Colorimetric Detection of Oligonucleotides. *J Am Chem Soc* 2000;122(15):3795-3800.
37. Mirkin CA, Letsinger RL, Mucic RC, Storhoff JJ. A DNA-based method for rationally assembling nanoparticles into macroscopic materials. *Nature* 1996;382(6592):607-609.
38. Alivisatos AP, Johnsson KP, Peng X, Wilson TE, Loweth CJ, Bruchez MP Jr, Schultz PG. Organization of 'nanocrystal molecules' using DNA. *Nature* 1996;382(6592):609-611.
39. <http://www.abraxisbio.com/>
40. Ochekepe NA, Olorunfemi PO, Ngwuluka NC. Nanotechnology and Drug Delivery Part 2: Nanostructures for Drug Delivery. *Trop J Pharm Res* 2009;8(3):275-287.

41. Wagner V, Dullaart A, Bock AK, Zweck A. The emerging nanomedicine landscape. *Nat Biotechnol* 2006;24(10):1211-1217.
42. Parak WJ, Gerion D, Pellegrino T, Zanchet D, Micheel C, Williams SC, *et al.* Biological applications of colloidal nanocrystals. *Nanotechnology* 2003;14(7):R15–R27.
43. Katz E, Willner I. Integrated nanoparticle-biomolecule hybrid systems: Synthesis, properties, and applications. *Angew Chem Int Ed Engl* 2004;43(45):6042-6108.
44. Pitsillides CM, Joe EK, Wei X, Anderson RR, Lin CP. Selective cell targeting with light-absorbing microparticles and nanoparticles. *Biophys J* 2003;84(6):4023–4032.
45. Zharov VP, Galitovsky V, Viegas M. Photothermal detection of local thermal effects during selective nanophotothermolysis. *Appl Phys Lett* 2003;83(24):4897–4899.
46. Decher G, Hong JD. Buildup of ultrathin multilayer films by a self-assembly process: I. consecutive adsorption of anionic and cationic bipolar amphiphiles. *Makromol Chem Macromol Symp* 1991;46:321-327.
47. Decher G, Hong JD, Schmitt J. Buildup of ultrathin multilayer films by a self-assembly process: III. Consecutively alternating adsorption of anionic and cationic polyelectrolytes on charged surfaces. *Thin Solid Films* 1992;210(1-2):831-835.
48. Decher G, Schmitt J. Fine-tuning of the film thickness of ultrathin multilayer films composed of consecutively alternating layers of anionic and cationic polyelectrolytes. *Prog Colloid Polymer Sci* 1992;89:160-164.
49. Decher G, Hong J-D. Buildup of ultrathin multilayer films by a self-assembly process: II. consecutive adsorption of anionic and cationic bipolar amphiphiles and polyelectrolytes on charged surfaces. *Ber Bunsenges Phys Chem* 1991;94:1430-1434.

50. Lvov Y, Ariga K, Ichinose I, Kunitake T. Formation of ultrathin multilayer and hydrated gel from montmorillonite and linear polycations. *Langmuir* 1996;12:3038-3044.
51. Keller SW, Johnson SA, Brigham ES, Yonemoto EH, Mallouk TE. Photoinduced charge separation in multi-layer thin film grown by sequential adsorption of polyelectrolytes. *J Am Chem Soc* 1995;117(51):12879-12880.
52. Hammond PT. Recent explorations in electrostatic multilayer thin film Assembly. *Current Opinion in Colloid & Interface Science* 2000;4(6):430-442.
53. Decher G. Fuzzy Nanoassemblies: Toward Layered Polymeric Multicomposites. *Science* 1997;277(5330):1232-1237.
54. Krol S. "Encapsulation of stone surfaces of civil infrastructure or ancient stone objects with polyelectrolyte multilayers as protection against pollutants in air or rain as well as mechanical degradation. Italian patent application TO2003A000997.
55. Keller SW, Kim HN, Mallouk TE. Layer-by-Layer Assembly of Intercalation Compounds and Heterostructures on Surfaces: Towards Molecular "Beaker" Epitaxy. *J Am Chem Soc* 1994;116(19), 8817-8818.
56. Kong W, Zhang X, Gao ML, Zhou H, Li W, Shen JC. A new kind of immobilized enzyme multilayer based on cationic and anionic interaction. *Makromol Chem Rapid Commun* 1994;15(5):405-409.
57. Lvov Y, Ariga K, Kunitake T. Assembly of Multicomponent Protein Films by Means of Electrostatic Layer-by-Layer Adsorption. *J Am Chem Soc* 1995;117(22):6117-6123.
58. Kleinfeld ER, Ferguson GS. Stepwise formation of multilayered nanostructural films from macromolecular precursors. *Science* 1994;265(5170):370-373.

59. Ferguson GS, Kleinfeld ER. Mosaic tiling in molecular dimensions. *Adv Mater* 1995;7(5):414-416.
60. Ferguson GS, Kleinfeld ER. Rapid, Reversible Sorption of Water from the Vapor by a Multilayered Composite Film: A Nanostructured Humidity Sensor. *Chem Mater* 1995;7(12):2327-2331.
61. Lvov Y, Haas H, Decher G, Moehwald H, Mikhailov A, Mtchedlishvily B, *et al.* Successive Deposition of Alternate Layers of Polyelectrolytes and a Charged Virus. *Langmuir* 1994;10(11):4232-4236.
62. Schmitt J, Decher G, Dressick WJ, Brandow SL, Geer RE, Shashidhar R, *et al.* Metal nanoparticle/polymer superlattice films: Fabrication and control of layer structure. *Adv Mater* 1997;9(1):61-65.
63. Feldheim DL, Grabar KC, Natan MJ, Mallouk TE. Electron Transfer in Self-Assembled Inorganic Polyelectrolyte/Metal Nanoparticle Heterostructures. *J Am Chem Soc* 1996;118(32):7640-7641.
64. Yoo D, Shiratori SS, Rubner MF. Controlling Bilayer Composition and Surface Wettability of Sequentially Adsorbed Multilayers of Weak Polyelectrolytes. *Macromolecules* 1998;31(13):4309-4318.
65. Shiratori S, Rubner MF. pH Dependent thickness behavior of sequentially adsorbed layers of weak polyelectrolytes. *Macromolecules* 2000;33(11):4213-4219.
66. Ladam G, Schaad P, Voegel JC, Scaaf P, Decher G, Cuisinier F. In Situ Determination of the Structural Properties of Initially Deposited Polyelectrolyte Multilayers. *Langmuir* 2000;16:1240-1255.
67. Bohren CF, Huffman DR. Absorption and Scattering of Light by Small Particles. New York: Wiley, 1983.

68. Willets KA, Van Duyne RP. Localized surface plasmon resonance spectroscopy and sensing. *Annu Rev Phys Chem* 2007;58:267-297.
69. Mie G. Beiträge zur Optik trüber Medien, speziell kolloidaler Metallösungen. *Ann Phys* 1908;330:377-445.
70. Link S, El-Sayed MA. Shape and size dependence of radiative, non-radiative and photothermal properties of gold nanocrystals. *Int Reviews Phys Chem* 2000;19(3):409-453.
71. Sönnichsen C, Franzl T, Wilk T, von Plessen G, Feldmann J, Wilson O, *et al.* Drastic reduction of plasmon damping in gold nanorods. *Phys Rev Lett*;88(7):077402.
72. Gans R. Form of ultramicroscopic particles of silver. *Ann Phys* 1915;47(10):270-284.
73. El-Sayed IH, Huang X, El-Sayed MA. Selective laser photo-thermal therapy of epithelial carcinoma using anti-EGFR antibody conjugated gold nanoparticles. *Cancer Lett* 2006;239(1):129-135.
74. Huang X, Jain PK, El-Sayed IH, El-Sayed MA. Determination of the minimum temperature required for selective photothermal destruction of cancer cells with the use of immunotargeted gold nanoparticles. *Photochem Photobiol* 2006;82(2):412-417.
75. Du H, Fuh RA, Li J, Corkan A, Lindsey JS. PhotochemCAD: A Computer-Aided Design and Research Tool in Photochemistry. *Photochem Photobiol* 1998;68(2):141-412.
76. Hydrophobic solutions. In. Van De Hulst HC, editor. *Light Scattering by Small Particles*. New York: Dover, 1981. p. 397–400.
77. Kerker M. *The Scattering of Light and Other Electromagnetic Radiation*. New York: Academic Press, 1969. p. 34-37.

78. West JL, Halas NJ. Engineered nanomaterials for biophotonics applications: improving sensing, imaging, and therapeutics. *Annu Rev Biomed Eng* 2003;5:285-92.
79. Huang X, El-Sayed IH, El-Sayed MA. Cancer cell imaging and photothermal therapy in the near-infrared region by using gold nanorods. *J Am Chem Soc* 2006;128(6):2115–2120.
80. Huang X, Jain PK, El-Sayed IH, El-Sayed MA. Plasmonic photothermal therapy (PPTT) using gold nanoparticles. *Lasers Med Sci* 2008;23(3):217-228.
81. Daniel MC, Astruc D. Gold nanoparticles: assembly, supramolecular chemistry, quantum-size-related properties, and applications toward biology, catalysis, and nanotechnology. *Chem Rev* 2004;104(1):293-346.
82. Xia Y, Halas NJ. Shape-controlled synthesis and surface plasmonic properties of metallic nanostructures. *MRS Bull* 2005;30(5):338–343.
83. Zharov VP, Galitovskaya E, Viegas M. Photothermal guidance for selective photothermolysis with nanoparticles. *Proc SPIE* 2004;5319:291–300.
84. Hainfeld JF, Slatkin DN, Smilowitz HM. The use of gold nanoparticles to enhance radiotherapy in mice. *Phys Med Biol* 2004;49(18):N309-N315.
85. Zharov VP, Galitovskaya EN, Johnson C, Kelly T. Synergistic enhancement of selective nanophotothermolysis with gold nanoclusters: potential for cancer therapy. *Lasers Surg Med* 2005;37(3):219–226.
86. Khlebtsov B, Zharov V, Melnikov A, Tuchin V, Khlebtsov N. Optical amplification of photothermal therapy with gold nanoparticles and nanoclusters. *Nanotechnology* 2006;17:5167–5179.

87. Takahashi H, Niidome T, Nariai A, Niidome Y, Yamada S. Gold nanorod-sensitized cell death: Microscopic observation of single living cells irradiated by pulsed near-infrared laser light in the presence of gold nanorods. *Chem Lett* 2006;35(5):500–501.
88. Takahashi H, Niidome T, Nariai A, Niidome Y, Yamada S. Photothermal reshaping of gold nanorods prevents further cell death. *Nanotechnology* 2006;17(17):4431–4435.
89. Huff TB, Tong L, Zhao Y, Hansen MN, Cheng JX, Wei A. Hyperthermic effects of gold nanorods on tumor cells. *Nanomedicine (Lond)* 2007;2(1):125–132.
90. Hirsch LR, Stafford RJ, Bankson JA, Sershen SR, Price RE, Hazle JD, Halas NJ, West JL, *et al.* Nanoshell-mediated near infrared thermal therapy of tumors under magnetic resonance. *Proc Natl Acad Sci* 2003;100(23):13549–13554.
91. Loo C, Lin A, Hirsch L, Lee MH, Barton J, Halas N, *et al.* Nanoshell-enabled photonics-based imaging and therapy of cancer. *Technol Cancer Res Treat* 2004;3(1):33-40.
92. O’Neal DP, Hirsch LR, Halas NJ, Payne JD, West JL. Photothermal tumor ablation in mice using near infrared absorbing nanoshells. *Cancer Lett* 2004;209:171–176.
93. Loo C, Lowery A, Halas NJ, West JL, Drezek R. Immunotargeted nanoshells for integrated cancer imaging and therapy. *Nano Lett* 2005;5(4):709–711.
94. Chen J, Wiley B, Li ZY, Campbell D, Saeki F, Cang H, Au *et al.* Gold nanocages: engineering their structure for biomedical applications. *Adv Mater* 2005;17:2255–2261.
95. Hu M, Petrova H, Chen J, McLellan JM, Siekkinen AR, Marquez M, *et al.* Ultrafast laser studies of the photothermal properties of gold nanocages. *J Phys Chem B* 2006;110(4):1520–1524.

96. Shi Kam NW, O'Connell M, Wisdom JA, Dai H. Carbon nanotubes as multifunctional biological transporters and nearinfrared agents for selective cancer cell destruction. *Proc Natl Acad Sci* 2005;102(33):11600–11605.
97. Zavelani-Rossi M, Celebrano M, Biagioni P, Polli D, Finazzi M, Duo L. Near-field second-harmonic generation in single gold nanoparticles. *Appl Phys Lett* 2008;92(9):093119 - 093121.
98. Weitman SD, Lark RH, Coney LR, Fort DW, Frasca V, Zurawski VR Jr, *et al.* Distribution of the folate receptor GP38 in normal and malignant cell lines and tissues. *Cancer Res* 1992;52(12):3396-3401.
99. Franklin WA, Waintrub M, Edwards D, Christensen K, Prendergrast P, Woods J, *et al.* New anti-lung-cancer antibody cluster 12 reacts with human folate receptors present on adenocarcinoma. *Int J Cancer Suppl* 1994;8:89-95.
100. Coney LR, Tomassetti A, Carayannopoulos L, Frasca V, Kamen BA, Colnaghi MI *et al.* Cloning of a tumor-associated antigen: MOv18 and MOv19 antibodies recognize a folate-binding protein. *Cancer Res* 1991;51(22):6125-6132.
101. Garin-Chesa P, Campbell I, Saigo PE, Lewis JL Jr, Old LJ, Rettig WJ. Trophoblast and ovarian cancer antigen LK26. Sensitivity and specificity in immunopathology and molecular identification as a folate-binding protein. *Am J Pathol* 1993;142(2):557-567.
102. Campbell IG, Jones TA, Foulkes WD, Trowsdale J. Folate-binding protein is a marker for ovarian cancer. *Cancer Res* 1991;51(19):5329-5338.
103. Antony AC. The biological chemistry of folate receptors. *Blood* 1992;79(11):2807-2820.

104. Rothberg KG, Ying YS, Kolhouse JF, Kamen BA, Anderson RG. The glycopospholipid-linked folate receptor internalizes folate without entering the clathrin-coated pit endocytic pathway. *J Cell Biol* 1990;110(3):637-649.
105. Wang S, Lee RJ, Mathias CJ, Green MA, Low PS. Synthesis, purification, and tumor cell uptake of <sup>67</sup>Ga-deferoxamine-folate, a potential radiopharmaceutical for tumor imaging. *Bioconjugate Chem* 1996;7(1):56-62.
106. Lee RJ, Low PS. Delivery of liposomes into cultured KB cells via folate receptor-mediated endocytosis. *J Biol Chem* 1994;269(5):3198-3204.
107. Wang S, Low PS. Folate-mediated targeting of antineoplastic drugs, imaging agents, and nucleic acids to cancer cells. *J Control Release* 1998;53(1-3):39-48.
108. Gabizon A, Horowitz AT, Goren D, Tzemach D, Mandelbaum-Shavit F, Qazen MM, *et al.* Targeting folate receptor with folate linked to extremities of poly(ethylene glycol)-grafted liposomes: in vitro studies. *Bioconjug Chem* 1999;10(2):289-298.
109. Malmqvist M. Biospecific interaction analysis using biosensor technology. *Nature* 1993;361(6408):186-187.
110. Corsi K, Chellat F, Yahia L, Fernandes JC. Mesenchymal stem cells, MG63 and HEK293 transfection using chitosan-DNA nanoparticles. *Biomaterials* 2003;24(7):1255-1264.
111. Dash PR, Read ML, Barrett LB, Wolfert MA, Seymour LW. Factors affecting blood clearance and in vivo distribution of polyelectrolyte complexes for gene delivery. *Gene Ther* 1999;6(4):643-650.
112. Murphy RF, Jorgensen ED, Cantor CR. Kinetics of histone endocytosis in Chinese hamster ovary cells. A flow cytometric analysis. *J Biol Chem* 1982;257(4):1695-1701 .

113. Murphy RF, Powers S, Verderame M, Cantor CR, Pollack R. Flow cytometric analysis of insulin binding and internalization by Swiss 3T3 cells. *Cytometry* 1982;2(6):402-406 .
114. Tycko B, Maxfield FR. Rapid acidification of endocytic vesicles containing alpha 2-macroglobulin. *Cell* 1982;28(3):643-651.
115. van Renswoude J, Bridges KR, Harford JB, Klausner RD. Receptor-mediated endocytosis of transferrin and the uptake of Fe in K562 cells: identification of a nonlysosomal acidic compartment. *Proc Natl Acad Sci U S A* 1982;79(20):6186-6190.
116. Lacey SW, Sanders JM, Rothberg KG, Anderson RG, Kamen BA. Complementary DNA for the folate binding protein correctly predicts anchoring to the membrane by glycosyl-phosphatidylinositol. *J Clin Invest* 1989;84(2):715-720.
117. Elwood PC. Molecular cloning and characterization of the human folate-binding protein cDNA from placenta and malignant tissue culture (KB) cells. *J Biol Chem* 1989;264(25):14893-14901.
118. Ratnam M, Marquardt H, Duhring JL, Freisheim JH. Homologous membrane folate binding proteins in human placenta: cloning and sequence of a cDNA. *Biochemistry*. 1989;28(20):8249-54.
119. Brigle KE, Westin EH, Houghton MT, Goldman ID. Insertion of an intracisternal A particle within the 5'-regulatory region of a gene encoding folate-binding protein in L1210 leukemia cells in response to low folate selection. Association with increased protein expression. *J Biol Chem* 1992; 267:22351-22355.
120. Wang X, Shen F, Freisheim JH, Gentry LE, Ratnam M. Differential stereospecificities and affinities of folate receptor isoforms for folate compounds and antifolates. *Biochem Pharmacol*. 1992;44(9):1898-1901.

121. Brigle KE, Spinella MJ, Westin EH, Goldman ID. Increased expression and characterization of two distinct folate binding proteins in murine erythroleukemia cells. *Biochem Pharmacol* 1994;47(2):337-45.
122. Luhrs CA, Slomiany BL. A human membrane-associated folate binding protein is anchored by a glycosyl-phosphatidylinositol tail. *J Biol Chem* 1989;264(36):21446–21449.
123. Verma RS, Gullapalli S, Antony AC. Evidence that the hydrophobicity of isolated, in situ, and de novo-synthesized native human placental folate receptors is a function of glycosyl-phosphatidylinositol anchoring to membranes. *J Biol Chem* 1992;267(6):4119-4127.
124. Yan W, Ratnam M. Preferred sites of glycosylphosphatidylinositol modification in folate receptors and constraints in the primary structure of the hydrophobic portion of the signal. *Biochemistry* 1995;34(44):14594-14600.
125. Leamon CP, Low PS. Delivery of macromolecules into living cells: a method that exploits folate receptor endocytosis. *Proc Natl Acad Sci U S A.* 1991;88(13):5572-5576.
126. Turek JJ, Leamon CP, Low PS. Endocytosis of folate-protein conjugates: ultrastructural localization in KB cells. *J Cell Sci* 1993;106( Pt 1):423-430.
127. Shen F, Wu M, Ross JF, Miller D, Ratnam M. Folate receptor type gamma is primarily a secretory protein due to lack of an efficient signal for glycosylphosphatidylinositol modification: protein characterization and cell type specificity. *Biochemistry* 1995;34(16):5660-5665.
128. Habeck LL, Leitner TA, Shackelford KA, Gossett LS, Schultz RM, Andis SL, *et al.* A novel class of monoglutamated antifolates exhibits tight-binding inhibition of human

- glycinamide ribonucleotide formyltransferase and potent activity against solid tumors. *Cancer Res* 1994;54(4):1021-1026.
129. Ross JF, Chaudhuri PK, Ratnam M. Differential regulation of folate receptor isoforms in normal and malignant tissues in vivo and in established cell lines. Physiologic and clinical implications. *Cancer* 1994;73(9):2432-2443.
130. Westerhof GR, Schornagel JH, Kathmann I, Jackman AL, Rosowsky A, Forsch RA, *et al.* Carrier- and receptor-mediated transport of folate antagonists targeting folate-dependent enzymes: correlates of molecular-structure and biological activity. *Mol Pharmacol* 1995;48(3):459-471.
131. Bolhuis RL, Lamers CH, Goey SH, Eggermont AM, Trimbos JB, Stoter G, *et al.* Adoptive immunotherapy of ovarian carcinoma with bs-MAb-targeted lymphocytes: a multicenter study. *Int J Cancer Suppl* 1992;7:78-81.
132. Canevari S, Mezzanzanica D, Ménard S, Ferrini S, Moretta L, Colnaghi MI. Possible targets on carcinoma for bMAb retargeting of lymphocyte or drug cytotoxicity. *Int J Cancer Suppl* 1992;7:42-744.
133. Ferrini S, Cambiaggi A, Sforzini S, Canevari S, Mezzanzanica D, Colnaghi MI, *et al.* Use of anti-CD3 and anti-CD16 bispecific monoclonal antibodies for the targeting of T and NK cells against tumor cells. *Cancer Detect Prev* 1993;17(2):295-300.
134. Leamon CP, Low PS. Selective targeting of malignant cells with cytotoxin-folate conjugates. *J Drug Target* 1994;2(2):101-112.
135. Mazzoni A, Mezzanzanica D, Jung G, Wolf H, Colnaghi MI, Canevari S. CD3-CD28 costimulation as a means to avoiding T cell preactivation in bispecific monoclonal antibody-based treatment of ovarian carcinoma. *Cancer Res* 1996;56(23):5443-5449.

136. Mathias CJ, Wang S, Lee RJ, Waters DJ, Low PS, Green MA. Tumor-selective radiopharmaceutical targeting via receptor-mediated endocytosis of gallium-67-deferoxamine-folate. *J Nucl Med* 1996;37(6):1003-1008.
137. Wang S, Lee RJ, Cauchon G, Gorenstein DG, Low PS. Delivery of antisense oligodeoxyribonucleotides against the human epidermal growth factor receptor into cultured KB cells with liposomes conjugated to folate via polyethylene glycol. *Proc Natl Acad Sci U S A* 1995;92(8):3318-3322.
138. Elnakat H, Ratnam M. Role of folate receptor genes in reproduction and related cancers. *Front Biosci* 2006;11:506–519.
139. Sandoval RM, Kennedy MD, Low PS, Molitoris BA. Uptake and trafficking of fluorescent conjugates of folic acid in intact kidney determined using intravital two-photon microscopy. *Am J Physiol Cell Physiol* 2004;287:C517–C526.
140. Kamen BA, Smith AK. A review of folate receptor alpha cycling and 5-methyltetrahydrofolate accumulation with an emphasis on cell models in vitro. *Adv Drug Deliv Rev* 2004;56(8):1085–1097.
141. Weitman SD, Lark RH, Coney LR, Fort DW, Frasca V, Zurawski VR Jr, *et al.* Distribution of the folate receptor GP38 in normal and malignant cell lines and tissues. *Cancer Res* 1992;52(12):3396–3401.
142. Leamon CP, Low PS. Delivery of macromolecules into living cells: a method that exploits folate receptor endocytosis. *Proc Natl Acad Sci U S A* 1991;88(13):5572–5576.
143. Salazar MD, Ratnam M. The folate receptor: what does it promise in tissue-targeted therapeutics? *Cancer Metastasis Rev* 2007;26(1):141–152.

144. Reddy JA, Allagadda VM, Leamon CP. Targeting therapeutic and imaging agents to folate receptor positive tumors. *Curr Pharm Biotechnol* 2005;6(2):131–150.
145. Parker N, Turk MJ, Westrick E, Lewis JD, Low PS, Leamon CP. Folate receptor expression in carcinomas and normal tissues determined by a quantitative radioligand binding assay. *Anal Biochem* 2005;338(2):284–293.
146. Knutson KL, Krco C, Goodman K, Goodman K, Kelemen LE, Wettstein PJ, *et al.* T cell immunity to the folate receptor alpha is prevalent in women with breast or ovarian cancer. *J Clin Oncol* 2006;24(26):4254–4261.
147. Ebel W, Routhier EL, Foley B, Jacob S, McDonough JM, Patel RK, *et al.* Preclinical evaluation of MORAb-003, a humanized monoclonal antibody antagonizing folate receptor-alpha. *Cancer Immun* 2007;7:6.
148. Toffoli G, Russo A, Gallo A, Cernigoi C, Miotti S, Sorio R, *et al.* Expression of folate binding protein as a prognostic factor for response to platinum-containing chemotherapy and survival in human ovarian cancer. *Int J Cancer* 1998;79(2):121–126.
149. Jaroszewski L, Rychlewski L, Li Z, Li W, Godzik A. FFAS03: a server for profile--profile sequence alignments. *Nucleic Acids Res.* 2005;33(Web Server issue):W284-W288.

## **CHAPTER 1**

*Novel generation of non-aggregating targeted functionalized gold nanoparticles and a detailed surface enhanced Raman spectroscopic characterization.\**

### **1.1. Aim of the present work**

Gold nanoparticles (AuNP) became increasingly interesting for nanomedical applications due to its broad spectrum of possible functions in therapy but also in diagnostics. The main features which make them so useful are the fact that they are inert and not toxic and can be visualized by different optical techniques. As the properties of the nanoparticle are mainly determined by its surface in this section of the thesis I will investigate in detail the properties of the polyelectrolytes capsule in contact with the gold nanoparticles. Moreover I will introduce a novel polyelectrolyte (PE) multilayer encapsulation protocol aimed to improve the long-term stability (shelf life) and the resistance AGAINST AGGREGATION IN PRESENCE OF SMALL IONS of coated gold nanoparticles.

Initially the binding of the first polyelectrolyte layer, either the positive or the negative one, and the orientation of the polymers toward the gold surface was studied by surface enhanced Raman spectroscopy (SERS). Then I have functionalized the PE coated gold nanoparticles (PNGs) by electrostatically conjugating folic acid for targeted delivery in breast cancer cell lines, VP 229 and MDA MB 231 which over-express folate-receptors. . After incorporation of B-10 in the layers of the multi-layers of the PNGs (<sup>10</sup>BPNGs) the particles were tested for a potential application in Boron Neutron Capture Therapy (BNCT), a novel treatment for cancer.

\*  
*Manuscript accepted by Langmuir*

## **CHAPTER 2**

### **2.1. Introduction**

Nanotechnology in medicine promises a completely new and revolutionary way for diagnosing and treating diseases. However this has led to an increasing interest in multifunctional nanoparticles.

Colloidal gold nanoparticles (AuNPs) and gold salts have a long tradition in medical [1-4]. Their unique properties, such as being non-toxic, inert against chemical modifications and emitting luminescence, make them a very attractive tool for “theranostics”, the combination of drug or drug delivery with diagnostic features. AuNPs can be used as drug for microwave induced cancer lesion treatment by radiotherapy and thermotherapy [3, 4]. Some examples of diagnostic applications which are in development are the visualization of receptors or other targets in electron microscopy [5] and as fluorescence label for antibody binding [6-8]. The main obstacle for using AuNP for medical preparation is the fact that functionalized AuNPs tend to aggregate, as in the case of thiol-stabilized AuNPs [9-11], or to become cytotoxic due to coating or size [12, 13]. Especially the work of Decher and Schneider [14] indicates that polyelectrolyte multilayer coated AuNPs (PNGs) are aggregating in presence of ions. On the other hand polyelectrolyte multilayer coating is an appealing method to functionalize AuNP for drug delivery or theranostics via electrostatic forces [15-19].

In the present work, we address most of the above mentioned drawbacks by introducing a new protocol for non-aggregating, targeted PNG preparation. As working hypothesis we assumed that the low stability against agglomeration reported by Decher and Schneider [14] may be due to the excessive length of the polyelectrolytes (PEs) with respect to the particle

size leading to incomplete wrapping and in turn to bridging flocculation. Therefore we decided to collapse the PE by incubating them in the ionic solution and then coating the AuNP with these random coil polymers. In the literature related to weak polyelectrolytes [15], it has been reported that they can change their conformation in dependence of the ionic strength and that a shielding of the intramolecular repulsive forces induce a structural change from the extended chain to a random coil structure [20]. The resulting were tested for aggregation behaviour in Ringer's solution as a typical injection solution in medicine, or at high ionic strength (0.5M NaCl). Targeting against cancer cells was possible with the electrostatic binding of Fo.

Folic acid was chosen as a model for receptor-mediated up-take of the targeted PNG. FRs are significantly over-expressed in the majority of human cancers [20-25] because they require high amounts of folic acid for rapid nucleic acid biosynthesis [26, 27].

The binding of poly-allylamine hydrochloride (PAH) as well as poly-styrene-4-sulfonate (PSS) to the AuNPs surface is not yet fully understood and therefore was characterized in more detail by Surface Enhanced Raman Spectroscopy (SERS) in the present work.

The key attribute of nanoparticle-based agents is its multifunctionality. This feature enable in conjugating various therapeutic drugs, targeting ligands, imaging label and other functionalities can all be integrated to allow for targeted molecular imaging and molecular therapy of cancer. As an application for the multifunctional targeted gold nanoparticles I studied the development of a possible nanodrug for Neutron Capture Therapy (BNCT). A major challenge in the translation of experimental BNCT into a routine clinical therapy is the selective delivery of boron compounds to tumors in addition to safety concerns.

In radiation therapy, BNCT is a bimodal method, which offer a great promise in the search for the ideal cancer therapy, with the potential for selective destruction of tumor cells

while sparing normal cells/tissue. BNCT takes advantage of the ability of the stable isotope 10-Boron ( $^{10}\text{B}$ ) to capture neutrons. When  $^{10}\text{B}$  is irradiated with low energy thermal neutrons, there nuclear capture and fission reactions occur that results in high-energy particles [ $\alpha$ -particle (1.47 MeV) and Li-7 ion (0.84 MeV)]. The Linear Energy Transfer (LET) of these highly charged energy particles ranges within approximately one cell diameter [28], which confines the radiation damage within the cell from which they arise. Therefore, minimizing the cytotoxic effects on the surrounding tissue.

Selective delivery of a sufficient number of  $^{10}\text{B}$  atoms to malignant cells ( $10^9$  atoms/cell, which translates to approximately  $35\mu\text{g } ^{10}\text{B}$  per gram of tissue) [29] is a critical prerequisite for successful BNCT. Furthermore, enough thermal neutrons must be absorbed by them to “activate” the high lethal dosage during neutron capture reaction within the cancer cell. The damage of the healthy tissue in the path of the neutron beam can be prevented if the surrounding tissue should contain  $< 5\mu\text{g}$  of  $^{10}\text{B}$  per gram of tissue.

Hence, the most critical challenge to the translation of experimental BNCT into a routine clinical therapeutic option for cancer is the selective delivery of boron compounds to the tumor tissue while sparing the healthy one and their safety.

To date, only two boron delivery agents, borocaptate sodium (BSH) and boronophenylalanine (BPA) are clinically approved for BNCT. Despite the possibility to attain average tumor-to-normal tissue ratios of therapeutic significance after infusion of BPA, the outcome of pre-clinical and clinical BNCT trials has been limited. In a report by Zonta et al [30], residual viable tumor cells were observed at the periphery of a tumor mass biopsied after extracorporeal liver BNCT of liver metastases. The patient went on to develop a recurrence of the disease. In another noteworthy observation, Altieri et al [31] found a

heterogeneous micro distribution of boron was observed within the tumor masses after BPA infusion in patients. Thus uniform distribution is lacking.

These observations suggest that the low accumulation of boron in certain areas of a tumor, either due to inherent accumulation properties of different subpopulations of malignant cells, or to external conditions, such as poor vascularisation, limit the therapeutic outcome of BNCT [31].

In this study I describe the synthesis of multi-functional nanoparticles for targeted boron delivery and molecular imaging, with a perspective application in BNCT. These multilayers coated AuNPs were equipped with fluorophores for visualization, folic acid molecules for targeted and receptor guided delivery and the layer-wise deposition of the polymers allowed electrostatically conjugating boron containing molecules like Boronophenylalanine (BPA). The architecture of the resulting nanostructures was characterized by Transmission electron microscopy (TEM) while neutron autoradiography was used to validate the amount of incorporated boron. Colloidal stability of the nanoparticles was tested in physiological solutions. biocompatibility/toxicity and receptor mediated cellular uptake was evaluated by using in vitro various cancer cell lines. Fluorescence microscopy revealed that the nanoparticles were internalized and accumulated in the perinuclear region of the cancer cells. A MTT assay showed low overall toxicity in both non-cancerous cell line i.e. IHH (immortalized liver cell line) and J774.2 (macrophage cell line) and cancerous cell line i.e. JHH6 (Hepatocellular carcinoma cell line), HL60 (leukemic cell line) and MDA MB 231 (breast cancer cell line).

## **2.2. References**

1. Daniel MC, Astruc D. Gold nanoparticles: Assembly, Supramolecular chemistry, Quantum-Size-Related Properties, and Application towards Biology, Catalysis and Nanotechnology. *Chem Rev* 2004;104 (1):293-346.
2. Bajaj S, Vohora SB. Analgesic activity of gold preparations used in Ayurveda & Unani-Tibb. *Indian J Med Res* 1998;108:104-111.
3. Hainfeld JF, Slatkin DN, Smilowitz, H.M. The use of gold nanoparticles to enhance radiotherapy in mice. *Phys. Med. Biol* 2004;9:N309-N315.
4. Visaria RK, Griffin RJ, Williams BW, Ebbini ES, Paciotti GF, Song CW, *et al.* Enhancement of tumor thermal therapy using gold nanoparticle-assisted tumor necrosis factor- $\alpha$  delivery. *Mol Cancer Ther* 2006;5(4):1014–1020.
5. Jian Z, Yong-Chang W, Shi-Nong Y. Fluorescence Spectrum Characteristics of Gold Nanorods. *Chin Phys Lett* 2004;21(3):559-561.
6. Sato T, Brown D, Johnson BFG. Nucleation and growth of nano-gold colloidal lattices. *Chem Commun* 1997;11:1007-1008.
7. Lee SY, Royston E, Culver JN, Harris MT. Improved metal cluster deposition on a genetically engineered tobacco mosaic virus template. *Nanotech* 2005;16:S435-S441.
8. Mukherjee P, Bhattacharya R, Patra CR, Mukhopadhyay D. Gold nanoparticles in Cancer Therapy and Diagnosis. In Kumar C, editor. *Nanotechnologies for the Life Sciences*. Weinheim: Wiley-VCH, 2007. p. 86-120.
9. Brust M, Walker M, Bethell D, Schiffrin DJ, Whyman R. Synthesis of Thiol Derivatized Gold Nanoparticles in a 2-Phase Liquid-Liquid System. *J Chem Soc Chem Commun* 1994;7:801-802.

10. Pasquato L, Pengo P, Scrimin P. Functional Gold nanoparticles for recognition and Catalysis. *J Mater Chem* 2004;14(24):3481-3487.
11. Hong R, Fernández JM, Nakade H, Arvizo R, Emrick T, Rotello VM. *In situ* observation of place exchange reactions of Gold nanoparticles. Correlation of monolayer structure and stability. *J Chem Commun* 2006;22:2347-2349.
12. Biaglow JE, Issels RW, Gerweck LE, Varnes ME, Jacobson B, Mitchell JB, *et al.* 1984 Factors Influencing the Oxidation of Cysteamine and Other Thiols: Implications for Hyperthermic Sensitization and Radiation Protection. *Radiat Res* 1984;100(2):298-312.
13. Folkes LK, Rossiter S, Wardman P. Reactivity toward thiols and cytotoxicity of 3-methylene-2-oxindoles, cytotoxins from indole-3-acetic acids, on oxidation by peroxidases. *Chem Res Toxicol* 2002;15(2):877-882.
14. Schneider G, Decher G. Functional core/shell nanoparticles via layer-by-layer assembly. Investigation of the experimental parameters for controlling particle aggregation and for enhancing dispersion stability. *Langmuir* 2008;24(5):1778-1789.
15. Decher G. Fuzzy nanoassemblies: Toward Layered Polymeric Multicomposites. *Science* 1997;277(5330):1232-1237.
16. Schneider G, Decher G. From Functional Core/Shell Nanoparticles Prepared via Layer-by-Layer Deposition to Empty Nanospheres. *NanoLetters* 2004;4(10):1833-1839.
17. Chanana M, Gliozzi A, Diaspro A, Chodnevskaja I, Huewel S, Moskalenko V, *et al.* Interaction of polyelectrolytes and their composites with living cells. *NanoLetters* 2005;5(12):2605-2612.

18. Schneider GF, Subr V, Ulbrich K, Decher G. Multifunctional cytotoxic stealth nanoparticles. A model approach with potential for cancer therapy. *Nano Lett* 2009;9(2):636-642.
19. Labouta HI, Schneider M. Tailor-made biofunctionalized nanoparticles using layer-by-layer technology. *Int J Pharm* 2010;395(1-2):236-242.
20. Decher G. Polyelectrolyte multilayers, an Overview. In: Decher G, Schlenoff GF, editors. *Multilayer thin films*. Weinheim: Wiley-VCH, 2003. p. 1-17.
21. Leamon CP, Low PS. Folate-mediated targeting: from diagnostics to drug and gene delivery. *Drug Discov Today* 2001;6(1):44-51.
22. Franklin WA, Waintrub M, Edwards D, Christensen K, Prendegast P, Woods J, *et al.* New anti-lung cancer antibody cluster 12 reacts with human folate receptors present on adenocarcinoma. *Int J Cancer Suppl* 1994;8:89-95.
23. Weitman SD, Lark RH, Coney LR, Fort DW, Frasca V, Zurawski VR Jr, *et al.* Distribution of the folate receptor GP38 in normal and malignant cell lines and tissues. *Cancer Res* 1992;52(12):3396–3401.
24. Pan J, Feng Si-S. Targeted delivery of paclitaxel using folate-decorated poly(lactide)–vitamin E TPGS nanoparticles. *Biomaterials* 2008;29(17):2663-2672.
25. Reddy JA, Low PS. Enhanced folate receptor mediated gene therapy using a novel pH-sensitive lipid formulation. *J. Controlled Release* 2000;64(1-3):27-37.
26. Stella B, Arpicco S, Peracchia MT, Desmaële D, Hoebeke J, Renoir M, *et al.* Design of folic acid conjugated nanoparticles for drug targeting. *J Pharm Sci* 2000;89(11):1452-1464.
27. Kaman B. Folate and antifolate pharmacology. *Semin Oncol* 1997;24(5 Suppl. 18):S18-30-S18-39.

28. Soloway AH, Tjarks W, Barnum BA, Rong FG, Barth RF, Codogni IM, *et al.* The chemistry of neutron capture therapy. *Chem Rev* 1998;98(6):2389-2390.
29. Fairchild RG, Bond VP. Current status of <sup>10</sup>B neutron capture therapy: enhancement of tumore dose via beam filtration and dose rate, and the effects of these parameters on minimum boron content: a theoretical evaluation. *Int J Radiat Oncol Biol Phys* 1985;11:831-840.
30. Zonta A, Pinelli T, Prati U, Roveda L, Ferrari C, Clerici AM, *et al.* Extra corporeal liver BNCT for the treatment of diffuse metastases: what was learned and what is still to be learned. *Appl Rad Isot* 2009;67:S67-S75.
31. Altirei S, Bortolussi S, Bruschi P, Chiari P, Fossati F, Stealla S, *et al.* Neutron autoradiography imaging of selective boron uptake in human metastatic tumours. *Appl Rad Isot* 2008;66:1850-1855.

## CHAPTER 3

### Materials and Methods

#### 3.1. Materials

The cationic PE poly(allylamine hydrochloride)(PAH) (MW. 15 kDa), poly(fluorescein allylamine hydrochloride)(FITC-PAH) (MW. 15 kDa), the anionic PE poly(sodium 4-styrenesulfonate)(PSS) (MW. 4.3 kDa), folic acid (Fo), sodium tetrachloroaurate(III) dihydrate ( $\text{NaAuCl}_4 \cdot 2\text{H}_2\text{O}$ ), sodium citrate tribasic dihydrate, sodium chloride (NaCl), potassium chloride (KCl), 10-boronophenylalanine ( $^{10}\text{BPA}$ ) and calcium chloride ( $\text{CaCl}_2$ ) were purchased from Sigma, Aldrich (Milan, Italy) and used without further purification. MEGM<sup>®</sup> SingleQuots medium, foetal bovine serum (FBS), foetal calf serum (FCS) and DMEM medium were purchased from Lonza (USA). For all experiments and washing steps Milli-Q (MQ) water with a resistance approximately  $18.2 \text{ M}\Omega/\text{cm}^2$  was used (if mentioned otherwise).

#### 3.2. Methods

##### 3.2.1. Gold nanoparticle preparation, coating and functionalisation

Gold nanoparticles (AuNPs) were prepared according to the technique described by Turkevich (fig. 3-1) [1]. The absorption of the colloidal gold solution was determined at  $\lambda=518 \text{ nm}$  with the UV-Vis spectrophotometer DU<sup>®</sup>730 (BeckmanCoulter, Italy). Then the concentration was calculated according to the Lambert-Beer equation using the values for  $\epsilon$  from Liu *et al.* [2] to be  $35 \pm 0.52 \text{ nM}$ . This solution was stable for at least three months without a visually significant agglomeration. The particle size was determined with a

Transmission Electron microscope (TEM) JEM-2100F (JEOL, UK) while the polydispersity index (PDI), hydrodynamic diameter and surface charge were measured by Dynamic Light Scattering (DLS) and  $\zeta$ -potential analysis on Zeta-sizer (Nano-ZS, Malvern, UK). TEM measurements showed AuNPs with a diameter of  $15 \pm 1$  nm, whilst the analysis determines the particle diameter with  $21 \pm 2$  nm. In general, DSL serves as a quality control of the preparation. Gold nanoparticles preparations with one single peak in DLS and a PDI below 0.2 were used for further experiments. The size difference between TEM and DSL can be explained by the citrate/structured water shell around the particles which stabilizes the AuNPs in solution and influences the measurement with DSL, but is not visible in TEM. In recent studies it was shown that DLS is a highly sensitive technique for the detection of aggregates [3-5].

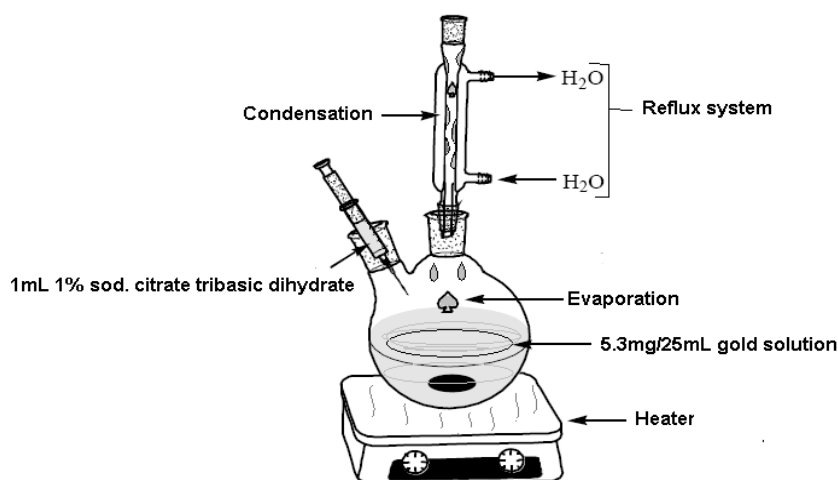


Fig. 3-1. Synthesis of 15 nm gold nanospheres with the technique of Turkevich [1].

The multilayer coating was performed according to a modified protocol of Chanana *et al.* [6]. The first 5 layers were deposited from PEs solved in pure Milli-Q-grade water. The following layers were deposited from PE solutions prepared with 0.5M NaCl. All PE solutions were prepared one day in advance. PSS was used in a supersaturated concentration of 10mg/mL, PAH with 2 or 3mg/mL, solved in either in MQ-water or 0.5M NaCl solution.

For the first layer, the AuNPs stock solution was added drop-wise under continuous vortexing either to the polycation or polyanion solution. Then the mixture was kept for 20min in the dark to allow a sufficient and homogenous coating of the nanoparticles. The protection from light is only a precaution to avoid light-induced aggregation of the AuNPs. Next the PE coated AuNPs i.e. PNGs, were washed twice in MQ-water by centrifugation 18,000×g for 30min, removal of the supernatant and re-dispersion of the pellet in MQ-water. For the next layer, the procedure was repeated with an oppositely charged PE. Again the coated AuNPs was added drop-wise to the PE solution. For the normal PNGs this procedure was repeated until the desired number of layers was reached. For fluorescently labeled PE coating on the AuNPs (FPNG), FITC-PAH (2 mg/mL) was used instead of unlabeled PAH.

The 0.5M PNGs consist of five layers were prepared according to the protocol described above with aqueous PEs but all following outer layers were prepared with PEs dissolved in 0.5M NaCl. For these layers, washing and removal of unbound PEs was performed by twice

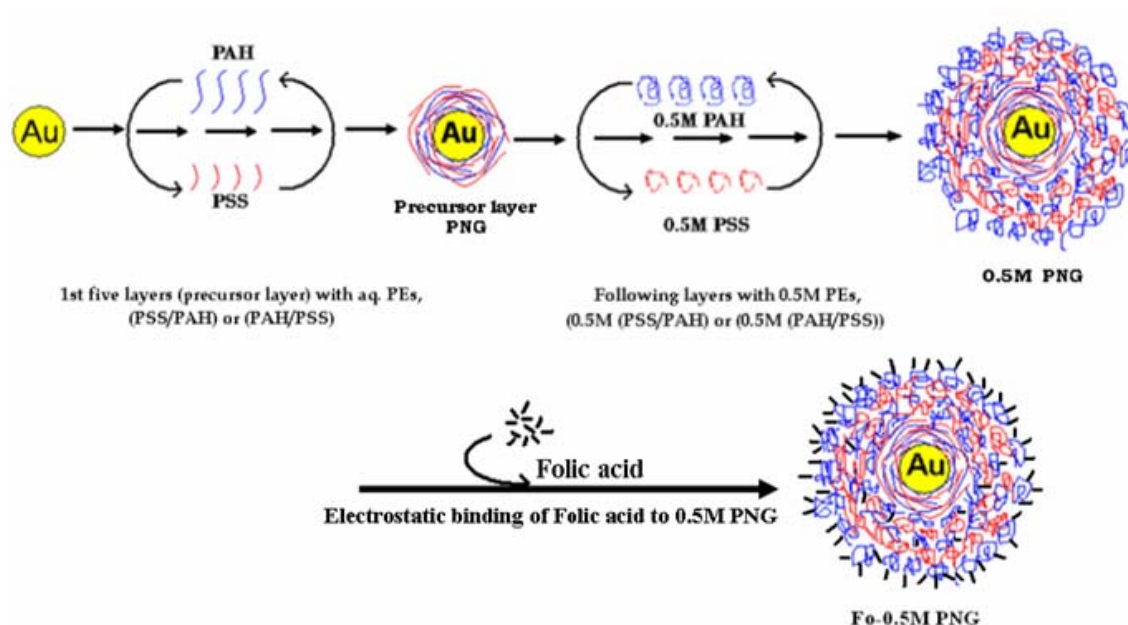


Fig. 3-2. Scheme of the multilayer PE sequence deposited on the gold nanoparticles as core according to the novel protocol and functionalisation by electrostatic binding of folate as a targeting molecule for the cancer cell.

repeating a centrifugation at 12,000×g for 30min and re-suspension in fresh 0.5M NaCl solution. The PDI value for citrate stabilized AuNPs was usually 0.192±0.017 whereas for coated particles the value varies from 0.23 to 0.27. A detailed coating procedure is schematically depicted in fig. 3-2.

For the conjugation of 10-Boron (10-B) between the layers, PSS 10 mg/mL was dissolved along with 2 mg/mL <sup>10</sup>BPA, whereas to 3 mg/mL PAH with solution 0.5 mg/ml <sup>10</sup>BPA was dissolved in MQ-water. After 5<sup>th</sup> layer, coating was done with 10 mg/mL PSS and 3 mg/mL PAH dissolved in 0.5 M NaCl solution (0.5M PEs), respectively. All the boronated polyelectrolyte (<sup>10</sup>BPE) solutions were prepared one day in advance, to get maximum boron conjugation on the PEs. The coating is done described above in this section. To differential PNGs from <sup>10</sup>BPA conjugated PNGs, they are called as <sup>10</sup>BPNG and in case of penultimate and ultimate layered 0.5M PE coated <sup>10</sup>BPNGs are termed as 0.5M <sup>10</sup>BPNGs.

For functionalized PNG for receptor-mediated up-take in cancer cells was prepared by adding drop-wise a folic acid (0.07 mg/mL) colloidal solution (solubility limit for folic acid: 1.6µg/mL) to 0.5M PNGs coated with the layer sequence [(PAH/PSS)<sub>2</sub>/PAH/(0.5 PSS/PAH)] under constant vortexing, followed by 30 minutes incubation in the dark. The particles were used after 4 washing steps. In order to visualize the folate receptor-mediated endocytosis by confocal microscopy, FPNGs with the following sequence of layers [(FITC-PAH/PSS)<sub>2</sub>/FITC-PAH/(0.5M PSS/0.5M FITC-PAH)] were functionalized with folic acid. Then the particles were stored for 2 h in the dark at room temperature before they were further characterized.

The same above procedure was followed for 0.5M <sup>10</sup>BFPNG preparation (fig. 3-3). The layering was started with <sup>10</sup>BPAH (<sup>10</sup>BPA conjugated PAH) PEs followed by <sup>10</sup>BPSS (<sup>10</sup>BPA conjugated PSS) coating and so on. The first 5 layers were coated using <sup>10</sup>BPEs solubilized in

MQ water. Following the 6th and 7th layering was with PEs dissolved in 0.5M NaCl. Thus, the sequence of layering was [(FITC-<sup>10</sup>BPAH/<sup>10</sup>BPSS)<sub>2</sub>/FITC-<sup>10</sup>BPAH/(0.5M PSS/0.5M FITC-PAH)]. The presence of folic acid on the FPNGs (Fo-FPNG) was proven by an increase in diameter in DLS, and the folic acid signal by surface enhanced Raman spectroscopy (SERS). Each measurement was repeated for a minimum of ten times.

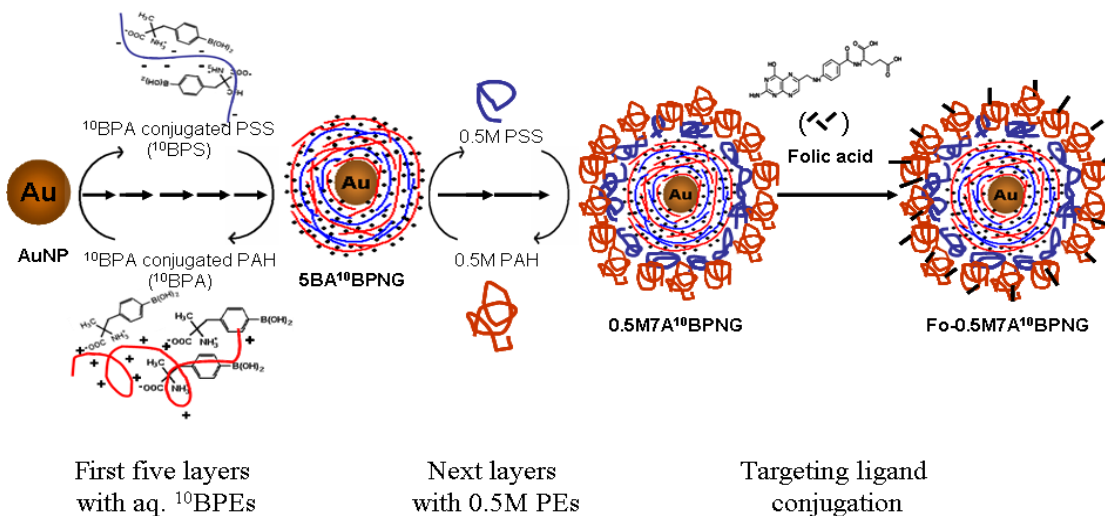


Fig. 3-3. Schematic representation of the design and synthesis of <sup>10</sup>BPA conjugated Fo-0.5M <sup>10</sup>BPNG according to the novel protocol to be used as probe for the BNCT.

### 3.2.2. Particle agglomeration by small ions

The stability of the PNGs was tested in various media. In order to study the particle agglomeration in presence of ions, coated and uncoated gold nanoparticles were centrifuged. Then the particles were resuspended in MQ-water, 0.5 M NaCl solution and Ringer's solution ([NaCl]=0.147 M, [KCl]=0.004 M, [CaCl<sub>2</sub>]=0.0033 M), respectively. After 2h, the particles were characterized by DSL. For each preparation in solution a UV-Vis spectrum was recorded because bigger particles or aggregates usually show a color change from wine red to blue or black precipitates. Each measurement was repeated for a minimum of five times.

In order to study the stability of Fo-0.5M PNG in serum, 2.5pM Fo-0.5M PNG was incubated in 10% BSA for 2h at room temperature, followed by DLS studies. The experiments were repeated at least three times.

### **3.2.3. Surface characterization by SERS and Raman measurements**

SERS spectroscopy yields information about the molecules adsorbed on the gold surface. The vibrational Raman spectra of molecules or molecular moieties in direct contact to certain metals can be strongly enhanced [7-8].

The adsorption of one or two PE layers onto the surface of AuNP was followed by SERS measurements with a Raman system (Renishaw plc, Wotton-under-Edge, UK). The laser (632.8 nm He-Ne laser, Melles-Griot, Albuquerque NM, USA) was focused by a 10× objective (0.25 NA) on the sample, consisting of a 10μL drop of AuNP dispersion (previously concentrated upon centrifugation) on a CaF<sub>2</sub> slide (OEC Optoelectronic Components GmbH, Zusmarshausen, Germany) for SERS measurements or aqueous solutions of PSS (80mg/mL), PAH (160mg/mL) or sodium citrate (160mg/mL) for normal Raman measurement. The laser power at the sample was 15mW. The total acquisition time was 30s per spectrum.

In order to understand if folic acid is binding stably to the AuNPs were coated only with one PAH layer followed after washing by immersion of the coated particles in folic acid and investigation in SERS. It was necessary to limit the number of polyelectrolyte layers to one between the gold surface and the folic acid because SERS signals can be measured only close to the gold surface. However, the electrostatic folic acid binding to polycation layers other than the first is supposed to be comparable. SERS measurements of the Fo-PNG were performed with an excitation wavelength of 785nm (Renishaw HP-NIF diode laser) and a

laser power at the sample 90 mW. For comparison the pure folic acid crystals were measured by Raman spectroscopy.

#### **3.2.4. Cellular nanoparticle up-take**

For the folate receptor-mediated up-take of Fo-FPNGs, VP229 and MDA MB 231 (breast cancer cell lines, ECACC and ATCC HTB 26, Sigma-Aldrich, Milan, Italy) were seeded onto 22 X 22 mm cover-slips to a density of  $10^5$  cells per plate in MEGM, supplemented with glutamine and 2% FCS but without antibiotics and DMEM medium supplemented with 10% heat-inactivated FBS, penicillin (100units/ml), streptomycin (100 $\mu$ g/ml) and gentamicin (10 $\mu$ g/ml). They were grown for 24h in an incubator at 37°C and 5% CO<sub>2</sub>, prior to treatment. The cells were then incubated for 2h along with FPNGs or Fo-FPNGs at the concentration of 2.4pM and 2.6pM, respectively. After washing twice with serum-free medium, time-relapsed confocal fluorescence microscopic studies were performed to visualized FPNGs and Fo-FPNGs uptake by the cells. The experiments were repeated at least three times on each cell line.

In order to exclude other mechanisms than folate-receptor mediated up-take a competition study with free folic acid was performed. For this,  $2 \times 10^5$  cells/mL breast cancer cells (MDA MB 231) were seeded on a microscopic slide and incubated for 24h at 37°C and 5% CO<sub>2</sub> in serum containing medium, with different concentrations (0.567, 2.27, 4.54, 9.08, 18.16 and 27.24nM) of folic acid and 2.23pM Fo-FPNGs. After washing with serum-free medium, confocal fluorescence microscopic studies were performed to visualize Fo-FPNGs internalized in cells. From one slide at least 15 regions of interest were taken for the calculation. The experiments were repeated at least for three times.

The immune recognition of the coated particles was tested with a macrophage cell line as model system for immune response. The macrophages cell line, J774.2 (ECACC, Mouse BALB/C monocyte macrophage) (a generous gift from Prof. A. Nistri, Neurobiology sector, SISSA) ( $4 \times 10^4$  cells/ml) were grown on 22 X 22 mm cover-slips in Petri-dishes. They were grown for 24h in an incubator at 37°C and 5% CO<sub>2</sub>. The cells were rinsed with DMEM medium, followed by incubation for 4h with Fo-0.5 M FPNGs (2.4pM) or with 0.5M FPNGs (2.9pM). The cells were rinsed three times as described above. Time-lapse confocal fluorescence microscopy was performed to visualize the uptake of these particles by the cells. Each experiment was repeated five times (for each experiment ~1000 cells were studied). Statistical analysis was performed by SigmaStat and Origin8 software.

Image acquisition was preformed with a Nikon C1*si* laser scanning confocal unit (Nikon D-eclipse C1, Japan) attached to an inverse fluorescence microscope (Nikon D-eclipse C1, Japan) with 100X/1.49 oil Apo TIRF objective (Nikon, Japan). Excitation was performed with an air-cooled argon laser emitting at 488 nm and appropriate filter sets were used to collect the fluorescence emission. Images were acquired and processed using the NIKON software EZ-C1.

### **3.3. References**

1. Turkevich J, Stevenson PC, Hillier J. A study of the nucleation and growth processes in the synthesis of colloidal gold. *J Disc Farad Soc* 1951;11:55-75.
2. Liu X, Atwater M, Wang J, Huo Q. Extinction coefficient of gold nanoparticles with different sizes and different capping ligands. *Colloids Surf B Biointerfaces* 2007;58(1):3-7.
3. Ahonen P, Laaksonen T, Nykänen A, Ruokolainen J, Kontturi K. Formation of stable Ag-nanoparticle aggregates induced by dithiol cross-linking. *J Phys Chem B* 2006;110(26):12954-12958.
4. Soman CP, Giorgio TD. Quantum dot self-assembly for protein detection with sub-picomolar sensitivity. *Langmuir* 2008;24(8):4399-4404.
5. Bogdanovic J, Colon J, Baker C, Huo Q. A label-free nanoparticle aggregation assay for protein complex/aggregate detection and study. *Anal Biochem* 2010;405(1):96-102.
6. Chanana M, Gliozzi A, Diaspro A, Chodnevskaja I, Huewel S, Moskalenko V, *et al.* *NanoLetters* 2005;5(12):2605-2612.
7. Chang RK, Furtak TE. *Surface Enhanced Raman Scattering*. Plenum Press: New York, 1982.
8. Edwards HGM, Brown DR, Dale JA, Plant S. Raman spectroscopy of sulfonated polystyrene resins. *Vibr Spectr* 2000;24(2):213-224.

## CHAPTER 4

### Results and Discussion

#### 4.1. Surface characterization by SERS and Raman measurements

In order to understand the binding of the first PE layer, SERS measurements were performed. Raman and SERS experiments give information about the orientation and composition of the molecules adsorbed directly onto the surface of metal (most commonly Ag or Au) nanoparticles.

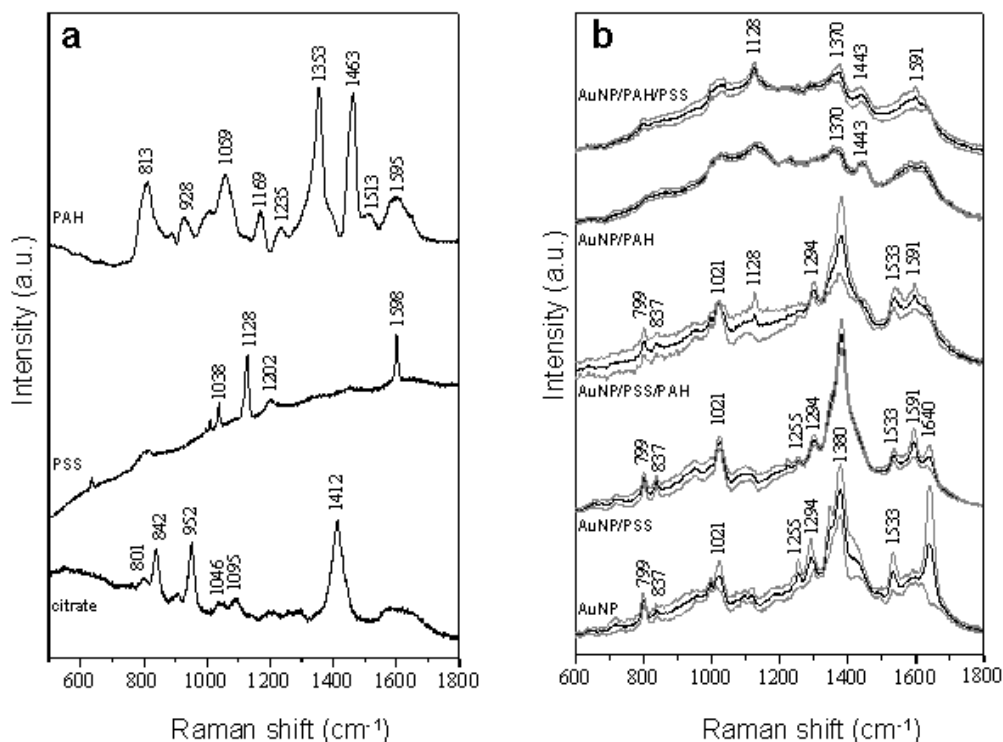


Fig. 4-1. (a) Normal Raman spectra of citrate, PSS and PAH (bottom to top) measured in water. (b) SERS spectra of uncoated and coated AuNP. For SERS spectra, average spectra (over 4 samples) are reported as black lines, and standard deviations as gray lines. The excitation wavelength was 632.8 nm and the power at the sample was 15 mW. Acquisition time was 30s.

In fig. 4-1a the normal Raman of sodium citrate, PSS and PAH aqueous solutions are reported, together with the average SERS spectra of citrate stabilized AuNPs and AuNP coated with PAH or PSS (fig. 4-1b). The SERS spectrum of citrate stabilized AuNP is in substantial agreement with those previously reported in literature [1]. The intense SERS bands corresponding to the anti-symmetric ( $1640$  and  $1533\text{ cm}^{-1}$ ) and symmetric ( $1380\text{ cm}^{-1}$ ) stretching of citrate carboxylates are down-shifted with respect to the normal Raman spectrum, indicating an adsorption on the metal surface via the  $\text{COO}^-$  moieties. The presence of intense bands for both anti-symmetric and symmetric stretching suggests a variability of orientations for the adsorbed citrate, in which the carboxylate moieties are oriented with the line joining the two oxygen atoms both parallel and perpendicular to the metal surface [2].

The SERS spectrum of PSS-coated AuNP (AuNP/PSS) show a striking similarity with that of citrate stabilized AuNP, indicating the persistence of the adsorbed citrate layer on the gold surface upon the addition of PSS. In spite of this resemblance, some significant differences were observed, such as, the emergence of a band at  $1591\text{ cm}^{-1}$  and the decrease in intensity of the band at  $1640\text{ cm}^{-1}$ . The band at  $1591\text{ cm}^{-1}$  can be attributed to the aromatic C-C stretching of the PSS benzene ring, which is present as an intense and narrow band at  $1598\text{ cm}^{-1}$  in the normal Raman spectrum of PSS [3]. The occurrence of this band suggests the presence of the PSS near the metal surface. Moreover, SERS spectra of AuNP/PSS show less variability than those of citrate stabilized AuNP, as indicated by the respective intensity standard deviations in the spectral regions of the anti-symmetric and symmetric carboxylate stretching (depicted as grey lines in Fig. 4-1, right panel). This observation suggests that the adsorption of PSS perturbs the pre-existing citrate layer, inducing the adsorption of citrate molecules onto the gold with the carboxylates having a preferential orientation with the line joining the two oxygen atoms parallel to the surface. The presence of PSS on the citrate-

coated particle surface is inferred from both indirect (fig.4-1b, AuNP/PSS) and direct (fig. 4-1b, AuNP/PSS/PAH) experimental evidences. The electrostatic repulsion between the citrate-coated surface and PSS is likely to be shielded by the well-known "counterion condensation" effect, which can even lead to a counter-intuitive phenomenon of an attractive interaction between like-charged PEs or nanoparticles [4-6].

The addition of PAH as second layer in AuNP/PSS/PAH samples significantly perturbs the pre-existing layers (fig. 4-1b), as shown by its SERS spectrum (fig. 4-1a). The spectral features due to the adsorbed citrate are still present, indicating the persistence of the citrate layer, but the intensity standard deviation increases upon PAH binding. Additionally, the PSS layer is still present, as suggested by the PSS band at  $1591\text{ cm}^{-1}$ . Interestingly, a band appears at  $1128\text{ cm}^{-1}$  upon PAH binding. Due to the uncertain assignment of this band, it is difficult to postulate about the nature of this interaction, which needs further investigation.

On the other hand, the citrate layer appears to be displaced by PAH in AuNP/PAH samples, as indicated by the SERS spectrum (fig. 4-1b). In fact, in the spectra of AuNP/PAH, the characteristic carboxylate stretching bands, which are due to citrate, disappear, and are replaced by a group of weak and broad bands, which are in agreement with previously reported PAH SERS spectra [3, 7]. These bands are difficult to assign to PAH vibrations. The two broad bands at  $1370$  and around  $1600\text{ cm}^{-1}$  could be due to the formation of amorphous carbon upon laser irradiation [8] which are often observed in SERS spectra of polymers. On the other hand, the  $1300\text{-}1700\text{ cm}^{-1}$  region in the SERS spectrum of PAH bears some resemblance to the normal PAH Raman spectrum, with SERS bands at  $1600$ ,  $1443$  and  $1370\text{ cm}^{-1}$  corresponding to the normal Raman bands at  $1595$ ,  $1463$  and  $1353\text{ cm}^{-1}$ . Indeed, the band at  $1600\text{ cm}^{-1}$  could be due to the vibrations of the  $\text{-NH}_2$  groups of PAH which interact with the metal surface. In fact, amino groups are known to have a stronger affinity for metals

rather than carboxylates [9], and therefore PAH is likely to displace citrate, by adsorbing directly onto the gold surface via its  $-NH_2$ . This latter hypothesis is supported by the SERS band at  $1443\text{ cm}^{-1}$ , which can be assigned to the bending or the  $-CH_2-$  groups of PAH backbone [10].

The SERS spectrum of AuNP/PAH/PSS is almost identical to that of AuNP/PAH, indicating that the addition of PSS does not significantly perturb the pre-existing PAH layer. The presence of an additional PSS layer, however, is inferred from the appearance of the two weak bands at  $1128$  and  $1591\text{ cm}^{-1}$ , which are attributed to the S=O stretching of the undissociated form of PSS and to the aromatic C-C stretching of the PSS benzene ring. It is interesting to note that in all the samples in which PSS is associated with PAH (i.e. in AuNP/PSS/PAH and AuNP/PAH/PSS) the band at  $1128\text{ cm}^{-1}$  is present, whereas in AuNP/PSS it is absent. This observation was also observed in case of AuNP/PSS/PAH.

#### **4.2. Synthesis of non-aggregating polyelectrolyte multilayer PNGs**

Although surface-functionalized PNGs are good candidates for targeted drug delivery or therapeutic approaches as in local radio- and hyperthermal therapy for cancer treatment, the major obstacle in its use, is its low stability against aggregation in presence of ions and its low shelf life due to light induced agglomeration.

In order to overcome particle aggregation, which could be due to bridging flocculation induced by a mismatch of particle size and PE length or incomplete PE attachment to the particle surface, the PEs were pre-incubated in a  $0.5\text{ M NaCl}$  solution. This causes the collapse of the polyions from extended chains (because in water, polyions are fully charged and this imparts a repulsion between the single monomers and hence maximally extension) to random coils. It was observed that for up to the first 5 layers, coating with  $0.5\text{ M NaCl}$  solved

PE (0.5M PEs) induced immediate aggregation because of the presence of the ions. This was proven by instant colour change from red to blue and a drastic increase in the particle diameter to >3000 nm as measured by DLS.

In contrast if the first layers are deposited from water solved PE solutions and the latter layers are deposited from a 0.5M PE solution, no colour change was detected. The surface charge (fig. 4-2a) and hydrodynamic diameter (fig. 4-2b) versus the number of layers on the AuNP prepared according to the novel protocol were measured by DSL and  $\zeta$ -potential. It was noted that the hydrodynamic diameter of the PNGs became larger, when coating was accomplished by the deposition of 0.5M PEs (0.5M PNGs) (fig. 4-2b) rather than the aq. PEs (aq. PNGs) (inset in fig. 4-2b). This is in good agreement with the hypothesis that the PE is binding as a collapsed random coil to the PNG surface. In addition, the large increase in diameter is

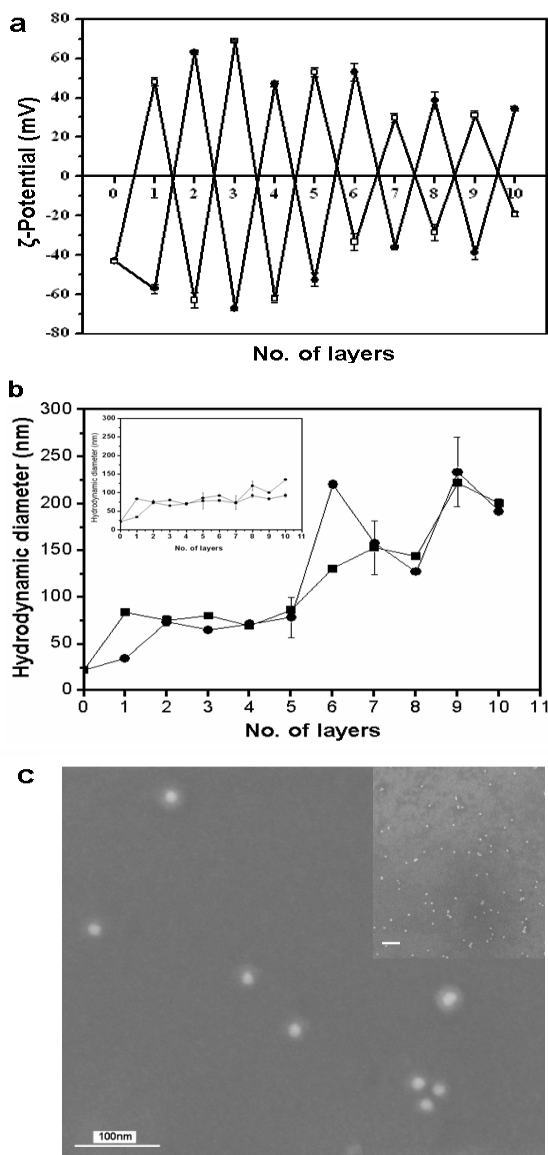


Fig. 4-2. (a)  $\zeta$ -potential versus No. of deposited layers during 0.5M PNGs preparation. The arrows indicate the change in the encapsulation method from aq. PEs to 0.5M PEs deposition. The circles represent the surface charge on the PNGs at every step of the preparation starting with PSS, whereas the squares represent the surface charge on the PNGs, starting with PAH as layer 1<sup>st</sup> layer. (b) Hydrodynamic radius versus No. of layers according to the novel 0.5M PNG preparation protocol. Inset: Hydrodynamic radius versus No. of layers during the aq. PNG preparation protocol with all layers deposited from aq. PEs.

not due to particle aggregation was verified from the SEM images (fig. 4-2c & inset). Moreover, it was observed that with the deposition of PSS, solved in 0.5 M NaCl (0.5M PSS) as 6<sup>th</sup> layer, the surface charge significantly decreased from -60 mV for the 4<sup>th</sup> layer to -40 mV for the 6<sup>th</sup> layer while for PAH the value of +50 mV is the same for the 4<sup>th</sup> and the 6<sup>th</sup> layer (fig. 4-2a). A possible explanation could be the nature of the underlying 5<sup>th</sup> layer, which in case of PSS as 6<sup>th</sup> layer, is composed of PAH. PAH is more sensitive to counter ions because it is a weak polyion. Once in contact with the 0.5M PSS solution containing Na<sup>+</sup> and Cl<sup>-</sup>, Cl<sup>-</sup> ions most probably penetrate the layer and shield some of the positive charges of PAH. This will reduce the number of polyanions, binding as next layer. However, in the case of PAH as a 6<sup>th</sup> layer, the situation is different. PSS (5<sup>th</sup> layer) is a strong PE and is not affected by the presence of counter ions [11]. Thus, the negative surface charge remains unaffected. Nevertheless, the shielding ions in the collapsed polycation causes a reduced number of free charges in PAH in comparison to aq. PAH and hence a significantly higher amount of 0.5M PAH binds to over-compensate the negative charge of the underlying layer. This explanation, was supported by the fact that a significant increase in the hydrodynamic diameter of PNG was observed when PNG were coated with 0.5M PSS as the 6<sup>th</sup> layer as determined by DSL (fig. 4-2b). In the SEM image shown in fig. 4-2c, the thickness of the collapsed polymeric shell (bright rim around the AuNP) completely deprived by water can be estimated to be 8 nm.

### **4.3. Stability of aq. PNGs and 0.5M PNGs against aggregation in presence of small ions**

As shown by Schneider and Decher [12], the presence of ions (NaCl or Ringer solution) causes immediate aggregation of citrate-stabilized AuNP (fig. 4-3 & 4-4a) or aq. PNG (fig 4-

3 & 4-4b to c). The particle's hydrodynamic diameter (fig. 4-3) shows a strong increase, indicating particle aggregation, especially for AuNP and PNGs in Ringer solution. This is supported by the observation that the absorption spectrum for AuNP (fig. 3-4a) and PNGs (fig. 4-4b, c) has a red shift of the spectra. Moreover, in case of AuNP the peak intensity decreases dramatically, indicating that most particles disappear from the solution (fig. 4-4a) while in the case of aq. PNG, the decrease in the intensity of absorbance was not so prominent. However, most of the particles are

Fig. 4-4. The stability analysis of AuNPs and aq. PNGs by UV-Visible spectrophotometer studies, after 2h incubation at RT in respective solutions. (a) Absorption spectrum of mono-dispersed AuNPs in MQ-water (solid line), in 0.5M NaCl solution (dashed line) & Ringer's solution (dotted line). (b) Absorption spectrum of aq. 7S PNG, (with [(PSS/PAH)<sub>3</sub>PSS] layer pattern) in MQ-water (solid line), in 0.5M NaCl solution (dashed line) and in Ringer solution (dotted line). (c) Absorption spectrum of aq. 7A PNG, where AuNPs coated as [(PAH/PSS)<sub>3</sub>PAH] (solid line) in MQ-water, in 0.5M NaCl solution (dashed line) and in Ringer solution (dotted line.). All the absorption spectra were presented after base subtraction to visualise properly the red shift due to aggregation.

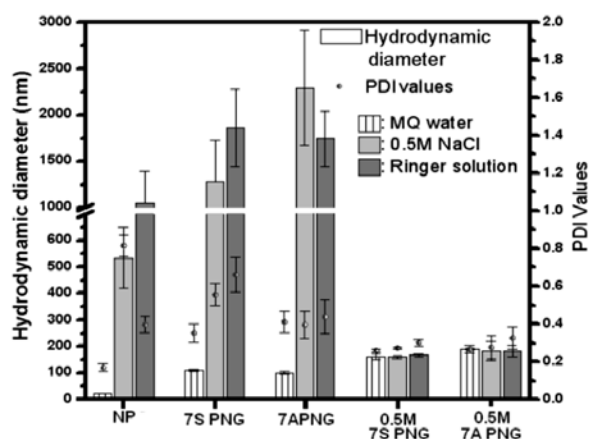
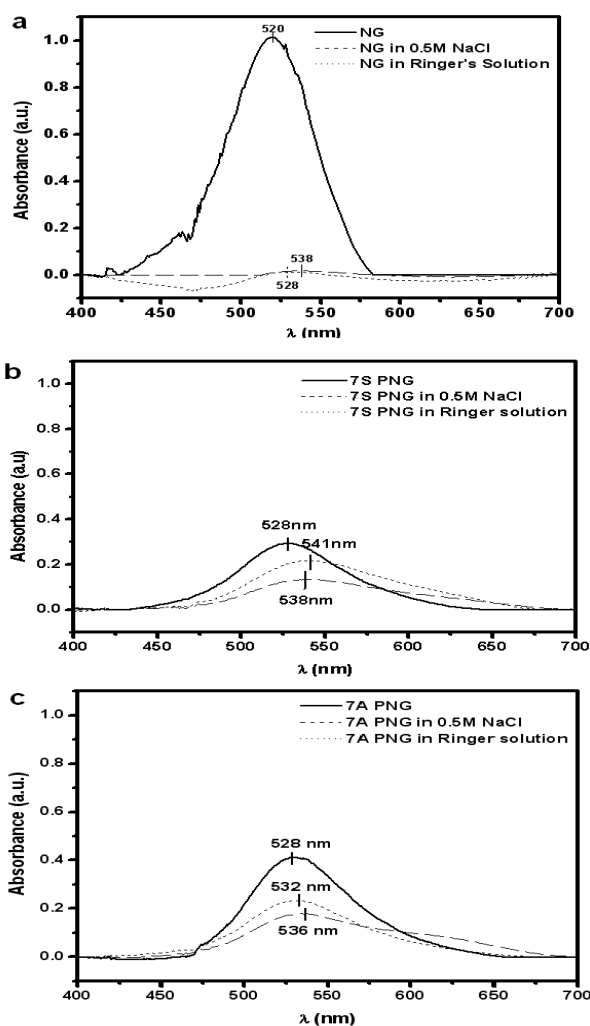


Fig. 4-3. (a) Agglomeration of NGs, PNGs and 0.5 M PNGs in absence or presence of small ions. The particle diameter was measured in MQ water, 0.5 M NaCl, or Ringer's solution. DLS measurement of the hydrodynamic diameter (columns) and the PDI (circles) versus particle preparation and stored in different solutions.



observed to precipitate after incubation and the remaining measurable PNGs are influenced by the ions in solution, as deduced from the red shift in the absorption spectrum (fig. 4-5b, c).

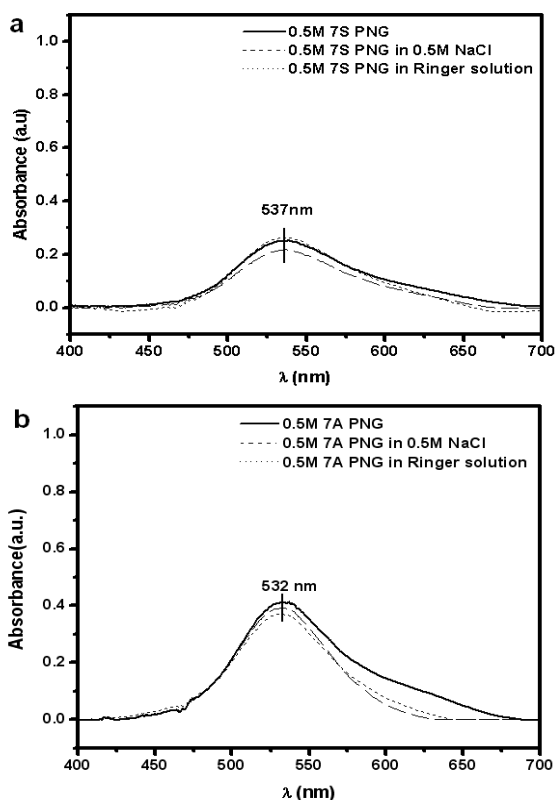


Fig. 4-5. The stability analysis of 0.5M PNGs by UV-Visible spectrophotometric studies, after 2h incubation at RT in respective solutions. (a) Absorption spectrum of 0.5M 7S PNG, where AuNPs coated as [(PSS/PAH)<sub>2</sub>PAH/0.5M PSS/0.5M PAH] in MQ-water (solid line), in 0.5M NaCl (dashed line) and in Ringer solution (dotted line). (b) Absorption spectrum of 0.5M 7A PNG, where AuNPs coated as [(PAH/PSS)<sub>2</sub>PSS/0.5M PAH/0.5M PSS] in water (solid line), in 0.5M NaCl solution (dashed line) and in Ringer solution (dotted line). All the absorption spectra were presented after base subtraction to visualise properly the red shift due to aggregation.

Here, the effect of the novel preparation protocol was even more striking (fig. 4-3 & 4-5). The 0.5M PNGs (fig. 4-5a) do not aggregate in ion-containing solutions. This is concluded from the fact that the absorption spectrum of the coated 0.5M PNG in ionic solution does not show any shift (fig. 4-5b) as well as that no significant increase in diameter can be observed in DLS. This highlights that 0.5 M PNGs are significantly more stable in medicinal solution (Ringer's solution).

The improved stability of particles coated by 0.5M PE, cannot be explained by electrostatic repulsion, since the surface charge decreases, as measured by the zeta-potential.

In a model proposed for the layer-by-layer technique it was assumed that the first

“precursor” layers on flat surfaces differ from latter layers because the deposition is still influenced by the template [13]. Moreover these layers are supposed to contain small counter ions and they are charged. We assume that the same is true for curved templates like gold nanoparticles. From the experiments we deduce that on NG the first 5 layers are precursor layers and that they are more prone to be affected by small counter ions. Then probably the

neutral layers from zone II stabilize the capsule and the exposure to small ions did not cause agglomeration any longer [14].

Bridging flocculation due to the excess length of one of the polyelectrolytes was the main reason Schneider and Decher identified for the nanoparticle agglomeration caused by small ions [12]. It is known that the polycation PAH in presence of a concentration higher than 0.3 M NaCl collapse into a random coiled structure [14]. This can explain why we observe an increased stability against agglomeration of nanoparticles coated with PEs from a 0.5 M NaCl solution while their equivalent particles coated from pure water aggregate. Thus, a possible explanation for the higher stability can be that the collapsed structure of the PEs prevents bridging flocculation.

#### **4.4. Electrostatic functionalisation of 0.5M FPNG with folic acid for cancer cell targeting**

The electrostatic binding of folic acid was assayed as an example for targeting cancer cells. In order to orientate the folic acid molecules in the way that it binds with the  $\alpha$ - and  $\gamma$ -COOH (glutamic acid moiety) to assures receptor recognition [15] through free pteronic acid moiety (see fig.1-21 of part1 overview chapter) and to follow the particle up-take in real-time, the folic acid (Fo) was bound to fluorescently labelled 0.5M FPNGs with a positive surface charge. An increase in the hydrodynamic diameter from  $174\pm 5$  nm to  $213\pm 14$  nm of 0.5M FPNG [(FITC-PAH/PSS)<sub>2</sub> FITC-PAH/ 0.5M PSS/0.5M FITC-PAH] and decrease in the surface charge from  $32.4\pm 0.6$  mV to  $19\pm 3.5$  mV was observed upon folic acid binding (Fig. 4-6a).

Folic acid absorbs in the UV region with absorption peaks at 280 and 350 nm. The absorption spectrum of Fo-0.5M FPNGs shows prominent peaks at these wavelengths,

confirming the binding of Fo, in conjunction with the absorption peak at 533 nm for 0.5M FPNGs (Fig. 4-6b).

Furthermore the presence of folic acid was confirmed by SERS. Because of the short-range of the SERS effect the spectrum of AuNP coated with only 1 layer of PAH and folic acid was measured (Fig. 4-7a). The spectrum shows intense bands, which are very similar in both, relative intensity and frequency, to those of the normal Raman spectrum of folic acid.

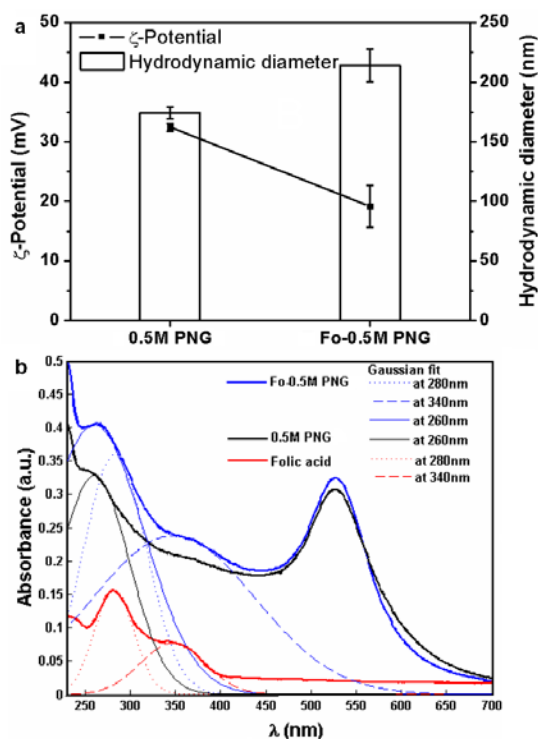


Fig. 4-6. (a) Hydrodynamic diameter and zeta potential of the coated 0.5M FPNG before and after folic acid binding. (b) UV/VIS-spectrum of the coated 0.5M FPNG before (black bold line) and after folic acid binding (blue bold line), along with pure Fo spectra (red bold line). Gaussian fit represent the major peaks of folic acid alone (red, dashed line for 350nm; dotted line for 280nm), spectra from Fo-0.5M PNGs (blue, solid line at 260nm coming from the coated particle, whereas dotted line for 280nm and dashed line for 350nm coming from bound folic acid); of 0.5M PNGs (black, solid line).

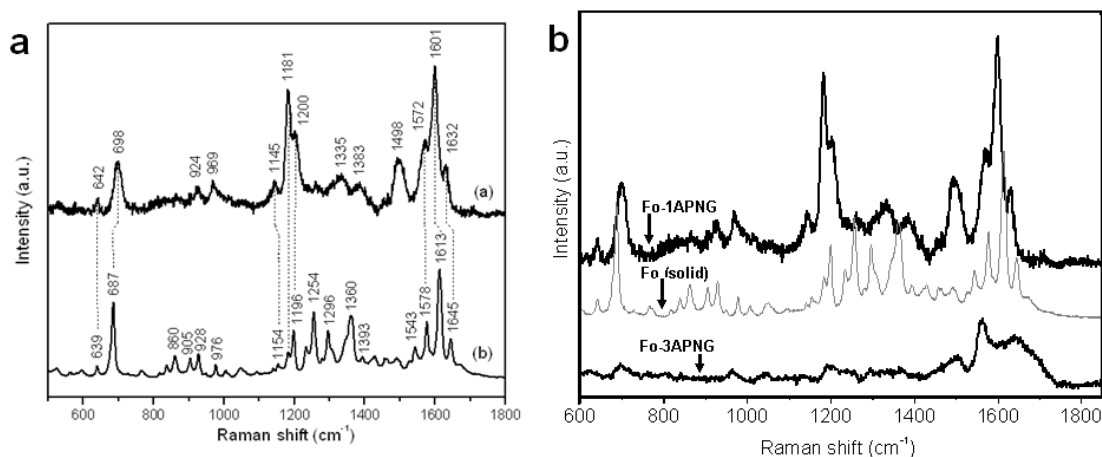


Fig. 4-7. SERS spectrum of Fo conjugated PNG. (a) Fo-PNG only with 1 layer of PAH followed by folic acid binding, [(PAH)-Fo] (top); normal Raman spectrum of folic acid (powder) (bottom). (b) Fo-PNG only with 1 layer as [(PAH)-Fo] (Fo-1APNG) (top); normal Raman spectrum of folic acid (powder) and 3 layered PNG [(PAH)/PSS/(PAH)-Fo] (Fo-3APNG) (bottom). Excitation was at  $\lambda=785$  nm, power at the sample 90 mW.

Moreover, it is significantly different from the SERS of PAH-coated nanoparticles. These findings clearly indicate that folic acid is adsorbed onto the surface of the AuNPs. Experiments with folic acid attached to the 3<sup>rd</sup> layer did not give any signal in SERS (fig. 4-7b). From this observation it was deduced that folic acid was not able to penetrate deeply into the PE matrix but remained attached to the surface otherwise a signal from folic acid molecules which come close to the surface must be visible as SERS is a highly sensitive technique. Despite some differences, most likely due to the different nature of the surface, the SERS spectrum of folic acid on PAH-coated AuNPs shares many spectral features with the SERS spectrum of folic acid on silver nanoparticles, as recently reported by Stokes *et al.* [16].

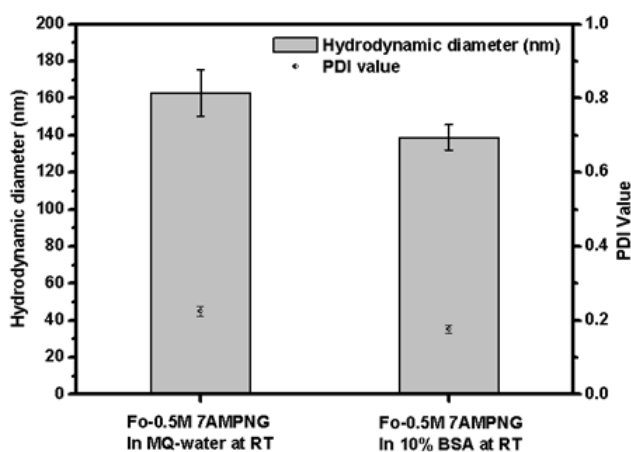


Fig. 4-8. 10% BSA stability analysis by DLS measurement of Fo-0.5M PNGs. The graph represents hydrodynamic diameter (columns) and the PDI (half black circles) versus particle preparation and stored in different solutions.

The stability study of Fo-0.5M PNG in 10% BSA ((fig. 4-8), shows a decrease in the hydrodynamic diameter of coated particles from 163±12 nm to 139±7nm, along with an improved PDI value from 0.225±0.015 to 0.179±0.011. This

indicates that BSA induces a compaction of the polymeric layer on the AuNP surface.

#### 4.5. Target specific internalization of Fo-0.5M FPNGs in cancer cell lines

The receptor-mediated endocytosis by folate receptors is known to guide the content directly to the nucleus (fig. 4-9a, schematic diagram) [17]. In fig. 4-9b, a representative

image visualized by confocal fluorescence microscopy, shows the endocytosis of Fo-0.5M FPNG into VP229 breast cancer cells. Due the fact that the cells were not synchronized,

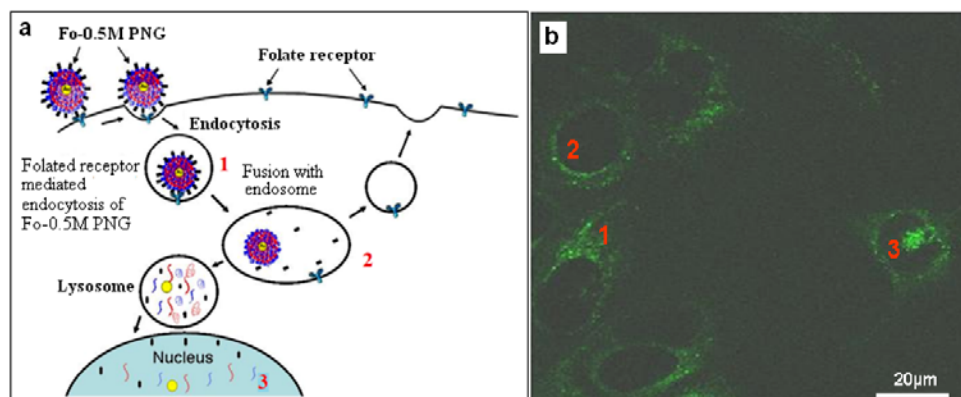


Fig. 4-9. (a) Scheme of the folate-receptor endosomal pathway. (b) Confocal micrograph of VP229 (breast cancer) cell line internalizing Fo-FPNG by folate-receptor mediated endocytosis. Red arrows are indicating aggregates of Fo-FPNGs. The numbers correspond to different steps of internalization depicted in the scheme in (a).

different cells are in different stages in the endosomal pathway (as in scheme and tags of fig. 4-9a). The cells tagged as 1 represent particle bearing endosomes (green) still homogeneously distributed within the cytosol. The endosomes in cells with the tag 2 show particle accumulation closer to the nucleus. Whereas, in the cells tagged as 3, it was observed that the particles are released into the nucleus (fig. 4-9b).

The uptake of Fo-0.5MFPNG was followed in two different breast cancer cell lines, i.e.

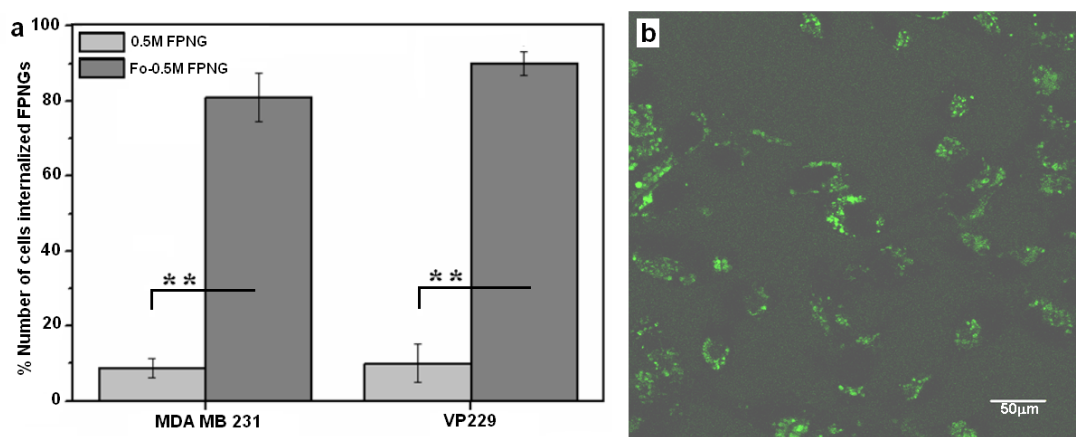


Figure 4-10. (a) Statistical analysis of cells with internalised FPNG with and without folic acid in two breast cancer cell lines displayed as a % of the cells with internalised FPNG. (b) Confocal micrograph of MDA MB 231 cells internalizing Fo-FPNG. Each experiments were repeated 3 times.

VP229 and MDA MB 231. It was observed that Fo functionalised 0.5M FPNGs (Fo-0.5MFPNGs) for receptor-mediated endocytosis, leads to a significantly ( $p \leq 0.001$ ) higher number of cells with internalised FPNGs than for FPNGs without Fo (fig. 4-10).

That the uptake is related to a folate receptor-mediated internalization was supported by the finding that if the folic acid functionalized particles are incubated with the MDA MB 231 cells in presence of increasing concentrations of folic acid the number of cells with internalized nanoparticles decreases (fig. 4-11).

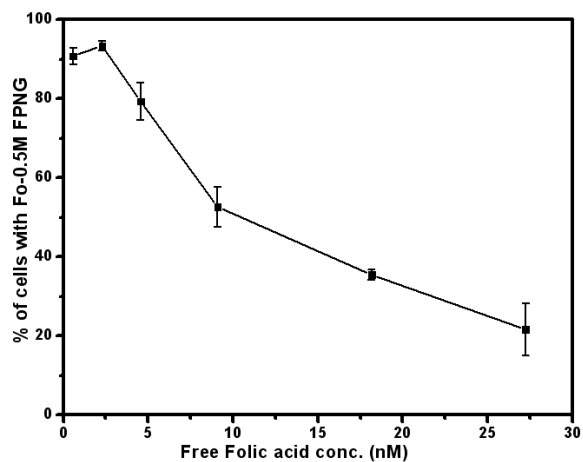


Figure 4-11. Binding competition assay of Fo-0.5M FPNG uptake in the presence of different concentrations of free folic acid. Each data point is the result of 3 independent experiments.

#### 4.6. Non-specific internalization of Fo-0.5M FPNGs in macrophage cell line

Macrophage recognition (i.e. innate immunological response) of charged nanoparticles is

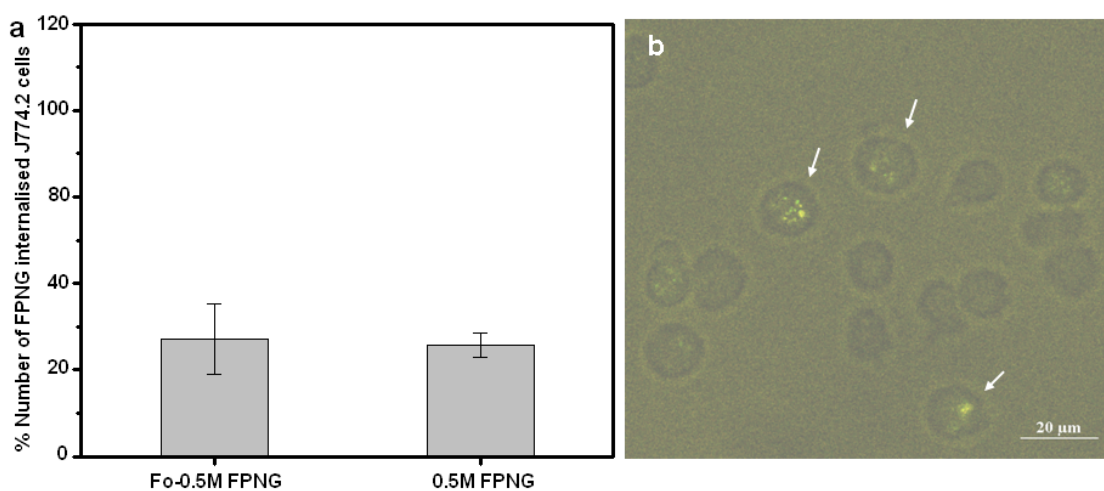


Figure 4-12. Non-specific uptake analysis in macrophage cell line (J774.2). (a) Statistical study of the % of the marked cells with internalised fluorescent 0.5M FPNGs or Fo-0.5M FPNGs (student 't' test,  $**P \leq 0.001$ ) ( $n=5$ ). (b) Confocal image showing macrophage cells treated with Fo-FAPNGs (Green). White arrow indicates cells which had internalised nanoparticles.

the main reason for the fast clearance of these drug delivery systems from the blood. Therefore, I evaluated the non-specific uptake of Fo-0.5MFPNGs and 0.5MFPNGs by means of confocal fluorescence microscopy, in non-activated macrophages after 24h after incubation. I found that only ~27% & ~25% of the macrophages show endocytosis of the Fo-FPNGs and FPNGs after 24h, respectively (fig. 4-12). As can be observed that number of particle containing endosomes in macrophage cell line (fig. 4-12b) were lower than in folate-receptor expressing cancer cell lines (fig. 4-9b). A possible explanation for this low up-take which is the same range than the up-take of coated nanogold without folic acid is that it is unspecific endocytosis or pinocytosis rather than receptor-mediated endocytosis because the macrophages do not have a folate-receptor. These results show that with folic acid coated nanoparticles a target specific delivery is possible while avoiding fast clearance from the blood.

#### **4.7. Boron conjugation within the layers of Fo-0.5M PNG as probe for BNCT**

##### **4.7.1. Synthesis of Fo-<sup>10</sup>BPNG and its stability in different solutions**

PNGs is a good candidate for targeted drug delivery. In the following a protocol was described for the Boron-10 (as <sup>10</sup>BPA) uploading in the PE multilayer matrix of targeted PNGs as probes and boron delivery system for BNCT in cancer treatment.

In order to maximize 10B loading on PNGs, both the PEs were electrostatically conjugated with <sup>10</sup>BPA (<sup>10</sup>BPEs). In fig. 3-3, the layer by layer coating of AuNP and targeting molecule conjugation is schematically depicted. The coating was performed by <sup>10</sup>BPAH (<sup>10</sup>BPA electrostatically bind with polyallylamine hydrochloride) PEs and <sup>10</sup>BPSS (<sup>10</sup>BBPA electrostatically bind with polystyrene sulfate) deposition. In order to prevent particle aggregation in presence of ionic media or blood fluids the first 5 layers were

constructed with  $^{10}\text{BPEs}$  solved in MQ water. Two final layer were deposited from pure PEs solved in 0.5 M NaCl to avoid exposure of  $^{10}\text{BPA}$  on the shell surface because it induces uptake in normal proliferating cells as well as to avoid aggregation.

The PNG hydrodynamic size and the surface charge versus the number of layers of coated AuNPs (AuNPs) prepared according to the novel protocol (described in the main part) was measured by Dynamic Light Scattering (DSL) and  $\zeta$ -potential (surface charge) analysis (Fig. 4-13a). The behavior of the boron containing polyion layers is exactly the same as observed for the pure PE layers. This is somehow surprising because the electrostatic interaction between the BPA and the polyelectrolyte should have an effect like ionic strength, hence changing the structure and the layer thicknesses of the PE layers. It is possible that the

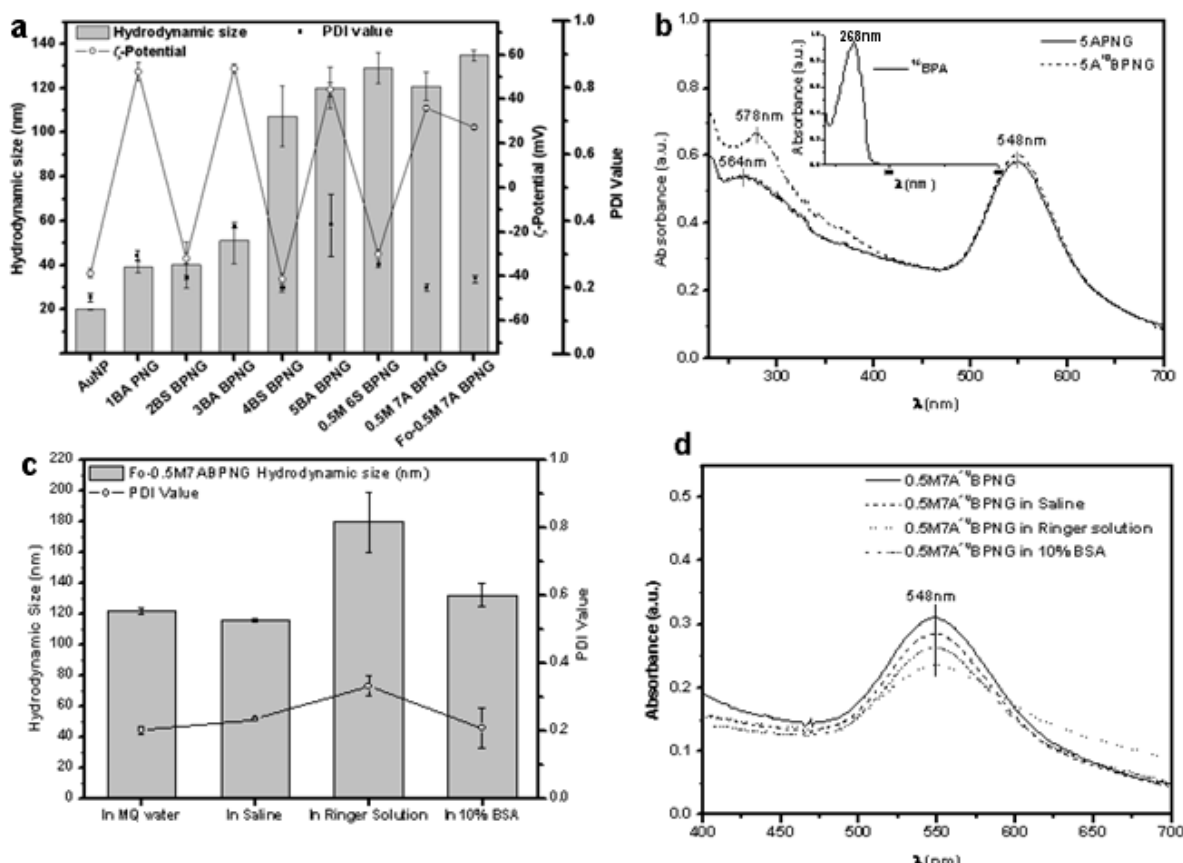


Figure 4-13. Characterization of the AuNPs by (a) hydrodynamic size, surface charge and PDI-value analysis after every layer deposition, (b) the verification of BPA upload, by UV-spectrophotometry. The stability analysis (c & d) Fo-0.5M 7A $^{10}$ BPNG in MQ-water, saline, Ringer solution and 10% BSA solutions by DLS and PDI-value (c) and UV-Visible spectrophotometry (d).

amount of boron compound is too low to influence significantly the layer architecture. Further investigation will be performed.

The presence of  $^{10}\text{BPA}$  was evaluated by UV-Vis spectrophotometric analysis (fig. 4-13b). The UV-absorbance at 278nm is due to phenylalanine of BPA shows the conjugation of  $^{10}\text{BPA}$ . BPA have a phenylalanine group in which the  $\pi$  electrons of the phenyl ring which can stack with other aromatic systems and often do within folded PEs, thus adding to the stability of the structure. As seen in the  $^{10}\text{BPA}$  absorbance spectra having peak at 268nm (fig. 4-13b, inset) but the absorbance peak in case of  $^{10}\text{BPA}$  on the  $^{10}\text{BPNG}$  was observed to have a 10nm shift to 278nm which can be a hint for ring-stacking (fig. 4-13b). Further detailed investigation is going on.

The binding of BPA was further validated by neutron autoradiography (fig. 4-14b). The

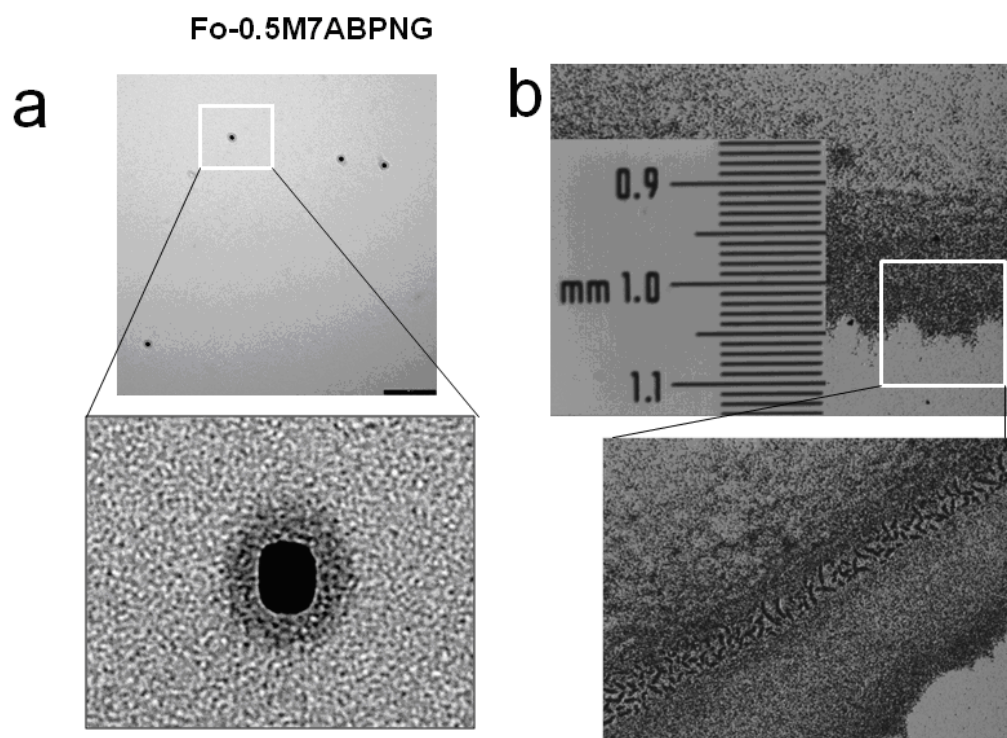


Figure 4-14. (a) TEM micrograph depicting the mono-dispersity (image up) and the architecture of the AuNP with a nano-gold core and PE capsule (image down). Black bar represents 200nm scale length. (b) Neutron autoradiography validating the significant uptake of  $^{10}\text{BPA}$  in the PNGs layers ( $^{10}\text{BPNG}$ ). The scale represents the size of the drop pipetted from the sediment of the suspension of Fo-0.5M 7A $^{10}\text{BPNG}$ . The spatial map represents the alpha particles liberated as a result of the exposure of the dried drop to neutron radiation.

neurographic plate, infers an extremely high density implies from Fo-0.5M  $^{10}\text{BPNG}$  predicting an equally high concentration of boron in the suspension (drop) that was exposed to neutrons. This result verifies the successful conjugation of  $^{10}\text{BPA}$  in between the layers of Fo-0.5M  $^{10}\text{BPNG}$ . The nanoparticles were rinsed several times until the wash through (supernatant) does not show negligibly low UV-Visible absorbance, before exposure to neutron radiation. This verifies that the alpha particles liberated are solely coming from the particles and not from the solution. The neurographic experiments efficiency of Fo-0.5M  $^{10}\text{BPNG}$  at cell line level (i.e. on non-cell line and cancerous cell line) are underway.

The PDI value (fig. 4-13a) and TEM image analysis (fig. 4-14a, up) of the 0.5M7A  $^{10}\text{BPNG}$  indicates that they are quite mono disperse. The overall architecture of the nanogold composite was visualized for particles with 7 layers exemplarily by TEM (fig. 4-14a, down).

While the presence of ions (saline or Ringer's solution) causes an immediate aggregation of PNGs coated from aq. PE, the 0.5M7A  $^{10}\text{BPNG}$  (7 layers PNGs with last 2 layers with 0.5M PEs and outermost layer of 0.5M PAH) were stable in in 0.5M NaCl solution and 10% BPA (fig. 4-13c & d). But some changes were observed if the coated particles were stored in Ringer's solution. The hydrodynamic size of the 0.5M7A  $^{10}\text{BPNG}$  increased from ~127nm to ~180nm and the UV-Vis spectrum shows a shoulder at 650 nm which may indicative particle aggregation (lit from Schneider and Decher [12]) (fig. 4-13c & d).

#### **4.7.2. Interaction of Fo-0.5M $^{10}\text{BFPNGs}$ with non-cancerous and cancer cells**

The uptake of Fo-0.5M 7A  $^{10}\text{BFPNGP}$  was followed in three different cancer cell lines, i.e. hepatocellular carcinoma (JHH6), leukemic (HL60) and breast cancer (MDA MB 231) as

well as in two non-cancerous cell line i.e. immortalized human hepatocyte (IHH) and J774.2 (macrophage cell line) by confocal fluorescence microscopy. In fig. 6-4, it can be seen that the targeting with Fo-0.5M 7AFPNGs led to a significantly ( $p \leq 0.001$ ) higher particle uptake in the tested cancer cell lines (fig. 4-15d-f) in comparison to the non-cancerous cell line (fig. 4-15a, b). The folate-receptor mediated endosomes are known to guide and liberate its content in the nucleus [18]. In fig. 4-15c, after 24 h of treatment, most of the cancer cells had

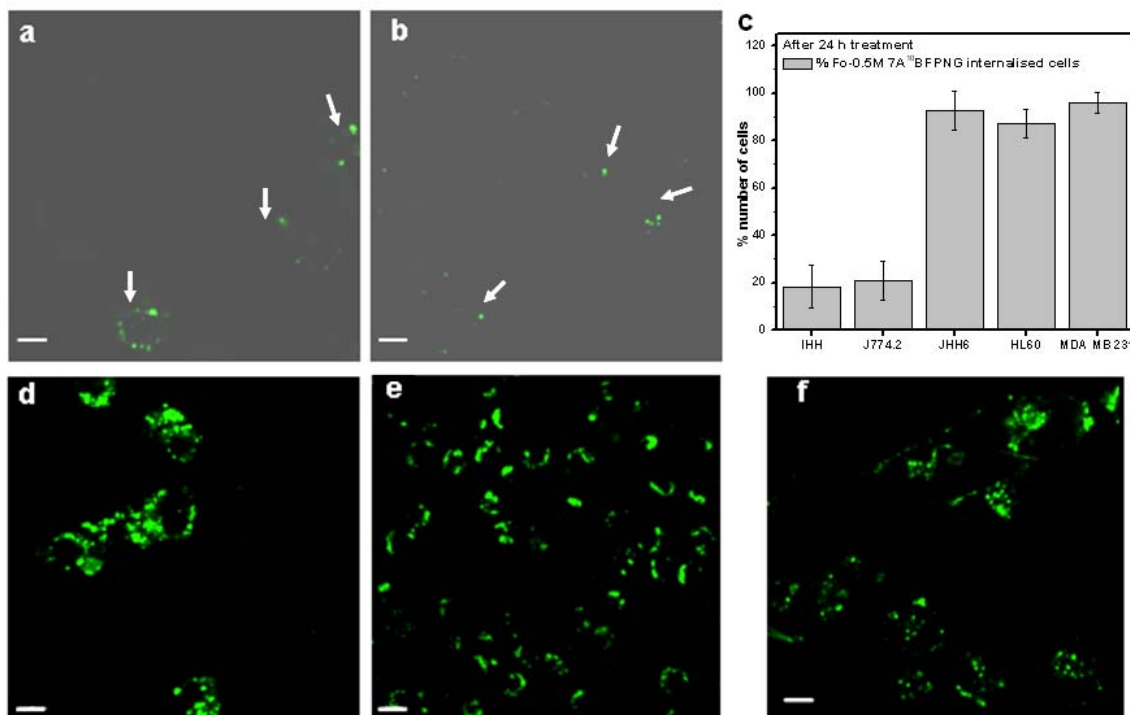


Fig. 4-15. Fluorescence confocal microscopy reveals negligible <sup>10</sup>BPNG uptake in noncancerous cells lines (a) IHH & (b) J774.2 while significant uptake is observed in tumor cell lines i.e. JHH6 (d), HL60 (e) and MDA MB 231 (f). (c) The graphically represented percentage of cells with <sup>10</sup>BPNG in non-cancerous and cancer cell lines. Each result represents mean  $\pm$ SD of 5 independent experiments. White bar reoresents 10 $\mu$ m scale length.

internalized the <sup>10</sup>BPNGs which accumulated in the perinuclear region, whereas in the non-cancerous cell lines, number of cells which have taken up the particles is significantly low.

Interaction with the macrophages (i.e. innate immunological response) was also assessed as an indicator of systemic drug biocompatibility. Macrophage recognition of PNGs is the main reason for fast clearance of charged drug delivery systems from blood. Due to the decrease in the surface charge by saturation of the PE capsule with folic acid, it was assumed that a quasi neutral surface charge could prevent recognition by macrophages. Therefore, to evaluate the above assumption, I did confocal imaging of macrophage cells (J774.2 cell line) after 24h treatment with the Fo-0.5 7A<sup>10</sup>BFPNGs (fig. 4-15c). For each experiment on average 1000 cells were analyzed and each experiment was repeated 3 times. I found that only ~20% macrophages could endocytosed the Fo-0.5M 7A<sup>10</sup>BFPNGs.

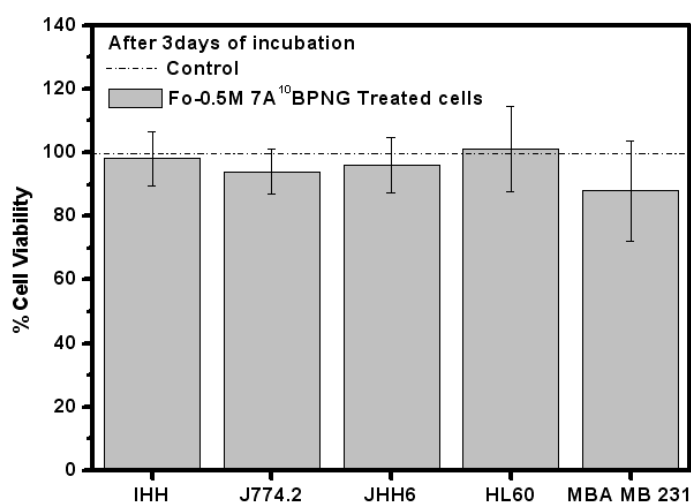


Figure 4-16. Cell toxicity profiles after 3days of the <sup>10</sup>BPNG uptake of the test cell lines. There was no significant difference between their respective control (untreated cells considered as 100%). Each result represents mean±SD of 5 independent experiments.

Furthermore, an adverse effect on the cell viability due to <sup>10</sup>BPNGs treatment was studied by a MTT assay. The cell viability was found to be between 90 and 100%. The only exception is the breast cancer cell line where it decreased to around 80% (fig. 4-16). This indicates a quite low toxicity of the coated particles themselves.

#### **4.8. References**

1. Mabuchi M, Takenaka T, Fujiyoshi Y, Uyeda N. Surface enhanced Raman scattering of citrate ions adsorbed on gold sol particles. *Surface Science* 1982;119(2-3):150-158.
2. Smith WE. Practical understanding and use of surface enhanced Raman scattering/surface enhanced resonance Raman scattering in chemical and biological analysis. *Chem Soc Rev* 2008;37(5):955-964.
3. Pristiniski D, Tan S, Erol M, Du H, Sukhishvili S. In situ SERS Study of Rhodamine 6G Adsorbed on Individually Immobilized Ag Nanoparticles. *J Raman Spectrosc* 2006;37(7):762-770.
4. Schiessel H, Pincus P. Counterion-condensation-induced collapse of highly charged polyelectrolytes. *Macromolecules* 1998;31(22):7953–7959.
5. Naji A, Netz RR. Attraction of like-charged macroions in the strong-coupling limit. *Eur Phys J E Soft Matter* 2004;13(1):43-59.
6. Pietronave S, Arcesi L, D'Arrigo C, Perico A. Attraction between like-charged polyelectrolytes in the extended condensation theory. *J Phys Chem B* 2008;112(50):15991-15998.
7. Kim K, Lee HS, Kim NH. Silver-particle-based surface-enhanced resonance Raman scattering spectroscopy for biomolecular sensing and recognition. *Anal Bioanal Chem* 2007;388:81-88.
8. Zucolotto V, Ferreira M, Cordeiro MR, Constantino CJL, Balogh DT, Zanatta, AR, *et al.* Unusual Interactions Binding Iron Tetrasulfonated Phthalocyanine and

- Poly(allylamine hydrochloride) in Layer-by-Layer Films. *J Phys Chem B* 2003;107(16):3733-3737.
9. Guerrini L, Jurasekova Z, Domingo C, Pérez-Méndez M, Leyton P, Campos-Vallette M, *et al.* Importance of metal-adsorbate interactions for the surface-enhanced Raman scattering of molecules adsorbed on plasmonic nanoparticles. *Plasmonics* 2007;2(3):147-156.
  10. Dong W-F, Sukhorukov GB, Moehwald H. Enhanced Raman Imaging and Optical Spectra of Gold Nanoparticle Doped Microcapsules. *Phys Chem Chem Phys* 2003;5:3003-3012.
  11. Papagiannopoulos A, Fernyhough CM, Waigh TA, Radulescu A. Scattering Study of the Structure of Polystyrene Sulfonate Comb Polyelectrolytes in Solution. *Macromolecular Chemistry and Physics* 2008;209(24):2475-2486.
  12. Schneider G, Decher G. Functional core/shell nanoparticles via layer-by-layer assembly. Investigation of the experimental parameters for controlling particle aggregation and for enhancing dispersion stability. *Langmuir* 2008;24(5):1778-1789.
  13. Schneider GF, Subr V, Ulbrich K, Decher G. Multifunctional cytotoxic stealth nanoparticles. A model approach with potential for cancer therapy. *Nano Lett* 2009;9(2):636-642.
  14. Decher G. Polyelectrolyte multilayers, an Overview. In. Decher G, Schlenoff GF, editors. *Multilayer thin films*. Weinheim: Wiley-VCH, 2003. p. 1-17.
  15. Kamen BA, Capdevila A. Receptor-mediated folate accumulation is regulated by the cellular folate content. *Proc Natl Acad Sci USA* 1986;83(16):5983-5987.

16. Stokes RJ, McBride E, Wilson CG, Girkin JM, Smith WE, Graham D. Surface-Enhanced Raman Scattering Spectroscopy as a Sensitive and Selective Technique for the Detection of Folic Acid in Water and Human Serum. *Appl Spectrosc* 2008;*62*:371-376.
17. Weitman SD, Lark RH, Coney LR, Fort DW, Frasca V, Zurawski VRJr, *et al.* Kamen, B.A. Distribution of the folate receptor GP38 in normal and malignant cell lines and tissues. *Cancer Res.* 1992; *52*(12):3396–3401.
18. Antony AC. The biological chemistry of folate receptors. *Blood* 1992;*79*:2807–2820.

## **CHAPTER 5**

### **5.1. Conclusions**

This is the first time that a study has described in detail orientation and binding of the first polycation (PAH) or polyanion (PSS) layer to the curved gold surface of nanoparticles. In the presented SERS study we confirmed the unexpected binding of PSS and clarified the underlying binding mechanism. The changes observed in the spectrum of the aromatic system of PSS and the fact that some of the peaks from the PSS spectrum are visible in the citrate-gold spectrum indicates that also PSS binds to the gold surface but without replacing the citrate shell. By SERS it was shown that the poly-allylamine is oriented with the primary amine groups towards the gold surface which was expected and in accordance to the results of other groups [1]. These results are supported by the surface charge measurement which showed an additional decrease in the negative charge of the citrate stabilized AuNP in case of PSS as first layer while the PAH induces a high positive surface charge. Another aim of the present study was to improve the stability of PNGs against aggregation in the presence of small ions, in order to allow injectability in medicinal solutions without losing the advantage of small size of single nanoparticles. It was shown by Schneider and Decher that encapsulation in the presence of ions such as sodium or chloride, leads to AuNPs aggregation [2]. I confirmed that this observation is true for the first 5 layers. However, if the first 5 layers were deposited from aq. PE followed by coating with 0.5 M PEs, the coated particles are stable against aggregation. The resulting nanoparticles showed also higher stability if stored in ionic solutions. In a model proposed for the layer-by-layer technique it was assumed that the first “precursor” layers on flat surfaces differ from latter layers because the

deposition is still influenced by the template [3]. Moreover these layers are supposed to contain small counter ions and they are charged. This effect could be true for curved templates such as AuNPs. From the experiments, it was deduced that on AuNP, the first 5 layers are the precursor layers and that they are more prone to be affected by small counter ions. Probably for a higher number of layers the neutral layers in zone II [3] stabilize the capsule and the exposure to small ions does not cause aggregation any longer.

As a possible reason for the low stability against aggregation of the nanoparticles coated with PEs from pure water, the excessive length of the PAH chains as compared to the particle diameter was identified. If the particle is smaller than the polyion length, this can lead to incomplete wrapping and in turn to bridging of several particles and hence flocculation.

It is known that the polycation PAH in the presence of a concentration higher than 0.3M NaCl, collapses into a random coiled structure [3]. This can explain the increased stability of nanoparticles coated with 0.5M PEs against aggregation while their equivalent aq. PE coated particles aggregate in the presence of ions.

After improving the stability of the coated particles for injection into body fluids, the next aim was to conjugate targeting molecule with them. I studied whether the electrostatic binding of a target molecule is strong enough to allow the recognition in ionic solutions such as complex cell culture media. Many recent reports describe the functionalization by covalently binding of folic acid for targeted nanoparticle delivery to cancer cells [4-9]. However, the covalent binding can always induce toxic by-products, reduce the efficacy of the drug, or influence the recognition by the targeted receptor. Therefore, functionalization was assessed via electrostatic interactions. The binding of folic acid to the multilayer capsule was verified by SERS,  $\zeta$ -potential and DSL analysis. The observed higher uptake by cancer cells of folic acid functionalized AuNPs is in good accordance to other studies described in

literature, for folic acid-poly-ethylenglycol conjugates [8, 9]. Moreover the fact that the uptake of particles without folic acid in cells without folate-receptor (macrophages) is lower supports its increased specificity.

The 10-B uploading in between the layers of the targeted multilayer coated AuNPs verify the potential applicability of the present system. Therefore, stabilised targeted multilayer coated AuNPs could be a potential drug delivery or diagnostic system (as drug molecules or imaging probes could be loaded in the PE matrix of the multilayers).

## 5.2. References

1. Mukhopadhyay K, Phadtare S, Vinod VP, Kumar A, Rao JM, Chaudhari RV, *et al.* Gold Nanoparticles Assembled on Amine-Functionalized Na–Y Zeolite: A Biocompatible Surface for Enzyme Immobilization. *Langmuir* 2003;19(9):3858–3863.
2. Schneider G, Decher G. Functional core/shell nanoparticles via layer-by-layer assembly. Investigation of the experimental parameters for controlling particle aggregation and for enhancing dispersion stability. *Langmuir* 2008;24(5):1778-1789.
3. Decher G. Polyelectrolyte multilayers, an Overview. In *Multilayer thin films.* (eds. G. Decher, B. Schlenoff), Weinheim: Wiley-VCH, 2003, p. 1-17.
4. Reddy JA, Low PS. Enhanced folate receptor mediated gene therapy using a novel pH-sensitive lipid formulation. *J. Controlled Release* 2000;64(1-3):27-37.
5. Pan J, Feng Si-S. Targeted delivery of paclitaxel using folate-decorated poly(lactide)–vitamin E TPGS nanoparticles. *Biomaterials* 2008;29(17):2663-2672.
6. Kaman B. Folate and antifolate pharmacology. *Semin Oncol* 1997;24(5 Suppl. 18):S18-30-S18-39.
7. Lee RJ, Low PS. Delivery of Liposomes to Cultured KB Cells via Folate Receptor-Mediated Endocytosis. *J Biol Chem* 1994; 269:3198-3204.
8. Cho, K.C.; Kim, S.H.; Jeong, J.H; Park, T.G. Folate Receptor-Mediated Gene Delivery Using Folate-Poly(ethylene glycol)-Poly(L-lysine) Conjugate. *Macromolecular Bioscience* 2005;5(6):512-519.
9. Gabizon A, Horowitz AT, Goren D, Tzemach D, Mandelbaum-Shavit F, Qazen MM, *et al.* Targeting folate receptor with folate linked to extremities of poly(ethylene glycol)-grafted liposomes: in vitro studies. *Bioconjug Chem.* 1999;10(2):289-298.

---

**Part 2:**

**Target specific polymeric coacervate  
nanoparticle approach**

## 1. A brief overview

Cancers are caused by abnormalities in the genetic material of transformed cells [1]. Most cancers have mutations in genes for one or more proteins which are crucial cell-cycle checkpoints that normally function to restrict progression through the G<sub>1</sub> stage of the cell cycle (Fig. 1-1). Defects in the apoptotic pathway allow cancer cells to survive for prolonged periods of time, accumulating more genetic errors, and live in a suspended state that permits metastatic spread. In the absence of tumor suppressor gene products and/or activation of other oncoproteins, oncogenes contribute to cancer formation by supporting accelerated proliferation, de-regulating cell cycle control or blocking apoptosis [2].

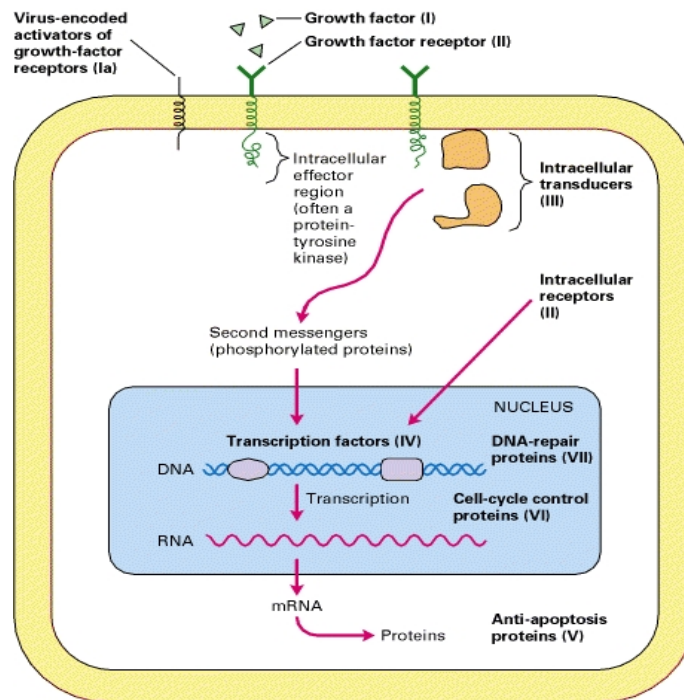
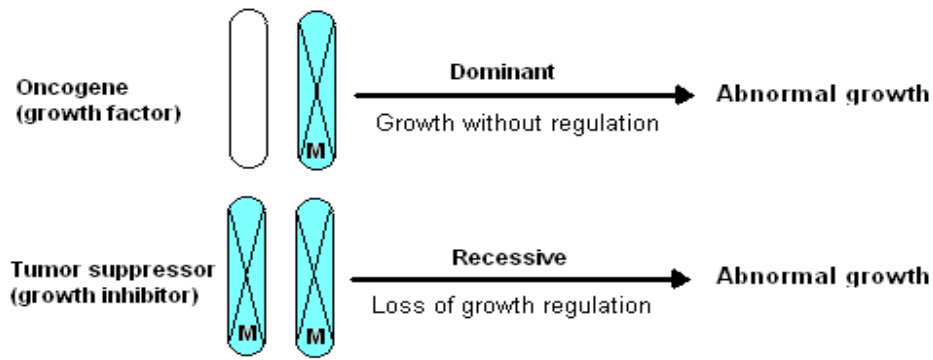


Fig. 1-1. The seven types of proteins that participate in controlling cell growth. Cancer can result from the expression of mutant forms of these proteins: growth factors (I), growth factor receptors (II), signal-transduction proteins (III), transcription factors (IV), pro- or anti-apoptotic proteins (V), cell cycle control proteins (VI), and DNA repair proteins (VII). Mutations changing the structure or expression of proteins in classes I–IV generally give rise to dominantly active oncogenes. The class VI proteins mainly act as tumor suppressors; mutations in the genes encoding these proteins act recessively to release cells from control and surveillance, greatly increasing the probability that the mutant cells will become tumor cells. Class VII mutations greatly increase the probability of mutations in the other classes. Virus-encoded proteins that activate growth-factor receptors (Ia) also can induce cancer [2].

Nanoparticles and nanocapsules have opened up a new ground in the field of cancer therapy because of their unique properties, such as small size, controlled release of drug and reduced toxic effects on healthy cells. Furthermore they can be multifunctionalized to make personalized target specific particles with long blood circulation times. But most importantly they can carry nucleic acids in form of plasmids or Ribonucleic acid (RNA) which could correct the major classes of mutations in cancer.

### **1.1 Oncogenes and tumor suppressor genes.**

Cell growth is regulated by both positive (proto-oncogenes) and negative (tumor suppressor genes) molecular factors. Thus, for a cell to divide or to enhance its growth, enhancement of positive factors or depletion of negative factors is required (fig. 1-2).



*Fig. 1-2. Mutation of oncogenes and tumor suppressor genes.*

#### **1.1.1. Gain-of-Function Mutations Convert Proto-Oncogenes into Oncogenes**

Most of the known oncogenes derive due to mutation in growth inducing genes of normal cellular genes (i.e., proto-oncogenes) whose products participate in cellular growth-controlling pathways. Because most proto-oncogenes are basic to life, they have been highly conserved [3].

Proto-oncogene conversion or activation into an oncogene generally involves a ‘*gain-of-function*’ mutation. At least three mechanisms can produce oncogenes from the corresponding proto-oncogenes [3].

- Point mutations in a proto-oncogene result in a constitutively acting protein products.
- Localized reduplication (gene amplification) of a Deoxyribonucleic acid (DNA) segment that includes a proto-oncogene, leading to overexpression of the encoded protein.
- Chromosomal translocation that changes the promoter for the growth-regulatory gene and causes inappropriate expression of the gene.

Oncogenes caused by the first mechanism, leads to modified oncoproteins that differ from the normal protein encoded by the corresponding proto-oncogene. In contrast, the latter two mechanisms produces oncogenes, whose protein products are identical with the normal proteins; the oncogenic effect is due to their overexpression or in cells where they normally are not expressed. However, the gain-of-function mutations which convert proto-oncogenes to oncogenes acts usually dominantly, i.e. mutation in only one of the two alleles is sufficient for induction of cancer [3].

#### **1.1.1.1. c-Myc oncoprotein and human cancer**

The human *c-myc* proto-oncogene is the genomic homologue of the transforming sequences found in MC29, an avian retrovirus that can cause myelocytomatosis, carcinoma, sarcoma and lymphoma [4-6]. The c-Myc protein encoded by the proto-oncogene is a multifunctional, nuclear phosphoprotein that plays a key role in cell cycle progression,

apoptosis and cellular transformation. It is a transcription factor regulating the transcription of specific target genes. Alterations in the structure or expression of c-Myc (fig. 1-3) was found to be

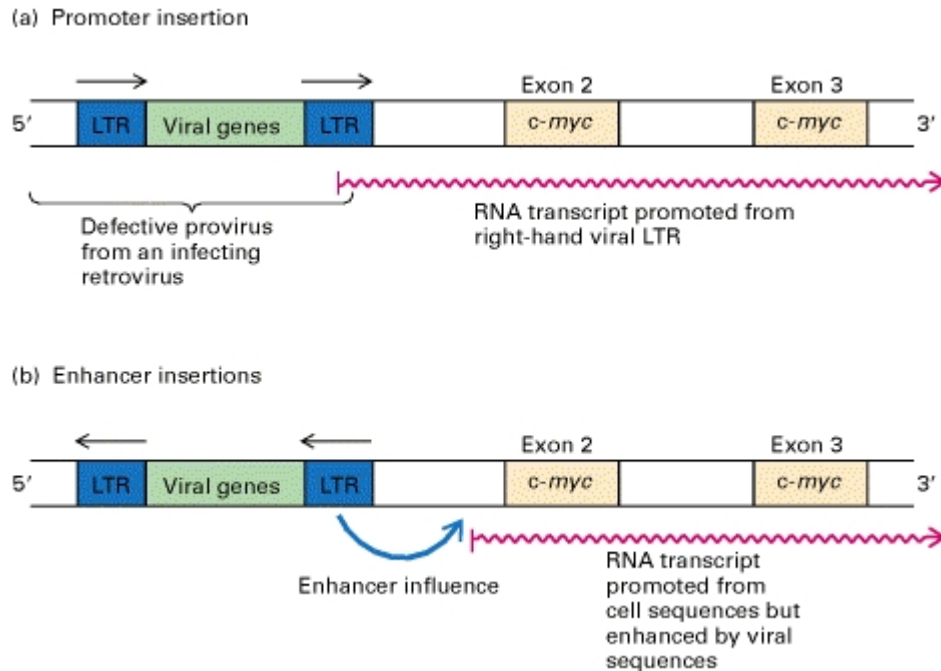


Fig. 1-3. Activation of the *c-myc* proto-oncogene by retroviral promoter and enhancer insertions (a) The promoter can be activated when the retrovirus inserts upstream (5') of the *c-myc* exons. The right-hand LTR may then act as a promoter if the provirus has a defect preventing transcription through to the right-hand LTR. The *c-myc* gene is shown as containing two exons; there is a further upstream exon but it has no coding sequences. (b) The *c-myc* gene can also be activated when a retrovirus inserts upstream of the *c-myc* gene in the opposite transcriptional direction; a viral LTR acts as an enhancer, activating transcription from the *c-myc* promoter sequence [3].

associated with several forms of neoplasia, including avian leukosis virus induced B-cell lymphoma, rodent plasmacytoma and human Burkitt's lymphoma, leukemia, colon carcinoma and variant small cell lung cancer [7-18]. Significantly elevated expression levels of c-Myc were measured in the majority of tumors. Due to gene rearrangement by transposition or by translocation of gene, sometimes if proto-oncogene is located under a strong constitutive promoter after the process, they start expressing the onco-protein. Transposon can do multiple transposition of the same gene thus causing amplification of the

number of gene, leading to enhanced gene expression. But so far no rearrangement or amplification of the c-myc gene has been demonstrated [18].

### **1.1.1.2. Structure of the c-Myc protein**

Myc is one of the few proteins which could be sufficient to drive the cell cycle and promote DNA synthesis into resting cells [19]. In line with this finding is that the constitutive

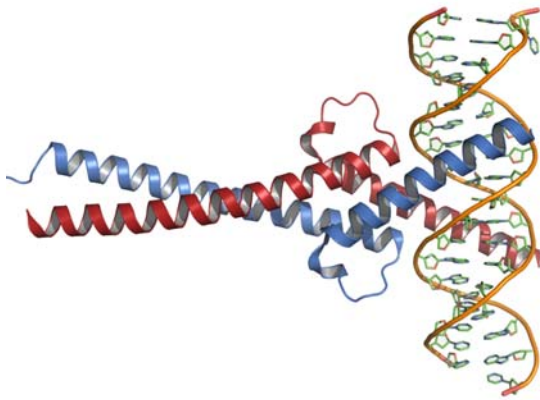


*Figure 1-4. Structure of the c-Myc (red) in complex with Max (blue) and DNA (PDB 1NKP). Both proteins are binding the major groove of the DNA by forming a fork-like structure [20].*

expression of Myc in cells blocks their differentiation. The growth stimulating properties are most likely to be responsible for the ability of Myc to initiate and promote tumor formation. Interestingly, Myc can also makes cells sensitive to apoptosis, suggesting that it is also a part of a life-and-death switch. In order to fulfill its function as a transcriptional regulator Myc needs to

heterodimerize with Max to exert the biological activities described above and to regulate gene transcription. Myc and Max are just two members of a growing family of proteins referred to as the Myc/Max/Mad network (fig. 1-4) [19, 20]. A hallmark of these proteins is that they possess a C-terminal basic region/helix-loop-helix/leucine zipper domain (bHLHZip). The bHLHZip domain specifies dimerization within the network and determines sequence specific DNA binding. Importantly this domain together with the N-terminal transactivation domain is essential for Myc biology [21].

### **1.1.2. Loss-of-Function Mutations in Tumor-Suppressor Genes Are Oncogenic**

Tumor-suppressor genes, in general, encode proteins that inhibit cell proliferation. Defeat in one or more of these “brakes” contributes to the development of many cancers. Five broad classes of proteins are normally recognized as being encoded by tumor-suppressor genes [3]:

- Intracellular proteins, such as the p16 cyclin-kinase inhibitor, that regulate or inhibit progression through a specific stage of the cell cycle
- Receptors for secreted hormones (e.g., tumor derived growth factor  $\beta$ ) that function to inhibit cell proliferation
- Checkpoint-control proteins that arrest the cell cycle if DNA is damaged or chromosomes are abnormal
- Proteins, such as p53 transcription factor, that promote apoptosis
- Enzymes that participate in DNA repair.

Although DNA-repair enzymes do not directly inhibit cell proliferation, cells that have lost the ability to repair errors, gaps, or broken ends in DNA accumulate mutations in many genes, including those that are critical in controlling cell growth and proliferation [3]. Thus, loss-of-function by mutations in the genes encoding DNA-repair enzymes promote inactivation of other tumor-suppressor genes not only initiated indirectly activation of oncogenes but also enhances the chance of tumorigenesis [3].

In generally, one copy of a tumor-suppressor gene is sufficient to control cell proliferation. Thus, oncogenic loss-of-function mutations in tumor-suppressor genes act recessively [3]. Hence in order to promote tumor development both alleles of a tumor-suppressor gene must be lost or inactivated.. Tumor-suppressor genes in many cancers have

deletions or point mutations that prevent production of protein or lead to production of a nonfunctional protein [3].

### **1.1.2.1. p53 and human cancers**

The *p53* gene is the first tumor suppressor gene to be identified and, ever since its discovery, scientists have found that the p53 pathway is altered in most human cancers. The p53 has been nicknamed “the Guardian of the Genome” as it is at the heart of the cell’s tumor suppressive mechanism. After receiving a “danger signal” such as DNA damage and cells in stress, it initiates several crucial cellular responses that suppress tumor formation (fig. 1-5) [22].

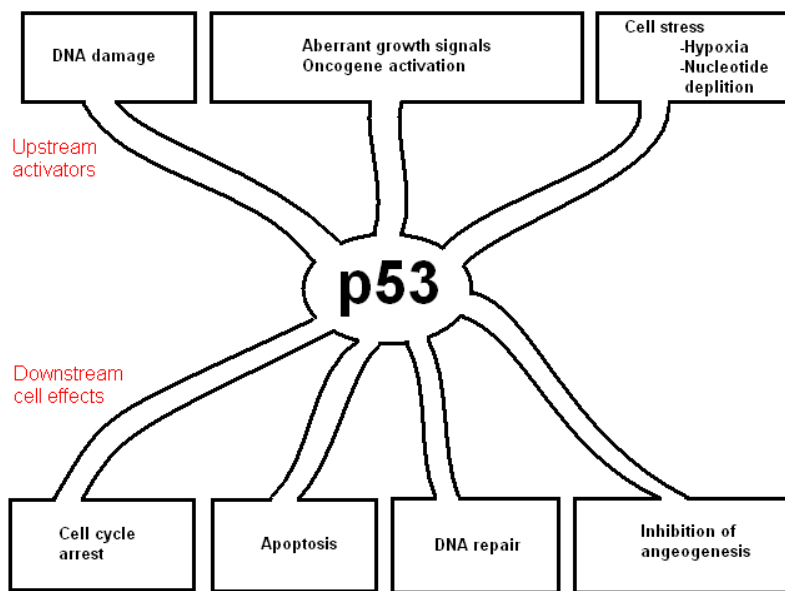


*Fig. 1-5. Activators and effects of p53 [22].*

### **1.1.2.2. Structure of the p53 protein**

The *p53* gene, located on chromosome 17p1, contains 11 exons that encode a 53kD phosphoprotein. The p53 protein is a transcription factor containing 4 distinct domains (fig. 1-6) [23, 24]:

- the N-terminus transactivation domain,
- the DNA binding domain containing a Zn<sup>2+</sup> ion,
- an oligomerization domain, and
- a C-terminus regulatory domain.

The p53 protein binds as a tetramer to a DNA response element containing 2 inverted repeats of the sequence 5'PuPuPuC(A/T)-3' (Pu represents purine base: A or G) in order to regulate transcription of its target genes by binding with approximately 300 different gene promoter regions.

The loss of function of p53, either through deletion, mutation, repression, or loss of expression is one of the most common events in tumorigenesis. The

restoration of p53 activity in cells with mutated or deleted p53 gene, in many *in vitro*

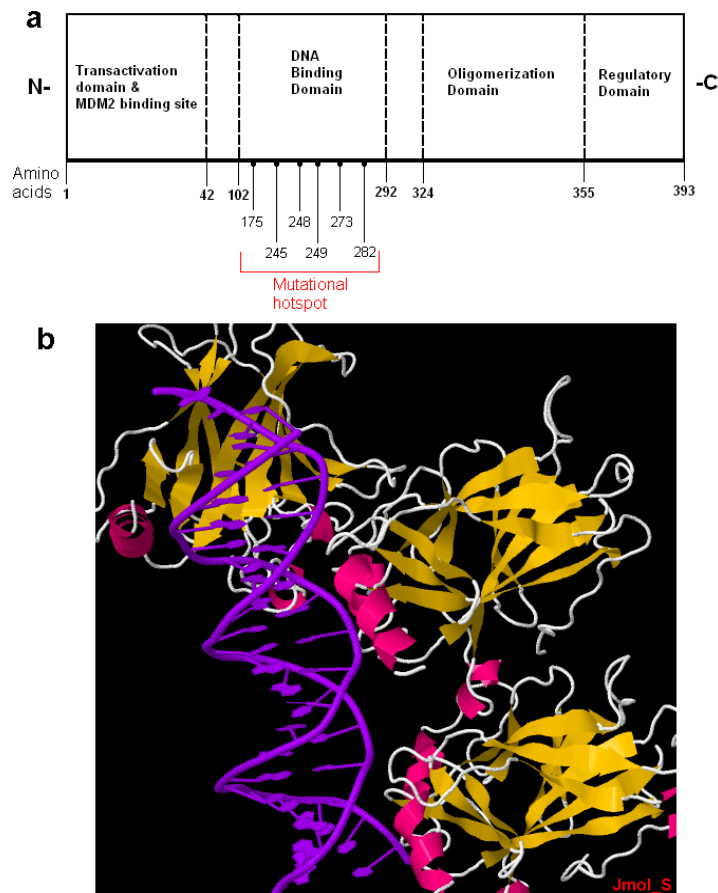


Figure 1-6. (a) Domains of the p53 protein and location of mutational hotspots. (b) Structure of the p53 in complex with DNA (PDB 3KZ8). Protein-DNA interactions occur at the major and minor grooves and at the DNA backbone [23].

studies shows that either it suppresses growth of the cells or induces apoptosis [25-29]. This led to the idea that gene therapy, aimed at restoring p53 activity in tumors might be a fruitful approach to a natural cancer treatment. Indeed a number of studies have shown that adenovirus- or retrovirus-driven delivery of the wt p53 gene can suppress tumor growth *in vivo* [30-35].

## 1.2. Nanomedicine and novel therapeutic strategies

While discovery of new drugs and cancer chemotherapy opened a new era for the treatment of tumors, optimized concentration of a drug at the target site is only possible at the expense of severe side effects [36]. Nanoscale carrier systems have shown to be the potential system with limited drug toxicity and achieve tumor localization [36].

These can be easily linked to tumor-targeting moieties, such as tumor-specific

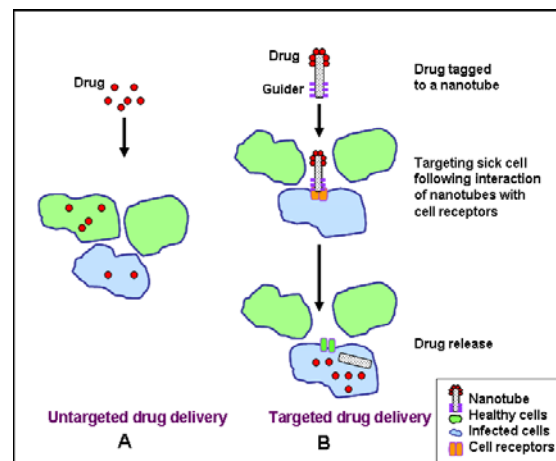


Fig. 1-7. Targeted drug deliver system [37].

ligands or monoclonal antibodies, the nanocarriers can be used to target cancer-specific receptors, tumor antigens, and tumor vasculatures with high affinity and precision. But unfortunately no proteins or receptors were found so far which are completely tumor specific, usually targeting nowadays aims to recognize markers on the cancer cell surface which is overexpressed in cancer cells. An effective drug delivery is based on three facts: (a) efficient encapsulation of drugs (b) targeted delivery and (c) successful release (fig. 1-7) [37].

### 1.2.1. Nanotechnology for antisense therapy

Recently, antisense oligonucleotides (ODN) have been used to inhibit the expression of a number of oncogenes and growth factors (fig. 1-8) [38, 39]. Antisense oligonucleotides directed against or upstream of the AUG region (protein translation start site) of a mRNA are

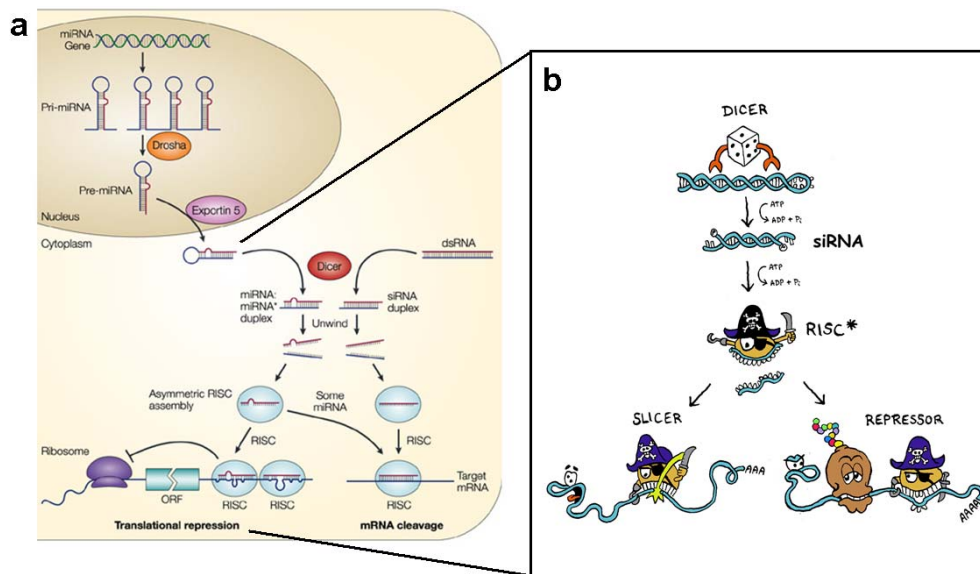


Figure 1-8. The siRNA/miRNA pathway. (a) overall pathway; (b) Cartoon of siRNA/miRNA induced cleavage mechanism of mRNA in the cytoplasm of a cell [38].

thought to hinder interaction of the RNA with the ribosome, thus interfering with its translocation [40].

The phenomenon of “RNA interference” (RNAi) was first reported by Napoli *et al.*[41] in 1990. RNAi mechanism are intended to regulate the endogenous gene expression. One of three type of small RNA molecule, is “small interfering RNA” (siRNA), which are involved in this mechanism (fig. 1-8). The siRNA bind to the target mRNA in a sequence specific manner. This binding causes localized double strand formation, which is then recognized by Dicer. Dicer is a member of the RNase III family of double-stranded RNA (dsRNA) specific endoribonuclease. After binding with siRNA/mRNA duplex, Dicer causes its cleavage which

in turn creating short double stranded siRNA/mRNA duplex with characteristic 2 nucleotide long 3'-overhang at each end [42]. The 2 nucleotide 3'overhang RNA duplex is then identified by the RNA-induced silencing complex (RISC). This complex includes 'slicer' and 'argonaute' protein with RNaseH like domain. Argonaute is an endonuclease causes degradation of messengerRNA (mRNA) whose sequence is complementary to that of the siRNA guide strand (strand which remain bound with RISC). In turn the siRNA guide strand (single strand) of RISC/siRNA complex again bind sequence specifically to the target mRNA, causing localize duplex formation as above [43]. Dicer recognizes this RISC/RNA duplex complex, but in this complex Dicer causes cleavage RNA duplex at the middle of the sequence. This short cleaved RNA is then identified as aberrant and are degraded. The RISC/siRNA guide strand after binding to mRNA by sequence specific manner may serve as a primer for RNA-dependent RNA polymerase (RDRP) enzyme, and polymerases the siRNA strand. This double stranded siRNA/mRNA act as template for Dicer and the same mechanism as above was followed. All this complex mechanism causes rapid degradation of the mRNA of the target protein mRNA, hence causes targeted silencing of the gene.

The study of optimal ODN length necessary to preserve the distinguished point mutation region of the oncogenic mRNA vs. the mRNA of the proto-oncogene, has provided us with new avenues in antisense ODN utilization for nanoparticle therapy in cancer tissue. This will stop uncontrolled proliferation in cancer cells to i.e., they enter into G<sub>0</sub>-phase of cell-cycle.

Various nano-technological carrier systems have been introduced. Quantum dots (QD) have been used for siRNA delivery [44]. Polylactic-co-glycolic (PLGA) and polylactic acid (PLA) based nanoparticles have also been used for *in vitro* RNAi delivery [45]. Although, the delivery of siRNA using the various nanomaterials, tracking their delivery and monitoring transfection efficiency has been success, but its, still difficult without a suitable tracking

agent or marker. Designing an efficient and traceable transfection agent for RNA interference is a big challenge. Recently, chitosan nanoparticles encapsulated with quantum dots or with fluorescent dyes have been synthesized and were uploaded with targeted siRNA to inhibit gene expression [46, 47].

### 1.2.2. Nanotechnology for gene therapy

Gene therapy is a therapy which causes insertion of target genes into individual cells of

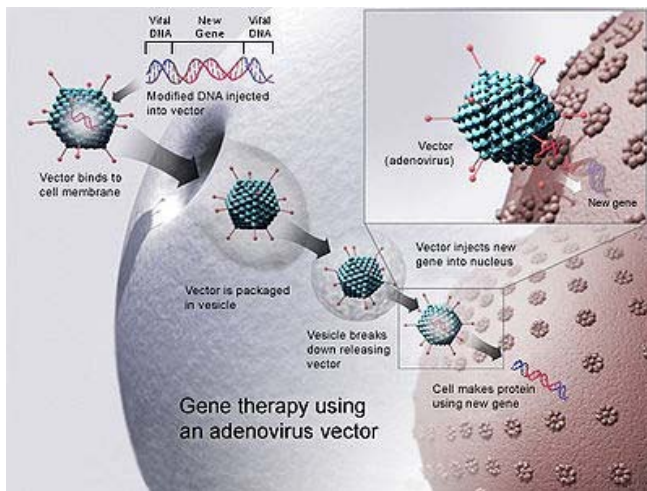


Figure 1-9. Adenovirus mediated gene therapy [48].

an individual to treat various diseases, such as cancer, where deleterious mutant alleles are replaced with functional ones (fig. 1-9) [48]. Viral vectors, bio-nanoparticles with diameters of 100 nm or less, have long been proven to be the most efficient

and stable transgene vectors into the cell and thus are suitable for vaccine and

gene therapy [49, 50]. Despite the fact that the viral gene delivery system has shown some successes in clinic trials, the FDA has not approved any therapeutic viral vectors because it shows a high transfection yield but has many disadvantages such as immunogenicity, oncogenicity, and potential virus recombination problems inherent in viral vector systems [36, 48]. Recently it has been reported that severe immunodeficiency leukemia patients have died following a retroviral vector treatment. The adenovirus therapy trial raised a red flag for viral vector-mediated gene transfer [51]. To this end, approaches have been developed to circumvent vector immunogenicity [52].

Safety concerns over the use of viral vectors have stimulated interest in developing substitute gene carriers. Nonviral nanoparticles may offer an alternative and perhaps a better approach, as they are relatively easy to prepare, are less immunogenic and oncogenic, and have no potential of virus recombination and limitation on the size of a transferred gene than viral vectors. The main drawback is the low transfection efficacy of non-viral gene delivery systems and the unspecific delivery to specific cells. In order to overcome the latter problem, they can be decorated to carry genetic materials to target cells. Nanoparticles have been successfully tested for both in vitro [52] and in vivo gene delivery [53]. Their high surface area to volume ratio increase increases their interaction area with the target cancer cell membrane which makes them ideal for nonviral gene transfer. This mechanism has been widely used in liposome and other polymer-mediated gene transfer systems [53-55]. Various other non-viral nano-carrier systems have also been developed for ODN and gene-delivery [56-57].

### **1.2.3. Ideal nanoscopic drug delivery system**

To deliver therapeutic agents to cancer cells in vivo, the following three issues have to be considered: (i) drug resistance at the tumor level due to physico-chemical barrier (non-cellular based mechanisms), (ii) drug resistance at the cellular level (cellular mechanisms), and (iii) distribution, metabolism & clearance of anticancer drugs in the body.

#### **1.2.3.1. Strategies to overcome tumor level resistance**

Various strategies must be considered and accordingly therapeutics should be developed in order to overcome tumor level resistance due to several mitigating factors.

Firstly, non-cellular drug-resistance mechanisms are poor vasculature, the acidic environment of the neoplastic tissue, high interstitial pressure and low micro-vascular pressure, and charge on the drug molecules, reducing drug access to the tumor and thus protecting cancerous cells from cytotoxicity [58]. Secondly, resistance due to cellular mechanisms which comprises altered activity of specific enzyme systems (e.g., topoisomerase activity), altered apoptotic regulation (i.e., mutation in the major tumor suppressor genes like p53, p16 etc.), or transport based mechanisms, such as P-glycoprotein efflux system, which is responsible for multi-drug resistance (MDR), or the multi-drug resistance proteins (MRP) [59, 60]. Thirdly and the most destructive fact is, that anticancer drugs are distributed throughout the body, causing damage in both, tumor and normal cells. The low efficacy of chemotherapy and radiotherapy is often limited due to this side effect [61]. This observation emphasizes that in order to develop efficient strategies for cancer therapy the nanoparticulated drug needs to be functionalities to overcome these non-cellular and cellular resistance mechanisms as well as increase the selectivity towards cancer cells while minimally affecting the normal tissues.

While innovative nanoparticles or nanocapsules have opened a new arena in the field of cancer therapy mainly two factors reduce the efficiency of these drug delivery systems i.e., short blood half-life (rapid elimination from the blood stream) and non-specific targeting. Identification by the macrophages of the mononuclear phagocytic system (MPS) as a consequence of the absorption of blood opsonin proteins on hydrophobic conventional nanoparticles causes their rapid elimination from the blood stream [62]. Thus, to obtain long-circulating nanoparticles, nanoparticles should be surface modified with hydrophilic, flexible and non-ionic polymers such as polyethylene glycol (PEG) [62, 63]. A major breakthrough in this field was the introduction of “stealth” hydrophilic polymers such as polyethylene glycol (PEG), polyxamine, poloxamers, polysaccharides [64, 65]. This dynamic ‘cloud’ of

hydrophilic and neutral chains, repel plasma proteins as modeled by Jeon et al. [65, 66]. In order to enhance the ability of nanoparticles to interact with cells and better permeation of the tissue, PEG can be covalently coupled to polylactic acid (PLA), polycaprolactone (PCL) and polycyanoacrylate (PCA) [66].

### **1.2.2. Target specific drug delivery**

A most significant drawback of conventional drug delivery system is the lack of site-specific targeting, i.e. tissue specificity, of nanoparticles. In first approaches to solve the problem, scientists have coupled targeting agents, such as monoclonal antibodies, with the nanoparticles [66-73]. But the dimension of antibodies (10nm) causes poor diffusion through biological barriers, and they induce a strong immunogenicity. One other strategy is the use of small non-antigenic ligands. Among various low molecular weight (MW) targeting agents, folic acid (MW 441Da) has been suggested as a target for cancer cells. Indeed, folic acid is a vitamin whose receptor is frequently overexpressed on the surface of the cancer cells [71, 72] as folate is required for the RNA and DNA synthesis. Moreover the receptor has also been reported as a tumor marker, especially in ovarian carcinoma, as it is highly restricted in most normal tissues [75-76]. Thus, the advantage of folic acid as targeting agent are that it is stable, inexpensive and non-immunogenic compared to monoclonal antibodies. Moreover, it has a very high affinity for its cell surface receptor ( $K_d \sim 1nM$ ) [78] and is effectively internalized within the cell [77-79], which makes it a valuable tool for intracellular delivery of anticancer agents [80-86].

**2. Reference:**

1. Bert V, Kinzler KW. Introduction. In: Bert V, Kinzler KW, editors. The genetic basis of human cancer, 2<sup>nd</sup> ed. New York: McGraw-Hill, Medical Pub. Division, 2002. p. 5.
2. Weinberg RA. Tumor suppressor genes. *Science* 1991;254(5035):1138-1146.
3. Lodish H, Berk A, Zipursky SL, Matsudaira P, Baltimore D, Darnell J, editors. *Molecular Cell Biology*, 4<sup>th</sup> ed. New York: W. H. Freeman, 2003.
4. Payne GS, Bishop JM, Varmus HE. Multiple arrangements of viral DNA and an activated host oncogene in bursal lymphomas. *Nature* 1982;295(5846):209-214.
5. Graf T, Beug H. Avian leukemia viruses: interaction with their target cells in vivo and in vitro. *Biochim Biophys Acta* 1978;516(3):269-299.
6. Enrietto PJ, Hayman MJ, Ramsay GM, Wyke JA, Payne LN. Altered pathogenicity of avian myelocytomatosis (MC29) viruses with mutations in the v-myc gene. *Virology* 1983;124(1):164-172.
7. Distaso A, Abatangelo L, Maglietta R, Creanza TM, Piepoli A, Carella M, *et al.* Biological and functional analysis of statistically significant pathways deregulated in colon cancer by using gene expression profiles. *Int J Biol Sci* 2008;4:368-378.
8. Neel BG, Gasic GP, Rogler CE, Skalka AM, Ju G, Hishinuma F, *et al.* Molecular analysis of the c-myc locus in normal tissue and in avian leukosis virus-induced lymphomas. *J Virol* 1982;44(1):158-166.
9. Payne GS, Bishop JM, Varmus HE. Multiple arrangements of viral DNA and an activated host oncogene in bursal lymphomas. *Nature* 1982;295(5846):209-214.

10. Shen-Ong GL, Keath EJ, Piccoli SP, Cole MD. Novel myc oncogene RNA from abortive immunoglobulin-gene recombination in mouse plasmacytomas. *Cell* 1982;31(2 Pt 1):443-452.
11. Collins S, Groudine M. Amplification of endogenous myc-related DNA sequences in a human myeloid leukaemia cell line. *Nature* 1982;298(5875):679-681.
12. Dalla-Favera R, Wong-Staal F, Gallo RC. Onc gene amplification in promyelocytic leukaemia cell line HL-60 and primary leukaemic cells of the same patient. *Nature* 1982;299(5878):61-63.
13. Crews S, Barth R, Hood L, Prehn J, Calame K. Mouse c-myc oncogene is located on chromosome 15 and translocated to chromosome 12 in plasmacytomas. *Science* 1982;218(4579):1319-1321.
14. Little CD, Nau MM, Carney DN, Gazdar AF, Minna JD. Amplification and expression of the c-myc oncogene in human lung cancer cell lines. *Nature* 1983;306(5939):194-196.
15. Ingvarsson S, Asker C, Axelson H, Klein G, Sümegi J. Structure and expression of B-myc, a new member of the myc gene family. *Mol Cell Biol* 1988;8(8):3168-3174.
16. Sümegi J, Spira J, Bazin H, Szpirer J, Levan G, Klein G. Rat c-myc oncogene is located on chromosome 7 and rearranges in immunocytomas with t(6:7) chromosomal translocation. *Nature* 1983;306(5942):497-498.
17. Alitalo K, Ramsay G, Bishop JM, Pfeifer SO, Colby WW, Levinson AD. Identification of nuclear proteins encoded by viral and cellular myc oncogenes. *Nature* 1983;306(5940):274-277.
18. Erisman MD, Rothberg PG, Diehl RE, Morse CC, Spandorfer JM, Astrin SM. Deregulation of c-myc gene expression in human colon carcinoma is not

- accompanied by amplification or rearrangement of the gene. *Mol Cell Biol* 1985;5(8):1969-1976.
19. Lüscher B, Larsson LG. The basic region/helix-loop-helix/leucine zipper domain of Myc proto-oncoproteins: function and regulation. *Oncogene* 1999;18(19):2955-2966.
  20. Nair SK, Burley SK (2003) X-Ray Structures of Myc-Max and Mad-Max Recognizing DNA. *Cell*. 2003;112(2):193-205.
  21. Rothberg PG, Erisman MD, Diehl RE, Rovigatti UG, Astrin SM. Structure and expression of the oncogene c-myc in fresh tumor material from patients with hematopoietic malignancies. *Mol Cell Biol* 1984;4(6):1096-1103.
  22. Lane DP. p53 and human cancers. *Br Med Bull* 1994;50(3):582-599.
  23. Bai L, Zhu WG. p53: Structure, Function and Therapeutic Applications. *J Cancer Mol* 2006;2(4):141-153,
  24. Kitayner M, Rozenberg H, Rohs R, Suad O, Rabinovich D, Honig B, *et al.* Diversity in DNA recognition by p53 revealed by crystal structures with Hoogsteen base pairs. *Nat Struct Mol Biol* 2010;17(4):423-429.
  25. Shaw P, Bovey R, Tardy S, Sahli R, Sordat B, Costa J. Induction of apoptosis by wild-type p53 in a human colon tumor derived cell line. *Proc Natl Acad Sci USA* 1992;89(10):4495-4499.
  26. Takahashi T, Carbone D, Takahashi T, Nau MM, Hida T, Linnoila I, *et al.* Wild-type but not mutant p53 suppresses the growth of human lung cancer cells bearing multiple genetic lesions. *Cancer Res* 1992;52(8):2340-2343.
  27. Baker SJ, Markowitz S, Fearon ER, Willson JK, Vogelstein B. Suppression of human colorectal carcinoma cell growth by wild-type p53. *Science* 1990;249(4971):912-915.

28. Liu TJ, Zhang WW, Taylor DL, Roth JA, Goepfert H, Clayman GL. Growth suppression of human head and neck cancer cells by the introduction of a wild-type *p53* gene via a recombinant adenovirus. *Cancer Res* 1994;54(14):3662-3667.
29. Lee JM, Bernstein A. Apoptosis, cancer and the *p53* tumour suppressor gene. *Cancer Metastasis Rev* 1995;14(2):149-161.
30. Fujiwara T, Cai DW, Georges RN, Mukhopadhyay T, Grimm EA, Roth JA. Therapeutic effect of a retroviral wild-type *p53* expression vector in an orthotopic lung cancer model. *J Natl Cancer Inst* 1994;86(19):1458-1462.
31. Wills KN, Maneval DC, Menzel P, Harris MP, Sutjipto S, Vaillancourt MT, *et al.* Development and characterization of recombinant adenoviruses encoding human *p53* for gene therapy. *Hum Gene Ther* 1994;5(9):1079-1088.
32. Lesoon-Wood LA, Kim WH, Kleinman HK, Weintraub BD, Mixson AJ. Systemic gene therapy with *p53* reduces growth and metastases of a malignant human breast cancer in nude mice. *Hum Gene Ther* 1995;6(4):395-405.
33. Hamada K, Alemany R, Zhang WW, Hittelman WN, Lotan R, Roth JA, *et al.* Adenovirus-mediated transfer of a wild-type *p53* gene and induction of apoptosis in cervical cancer. *Cancer Res* 1996;56(13):3047-3054.
34. Clayman GL, Liu TJ, Overholt SM, Mobley SR, Wang M, Janot F, *et al.* Gene therapy for head and neck cancer. Comparing the tumor suppressor gene *p53* and a cell cycle regulator WAF1/CIP1 (*p21*). *Arch Otolaryngol Head Neck Surg* 1996;122(5):489-493.
35. Bookstein R, Demers W, Gregory R, Maneval D, Park J, Wills K. *p53* gene therapy in vivo of herpatocellular and liver metastatic colorectal cancer. *Semin Oncol* 1996;23(1):66-77.

36. Mozafari MR, Pardakhty A, Azarmi S, Jazayeri JA, Nokhodchi A, Omri A. Role of nanocarrier systems in cancer nanotherapy. *J Liposome Res* 2009;19(4):310-321.
37. Suri SS, Fenniri H, Singh B. Nanotechnology-based drug delivery systems. *J Occup Med Toxicol* 2007;2:16.
38. Moghimi SM, Hunter AC, Murray JC. Long-Circulating and Target-Specific Nanoparticles: Theory to Practice. *Pharmacol Rev* 2001;53(2):283-318.
39. Calabretta B. Inhibition of protooncogene expression by antisense oligodeoxynucleotides: biological and therapeutic implications. *Cancer Res* 1991;51(17):4505-10.
40. Neckers L, Whitesell L, Rosolen A, Geselowitz DA. Antisense inhibition of oncogene expression. *Crit Rev Oncog* 1992;3(1-2):175-231.
41. Napoli C, Lemieux C, Jorgensen R. Introduction of a Chimeric Chalcone Synthase Gene into Petunia Results in Reversible Co-Suppression of Homologous Genes in trans. *Plant Cell* 1990;2(4):279-289.
42. Macrae IJ, Zhou K, Li F, Repic A, Brooks AN, Cande WZ, *et al*. Structural basis for double-stranded RNA processing by Dicer. *Science* 2006;311(5758):195-198.
43. Vermeulen A, Behlen L, Reynolds A, Wolfson A, Marshall WS, Karpilow J, *et al* he contributions of dsRNA structure to Dicer specificity and efficiency. *RNA* 2005y;11(5):674-82.
44. Chen AA, Derfus AM, Khetani SR, Bhatia SN. Quantum dots to monitor RNAi delivery and improve gene silencing. *Nucleic Acids Res* 2005;33(22):e190.
45. Shinde RR, Bachmann MH, Wang Q, Kasper R, Contag CH. PEG-PLA/PLGA Nanoparticles for In-Vivo RNAi Delivery. *NSTI Nano tech, California; 2007.*

46. Tan WB, Jiang S, Zhang Y. Quantum-dot based nanoparticles for targeted silencing of HER2/neu gene via RNA interference. *Biomaterials* 2007;28(8):1565-1571.
47. Howard KA, Rahbek UL, Liu X, Damgaard CK, Glud SZ, Andersen MØ, *et al.* RNA interference *in vitro* and in vivo using a novel chitosan/siRNA nanoparticle system. *Mol Ther* 2006;14(4):476-484.
48. Jin S, Ye K. Nanoparticle-Mediated Drug Delivery and Gene Therapy. *Biotechnol Prog* 2007;23:32-41.
49. Verma IM, Weitzman MD. Gene therapy: twenty-first century medicine. *Annu Rev Biochem* 2005;74:711-738.
50. Lundstrom K. Latest development in viral vectors for gene therapy. *Trends Biotechnol* 2003;21(3):117-122.
51. Tan W, Wang K, He X, Zhao XJ, Drake T, Wang L, *et al.* Bionanotechnology based on silica nanoparticles. *Med Res Rev* 2004;24(5):621-638.
52. Mastrobattista E, van der Aa MA, Hennink WE, Crommelin DJ. Artificial viruses: a nanotechnological approach to gene delivery. *Nat Rev Drug Discov* 2006;5(2):115-121.
53. Singh M, Briones M, Ott G, O'Hagan D. Cationic microparticles: A potent delivery system for DNA vaccines. *Proc Natl Acad Sci U S A* 2000;18;97(2):811-816.
54. Nomura T, Koreeda N, Yamashita F, Takakura Y, Hashida M. Effect of particle size and charge on the disposition of lipid carriers after intratumoral injection into tissue-isolated tumors. *Pharm Res* 1998;15(1):128-132.
55. Reszka R, Zhu JH, Weber F. Liposome mediated transfer of marker and cytokine genes into rat and human Glioblastoma, cells in vitro and in vivo. *J Liposome Res* 1995; 5(1):149-154.

56. Junghans M, Kreuter J, Zimmer A. Antisense delivery using protamine-oligonucleotide particles. *Nucleic Acids Res* 2000;28(10):E45.
57. Erbacher P, Zou S, Bettinger T, Steffan AM, Remy JS. Chitosan-based vector/DNA complexes for gene delivery: biophysical characteristics and transfection ability. *Pharm Res* 1998;15(9):1332-1339.
58. He X, Wang K, Tan W, Liu B, Liu X, Huang S, *et al.* A novel gene carrier based on amino-modified silica nanoparticles. *Chin Sci Bull* 2003;48(3):223-228.
59. Krishna R, Mayer LD. Multidrug resistance (MDR) in cancer. Mechanisms, reversal using modulators of MDR and the role of MDR modulators in influencing the pharmacokinetics of anticancer drugs. *Eur J Pharm Sci* 2000;11(4):265-283.
60. Links M, Brown R. Clinical relevance of the molecular mechanisms of resistance to anti-cancer drugs. *Expert Rev Mol Med* 1999;1999:1-21.
61. Brigger I, Dubernet C, Couvreur P. Nanoparticles in cancer therapy and diagnosis. *Adv Drug Deliv Rev* 2002;54(5):631-51.
62. Stolnik S, Illum L, Davis SS. 1995. Long circulating microparticulate drug carriers. *Adv Drug Del Rev* 16:195–214.
63. Gref R, Minamitake Y, Peracchia MT, Langer R. PEG-coated biodegradable nanospheres for intravenous drug administration. In: Cohen S, Bernstein H, editors. *Microparticulate systems for the delivery of proteins and vaccines*. New York: Marcel Dekker, 1996. p. 279–306.
64. Peracchia MT, Desmaële D, Couvreur P, d'Angelo J. Synthesis of a novel poly(MePEG cyanoacrylate-co-alkyl cyanoacrylate) amphiphilic copolymer for nanoparticle technology. *Macromolecules* 1997;30(4):846–851.

65. Peracchia MT, Fattal E, Desmaële D, Besnard M, Noël JP, Gomis JM, *et al.* Stealth PEGylated polycyanoacrylate nanoparticles for intravenous administration and splenic targeting. *J Control Release* 1999;60(1):121-128.
66. Blume G, Cevc G, Crommelin MD, Bakker-Woudenberg IA, Kluft C, Storm G. Specific targeting with poly(ethylene glycol)-modified liposomes: coupling of homing devices to the ends of the polymeric chains combines effective target binding with long circulation times. *Biochim Biophys Acta* 1993;1149(1):180-184.
67. Kaplan MR, Calef E, Bercovici T, Gitler C. The selective detection of cell surface determinants by means of antibodies and acetylated avidin attached to highly fluorescent polymer microspheres. *Biochim Biophys Acta* 1983;728(1):112–120.
68. Bourel D, Rolland A, Le Verge R, Genetet B. A new immunoreagent for cell labeling. CD3 monoclonal antibody covalently coupled to fluorescent polymethacrylic nanoparticles. *J Immunol Methods* 1988;106(2):161–167.
69. Adams GP, Weiner LM. Monoclonal antibody therapy of cancer. *Nat Biotechnol* 2005;23:1147-1157.
70. Adams GP, Tai MS, McCartney JE, Marks JD, Stafford WF 3rd, Houston LL, *et al.* Avidity-mediated enhancement of in vivo tumor targeting by single-chain Fv dimers. *Clin Cancer Res* 2006;12(5):1599-1605.
71. Cheng JD, Adams GP, Robinson MK, Weiner LM. Monoclonal antibodies. In: DeVita VT, Hellman S, Rosenberg SA. *Cancer Principles and Practice of Oncology*, 7<sup>th</sup> ed. Philadelphia, PA: Lippincott Williams & Wilkins, 2005. p. 445-456.
72. Chmielewski M, Hombach A, Heuser C, Adams GP, Abken H. T cell activation by antibody-like immunoreceptors: Increase in affinity of the single-chain fragment

- domain above threshold does not increase T Cell activation against antigen-positive target cells but decreases selectivity. *J Immunol* 2004;173(12):7647-53.
73. Horak E, Heitner T, Robinson MK, Simmons HH, Garrison J, Russeva M, *et al.* Isolation of scFvs to in vitro produced extracellular domains of EGFR family members. *Cancer Biother Radiopharm* 2005;20(6):603-613.
74. Franklin WA, Waintrub M, Edwards D, Christensen K, Prendegast P, Woods J, *et al.* New anti-lung cancer antibody cluster 12 reacts with human folate receptors present on adenocarcinoma. *Int J Cancer Suppl* 1994;8:89-95.
75. Weitman SD, Lark RH, Coney LR, Fort DW, Frasca V, Zurawski VR, *et al.* Distribution of the folate receptor GP38 in normal and malignant cell lines and tissues. *Cancer Res* 1992;52:3396-3401.
76. Coney LR, Tomassetti A, Carayannopoulos L, Frasca V, Kamen BA, Colnaghi MI, *et al.* Cloning of a tumor-associated antigen: Mov18 and Mov19 antibodies recognize a folate binding protein. *Cancer Res* 1991;51:6125-6132.
77. Garin-Chesa P, Campbell I, Saigo PE, Lewis JL, Old LJ, Rettig WJ. Trophoblast and ovarian cancer antigen LK26. Sensitivity and specificity in immunopathology and molecular identification as a folate- inducing protein. *Am J Pathol* 1993;142:557-567.
78. Antony AC. The biological chemistry of folate receptors. *Blood* 1992;79(11):2807-2820.
79. Rothberg KG, Ying YS, Kolhouse JF, Kamen BA, Anderson RG. The glycopospholipid-linked folate receptor internalizes folate without entering the clathrin-coated pit endocytic pathway. *J Cell Biol* 1990;110:637-649.

80. Campbell IG, Jones TA, Foulkes WD, Trowsdale J. Folate-binding protein is a marker for ovarian cancer. *Cancer Res* 1991;51:5329–5338.
81. Wang S, Lee RJ, Mathias CJ, Green MA, Low PS. Synthesis, purification, and tumor cell uptake of Gallium-67-deferoxamine-folate, a potential radiopharmaceutical for tumor imaging. *Bioconjugate Chem* 1996;7:56–62.
82. Lee RJ, Low PS. Delivery of liposomes into cultured KB cells via folate receptor-mediated endocytosis. *J Biol Chem* 1994;269:3198–3204.
83. Wang S, Low PS. Folate-mediated targeting of antineoplastic drugs, imaging agents, and nucleic acids to cancer cells. *J Controlled Release* 1998;53:39–48.
84. Gabizon A, Horowitz AT, Goren D, Tzemach D, Mandelbaum-Shavit F, Qazen MM, *et al.* Targeting folate receptor with folate linked to extremities of poly(ethylene glycol)-grafted liposomes: in vitro studies. *Bioconjugate Chem* 1999;10: 289–298.
85. Malmqvist M. Biospecific interaction analysis using biosensor technology. *Nature* 1993;361:186– 187.
86. Stella B, Arpicco S, Peracchia M.T., Desmaële D, Hoebeke J, Renoir M, D’Angelo J, Cattel L, Couvreur P. Design of Folic Acid-Conjugated Nanoparticles for Drug Targeting. *J Perma Sc* 2000;89(11):1452-1464.

## **CHAPTER 1**

*Double strike - Target specific polymeric coacervate nanoparticles inhibit proliferation and induce apoptosis in Cancer cell by integrating anti-sense and gene therapy.\**

### **1.1. Aim of the present work**

Cancer is a multi-mutation gathering disease. Mutations typically affect two general classes of genes i.e. proto-oncogenes and tumor suppressor genes. A novel therapeutic approach aims to develop nanoparticles correcting these mutations. This part of thesis describes the formulation, characterization and application of targeted (folate conjugated) Coacervate Polymeric particles (CPs) delivering siRNA (against oncogenic mRNA [c-myc]) and plasmid bearing wild-type tumor suppressor genes (p53 gene) for cancer therapy. Hence, with the formulation of this CP, I am able to integrate two therapeutic system i.e. antisense therapy and gene therapy.

\*

*Manuscript submitted in ASC Nano*

## **CHAPTER 2**

### **2.1. Introduction**

Cancer is a disease, in which alterations in the cellular genome affect the expression or function of genes which are controlling cell growth, differentiation and programmed cell death (apoptosis). There are two major classes of gene mutations present in most of cancer types: oncogenes and tumor suppressor genes.

Since gene therapy is currently being applied in the treatment of many different diseases such as cancer, AIDS, and cardiovascular diseases [1-6], numerous studies have been carried out or are in progress to develop non-viral gene delivery systems using nanoparticles.[7-14] Furthermore, there are several clinical trials test gene therapy protocols [15-21] and some of them have already been successful [22-24] in their outcome e.g. treatment of adenosine deaminase deficiency [25]. Moreover, in recent years, numerous research programs have been started in order to develop nanoparticles for anti-sense therapy. Several strategies were tested which involved uploading small interfering RNA (siRNA) onto the nanoparticles, in order to knock down the expression of the target gene at the messenger RNA (mRNA) level (hence the term RNA interference) [26-30]. This offers a novel therapeutic strategy to overcome the disease, because it could selectively down regulate protein production in cells.

In developing therapeutic agents for cancer at the cellular level three major issues have to be considered:

- a) Drug resistance (drug non-availability) at the tumor level due to possible physicochemical barriers (non-cellular based mechanisms) and at cellular level (cellular mechanisms),
- b) Bio-distribution (accumulation of the applied drug in the different organs), and
- c) Bio-transformation and clearance of the anticancer drug in the body.

Accordingly, in the present part the strategy has been to develop. My present work is aimed to develop polymeric Coacervate Particles (CPs) integrating antisense and gene therapeutic strategies for cancer therapy which should be selective to cancer cells and have a negligible toxicity for normal cells. Fig. 2-1 shows a scheme of the multilayered multifunctional nanoscopic system.

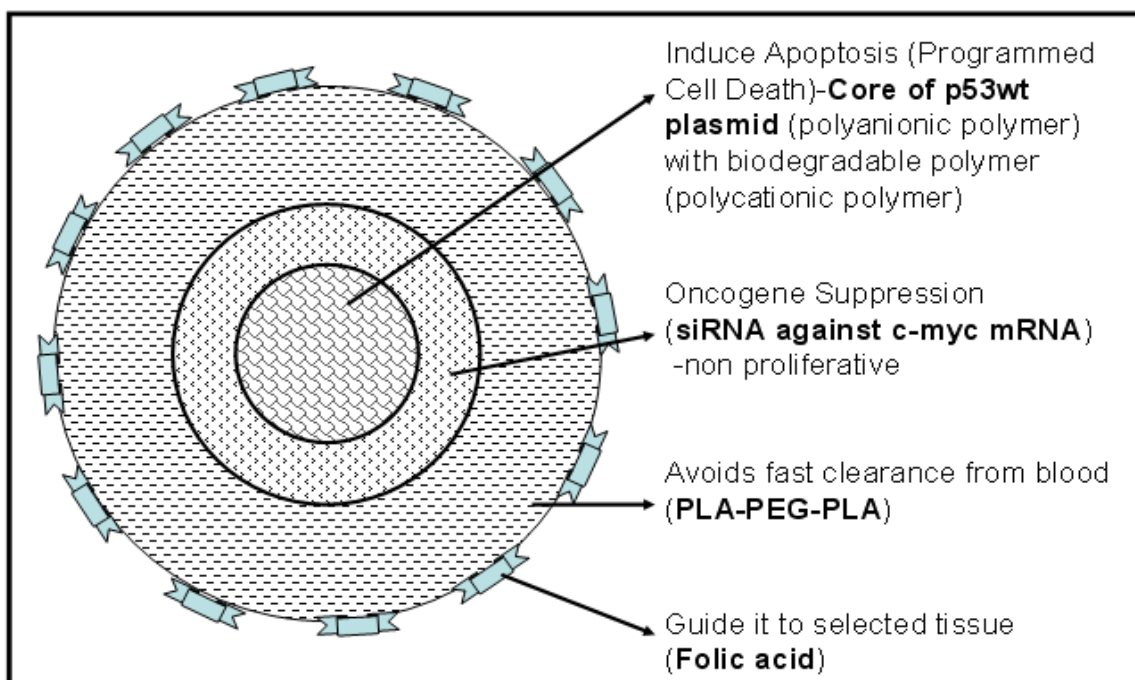


*Fig. 2-1. Schematic diagram of the multilayered multifunctional nanoscopic system.*

### **2.1.1. The core of the system: introducing gene therapy**

Mutations or deletion of the *p53* tumor suppressor gene, have been observed in more than 50% of human cancers [31-36]. This indicates the cell transformation ability of mutant *p53* genes goes beyond dominant-negative effects [34,35]. It has been already reported that induction of wild-type *p53* in cancer cells by infection resulted in extensive apoptosis and the death of a significant percentage of the infected cells [36-40]. Taking this into consideration, the strategy was to couple the delivery of siRNA against oncogenic mRNA of *c-myc* with that of a plasmid encoding for wild-type *p53* which, in turn, can activate apoptotic pathways in the haltered non-proliferating cancer cells.

### **2.1.2. The next layer introducing antisense therapy**

Mutations in *c-myc* proto-oncogene in most cancer cells cause deregulation and over-expression of Myc oncoprotein, a transcription factor which in turn contribute to tumorigenesis by inducing unrestrained cellular growth, proliferation, angiogenesis, and genomic instability [41-44]. Consequently, inhibition of Myc oncoprotein has become an attractive pharmacological target for treating diverse types of cancer. Previous studies have shown that targeting Myc inhibition, a common downstream trigger for many oncogenic signals, could be an effective, efficient and tumor-specific cancer therapy [45]. In view of the above argument I chose to deliver in a first step, siRNAs against the oncogenic mRNA of *c-myc* in different cancer cell lines, in order to induce down-regulation of Myc oncoprotein which can reverse tumorigenesis by inhibiting proliferation [46].

To deliver these therapeutically active nucleic acid systems I developed CPs, by precipitating by electrostatic interactions, the *p53* encoding plasmid with the biodegradable, biocompatible [47] cationic biopolymer chitosan (a polyaminosaccharide). In contrast to

most polycations, chitosan has a low immunogenicity [48]. Moreover, it also protects the uploaded nucleic acids from nuclease degradation [48-50].

### **2.1.3. The outermost layer reduces the uptake in macrophage system (MPS)**

The major limitation for intravenous delivery of polymeric nanoparticles is, however, their rapid elimination from the systemic circulation by blood monocytes and cells of the mononuclear phagocyte system (MPS) [51,52]. In particular, nanoparticles whose surfaces were modified by the incorporation of poly(ethylene glycol) (PEG) during nanoparticle formulation either through covalent attachment of PEG to surface functional groups or through physical adsorption of PEG to the surface. PEG can decrease MPS cell uptake and increase the blood circulation time to augment to the passive delivery by EPR [53-55]., therefore the CPs were coated with the tri-block polymer, polylactide-*block*-poly(ethylene glycol)-*block*-polylactide (PLA-PEG-PLA, P<sup>3</sup>) in order to obtain CPs combining the ability to avoid clearance by MPS along with an enhanced tissue and cell penetration [56-60].

In the multifunctional P<sup>3</sup> polymer, the PEG block, a non-toxic, amphiphilic polyglycoether, produces a dynamic, mobile and flexible molecular “cloud” over the particle surface due to the chain flexibility and electrical neutrality. This should reduce the adsorption of opsonins and other serum proteins by a “steric repulsion effect” [53-56]. Whereas PLA, an amorphous polymer widely used for medical and pharmaceutical applications, is known to enhance particle interaction with cells and hence allow for a better permeation in the tumor tissue [59-61]. Normally, targeted polymeric particles enter only in the first few cell layers of the tumor [62].

#### **2.1.4. CP decorated with cancer targeting molecule**

Most negative side-effects of anticancer drugs stem from the fact that they are widely distributed throughout the body, causing damage of both tumors along with normal cells. Consequently, the efficacy of chemotherapy and, similarly, radiotherapy is often limited, due to this problem that is normally tackled, in the case of chemotherapy by the use of small non-antigenic ligands targeted to cancer cells.

A low molecular weight (MW) targeting agent, Fo and the FR surface protein has emerged as one of the most [63-68] promising combinations for the development of selective cancer therapy. Specifically, malignant cells express significantly more of the receptor ( $\geq 20$  pmol [ $^3\text{H}$ ]folate/ $10^6$  cells) than normal epithelial cells and fibroblasts ( $\leq 1$  pmol [ $^3\text{H}$ ]folate/ $10^6$  cells).[64, 69-73] This receptor has also been reported as a tumor marker in most cancer forms [68], especially in ovarian carcinoma [72, 73]. Once the folic acid binds to the FR it is delivered directly to the nucleus of the cell, because folic acid is required for RNA synthesis [74, 75]. Thus, the advantages of Fo as targeting agent are that it is stable, inexpensive and non-immunogenic as compared to proteins such as monoclonal antibodies. [75] It has a very high affinity for its cell surface receptor ( $K_d \sim 1\text{nM}$ ) [74] and its efficiently internalized by the cell [75-79]. These properties make it a highly suitable molecule for intracellular delivery of anticancer agents.

The complete coacervate particles were characterized by zeta potential, dynamic light scattering, electron microscopy and UV-Vis spectroscopy. The interaction with cells such as uptake and transfection were studied in 3 different cancer cell lines: 1) HL-60, an undifferentiated leukemic cancer cell line with deleted p53 gene, 2) breast cancer cells with a mutated p53 gene and 3) hepato carcinoma cells, which are well-described in the literature as

targets for p53 gene therapy with even clinical trial phase III studies going on [81]. Finally the non-cancerous, immortalized hepatocyte cell line, IHH was used for comparison. The CPs showed a significant difference between cancer and non-cancer cells in cytotoxicity due to apoptosis induced by p53 expression.

## **2.2. References**

1. Chang MW, Barr E, Seltzer J, Jiang YQ, Nabel GJ, Nabel EG, *et al.* Cytostatic gene therapy for vascular proliferative disorders using a constitutively active form of Rb. *Science* 1995;267(5197):518-522.
2. Chang MW, Ohno T, Gordon D, Lu MM, Nabel GJ, Nabel EG, *et al.* Adenovirus-mediated transfer of the herpes simplex virus thymidine kinase gene inhibits vascular smooth muscle cell proliferation and neointima formation following balloon angioplasty of the rat carotid artery. *Mol Med* 1995;1(2):172-181.
3. Dachs GU, Dougherty GJ, Stratford IJ, Chaplin DJ. Targeting gene therapy to cancer: a review. *Oncol Res* 1997;9(6-7):313-325.
4. Cattaneo R. Paramyxovirus entry and targeted vectors for cancer therapy. *PLoS Pathog.* 2010;6(6):e1000973.
5. DiGiusto DL, Krishnan A, Li L, Li H, Li S, Rao A, *et al.* RNA-based gene therapy for HIV with lentiviral vector-modified CD34(+) cells in patients undergoing transplantation for AIDS-related lymphoma. *Sci Transl Med* 2010;2(36):36ra43.
6. Nikol S. Gene therapy of cardiovascular disease. *Curr Opin Mol Ther* 2008;10(5):479-492.
7. Roy K, Mao HQ, Huang SK, Leong KW. Oral gene delivery with chitosan–DNA nanoparticles generates immunologic protection in a murine model of peanut allergy. *Nat Med* 1999;5:387–391.
8. Cole-Strauss A, Yoon K, Xiang Y, Byrne BC, Rice MC, Gryn J, *et al.* Correction of the mutation responsible for sickle cell anemia by an RNA–DNA oligonucleotide. *Science* 1996;273:1386–1389.

9. Kren BT, Parashar B, Bandyopadhyay P, Chowdhury NR, Chowdhury JR, Steer CJ. Correction of the UDP-glucuronosyltransferase gene defect in the Gunn rat model of Crigler–Najjar syndrome type I with a chimeric oligonucleotide. *Proc Natl Acad Sci* 1999;96:10349–10354.
10. Yew NS, Wang KX, Przybylska M, Bagley RG, Stedman M, Marshall J, *et al.* Contribution of plasmid DNA to inflammation in the lung after administration of cationic lipid:pDNA complexes. *Hum Gene Ther* 1999;10:223–234.
11. Nabel GJ, Nabel EG, Yang ZY, Fox BA, Plautz GE, Gao X, *et al.* Direct gene transfer with DNA–liposome complexes in melanoma: expression, biologic activity, and lack of toxicity in humans. *Proc Natl Acad Sci* 1993;90:11307–11311.
12. Caplen NJ, Alton EW, Middleton PG, Dorin JR, Stevenson BJ, Gao X, *et al.* Liposome-mediated CFTR gene transfer to the nasal epithelium of patients with cystic fibrosis. *Nat Med* 1995;1:39–46.
13. Xing J, Deng L, Guo S, Dong A, Liang XJ. Polycationic nanoparticles as nonviral vectors employed for gene therapy in vivo. *Mini Rev Med Chem* 2010;10(2):126-137.
14. Viola JR, El-Andaloussi S, Oprea II, Smith CI. Non-viral nanovectors for gene delivery: factors that govern successful therapeutics. *Expert Opin Drug Deliv* 2010;7(6):721-35.
15. Nabel GJ, Nabel EG, Yang Z, Fox B, Plautz G, Gao X, *et al.* Direct gene transfer with DNA liposome complexes in melanoma: expression, biologic activity and lack of toxicity in humans. *Proc Natl Acad Sci* 1993;90:11307-11311.

16. Nabel EG, Yang ZY, Muller D, Chang AE, Gao X, Huang L, *et al.* Safety and toxicity of catheter gene delivery to the pulmonary vasculature in a patient with metastatic melanoma. *Hum Gene Ther* 1994;5:1089-1094.
17. Miller AD. Human gene therapy comes of age. *Nature* 1992;357:455-460.
18. Human Gene Marker/Therapy Clinical Protocols (Complete Updated Listings). *Hum Gene Ther* 1996;7(13):1621-1647.
19. Zabner J, Couture LA, Gregory RJ, Graham SM, Smith AE, Welsh MJ. Adenovirus-mediated gene transfer transiently corrects the chloride transport defect in nasal epithelia of patients with cystic fibrosis. *Cell* 1993;75:207-216.
20. Crystal RG, McElvaney NG, Rosenfeld MA, Chu CS, Mastrangeli A, Hay JG, *et al.* Administration of an adenovirus containing the human CFTR cDNA to the respiratory tract of individuals with cystic fibrosis. *Nat Genet* 1994;8:42-50.
21. Wilson JM, Engelhardt JF, Grossman M, Simon RH, Yang Y. Gene therapy of cystic fibrosis lung disease using E1 deleted adenoviruses: a phase I trial. *Hum Gene Ther* 1994;5:501-519.
22. Zeitlin PL. Cystic fibrosis gene therapy trials and tribulations. *Mol Ther* 2000;1(1):5-6.
23. Somia N, Verma IM. Gene therapy: trials and tribulations. *Nat Rev Genet* 2000;1(2):91-99.
24. <http://oba.od.nih.gov/oba/rac/panelrep.pdf>
25. Aiuti A, Ficara F, Cattaneo F, Bordignon C, Roncarolo MG. Gene therapy for adenosine deaminase deficiency. *Curr Opin Allergy Clin Immunol* 2003;3(6):461-466.

26. Lu PY, Xie F, Woodle MC. In vivo application of RNA interference: from functional genomics to therapeutics. *Adv Genet* 2005;54:117-142.
27. Maksimenko A, Malvy C. Oncogene-targeted antisense oligonucleotides for the treatment of Ewing sarcoma. *Expert Opin Ther Targets* 2005;9(4):825-830.
28. Putral LN, Gu W, McMillan NA. RNA interference for the treatment of cancer. *Drug News Perspect* 2006;19(6):317-324.
29. Moreira JN, Santos A, Moura V, Pedroso de Lima MC, Simões S. Non-viral lipid-based nanoparticles for targeted cancer systemic gene silencing. *J Nanosci Nanotechnol* 2008;8(5):2187-2204.
30. Fattal E, Barratt G. Nanotechnologies and controlled release systems for the delivery of antisense oligonucleotides and small interfering RNA. *Br J Pharmacol* 2009;157(2):179-194.
31. Sigal A, Rotter V. Oncogenic mutations of the p53 tumor suppressor: The demons of the guardian of the genome. *Cancer Res* 2000;60:6788-6793.
32. Maxwell SA, Davis GE. Differential gene expression in p53-mediated apoptosis-resistant vs. apoptosis-sensitive tumor cell lines. *Proc Natl Acad Sci U S A* 2000;97(24):13009-13014.
33. Hainaut P, Hollstein M. p53 and human cancer: the first ten thousand mutations. *Adv Cancer Res* 2000;77:81-137.
34. Hollstein M, Rice K, Greenblatt MS, Soussi T, Fuchs R, Sørliie T, *et al.* Database of p53 gene somatic mutations in human tumors and cell lines. *Nucleic Acids Res* 1994;22(17):3551-3555.

35. Hsiao M, Low J, Dorn E, Ku D, Pattengale P, Yeargin J, *et al.* Gain-of-function mutations of the p53 gene induce lymphohematopoietic metastatic potential and tissue invasiveness. *Am J Pathol* 1994;145(3):702-714.
36. Gostissa M, Hengstermann A, Fogal V, Sandy P, Schwarz SE, Scheffner M, *et al.* Activation of p53 by conjugation to the ubiquitin-like protein SUMO-1. *EMBO J* 1999;18(22):6462–6471.
37. Santoso JT, Tang DC, Lane SB, Hung J, Reed DJ, Muller CY, *et al.* Adenovirus-based p53 gene therapy in ovarian cancer. *Gynecol Oncol* 1995;59(2):169-170.
38. von Gruenigen VE, Santoso JT, Coleman RL, Muller CY, Miller DS, Mathis JM. In vivo studies of adenovirus-based p53 gene therapy for ovarian cancer. *Gynecol Oncol* 1998;69(3):197-204.
39. Armandola EA. Gene Therapy in Cancer Patients. *Medscape General Medicin: Hematology-Oncology Expert Column* 2002. Available from URL:  
[http://www.medscape.com/viewarticle/445128\\_2](http://www.medscape.com/viewarticle/445128_2)
40. Jiang H, Gomez-Manzano C, Lang FF, Alemany R, Fueyo J. Oncolytic adenovirus: preclinical and clinical studies in patients with human malignant gliomas. *Curr Gene Ther* 2009;9(5):422-427.
41. Oster SK, Ho CS, Soucie EL, Penn LZ. The myc oncogene: Marvelously complex. *Adv Cancer Res* 2002;84:81-154.
42. Knies-Bamforth UE, Fox SB, Poulsom R, Evan GI, Harris AL. c-Myc interacts with hypoxia to induce angiogenesis in vivo by a vascular endothelial growth factor-dependent mechanism. *Cancer Res* 2004;64(18):6563-6570.
43. Ingvarsson S. The myc gene family proteins and their role in transformation and differentiation. *Semin. Cancer Biol* 1990;1(6):359-369.

44. Eisenman RN. Deconstructing myc. *Genes Dev* 2001;15(16):2023–2030.
45. Soucek L, Whitfield J, Martins CP, Andrew J, Finch AJ, Murphy DJ, *et. al.* Modelling Myc inhibition as a cancer therapy. *Nature* 2008;455:679-683.
46. Arvanitis C, Felsher DW. Conditionally MYC:insights from novel transgenic models. *Cancer Lett* 2005;226:95-99.
47. Muzzarelli RAA. Chitosan. In: Belcher R, Freiser H, editors. *Natural Chelating Polymers; Alginic acid, Chitin, and Chitosan*. Oxford: Pergamon Press, 1973. p. 144-176.
48. Cui Z, Mumper RJ. Chitosan-based nanoparticles for topical genetic immunization. *J Control Release* 2001;75(3):409-419.
49. Illum L, Jabbal-Gill I, Hinchcliffe M, Fisher AN, Davis SS. Chitosan as a novel nasal delivery system for vaccines. *Adv Drug Deliv Rev* 2001;51(1-3):81-96.
50. S. Aiba. Molecular structures and properties of partially *N*-acetylated chitosans. In: Brine CJ, Sandford PA, Zikakis JP, editors. *Advances in Chitin and Chitosan*, London: Elsevier, 1992. p. 137-144.
51. Grislain L, Couvreur P, Lenaerts V, Roland M, Deprez-Decampeneere D, Speiser P. Pharmacokinetics and distribution of a biodegradable drug-carrier. *Int J Pharm* 1983;15:335-345.
52. Allémann E, Gurny R, Doelker E. Drug-loaded nanoparticles-preparation methods and drug targeting issues. *Eur. J Pharm Biopharm* 1993;39:173-191.
53. Mosqueira VC, Legrand P, Gref R, Heurtault B, Appel M, Barratt G. Interactions between a macrophage cell line (J774A1) and surface-modified poly (D,L-lactide) nanocapsules bearing poly(ethylene glycol). *J Drug Target* 1999;7(1):65-78.

54. Gref R, Domb A, Quellec P, Blunck T, Muller RH, Verbavatz JM, *et al.* The controlled intravenous delivery of drugs using PEG-coated sterically stabilized nanospheres. *Adv Drug Deliv Rev* 1995;16(2):215-233.
55. Gref R, Lück M, Quellec P, Marchand M, Dellacherie E, Harnisch S, *et al.* 'Stealth' corona-core nanoparticles surface modified by polyethylene glycol (PEG): influences of the corona (PEG chain length and surface density) and of the core composition on phagocytic uptake and plasma protein adsorption. *Colloids Surf. B: Biointerfaces* 2000;18(3-4):301-313.
56. Leroux JC, De Jaeghere F, Anner B, Doelker E, Gurny R. An investigation on the role of plasma and serum opsonins on the internalization of biodegradable poly(D,L-lactic acid) nanoparticles by human monocytes. *Life Sci* 1995;57(7):695-703.
57. Gbadamosi JK, Hunter AC, Moghimi SM. PEGylation of microspheres generates a heterogeneous population of particles with differential surface characteristics and biological performance. *FEBS Lett* 2002;532(3):338-344.
58. Mauduit J, Bukh N, Vert M. Gentamycin/poly(lactic acid) blends aimed at sustained release local antibiotic therapy administered peroperatively. I. The case of gentamycin base and gentamycin sulfate in poly (lactic acid) oligomers. *J Control Release* 1993;23(3):221-230.
59. Perrin DE, English JP. Polyglycolide and Polylactate. In: Domb AJ, Kost J, Wiseman DM, editors. *Handbook of Biodegradable Polymers*. Amsterdam: Harwood Academic, 1997. p. 3-27.
60. Ogris M, Wagner E. Tumor-targeted gene transfer with DNA polyplexes. *Somat Cell Mol Genet* 2002;27(1-6):85-95.

61. Weitman SD, Lark RH, Coney LR, Fort DW, Frasca V, Zurawski VR Jr, *et al.*  
Distribution of the folate receptor GP38 in normal and malignant cell lines and tissues.  
*Cancer Res* 1992;52(12):3396-3401.
62. Ogris M, Wagner E. Tumor-targeted gene transfer with DNA polyplexes. *Somat Cell Mol Genet* 2002;27(1-6):85-95.
63. Franklin WA, Waintrub M, Edwards D, Christensen K, Prendergrast P, Woods J, *et al.*  
New anti-lung-cancer antibody cluster 12 reacts with human folate receptors present on adenocarcinoma. *Int J Cancer Suppl* 1994;8:89-95.
64. Coney LR, Tomassetti A, Carayannopoulos L, Frasca V, Kamen BA, Colnaghi MI *et al.*  
Cloning of a tumor-associated antigen: MOv18 and MOv19 antibodies recognize a folate-binding protein. *Cancer Res* 1991;51(22):6125-6132.
65. Garin-Chesa P, Campbell I, Saigo PE, Lewis JL Jr, Old LJ, Rettig WJ. Trophoblast and ovarian cancer antigen LK26. Sensitivity and specificity in immunopathology and molecular identification as a folate-binding protein. *Am J Pathol* 1993;142(2):557-567.
66. Campbell IG, Jones TA, Foulkes WD, Trowsdale J. Folate-binding protein is a marker for ovarian cancer. *Cancer Res* 1991;51(19):5329-5338.
67. Antony AC. The biological chemistry of folate receptors. *Blood* 1992;79(11):2807-2820.
68. Rothberg KG, Ying YS, Kolhouse JF, Kamen BA, Anderson RG. The glycopospholipid-linked folate receptor internalizes folate without entering the clathrin-coated pit endocytic pathway. *J Cell Biol* 1990;110(3):637-649.

69. Wang S, Lee RJ, Mathias CJ, Green MA, Low PS. Synthesis, purification, and tumor cell uptake of <sup>67</sup>Ga-deferoxamine-folate, a potential radiopharmaceutical for tumor imaging. *Bioconjugate Chem* 1996;7(1):56-62.
70. Lee RJ, Low PS. Delivery of liposomes into cultured KB cells via folate receptor-mediated endocytosis. *J Biol Chem* 1994;269(5):3198-3204.
71. Wang S, Low PS. Folate-mediated targeting of antineoplastic drugs, imaging agents, and nucleic acids to cancer cells. *J Control Release* 1998;53(1-3):39-48.
72. Gabizon A, Horowitz AT, Goren D, Tzemach D, Mandelbaum-Shavit F, Qazen MM, *et al.* Targeting folate receptor with folate linked to extremities of poly(ethylene glycol)-grafted liposomes: in vitro studies. *Bioconjug Chem* 1999;10(2): 289-298.
73. Malmqvist M. Biospecific interaction analysis using biosensor technology. *Nature* 1993;361(6408):186-187.
74. Corsi K, Chellat F, Yahia L, Fernandes JC. Mesenchymal stem cells, MG63 and HEK293 transfection using chitosan-DNA nanoparticles. *Biomaterials* 2003;24(7):1255-1264.
75. Pendley C, Schantz A, Wagner C. Immunogenicity of therapeutic monoclonal antibodies. *Curr Opin Mol Ther* 2003;5(2):172-179.
76. Dash PR, Read ML, Barrett LB, Wolfert MA, Seymour LW. Factors affecting blood clearance and in vivo distribution of polyelectrolyte complexes for gene delivery. *Gene Ther* 1999;6(4):643-650.
77. Murphy RF, Jorgensen ED, Cantor CR. Kinetics of histone endocytosis in Chinese hamster ovary cells. A flow cytofluorometric analysis. *J Biol Chem* 1982;257(4):1695-1701 .

78. Murphy RF, Powers S, Verderame M, Cantor CR, Pollack R. Flow cytofluorometric analysis of insulin binding and internalization by Swiss 3T3 cells. *Cytometry* 1982;2(6):402-406 .
79. Tycko B, Maxfield FR. Rapid acidification of endocytic vesicles containing alpha 2-macroglobulin. *Cell* 1982;28(3):643-651.
80. van Renswoude J, Bridges KR, Harford JB, Klausner RD. Receptor-mediated endocytosis of transferrin and the uptake of fe in K562 cells: identification of a nonlysosomal acidic compartment. *Proc Natl Acad Sci U S A* 1982;79(20):6186-6190.
81. Guan YS, La Z, Yang L, He Q, Li P. p53 gene in treatment of hepatic carcinoma: Status quo. *World J Gastroenterol.* 2007;13(7):985-992.

## CHAPTER 3

### Materials and Methods

#### 3.1. Materials

The cationic polymer, low molecular weight chitosan (LMW-CHI: MW 50-190KDa), polylactide-*block*-poly(ethyleneglycol)-*block*-polylactide (PLA-PEG-PLA; P<sup>3</sup>: M<sub>n</sub> 3.9KDa), folic acid (Fo: MW 0.441KDa), sodium acetate, glacial acetic acid, sodium chloride (NaCl), trypan blue solution (T8154), dimethylsulfoxide (DMSO), potassium chloride (KCl), calcium chloride (CaCl<sub>2</sub>), and fluorescein isothiocyanate (FITC) as well as the chemicals for the lysis buffer were purchased from Sigma, Aldrich (Milan, Italy) and used without further purification. MEGM<sup>®</sup> SingleQuots medium, fetal bovine serum (FBS), fetal calf serum (FCS) and DMEM medium was purchased from Lonza (Sigma, USA). The pcDNA<sub>3</sub>p53wt construct, used as anionic polymer, was a generous gift from Prof. G. Del Sal, (Laboratorio Nazionale Consorzio Interuniversitario Biotecnologie-LNCIB, Trieste, Italy) while the pAcGFP1 Actin vector was purchased from Clontech, Italy. The antisense oligonucleotide, *Silencer*<sup>®</sup> Select Pre-designed siRNA (Ambion:#4390818) against *c-myc* mRNA was purchased from Applied Biosystem, Italy. All experiments were performed with autoclaved Milli-Q grade water with a resistance of 18.2MΩ/cm<sup>2</sup> and treated with DEPC (Diethylpyrocarbonate) to prevent RNase degradation during the experiments.

The statistical analysis was performed using Origin8 and Graphpad Prism 5 software.

## 3.2. Methods

### 3.2.1. Coacervate particle preparation

The standard layer-by-layer protocol was followed for the preparation of the multilayered multifunctional CPs. Briefly, a charged core was assembled by electrostatic interaction between the polyanion, which is the plasmid encoding for wild-type p53 (pcDNA<sub>3</sub>p53wt) (fig. 3-1) and the polycation,

LWM-CHI solved in 1% acetate buffer (pH-5.5). Chitosan is a weak base polysaccharide (pKa value: 6.2–7.0 for the D-glucosamine residues), thus shows low solubility at neutral and alkaline pH. However, at low pH (pH-5.5) around 90% of the amine groups are protonated [1]. The LWM-CHI solution was sonicated followed by sterile filtration through a 0.22µm syringe filter. The polymer

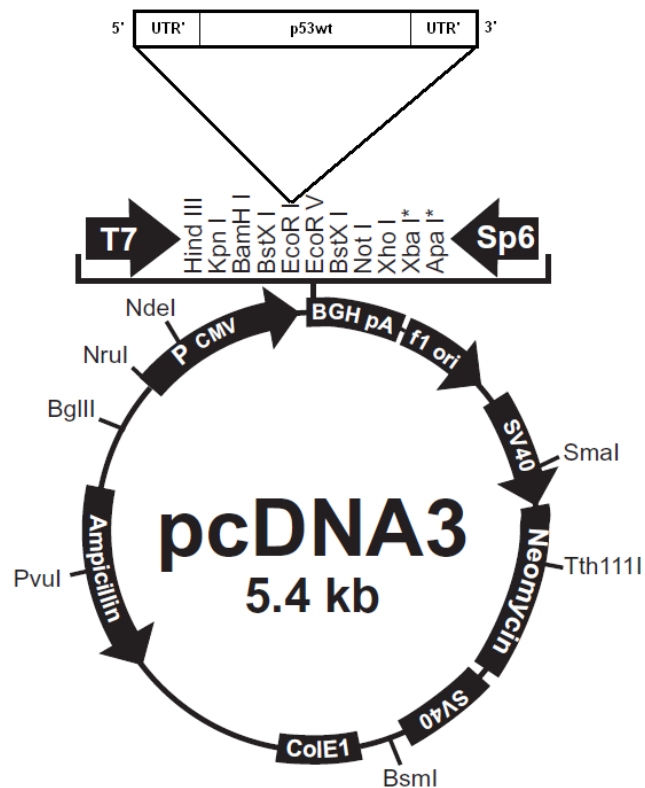


Fig. 3-1. The pcDNA<sub>3</sub>p53wt vector map.

solutions were heated to 42°C before the addition of the polyelectrolytes for the preparation of the core of the CPs at 37°C, in order to optimize the coacervation.

As the preparation procedure is a series of repeated deposition and washing steps, we summarize the details in table 3-1 and describe in the following only the general procedure.

*Table 3-1. Detailed step-by-step CP preparation method.*

CP	compound	Incubation step			Washing step			
		Conc ( $\mu$ M)	Final Volume ( $\mu$ L)	time (h)	Centrifugation			Re- suspension
					Speed ( $\times$ g)	Temp ( $^{\circ}$ C)	Time (min)	volume ( $\mu$ L)
Cp53	pcDNA <sub>3</sub> p53wt plasmid	0.0214	800	4	10,000	4	30	400
	LMW-CHI	0.04						
fCp53	pcDNA <sub>3</sub> p53wt plasmid	0.0214	800	4	10,000	4	30	400
	FITC-LMW-CHI	0.04						
CpAcGFPI	pAc GFPI-Mem	0.0214	800	4	10,000	4	30	400
	LMW-CHI	0.04						
iMCp53	siRNA (iM)	0.02	400	4	10,000	4	30	400
	Cp53							
P <sup>3</sup> iMCp53	P <sup>3</sup> (PLA-PEG-PLA)	128	400	4	8,000	4	30 (2)*	400
	iMCp53							
Fo- P <sup>3</sup> iMCp53	Fo (folic acid)	0.005	450	12	8,000	2	30 (4)*	400
	P <sup>3</sup> iMCp53							

\* In brackets: Repetition of washing steps

The particle suspension was added as drops to the polymer solution under intensive mixing to prevent local high particle concentration and hence agglomeration. Usually the unbound polymer was removed by three times centrifugation and re-suspension in a fresh DEPC treated water, followed by a brief sonication. Exceptions are indicated in the Table 3-1. The resulting CPs were characterized by size and polydispersity index (PDI) measurements with Dynamic Light Scattering (DLS) as well as the surface charge which was determined by the  $\zeta$ -potential using a Zetasizer (both: Nano-ZS; Malvern Instruments, Milan, Italy). Only CPs with PDI values of  $\sim$ 0.25 were used for the following coating steps. Particle concentrations were quantified by UV-Visible spectrophotometry (DU<sup>®</sup>730, Beckman

Coulter, Milan, Italy). The amount of bound nucleic acids was calculated from the optical density (OD) measured at  $\lambda=260\text{nm}$  and the assumption that OD is 1 for  $50\mu\text{g/mL}$  DNA and for  $40\mu\text{g/mL}$  RNA, respectively [2].

CPs for uptake and transfection efficiency determination by confocal fluorescence microscopy were prepared by varying the above described protocol. Furthermore to measure CP internalisation, fluorescent CPs, called fCPs [ $\text{P}^3\text{iMfCp53}$ ] were prepared by using FITC-labeled chitosan instead of the unlabelled one. FITC labeled chitosan was prepared in a 2-phase reaction. Chitosan flakes were suspended in water and mixed with FITC solved in DMSO for 1h. In this pH condition the amine groups are mainly uncharged and hence amenable to the covalent fluorophore binding. The success of the reaction can be seen from the bright orange color of the chitosan flakes and their solution. The unbound FITC was

removed by repeated washing of the chitosan flakes with pure water until the solution was no longer yellow. Then the flakes were dried and kept as powder until use. Finally, for transfection efficacy, reporter-gene containing CPs [ $\text{P}^3\text{iMCpAcGFP1}$ ] were prepared with pAcGFP1-Mem (4.8Kbps) vector as core encoding for AcGFP1 (fig. 3-2), a fusion protein of

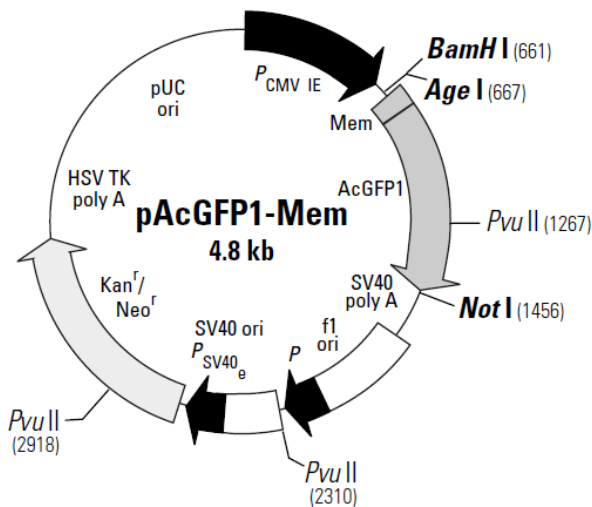


Fig. 3-2. The pAcGFP1-Mem vector map.

*Aequorea coerulea* Green Fluorescence Protein and the N-terminal 20 amino acids of neuromodulin. The neuromodulin fragment contains a signal for posttranslational

palmylation of cysteine 3 and 4 and hence the expressed GFP construct marks cellular membranes green.

### **3.2.2. CP stability analysis**

The stability of [Fo-P<sup>3</sup>iMCp53] CPs as well as [Fo-iMCp53] CPs was studied for the following conditions: (i) 2months at 4°C in MQ-water, (ii) 2h at room temperature in a Ringer solution ([NaCl]=0.147M, [KCl]=0.004M, [CaCl<sub>2</sub>]=0.0033M) and (iii) 2h at RT in MQ-water. The hydrodynamic size as well as the PDI was determined by DLS.

### **3.2.3. CPs Internalization and Transfection efficiency determination**

In order to determine the particle uptake by breast cancer cells, MDA MB 231 (ATCC HTB-26™), and Leukemic cell - HL60 (ATCC CCL-240™) line were incubated with green fluorescent P<sup>3</sup>iMfCp53 CPs for 24 h. For the transfection efficiency, the same cell lines were incubated with GFP expressing P<sup>3</sup>iMCpAcGFP1 CPs. In both cases, the coacervates were either with or without folic acid functionalisation.

Both cell lines were continuously maintained in DMEM medium supplemented with 10% heat-inactivated fetal bovine serum (FBS), penicillin (100units/ml), streptomycin (100µg/ml), gentamicin (10µg/ml) at 5% CO<sub>2</sub> and 37°C. The medium was changed every second day. A mycoplasma test was performed to exclude any possible contamination prior to performing all experiments.

For the CP uptake study, MDA MB 231 and HL60 cells (2×10<sup>5</sup> cells/mL), grown on WillCo-dish® Glass-Bottom dish (WillCo Wells BV, Netherlands) were treated with

P<sup>3</sup>iMfCp53 CPs (conc. approx. 40.5µg/mL) with or without folic acid and incubated for 24h at 37°C and 5% CO<sub>2</sub>. The short incubation time was necessary in order to avoid cell loss through apoptosis induced by the wild-type p53.

The transfection efficiency was determined as follows: 2mL of HL60 cell suspension (2×10<sup>5</sup> cells/mL) were incubated for 3days with P<sup>3</sup>iMCpAcGFP1 and Fo-P<sup>3</sup>iMCpAcGFP1 CPs (DNA-RNA concentration: approx. 40.5µg/mL), respectively.

The percentage of transfected cells were determined by counting the green fluorescent cells in comparison to the total number of cells. Therefore, confocal images were acquired with Nikon C1 laser scanning confocal microscope (Nikon D-eclipse C1Si, Japan) with 100X/1.49 oil Apo TIRF objective (Nikon, Japan). The fluorophore excitation was performed with an air-cooled argon laser at 488 nm and appropriate filter sets were used to collect the fluorescence emission. Images were acquired and analyzed using the Nikon provided operation EZ-C1 software. Each experiment was repeated 4 times (for each experiment ~1000 cells were included in the statistical analysis).

#### **3.2.4. Protein extraction and Western blot**

To evaluate variations in the protein expression induced by CP exposure (incubation procedure as described in section 2.3), the total cellular proteins were extracted either from untreated control (c) samples, from Fo-iMCpAcGFP1 (tc-treated control) or from Fo-iMCp53 (t-treated) CPs treated HL60 cells (deleted p53 gene). In the case of the breast cancer MDA MB cell line (mutated p53), proteins were only extracted from the control (c), and Fo-iMCp53 CPs treated (t) cells.

Briefly, after PBS washing, the HL60 cell pellets and the adhered MDA MB 231 cells were lysed for 5min on ice with 100 $\mu$ L and 400 $\mu$ L lysis buffer (20 mM Tris-HCl pH 7.0, 150mM NaCl, 1mM Na<sub>2</sub>EDTA, 1% Triton, 2.5mM sodium pyrophosphate, 1mM  $\beta$ -glycerophosphate, 1mM Na<sub>3</sub>VO<sub>4</sub>, 1 $\mu$ g/mL leupeptin), respectively . Cell debris was removed by centrifugation for 10 min at 14,000 $\times$ g at 4°C, followed by quick freezing of the supernatants. Protein concentrations were determined using the Bicinchoninic Acid Protein Assay Kit (SIGMA) in accordance to the manufacturer’s protocol. Subsequently, from the differently treated cells 20 $\mu$ g of total cellular protein was separated by gel electrophoresis in 8% SDS-polyacrylamide gel, followed by electro-blotting onto a nitrocellulose membrane. The electro-blotted membranes were then incubated for 1 h in 4% milk-TTBS (Tween-Tris Buffered Saline: 0.1% Tween-20 in 100 mM Tris-Cl [pH 7.5], 0.9% NaCl) for blocking and incubated over night at 4°C with primary antibodies in 4% milk-TTBS (details can be found in Table 3). After washing 3 times with 4% milk-TTBS, the immuno-blot was incubated for 2h with HRP (Horseradish Peroxidase) conjugated secondary antibodies (condition see: Table 3-2). Following 3-4 times washing with TTBS, detection was by the ECL kit, and performed in accordance to the manufacturer’s protocol (Amersham ECL Plus kit (RPN 2132)). For protein quantification, the intensity of the protein band was normalized to that of an actin standard, using ImageJ software.

*Table 3-2. Dilution of antibodies used in western blot analysis.*

<b>Primary Antibody</b>	<b>Dilution</b>	<b>Secondary Antibody</b>	<b>Dilution</b>
Mouse monoclonal anti-Myc (C-33:Sc-42, Santa Cruz Biotechnology)	1:200	Anti-mouse-HRP polyclonal (P0260,Dako Cytomation A/S)	1:2000
Goat polyclonal anti-p53 (sc-6243-G, Santa Cruz Biotechnology)	1:1000	Anti-goat-HRP polyclonal (PA1-32365, Pierce Antibodies)	1:10000
Rabbit anti-Actin (A2066, Sigma)	1:4000	Anti- rabbit-HRP polyclonal (P0448, Dako Cytomation A/S)	1:2000

### **3.2.5. CP induced apoptosis analysis**

During early apoptosis, phosphatidyl serine (PS) from the inner leaflet of the plasma membrane is transferred to the membrane surface for recognition by macrophages. Thus, PS becomes accessible to the Annexin-V/FITC conjugate and appears green in fluorescence microscopy [3]. On the other hand, propidium iodide (PI) red fluorescent staining allows the detection of late apoptotic cells with disrupted membrane and exposed DNA. In this way, early apoptotic cells will stain positive for Annexin-V/FITC and negative for PI, hence late apoptotic or necrotic cells, will stain positive for both, Annexin-V and PI, whereas normal viable cells in culture will be negative for both dyes.

For the staining procedure, MDA MB 231 cells were seeded onto glass cover-slips ( $2 \times 10^5$  cells/cover-slip) in a petri-dish under the previously mentioned growing conditions. After 24 h of treatment with Fo-P<sup>3</sup>iMCp53 (as above), the glass cover-slips were rinsed twice with PBS and washed with the binding buffer (10mM HEPES/NaOH, 140mM NaCl, 2.5mM CaCl<sub>2</sub>, pH-7.4). The cells were then incubated for 15min at room temperature (RT) with Annexin V–FITC (1:100, v/v) (Boehringer Ingelheim, Germany). After washing once with PBS, they were further incubated with propidium iodide (PI) (1:100, v/v) (molecular probes, USA).

Finally, the cells were washed twice in PBS and fixed with 4% paraformaldehyde for 20 min at RT. They were subsequently washed twice in PBS and to visualize the nucleus, the cells were incubated with Hoechst-33342 (molecular probes) (10 $\mu$ M) for 10mins. After washing again twice with PBS, coverlips were mounted with Vecta-shield (Vector Laboratories, Inc., Burlingame). The images were acquired with a Leica laser scanning confocal microscope (TCS SP2, Leica, Germany). Every experiment was repeated 3 times.

### **3.2.6. Cell Viability analysis**

Cell viability was determined by Trypan Blue dye exclusion, which is based on the fact that viable cells with an intact membrane, exclude the dye, while apoptotic cells or those with corrupted membrane integrity, will be stained. The non-cancerous liver cell line- IHH (immortalized human hepatocyte cell line, ATCC, Rockville, MD, USA) were used as a negative control. The viability of the treated non-cancerous cell line was compared to 3 cancer cell lines, JHH-6 (hepatocellular carcinoma, JCRB1030, Japan Health Science Research Resources Bank), HL-60 (leukaemia), and MDA MB 231 (breast cancer).

IHH cells were maintained in DMEM/F12 1× medium containing 15mM Hepes buffer, L-glutamine and pyridoxine HCl, 1µM dexametasone (Sigma-Aldrich), 5µg/mL bovine pancreas insulin (Sigma-Aldrich), antibiotics (10,000U/mL penicillin, and 10mg/mL streptomycin (Euro-clone)) and 10% (v/v) fetal bovine serum (FBS) (Invitrogen); whereas JHH6 were kept in William's E medium (Sigma-Aldrich, Missouri, USA W4128) supplemented 10% (v/v) fetal bovine serum (FBS), 2mM L-Glutamine (Euro-clone), and 1%(v/v) antibiotics (10,000U/mL penicillin, and 10mg/mL streptomycin); HL60 and MDA MB 231 cells were kept under the same conditions as described for the transfection efficiency. They were seeded at  $12 \times 10^4$  cells/well in 6 well-plates and transfected with Fo-P<sup>3</sup>iMCp53 CPs (concentration as before) and kept for 3 days at 37°C and 5%CO<sub>2</sub>, with respective untreated cells as control. After washing twice with PBS, these cells were incubated with 1:1 (v/v) of 4% trypan blue solution for 1 min and unstained cells (live cells) and total number of cells were counted on a haemocytometer with a Carl Zeiss light Microscope (Axiovert 40C, Zeiss, Milan, Italy). For each cell line, percentage cell viability

after treatment was determined on the basis of respective control (untreated) cells as 100% viability. Each experiment was repeated three times.

### **3.2.7. Macrophage recognition**

Fo-P<sup>3</sup>iMCp53 CPs uptake in macrophages was studied because they are the first responder in immune recognition, and hence the main reason for nanoparticle elimination from blood by the mononuclear phagocyte system (MPS).

Non-activated J774.2 macrophages (ECACC, Mouse BALB/C monocyte macrophage cell line, a generous gift from Prof. Andrea Nistri, Neurobiology sector, SISSA) were seeded ( $2 \times 10^5$  cells/ml) on a WillCo-dish® Glass-Bottom dish, in DMEM medium supplemented with 10% heat-inactivated FBS, penicillin (100units/ml), streptomycin (100µg/ml), gentamicin (10 µg/ml) at 5% CO<sub>2</sub> and 37°C for 48h. The cells were then incubated for 4h, 24h or 72h with Fo-P<sup>3</sup>iMfCp53 CPs (procedure as described in section 2.3), followed by three times rinsing with medium. The percentage of cells which had internalized Fo-P<sup>3</sup>iMfCp53 CPs was determined by fluorescence confocal microscopy. In order to evaluate the cell morphology, transmitted white light was collected through the second channel of the microscope to merge the fluorescence and transmission signal.

### **3.3. References**

1. S. Aiba. Molecular structures and properties of partially *N*-acetylated chitosans. In: Brine CJ, Sandford PA, Zikakis JP, eitors. *Advances in Chitin and Chitosan*, London: Elsevier, 1992. p. 137-144.
2. Sambrook J, Russell D. *Molecular Cloning: A Laboratory Manual*, 3rd ed. Cold Spring Harbor Laboratory Press, 2001.
3. Vermes I, Haanen C, Steffens-Nakken H, Reutelingsperger C. A novel assay for apoptosis - flow cytometric detection of phosphatidylserine expression on early apoptotic cells using fluorescein labelled Annexin V. *J Immunol Meth* 1995;184(1):39-51.

## CHAPTER 4

### Results and Discussion

#### 4.1. Synthesis and characterization of the multifunctional coacervate particles

As cancer is a disease caused by mutations in several genes which mainly regulate cell proliferation and apoptosis [1], a new generation of small multifunctional cancer cell targeted particles (Fo-P3iMCp53), correcting both of these mutations was been designed and produced in a multistep preparation. Fig. 4-1 shows a scheme of CP preparation by using a layer-by-layer approach. [2]

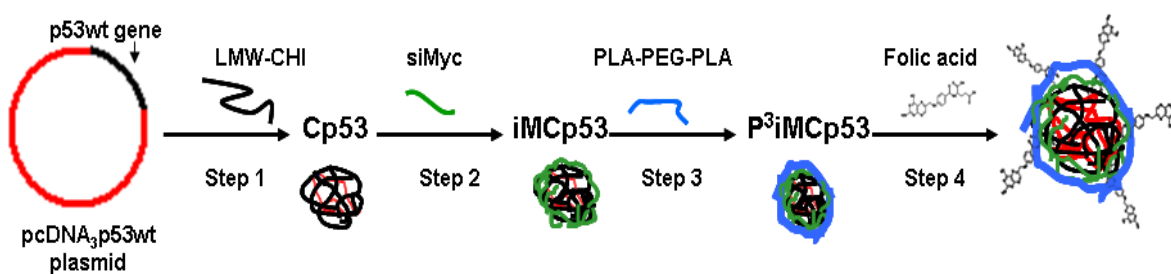


Figure 4-1. Scheme of the layer-wise construction of the [Fo-P<sup>3</sup>iMCp53] coacervate particles.

The first step was to create a charged core on which layer-wise several polymers with functional moieties could be deposited electrostatically. The positively charged core (Cp53) consists of a condensed polyanionic plasmid (due to the presence of polyphosphate group) bearing the wild-type p53 gene, complex with the biodegradable, non-toxic polycation,

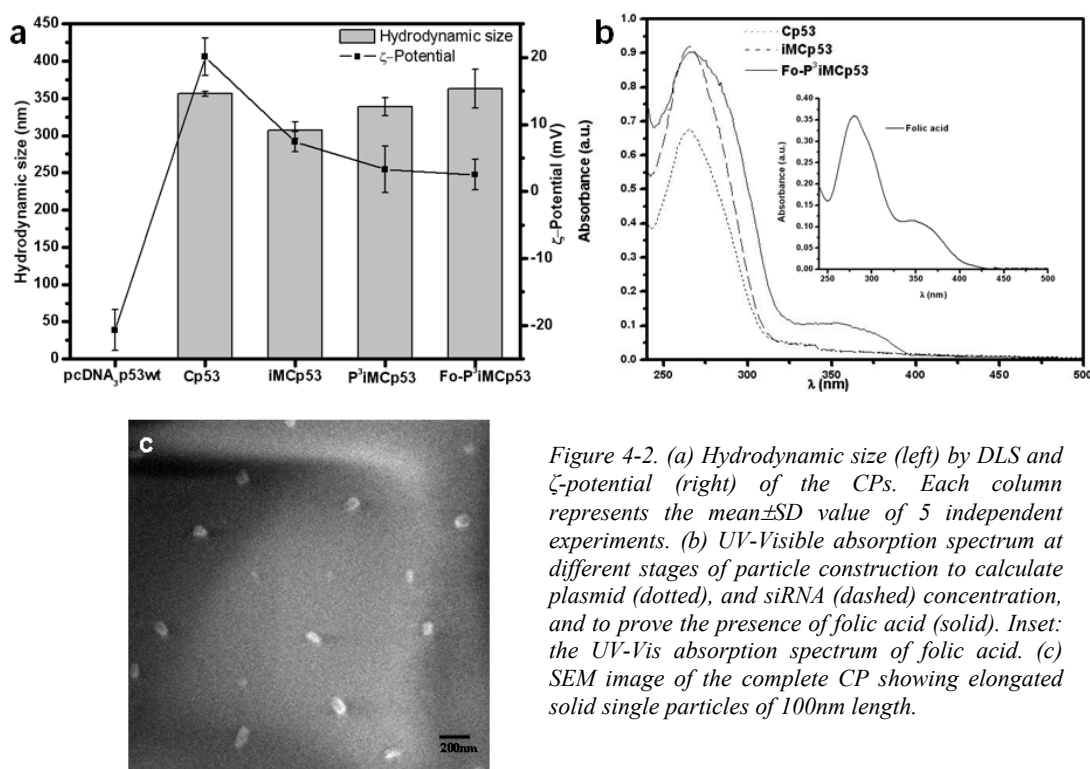


Figure 4-2. (a) Hydrodynamic size (left) by DLS and  $\zeta$ -potential (right) of the CPs. Each column represents the mean $\pm$ SD value of 5 independent experiments. (b) UV-Visible absorption spectrum at different stages of particle construction to calculate plasmid (dotted), and siRNA (dashed) concentration, and to prove the presence of folic acid (solid). Inset: the UV-Vis absorption spectrum of folic acid. (c) SEM image of the complete CP showing elongated solid single particles of 100nm length.

chitosan (due to the presence of primary amine group) (fig. 4-1, 4-2a) [3-5]. The polyanion (DNA) and polycation (LMW-CHI) were mixed with a charge ratio (N:P) of 20, assuming that polymers are completely charged. The resulting particles (pcDNA<sub>3</sub>p53wt) have a hydrodynamic size of 356 $\pm$ 3nm (fig. 4-2a). The change in the zeta-potential from -20 $\pm$ 3mV for the free plasmid to +20 $\pm$ 3mV for the coacervate core illustrates the binding of chitosan to DNA as well as the overcompensation of the negative charge. By UV-Vis spectroscopy the amount of bound plasmid was calculated by the absorption at 260 nm to be 33.85 $\mu$ g/mL (fig. 4-2b) (Table 4-1). Further the interaction of plasmid and polycation took place, was predicted

by the  $A_{260/280}$  ratio. As a result of polycation-plasmid intercalation, a reduction in the  $A_{260/280}$  ratio i.e. to be 1.28 was observed, whereas it is 1.8 for pure DNA. Due to the fact that chitosan has no absorption at these wavelengths, the uploaded amount of DNA was calculated to be 67.7% in the CP constructs.

The binding of chitosan ( $pK_a = 6.5$ ) to the negatively charged plasmid was triggered by the fact that the coacervation procedure was carried out at pH 5.5, at which the majority of amino groups is protonated [3]. An additional beneficial effect of chitosan binding to the plasmid is that it can prevent degradation by nucleases in the blood and in cells [6, 7].

The next layer deposited on the plasmid core was siRNA which was aimed to bind mRNA in order to down-regulate mutated oncoprotein growth factors such as c-Myc. and hence suppress cancer cell growth and proliferation. The excess positive charge of the Cp53 CP core was used to induce the electrostatic binding of siRNA (fig. 4-2a). The successful deposition of the siRNA against c-Myc mRNA was deduced from the reduction in zeta-potential from  $+20 \pm 3 \text{ mV}$  to  $+7 \pm 1.5 \text{ mV}$ . The reduction in zeta-potential value can be explained by the interaction of phosphate ( $\text{PO}_4^{3-}$ ) groups of siRNA with remaining free positively charged amino ( $\text{NH}_4^+$ ) groups of LMW-CHI. Moreover it could be observed that the hydrodynamic size decreased from  $356 \pm 3 \text{ nm}$  (Cp53) to  $307 \pm 11 \text{ nm}$  (iMCp53) (fig. 4-2a). A possible explanation for the decrease in the hydrodynamic size after siRNA deposition can be that the binding of siRNA condensate the polymeric core by reducing the repulsive forces induced by excess positive charges or binding free polycation loops which are also visible in the size as determined by DLS.

The amount of bound siRNA was calculated from UV-Vis spectroscopy (fig. 4-2b, Table 4-1). From the  $\text{OD}=0.924$  at 260 nm it was calculated that  $23.42 \pm 5.6 \mu\text{g/mL}$  of the initially added  $135.7 \mu\text{g/mL}$  are bound, which is a binding efficiency of 17.31% (table 3). Here the

dilution of the initial plasmid concentration by the RNA addition as well as the absorption at 260 nm due to the DNA had to be considered..

In order to induce a long circulating time in blood by “stealth” the particle surface and to improve the binding to cancerous cells, the biodegradable, neutral PLA-PEG-PLA (P<sup>3</sup>) was deposited.

Table 4-1. Calculation of the nucleic acid content of the CPs at different preparation steps.

CPNPs at different steps <sup>£</sup>	A=OD <sub>260</sub>	B (Abs. due to dil. )=A/dil. Factor i.e 2	C= Abs. difference at OD260 =A-B	G=Total Amount in CPNPs: DNA=A*50; RNA=C*40; (µg/mL) (± SD)	H=Amount used for uploading (µg/mL)	% Uploading efficiency=H*100/G
Cp53	0.677±0.12	0.3385		33.85±6	50	67.7
iMCp53	0.924±0.14		0.5855	23.42±5.6	135.7	17.31

& n=5

¥ Plasmid concentration = Absorbance at 260\*50

£ siRNA concentration = Absorbance at 260\*40

Upon P<sup>3</sup> binding only small changes in zeta potential from +7±1.5mV to +3±5 mV and hydrodynamic size from 307±11nm to 339±12nm were observed (fig. 4-2a). The small changes are due to the fact that the neutral polymer P<sup>3</sup> masks the remaining charged amine groups of LMW-CHI rather than neutralizing them. This assumption is supported by the observation that without the P<sup>3</sup> layer in presence of small ions (like those present e.g. in Ringer’s solution) the hydrodynamic size (477±50nm) and the PDI value (0.57±0.1) both increase with respect to the (hydrodynamic size: 311±27nm and PDI: 0.26±0.03) in pure

water (fig. 4-3b). This increase in diameter can be explained by an interaction of the free charges of the polyelectrolytes with small ions which can penetrate the polyelectrolyte matrix. If the P<sup>3</sup> layer is present as for the complete construct [Fo- P<sup>3</sup>iMCp53] no significant change in the size can be observed under the same experimental conditions (fig. 4-3a). In general it can be said that the particles with the P<sup>3</sup> layer are very stable, even over the period of 2 months. This could be due to the presence of dense surface coverage with hydrophilic PEG molecules which produce a hydrated nanoshell that may effectively screen the ions and later in blood it can repel effectively proteins and cells [8, 9].

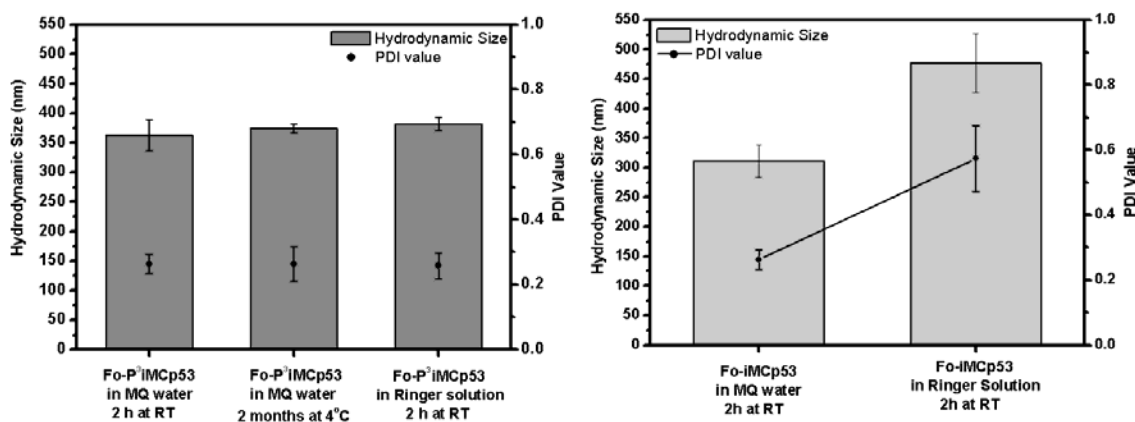


Figure 4-3. CP stability analysis in different storage condition determined by DLS studies. Stability of CPs (a) with and (b) without P<sup>3</sup> layer at different storage conditions. Hydrodynamic size (left) and Poly Dispersity Index (PDI) values (right) versus storage time and conditions. Each column represents mean $\pm$ SD values of 3 independent experiments.

In a final preparation step folic acid molecules as targeting ligand are immobilized onto the particle surface. While the binding of folic acid onto the [P<sup>3</sup>iMCp53] CPs [Fo-P<sup>3</sup>iMCp53] shows no differences in the surface charge ((+3 $\pm$ 5mV [P<sup>3</sup>iMCp53] CPs; +2.5 $\pm$ 2.5mV [Fo-P<sup>3</sup>iMCp53 CPs]) (fig. 4-2a), a slight increase in hydrodynamic size from 339 $\pm$ 11nm to 363 $\pm$ 26nm with PDI: 0.263 $\pm$ 0.03 was measured (fig. 4-2a). A final proof that folic acid is attached to the particles comes from UV-Vis measurements (fig. 4-2b). The UV-

Vis absorbance spectra of Fo-P<sup>3</sup>iMCp53 shows the characteristic absorption maximum of folic acid at 350 nm, as well as a broadening of the main peak between 260nm till 280nm, which is a characteristic peak of a folic acid spectrum (inset fig. 4-2b).

The Scanning Electron Microscopic (SEM) image of Fo-P<sup>3</sup>iMCp53 CPs (fig. 4-2c) also shows that they have a well-shape and compact structure, with an average size of 130±20nm. The difference in size between the SEM and DLS measurement can be explained by the fact that SEM works at ultra high vacuum and the particles are deprived of water. In contrast the DLS measurement determines CPs in a more realistic environment including the associated counter ions and the water shell of the particles.

## **4.2. CP multi-functionality analysis**

### **4.2.1. Folate-receptor mediated uptake efficiency of Fo-fCPs**

It is known [10] that the folic acid-folate receptor-mediated endosome delivers its content into the nucleus (fig. 4-4a). Hence, first I investigated the Fo-fCPs uptake efficiency in the breast cancer cell line and leukemic cell line. Both the selected cell lines are known to over express FR [11, 12]. Cellular uptake of CPs was analyzed by imaging with confocal fluorescence microscopy by using fluorescently labeled P<sup>3</sup>iMfCp53 particles in the two model cell lines: MDA MB 231, a breast cancer cell line as an adherent solid tumor model and HL60, a leukemic cell line in suspension as a circulating cancer model (fig. 4-4 c). In order to prevent that the cells may undergo apoptosis induced by the p53 plasmid the uptake experiment was limited to 24 h. Due to the fact that the cells are not synchronized, cells in different states of particle internalization can be observed by confocal microscopy. The tagging 1,2 and 3 in the fluorescent micrograph (fig. 4-4b) is in accordance to the scheme in fig. 4-4a. It can be clearly seen that the fluorescent construct was internalized into the cells by

an endocytic pathway (2) and that it is delivered to and entered into the nucleus (3) (fig. 4-4a,

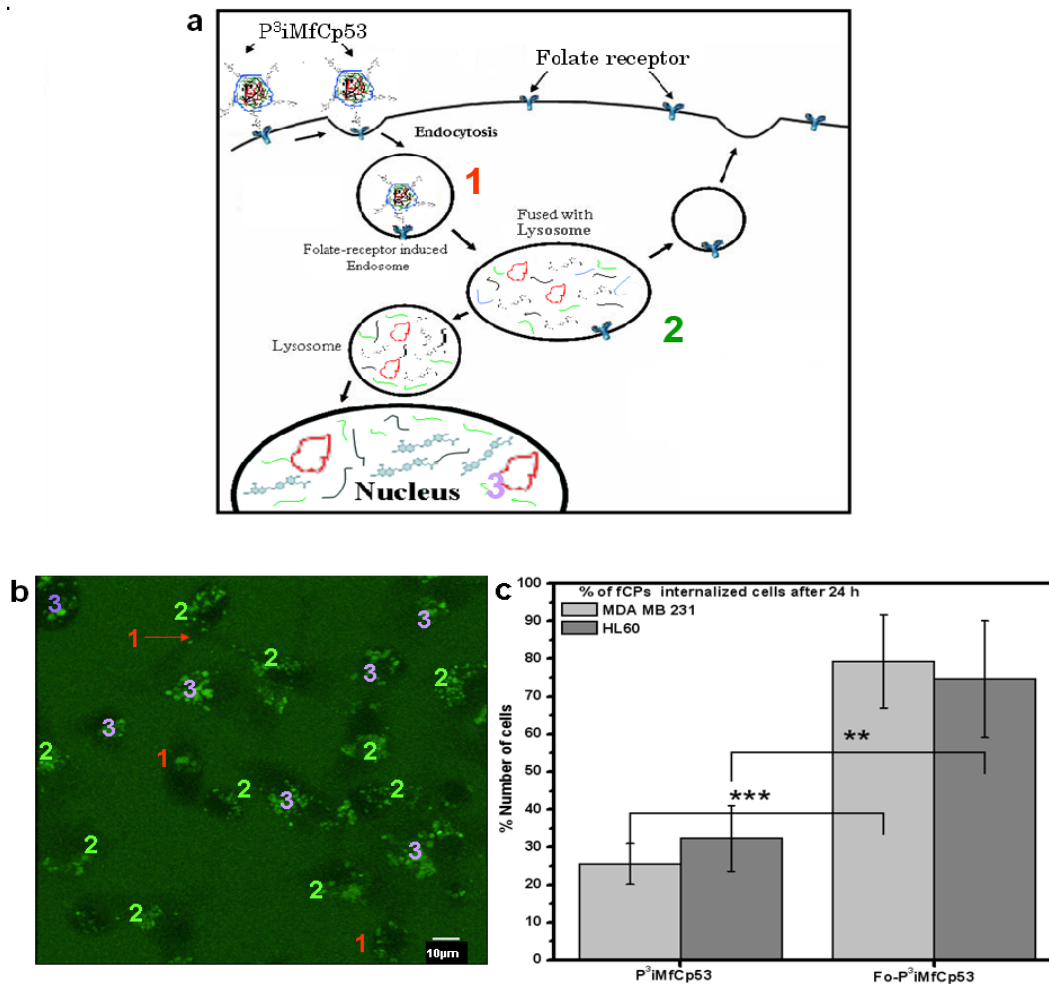


Fig. 4-4. (a) Scheme describing the folate-receptor mediated uptake of  $Fo-P^3iMfCp53$ . The tags 1, 2 and 3 show the major steps of folate-receptor mediated endosomal pathway. (b) Confocal fluorescence image of  $Fo-P^3iMfCp53$  (green) uptake in MDA MB 231 breast cancer cells, where 1, 2 and 3 are the steps in folate-receptor endosomal pathway as tagged in the scheme in (a). The scale bar represents 10  $\mu m$ . (c) Statistical study of the % of the CP internalised cells (green) after transfecting with the fluorescently labeled  $P^3iMfCp53$  or  $Fo-P^3iMfCp53$  (\*\*\*) represents  $P \leq 0.0005$ ; \*\* represents  $P \leq 0.005$ ). Each value represents the mean  $\pm$  SD of 4 independent experiments.

b). Moreover the importance of folic acid in the up-take mechanism becomes apparent by comparing the number of cells up-taking the particles with or without folic acid (fig. 4-4b). It was clearly seen that the number of cancer cells with fCPs are significantly higher in the presence of folic acid. The above result was further supported by a competition assay, where

the cells were incubated with particles in the presence of different concentrations of free folic acid. The number of cells with internalized fCPs decreased from 80 to 40-50% if the concentration increased (Fig. 4-5). Moreover, above analysis clearly supports that the uptake is FR mediated.

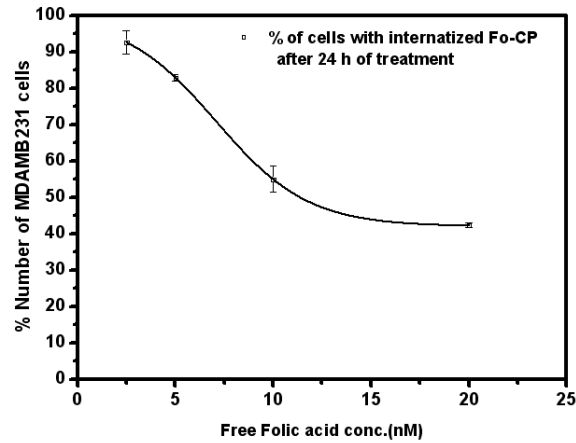


Figure 4-5. Folic acid competition assay for Fo-P<sup>3</sup>iMCp53 CPs to confirm the involvement of folate-receptor mediated endocytosis in the cellular uptake. The CPs were added in presence of different concentrations of free folic acid (2.5, 5, 10, 20nM). Each value represents mean±SD of 3 independent experiments. The black line represents the sigmoid fit.

#### 4.2.2. Transfection efficiency of Fo-CPs

In order to determine the influence of folic acid on the transfection efficacy, a pAcGFP1-

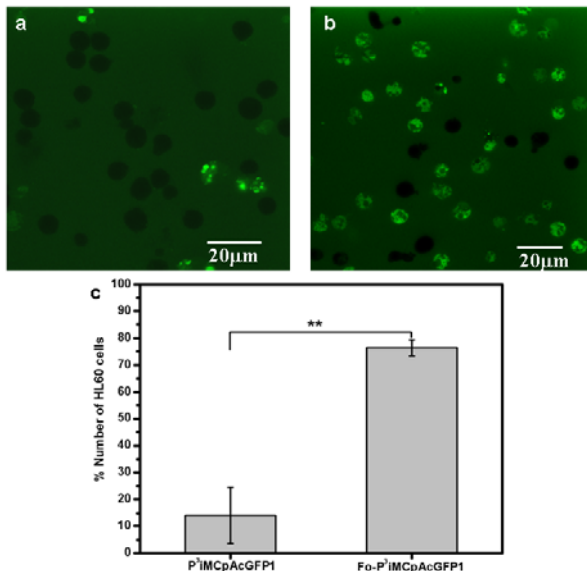


Figure 4-6. Confocal fluorescence micrographs of HL60 cells transfected (a) P<sup>3</sup>iMCpAcGFP1 CPs or (b) Fo-P<sup>3</sup>iMCpAcGFP1 CPs. The green fluorescence shows the expression of AcGFP1 3 days after transfection (c) Diagram of the % of the cells expressing AcGFP1 with and without folic acid mediated particle delivery (\*\* represents  $P \leq 0.005$ ). Each column represents the mean±SD value of 3 independent experiments.

mem vector encoding for the reporter membrane fusion AcGFP1 protein (Fo-P<sup>3</sup>iMCpAcGFP1) instead of pcDNA<sub>3</sub>p53wt vector was used. Fig. 4-6a & b, shows the results of the transfections of P<sup>3</sup>iMCpAcGFP1 and Fo-P<sup>3</sup>iMCpAcGFP1 CP in the HL60 cell line. Here, a significant difference for the transfection efficacy between cells exposed to the CPs with or without folic acid is found (fig. 4-6c). However, even more interesting was the difference of

GFP expression to plasmid uptake. While ~ 30% of the HL60 cells internalize the CPs without folic acid (fig. 4-6b) only ~14±10% are truly transfected (fig. 4-6c). Assuming that the up-take for the GFP encoding plasmid is the same as for the p53 encoding one this indicates that the up-take without folic acid leads to a release of the plasmid in the cytosol so that the GFP cannot be expressed properly while the uptake and the expression in case of folic acid labeling grows to approximately 75%. That indicates that folic acid not only enhances the particle uptake efficiency but also guides the release to the nucleus, thus the GFP expression efficiency significantly coincides with the particle internalization efficiency. These findings were in good agreement with the result of other groups reporting that folate is able to assist in particle up-take and guidance to the nucleus or cytosol [13, 14]. Even the presence of 10% FBS did not interfere with the transfection yield, indicating that the lack of interaction with serum protein during systemic administration [13].

### 4.2.3. CPs identification by the MPS

Finally, I tested the recognition by macrophages which are the first responder of the immune system. It was observed

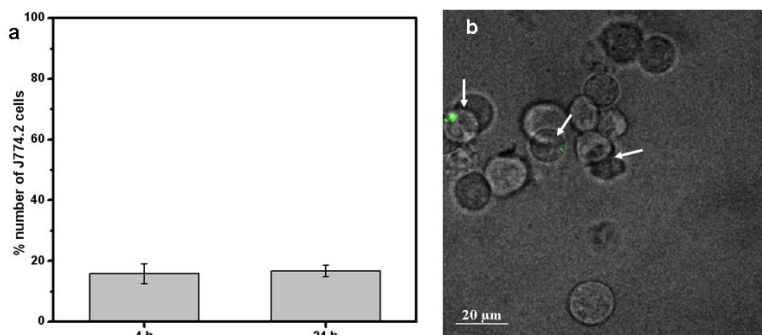


Figure 4-7. Fo- $P^3iMfCp53$  uptake in J774.2 macrophage. (b) Statistical study of the % of the J774.2 cells internalised CPs (green) after 4 h and 24 h treatment. Each column represents the mean±SD value of 5 independent experiments. (a) Confocal fluorescence image merged with a light transmission image of cells (grey) with internalized Fo-CPs (green).

that only a limited number of macrophages internalize the fCPs (Fig. 4-7). After 4h treatment with Fo-fCPs, only 15±3% of the macrophage cells (J774.2 cell line) shows

internalized fCPs, after 24h treatment it is  $16 \pm 2\%$  cells. Therefore there was no significant increase in uptake was observed (fig. 4-7a). There are two possible reasons for the favorable low uptake.. 1) the P<sup>3</sup> coating is preventing the recognition by the macrophages as described previously in literature [15-20]; or 2) the up-take observed in macrophages is in the same range as that for particles without folic acid taken up by cancer cells (fig. 4-4c). This can indicate that it is related to unspecific pinocytosis induced uptake in cells. In order to understand the reason for CP up-take into macrophages, I planned to conduct some future experiments with activated macrophages.

#### **4.2.4. Targeted antisense and gene therapeutic efficiency of the Fo-P<sup>3</sup>iMCp53 CPs**

##### **4.2.4.1. CP induces targeted protein down- or up-regulation**

In order to determine the efficacy of the multilayered antisense and gene therapeutic effect of CPs, several cancer cell line as well as non-cancerous cells were exposed to the complete CP construct (Fo-P<sup>3</sup>iMCp53). The CP was aimed to eventually inhibiting cancer cell proliferation by releasing siRNA against c-myc mRNA and to induce apoptosis by delivering the vector encoding for wild type p53.

First the expression level of wild-type p53 gene and c-Myc knockdown was quantified for HL60 cell line where the p53 gene is deleted and the MDA MB 231 cell line which has a mutation in p53 gene. The expression of p53 as well as the inhibition of c-Myc expression induced by Fo-P<sup>3</sup>iMCp53 particles in the treated cells was determined by Western blot analysis.

For MDA MB 231 cells, the control (untreated cells) showed, as expected, an expression of mutated p53 (fig. 4-8a). However, in the treated breast cancer cells, p53 expression was enhanced as indicated by an increase in the protein band intensity by ~50% higher when

compared to the protein band of the untreated cells. Fig. 4-8a, illustrates the efficacy of the CP to suppress c-myc oncogene expression, by the absence or low intensity of the protein band when comparing the treated cell with the untreated cells.

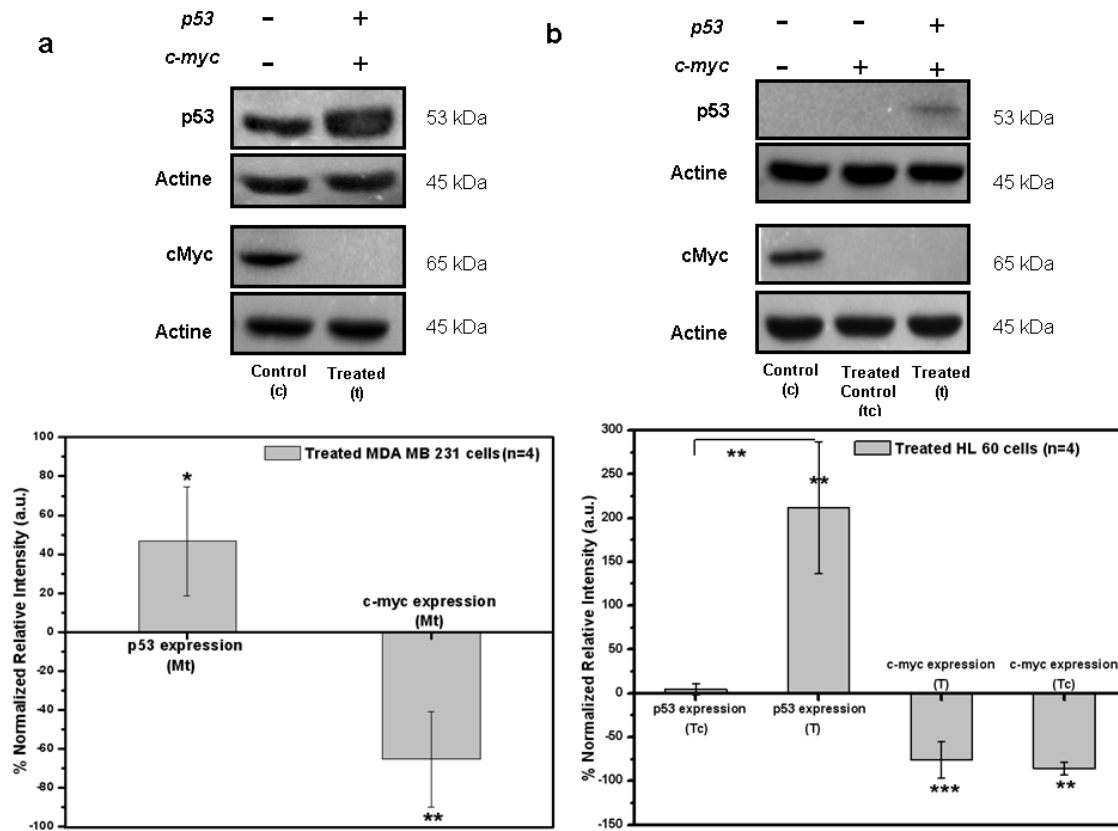


Figure 4-8. Western Blot of p53 protein and c-Myc protein expression level in whole cell lysates of MDA MB231 (a) and HL60 (b). (a) Upper panel- representative western blot results of p53 in control (c), and transfected (t) whole cell lysate along with the control actin band. Lower panel- Graph represents mean $\pm$ SD % of the intensity of p53 and c-Myc expression level relative to the expression without CP transfection and normalised to the actin band. (b) Upper panel- representative western blot results of p53 in control (c), treated control (tc) and treated (t) whole cell lysate along with the control band of actin. Lower panel- Graph represents mean $\pm$ SD % of the intensity of p53 and c-Myc expression level relative to the expression without CP transfection and normalised to the actin band. Each value represents 5 independent experiments (n=5).

In the case of HL60 cells (fig.4-8b), the experimental set-up was more complex, as it was my aim to see if both functional unities (p53 plasmid and siRNA) were released and became operative. Thus, I measured first the protein level for p53 and c-Myc in untreated control

(untreated) cells. As expected the p53 protein band was absent as in the HL60 cell line the p53 gene is deleted, but c-Myc was expressed (fig. 4-8b). However to determine the siRNA induced know-down of c-myc, I transfected the HL60 cells with Fo-P<sup>3</sup>iMCpAcGPF1 (treated control, tc) in order to inhibit c-Myc oncoprotein without inducing p53 expression. The western blot clearly showed the absence of p53 but the band intensity for c-Myc was diminished or disappeared completely, as observed for the treated breast cancer cells. Finally, the HL-60 cells were treated with the complete Fo-P<sup>3</sup>iMCp53 CP which led to a significant expression of wild-type p53 protein along with diminished c-Myc expression (Fig. 4-8b).

The results show that the CPs were able to release their content and they are biologically active showing respective effects in the treated cells.

#### 4.2.4.2. CP induced apoptosis in cancer cells

In order to confirm that the p53 protein was not only expressed by the treated cancer cells but also fully functional and hence induces apoptosis, an Annexin-V/PI assay was performed

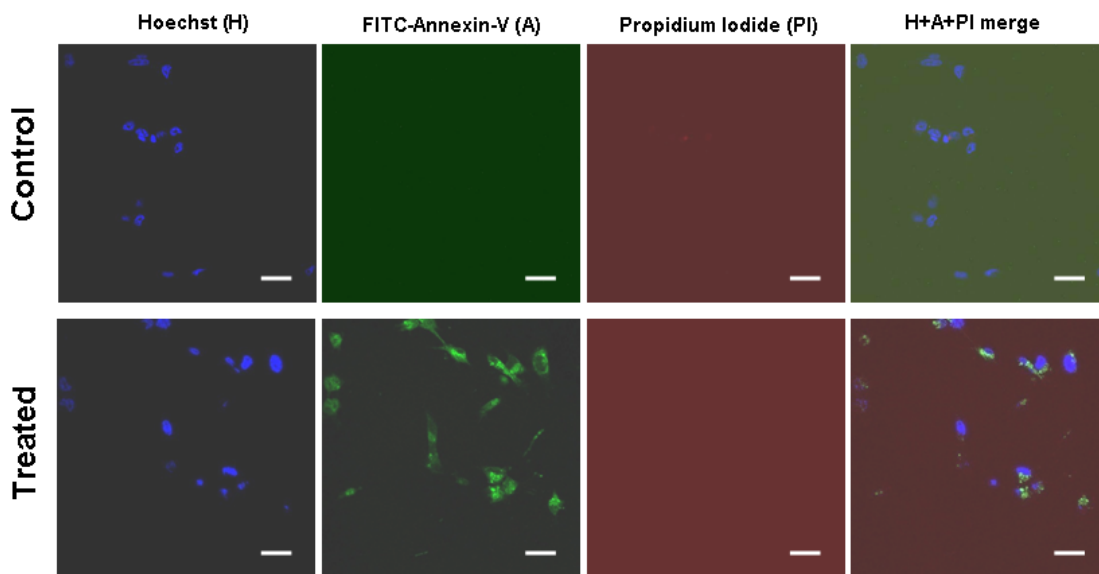


Figure 4-9. Immuno-fluorescence images of Annexin-V binding to external PS on the membrane of control (untreated) and Fo-P<sup>3</sup>iMCp53 CP treated MDA MB231 cells, after 3 days of treatment. FITC-labeled Annexin-V (green) represents the onset of apoptosis, PI stains necrotic cells (red) and the nucleus was visualized by staining with Hoechst-33342 (blue). Experiments were repeated 3 times. The scale bar represents 20 $\mu$ m.

(Fig. 4-9). The assay basically detects the externalization of phosphatidylserine (PS) to the outer membrane leaflet during early apoptosis (Annexin-V) and the decrease in membrane integrity (PI). During early apoptosis, phosphatidylserine (PS) is flipped from inner leaflet of the plasma membrane to the outer one. Thus PS becomes available to bind to the Annexin-V/FITC conjugate [21]. Cells that are destined to apoptosis will stain positive for Annexin-V/FITC and but negative for PI if they are in early apoptosis. Because PI can only enter the cells when the membrane integrity is disrupted, which happens at a later stage of apoptosis (PI entrance and intercalation in the DNA). By using a FITC-labeled Annexin-V and the red propidium iodide dye, I analyzed the apoptotic cells by fluorescence imaging. The treatment of MDA MB 231 cells with Fo-P<sup>3</sup>iMCp53 CPs at 37°C for 24 h results in a substantial increase in FITC-labeled Annexin-V positive, apoptotic cells as compared to control cells (fig. 4-9). By counting the labeled cells, it was found that approximately 80% were Annexin-V positive in complete CP treated MDA MB 231 cells (data not shown). No significant PI staining was found, which suggests that the cells are neither necrotic nor late apoptotic. Untreated cells were negative for FITC and PI staining as clearly seen in the micrographs in fig.4-9.

#### **4.2.4.3. CP causes decrease in cell viability**

Finally, the cell viability after Fo-P<sup>3</sup>iMCp53 treatment was determined by a trypan blue dye exclusion assay. A non-cancerous cell line i.e. the IHH (immortalized human hepatocytes) as well as its cancerous counterpart, the JHH-6 (hepato carcinoma), HL60 (leukemia), and MDA MB 231 (breast cancer) cells were treated with Fo-P<sup>3</sup>iMCp53 CPs for 3 days. For the non cancerous cell line IHH, which should not express the FR, only a low decrease in cell viability was observed (fig. 4-10). In contrast, for the three cancer cell lines, a significant

difference ( $P < 0.005$ ) was observed (fig. 4-10). The cell viability was estimated to be  $2.8 \pm 1.4\%$  (in HL60),  $4.9 \pm 0.44\%$  (in MDA MB 231) and  $14.9 \pm 3.5\%$  (in JHH).

The results of the cell viability study along with the high efficiency in targeting cancer cells, indicates that the multilayer CPs releases siRNA to know-down the c-myc expression and a plasmid expresses wild-type p53, support the idea of this novel therapeutic

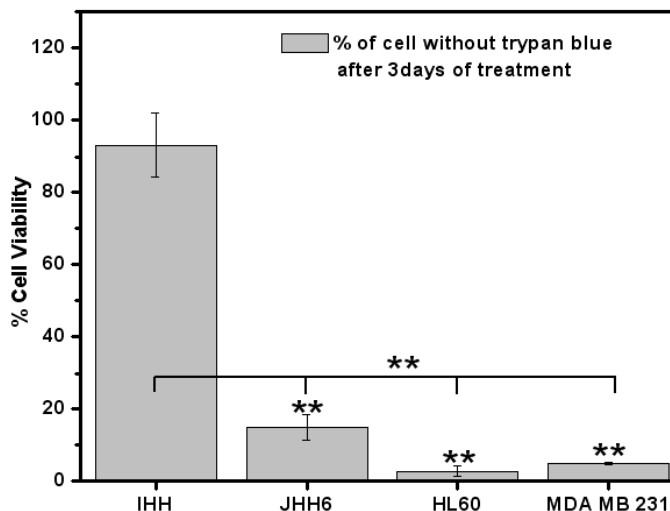


Figure 4-10. (a) Trypan Blue dye exclusion assay to determine the cell viability after 3 days of Fo-P<sup>3</sup>iMCp53 CP treatment in HL60 and MDA MB 231 cells. Untreated cells were considered as the control. The % viability after 3 days, were calculated by considering control (untreated) cell viability as 100% viability. Each value represents mean  $\pm$  SD of 3 independent experiments ( $n=3$ ).

approach, could be promising for systemic natural cancer treatment.

### 4.3. References

1. Vogelstein B, Kinzler KW. Introduction. In: Vogelstein B, Kinzler KW, editors. The genetic basis of human cancer, 2<sup>nd</sup> ed. McGraw-Hill, Medical Pub. Division: New York, 2002. p.3-6.
2. Ladam G, Gergely C, Senger B, Decher G, Voegel JC, Schaaf P, *et al.* Protein interactions with polyelectrolyte multilayers: interactions between human serum albumin and polystyrene sulfonate/polyallylamine multilayers. *Biomacromolecules* 2000;1(4):674-687.
3. S. Aiba. Molecular structures and properties of partially *N*-acetylated chitosans. In: Brine CJ, Sandford PA, Zikakis JP, eitors. *Advances in Chitin and Chitosan*, London: Elsevier, 1992. p. 137-144.
4. Muzzarelli RAA. Chitosan. In: Belcher R, Freiser H, editors. *Natural Chelating Polymers; Alginic acid, Chitin, and Chitosan*. Oxford: Pergamon Press, 1973. p. 144-176.
5. Cui Z, Mumper RJ. Chitosan-based nanoparticles for topical genetic immunization. *J Control Release* 2001;75(3):409-419.
6. Illum L, Jabbal-Gill I, Hinchcliffe M, Fisher AN, Davis SS. Chitosan as a novel nasal delivery system for vaccines. *Adv Drug Deliv Rev* 2001;51(1-3):81-96.
7. Grislain L, Couvreur P, Lenaerts V, Roland M, Deprez-Decampeneere D, Speiser P. Pharmacokinetics and distribution of a biodegradable drug-carrier. *Int J Pharm* 1983;15:335-345.

8. Gbadamosi JK, Hunter AC, Moghimi SM. PEGylation of microspheres generates a heterogeneous population of particles with differential surface characteristics and biological performance. *FEBS Lett* 2002;532(3):338-344.
9. Perrin DE, English JP. Polyglycolide and Polylactate. In: Domb AJ, Kost J, Wiseman DM, editors. *Handbook of Biodegradable Polymers*. Amsterdam: Harwood Academic, 1997. p. 3-27.
10. Lee RJ, Low PS. Delivery of liposomes into cultured KB cells via folate receptor-mediated endocytosis. *J Biol Chem* 1994;269:3198–3204.
11. Hartmann LC, Keeney GL, Lingle WL, Christianson TJ, Varghese B, Hillman D, *et al*. Folate receptor overexpression is associated with poor outcome in breast cancer. *Int J Cancer* 2007;121(5):938-942.
12. Parker N, Turk MJ, Westrick E, Lewis JD, Low PS, Leamon CP. Folate receptor expression in carcinomas and normal tissues determined by a quantitative radioligand binding assay. *Anal Biochem* 2005;338(2):284-293.
13. Sato T, Ishii T, Okahata Y. In vitro gene delivery mediated by chitosan. Effect of pH, serum, and molecular mass of chitosan on the transfection efficiency. *Biomaterials* 2001;22(15):2075-2080.
14. Park IK, Kim TH, Park YH, Shin BA, Choi ES, Chowdhury EH, *et al*. Galactosylated chitosan-graft-poly(ethylene glycol) as hepatocyte-targeting DNA carrier. *J Control Release* 2001;76(3):349-362.
15. Mosqueira VC, Legrand P, Gref R, Heurtault B, Appel M, Barratt G. Interactions between a macrophage cell line (J774A1) and surface-modified poly (D,L-lactide) nanocapsules bearing poly(ethylene glycol). *J Drug Target* 1999;7(1):65-78.

16. Gref R, Domb A, Quellec P, Blunck T, Muller RH, Verbavatz JM, Langer R. The controlled intravenous delivery of drugs using PEG-coated sterically stabilized nanospheres. *Adv Drug Deliv Rev* 1995;16(2):215-233.
17. Gref R, Lück M, Quellec P, Marchand M, Dellacherie E, Harnisch S, *et al.* 'Stealth' corona-core nanoparticles surface modified by polyethylene glycol (PEG): influences of the corona (PEG chain length and surface density) and of the core composition on phagocytic uptake and plasma protein adsorption. *Colloids Surf. B: Biointerfaces* 2000;18(3-4):301-313.
18. Leroux JC, De Jaeghere F, Anner B, Doelker E, Gurny R. An investigation on the role of plasma and serum opsonins on the internalization of biodegradable poly(D,L-lactic acid) nanoparticles by human monocytes. *Life Sci* 1995;57(7):695-703.
19. Stolnik S, Dunn SE, Garnett MC, Davies MC, Coombes AG, Taylor DC, Irving MP, Purkiss SC, Tadros TF, Davis SS, *et al.* Surface modification of poly(lactide-co-glycolide) nanospheres by biodegradable poly(lactide)-poly(ethylene glycol) copolymers. *Pharm Res* 1994;11(12):1800-8.
20. Mosqueira VC, Legrand P, Gref R, Heurtault B, Appel M, Barratt G. Interactions between a macrophage cell line (J774A1) and surface-modified poly (D,L-lactide) nanocapsules bearing poly(ethylene glycol). *J Drug Target* 1999;7(1):65-78.
21. Vermes I, Haanen C, Steffens-Nakken H, Reutelingsperger C. A novel assay for apoptosis - flow cytometric detection of phosphatidylserine expression on early apoptotic cells using fluorescein labelled Annexin V. *J. Immunol. Meth* 1995;184(1):39-51.

## **CHAPTER 5**

### **5.1. Conclusions**

Several *in vitro* and *in vivo* studies have shown that the restoration of wild-type p53 activity in cancer cells with mutated or deleted p53, either suppresses tumor growth or induces apoptosis [1-3]; thus supporting the idea that gene therapy focused on restoring p53 activity in tumors, might be a fruitful approach to cancer treatment. In the past the delivery of the wild type p53 containing plasmid is mainly triggered by adenovirus- or retrovirus [4, 5]. Most viral gene therapies bear the risk of infection with the remaining viral genome or immunogenicity making a repeated treatment impossible. This problem was tackled by the introduction of non-viral delivery systems such as polysomes or liposomes [6]. The main problem with polymeric delivery systems is that in comparison to viral systems they usually have a very low transfection efficiency. In order to improve it, a new generation of multifunctional polymeric particles was developed by us and by other researchers. Most researchers focus on the covalent conjugation of various moieties with the polymer for targeting, prevention of MPS recognition and/ or endosomal escape of the particles to the cytosol [7]. Another multifunctional approach used successfully is the polypeptide system for the different functionalities, in order to improve transfection efficiency and targeting especially for liver cancer [8].

In the present part, I develop a new multifunctional nanoparticles delivery system, which shows high transfection efficiency in different cancer cell lines but almost no effect in non-cancerous cells. The CPs with a size of around 350 nm carry various functionalities localized

in different layers of the construct. The particle size is nearly in the range (380-780 nm) which was found to extravasate preferentially in the tumor tissue rather than being diffusely delivered to every tissue like it is the case for smaller particles. [9] A plasmid encoding wild-type p53 was condensed into a charged core with the non-toxic cationic polysaccharide chitosan. On the surface of the core, siRNA against the mRNA of c-myc, was deposited by electrostatic self-assembly. Thus, CPs are aimed to induce proliferation arrest along with the induction of apoptosis by wild-type p53 expression in the cancer cells.

The surface of CP was coated with a neural tri-block copolymer PLA-PEG-PLA to stabilize and protect the CP, to induce *in vivo* long circulation due to “stealthiness”, and to allow a better penetration into the tumor mass. Finally, the particles were functionalized by electrostatically bound folic acid, for cancer cell targeting and for an assisted delivery of the construct to the nucleus, and to improve the transfection. Approximately 75% cells clearly showed uptake of the CPs into the cells. The improved internalization of the CPs into the cancer cells was due to the presence of the targeting moiety, folic acid. Moreover, the expression of the reporter gene AcGFP1 showed that with folic acid, the expression rate was in the same range than the up-take rate. In contrast, the transfection efficiency was significantly lower than the CP internalization without folic acid. This strongly support that the FR mediated endocytosis guides the delivery of the endosomes to the nucleus and hence facilitates the transfection. Transfection efficiency for the tested construct is comparable to that of virus infected cells [10].

Finally the expression efficacy, in terms of changes in the protein content for c-Myc as well as for p53, was measured by Western blot in two different cancer cell lines. A HL60 is a leukemic cell line, where p53 gene is absent due to p53 gene deletion [11]. Here the *di novo* p53 expression showed that the transfection was successful. Moreover, for hematopoietic

cells, substantial evidence indicates that the c-myc oncogene is linked to growth arrest and to the state of differentiation. In HL60 cells in which the differentiation is induced, the steady state level of c-myc RNA decreased and remained at low levels [12].

Moreover, it was supported by the fact that the expression of c-Myc was maximally down regulated by the silencing of the mRNA due to the release of siRNA from the construct. The same result was found for the MDA MB 231 breast cancer cells, which has a mutated p53 gene. Here the amount of p53 increased significantly by the expression of wild-type p53 and the c-Myc expression was extinguished.

The fluorescence microscopic analysis showed that the transfected cancer cell undergoes apoptosis induced by the delivered plasmid. The most important result was that the complete CP was able to deliver fully functional expression vector and siRNA. Hence, the cell survival reduced in the case of cancer, whereas non-cancer cells remained unaffected after incubation with the CPs for 3 days. For the non-cancer cells (IHH) the cell viability, with respect to the untreated control, was ~90%, while for JHH, a hepatocellular carcinoma (HCC), it was ~15% and for both, HL-60 and MDA MB breast cancer, it was <5%. This finding supports the idea that the folic acid receptor acts as a mediator for the transfection with p53 and the release of siRNA against c-Myc mRNA and, the combination in the form of an electrostatically ensembled submicrometric particle, is a promising novel strategy for systemic tumor-targeted gene therapy.

## 5.2. References

1. Gostissa M, Hengstermann A, Fogal V, Sandy P, Schwarz SE, Scheffner M, Del Sal G. Activation of p53 by conjugation to the ubiquitin-like protein SUMO-1. *EMBO J* 1999;18(22):6462–6471.
2. Santoso JT, Tang DC, Lane SB, Hung J, Reed DJ, Muller CY, *et al.* Adenovirus-based p53 gene therapy in ovarian cancer. *Gynecol Oncol* 1995;59(2):169-70.
3. von Gruenigen VE, Santoso JT, Coleman RL, Muller CY, Miller DS, Mathis JM. In vivo studies of adenovirus-based p53 gene therapy for ovarian cancer. *Gynecol Oncol* 1998;69(3):197-204.
4. Armandola EA. Gene Therapy in Cancer Patients. *Medscape General Medicin: Hematology-Oncology Expert Column* 2002. Available from URL:  
[http://www.medscape.com/viewarticle/445128\\_2](http://www.medscape.com/viewarticle/445128_2)
5. Jiang H, Gomez-Manzano C, Lang FF, Alemany R, Fueyo J. Oncolytic adenovirus: preclinical and clinical studies in patients with human malignant gliomas. *Curr Gene Ther.* 2009;9(5):422-427.
6. Ogris M, Wagner E. Tumor-targeted gene transfer with DNA polyplexes. *Somat Cell Mol Genet.* 2002;27(1-6):85-95.
7. Wang W, Yao J, Zhou JP, Lu Y, Wang Y, Tao L, *et al.* Urocanic acid-modified chitosan-mediated p53 gene delivery inducing apoptosis of human hepatocellular carcinoma cell line HepG2 is involved in its antitumor effect in vitro and in vivo. *Biochem Biophys Res Commun* 2008;377(2):567-572.

8. Lee TK, Han JS, Fan ST, Liang ZD, Tian PK, Gu JR, *et al.* Gene delivery using a receptor-mediated gene transfer system targeted to hepatocellular carcinoma cells. *Int J Cancer* 2001;93(3):393-400.
9. Hobbs SK, Monsky WL, Yuan F, Roberts WG, Griffith L, Torchilin VP, *et al.* Regulation of transport pathways in tumor vessels: role of tumor type and microenvironment. *Proc Natl Acad Sci U S A* 1998;95(8):4607-4612.
10. Santoso JT, Tang DC, Lane SB, Hung J, Reed DJ, Muller CY, *et al.* Adenovirus-based p53 gene therapy in ovarian cancer. *Gynecol Oncol* 1995;59(2):171-178.
11. Wolf D, Rotter V. Major deletions in the gene encoding the p53 tumor antigen cause lack of p53 expression in HL-60 cells. *Proc Natl Acad Sci U S A* 1985;82(3):790-794.
12. Roberts P, Jones M, Gale R, Thomas S, Tidman N, Linch D. The c-myc oncogene is regulated independently of differentiation in myeloid cell lines. *Leuk Res* 1989;13(8):651-659.

---

**Part 3:**  
**The Polycationic Approach**

## **1. A brief overview**

In recent decades, great progress has been made to extend the life span of cancer patients, but up to date, the definitive treatment that can defeat the disease, has not yet been found. Whilst the origin of cancer is still not completely understood, at present, depending upon the type of cancer, treatment may vary from surgery combined with chemotherapy which targets against DNA synthesis or inhibits cell division in fast dividing cells or radiation therapy. Today, the selective targeting of cancer cells is one of the major challenges in nano-medicine. Many approaches are dedicated to finding suitable biomarkers or targets [1], modifying the drug molecules or producing a protective delivery system [2] in order to decrease the collateral effects of chemotherapeutics and increase the tumoral drug concentration. I have used a polycation which enters preferentially cancer cells on the basis of differences in the physical properties of the cell membrane.

### **1.1. Differences in the physical properties of cancer and normal cells**

#### **1.1.1. Surface charge**

Mammalian cells in suspension migrate toward the anode in a direct current field, indicating they are predominantly anionic [3]. Evidently, in some cases, the electromobility studies have shown an increase in the net negative charge of cells during carcinogenesis [4-6] or during cell growth in general [7]. A critical study by Foley [8] showed that there are many differences in the surface membrane properties in between non-neoplastic and neoplastic cells. The negative membrane charge of cells is mainly due to carboxyl groups from sialic acids in the mucopolysaccharides (N- acetylneuraminic acid, N-glycolylneuraminic acid, etc.) on the cell surface [3, 9]. Although the present of negative phosphate and positive

ammonium charges also have some contribution on the surface charge properties of the cancer cell membrane [9]. The negative charge of the tumor cell membrane has been suggested to be involved with its invasive behavior [4]. Moreover the high negative surface charge on malignant cells and trophoblasts, may mediate the immune evasion [10].

The phospholipids are an integral part of the membrane and determine its structure. In the most cancer (table 1-1a-c) an increased amount of all phospholipids of cell membrane has been observed [11-14]. It has been considered that higher amounts of phospholipids can be due to enhanced cell membrane synthesis related to accelerated neoplasm cell replication [4].

The mechanisms responsible for an increase of phospholipids can vary depending upon cell nature, cell growth phase and its malignancy [14, 15]. The characteristic parameters of phospholipids presented in Tables 1-1 a-c, show that the content of phosphatidylcholine in cancer cells is higher than that of normal mucosa in comparison to other phospholipids [11].

This has been supported by the finding that malignant neoplastic cells with high number of metastases are characterized by a higher phosphatidylcholine/phosphatidylethanolamine ratio than malignant neoplasm cells which have a lower number of metastases [16]. It was found that an increased amount of phospholipids can increase surface density of negatively charged groups in cell membrane at low pH values and that of positively charged ones at high pH [17]. The pH in tumor tissue was found to be 6.5 instead of 7.3 [18] in normal tissue, this can explain why the cell membrane of tumor tissue expose a high negative surface charge.

**Table 1-1. Content of phospholipids and CTA i CTB of human large intestine of pT3 stage, G3 grade and with metastasis (N+) (a) [11].**

No. of patients	Phospholipids	HPLC method				Electrophoretic method					
		Content of phospholipid of plasma/serum (mg/g tissue)		Surface concentration of phospholipids ( $10^{-7}$ mol/m <sup>2</sup> )		Fraction of surface of occupied by phospholipids		$C_{TB}$ ( $10^{-7}$ mol/m <sup>2</sup> )			
		Control	Tumour	Control	Tumour	Control	Tumour	Control	Tumour		
1	PI	0.010 ± 0.002	0.225 ± 0.020 <sup>a</sup>	0.042 ± 0.002	0.996 ± 0.002 <sup>a</sup>	0.003 ± 0.001	0.063 ± 0.002 <sup>a</sup>	2.71 ± 0.10	3.73 ± 0.12 <sup>a</sup>	0.90 ± 0.05	1.35 ± 0.08 <sup>a</sup>
	PS	0.016 ± 0.003	0.100 ± 0.010 <sup>a</sup>	0.076 ± 0.007	0.465 ± 0.020 <sup>a</sup>	0.003 ± 0.001	0.020 ± 0.001 <sup>a</sup>				
	PE	0.550 ± 0.010	0.890 ± 0.030 <sup>a</sup>	2.445 ± 0.120	3.950 ± 0.160 <sup>a</sup>	0.060 ± 0.001	0.101 ± 0.099 <sup>a</sup>				
2	PC	0.675 ± 0.011	1.100 ± 0.061 <sup>a</sup>	3.181 ± 0.254	5.170 ± 0.361 <sup>a</sup>	0.163 ± 0.010	0.265 ± 0.022 <sup>a</sup>				
	PI	0.012 ± 0.003	0.239 ± 0.040 <sup>a</sup>	0.051 ± 0.003	1.018 ± 0.080 <sup>a</sup>	0.003 ± 0.001	0.065 ± 0.003 <sup>a</sup>	1.92 ± 0.12	3.25 ± 0.12 <sup>a</sup>	0.63 ± 0.04	1.24 ± 0.06 <sup>a</sup>
	PS	0.028 ± 0.002	0.151 ± 0.022 <sup>a</sup>	0.132 ± 0.015	0.710 ± 0.044 <sup>a</sup>	0.005 ± 0.001	0.030 ± 0.001 <sup>a</sup>				
3	PE	0.510 ± 0.020	0.740 ± 0.081 <sup>a</sup>	2.260 ± 0.208	3.290 ± 0.160 <sup>a</sup>	0.060 ± 0.001	0.080 ± 0.009 <sup>a</sup>				
	PC	0.116 ± 0.010	1.237 ± 0.099 <sup>a</sup>	2.870 ± 0.228	4.400 ± 0.234 <sup>a</sup>	0.150 ± 0.020	0.225 ± 0.013 <sup>a</sup>				
	PI	0.074 ± 0.008	0.081 ± 0.007	0.314 ± 0.010	0.348 ± 0.010 <sup>a</sup>	0.020 ± 0.011	0.022 ± 0.012	2.41 ± 0.12	2.84 ± 0.09 <sup>a</sup>	0.74 ± 0.07	0.97 ± 0.08 <sup>a</sup>
4	PS	0.086 ± 0.006	0.131 ± 0.010 <sup>a</sup>	0.399 ± 0.018	0.620 ± 0.030 <sup>a</sup>	0.016 ± 0.009	0.025 ± 0.018				
	PE	0.494 ± 0.021	0.902 ± 0.051 <sup>a</sup>	2.200 ± 0.290	4.010 ± 0.201 <sup>a</sup>	0.060 ± 0.021	0.103 ± 0.020 <sup>a</sup>				
	PC	0.648 ± 0.024	1.240 ± 0.085 <sup>a</sup>	3.040 ± 0.330	5.810 ± 0.385 <sup>a</sup>	0.156 ± 0.021	0.297 ± 0.026 <sup>a</sup>				
5	PI	0.087 ± 0.009	0.248 ± 0.020 <sup>a</sup>	0.368 ± 0.015	1.056 ± 0.065 <sup>a</sup>	0.023 ± 0.012	0.067 ± 0.012 <sup>a</sup>	2.08 ± 0.09	2.45 ± 0.11 <sup>a</sup>	0.67 ± 0.04	1.15 ± 0.06 <sup>a</sup>
	PS	0.097 ± 0.007	0.097 ± 0.006	0.451 ± 0.022	0.450 ± 0.022	0.019 ± 0.010	0.018 ± 0.001				
	PE	0.901 ± 0.050	0.932 ± 0.050	4.000 ± 0.250	4.130 ± 0.230	0.102 ± 0.018	0.106 ± 0.019				
6	PC	1.139 ± 0.061	1.245 ± 0.089 <sup>a</sup>	5.347 ± 0.320	5.834 ± 0.310	0.274 ± 0.026	0.299 ± 0.021				
	PI	0.064 ± 0.005	0.109 ± 0.010 <sup>a</sup>	0.280 ± 0.020	0.468 ± 0.020 <sup>a</sup>	0.018 ± 0.001	0.030 ± 0.009 <sup>a</sup>	2.24 ± 0.11	2.91 ± 0.22 <sup>a</sup>	0.91 ± 0.05	1.39 ± 0.06 <sup>a</sup>
	PS	0.086 ± 0.004	0.114 ± 0.015 <sup>a</sup>	0.415 ± 0.030	0.529 ± 0.031 <sup>a</sup>	0.017 ± 0.002	0.022 ± 0.008				
7	PE	0.498 ± 0.012	0.768 ± 0.080 <sup>a</sup>	2.210 ± 0.160	3.410 ± 0.124 <sup>a</sup>	0.060 ± 0.020	0.090 ± 0.019				
	PC	0.677 ± 0.018	1.054 ± 0.095 <sup>a</sup>	3.170 ± 0.200	4.940 ± 0.281 <sup>a</sup>	0.162 ± 0.019	0.253 ± 0.022 <sup>a</sup>	2.19 ± 0.08	2.81 ± 0.14 <sup>a</sup>	0.69 ± 0.05	1.65 ± 0.06 <sup>a</sup>
	PI	0.020 ± 0.002	0.056 ± 0.006 <sup>a</sup>	0.085 ± 0.012	0.238 ± 0.012 <sup>a</sup>	0.005 ± 0.001	0.015 ± 0.001 <sup>a</sup>				
8	PS	0.024 ± 0.002	0.096 ± 0.009 <sup>a</sup>	0.112 ± 0.018	0.310 ± 0.018 <sup>a</sup>	0.005 ± 0.001	0.013 ± 0.001 <sup>a</sup>				
	PE	0.432 ± 0.012	0.951 ± 0.092 <sup>a</sup>	1.920 ± 0.201	4.220 ± 0.180 <sup>a</sup>	0.050 ± 0.009	0.108 ± 0.020 <sup>a</sup>				
	PC	0.707 ± 0.019	1.368 ± 0.101 <sup>a</sup>	3.320 ± 0.202	6.420 ± 0.202 <sup>a</sup>	0.169 ± 0.012	0.329 ± 0.025 <sup>a</sup>	1.56 ± 0.14	1.69 ± 0.12	0.66 ± 0.04	0.77 ± 0.04 <sup>a</sup>
9	PI	0.009 ± 0.001	0.030 ± 0.015 <sup>a</sup>	0.035 ± 0.016	0.132 ± 0.021 <sup>a</sup>	0.002 ± 0.001	0.008 ± 0.001 <sup>a</sup>				
	PS	0.010 ± 0.011	0.021 ± 0.010	0.049 ± 0.018	0.098 ± 0.030 <sup>a</sup>	0.002 ± 0.001	0.004 ± 0.001				
	PE	0.419 ± 0.023	0.828 ± 0.052 <sup>a</sup>	1.860 ± 0.099	3.680 ± 0.160 <sup>a</sup>	0.050 ± 0.015	0.090 ± 0.017 <sup>a</sup>				
10	PC	0.675 ± 0.034	1.182 ± 0.065 <sup>a</sup>	3.160 ± 0.150	5.540 ± 0.390 <sup>a</sup>	0.162 ± 0.016	0.284 ± 0.019 <sup>a</sup>				
	PI	0.036 ± 0.012	0.136 ± 0.016 <sup>a</sup>	0.153 ± 0.018	0.581 ± 0.081 <sup>a</sup>	0.010 ± 0.013	0.037 ± 0.003 <sup>a</sup>	2.45 ± 0.12	2.66 ± 0.21	0.61 ± 0.03	0.72 ± 0.05 <sup>a</sup>
	PS	0.042 ± 0.015	0.103 ± 0.050 <sup>a</sup>	0.197 ± 0.060	0.488 ± 0.079 <sup>a</sup>	0.008 ± 0.001	0.020 ± 0.009 <sup>a</sup>				
11	PE	0.468 ± 0.028	0.895 ± 0.039 <sup>a</sup>	2.080 ± 0.101	3.980 ± 0.210 <sup>a</sup>	0.050 ± 0.008	0.102 ± 0.012 <sup>a</sup>				
	PC	0.686 ± 0.039	1.287 ± 0.070 <sup>a</sup>	3.210 ± 0.155	6.030 ± 0.528 <sup>a</sup>	0.164 ± 0.012	0.309 ± 0.018 <sup>a</sup>				

PI: phosphatidylinositol; PS: phosphatidylserine; PE: phosphatidylethanolamine; PC: phosphatidylcholine.

Statistically significant differences for  $p < 0.05$ .

<sup>a</sup>In comparison with control.

**Table 1-1. Content of phospholipids and CTA i CTB of human large intestine of pT3 stage, G3 grade and with metastasis (N+) (b) [11].**

No. of patients	Phospholipids	HPLC method						Electrophoretic method			
		Content of phospholipid of plasmalemma (mg/g tissue)		Surface concentration of phospholipids ( $10^{-7}$ mol/m <sup>2</sup> )		Fraction of surface of occupied by phospholipids		$C_{TA}$ ( $10^{-7}$ mol/m <sup>2</sup> )		$C_{TB}$ ( $10^{-7}$ mol/m <sup>2</sup> )	
		Control	Tumour	Control	Tumour	Control	Tumour	Control	Tumour	Control	Tumour
9	PI	0.044 ± 0.002	0.225 ± 0.011 <sup>a</sup>	0.186 ± 0.009	0.961 ± 0.020 <sup>a</sup>	0.012 ± 0.002	0.061 ± 0.003 <sup>a</sup>	1.88 ± 0.10	2.23 ± 0.16 <sup>a</sup>	0.70 ± 0.05	0.91 ± 0.08 <sup>a</sup>
	PS	0.043 ± 0.002	0.145 ± 0.009 <sup>a</sup>	0.201 ± 0.007	0.679 ± 0.015 <sup>a</sup>	0.008 ± 0.001	0.028 ± 0.002 <sup>a</sup>				
	PE	0.642 ± 0.011	0.909 ± 0.019 <sup>a</sup>	2.850 ± 0.135	4.040 ± 0.301 <sup>a</sup>	0.070 ± 0.002	0.103 ± 0.008 <sup>a</sup>				
	PC	0.783 ± 0.012	1.406 ± 0.025 <sup>a</sup>	3.680 ± 0.148	6.580 ± 0.399 <sup>a</sup>	0.188 ± 0.008	0.337 ± 0.009 <sup>a</sup>				
10	PI	0.150 ± 0.009	0.160 ± 0.008	0.633 ± 0.012	0.682 ± 0.016 <sup>a</sup>	0.040 ± 0.005	0.043 ± 0.005	2.71 ± 0.12	4.94 ± 0.11 <sup>a</sup>	0.77 ± 0.07	1.03 ± 0.08 <sup>a</sup>
	PS	0.055 ± 0.003	0.055 ± 0.003	0.250 ± 0.009	0.250 ± 0.009	0.010 ± 0.003	0.010 ± 0.003				
	PE	0.540 ± 0.012	0.545 ± 0.013	2.390 ± 0.140	2.420 ± 0.108	0.060 ± 0.003	0.060 ± 0.003				
	PC	0.925 ± 0.022	1.555 ± 0.028 <sup>a</sup>	4.341 ± 0.205	7.305 ± 0.505 <sup>a</sup>	0.222 ± 0.009	0.374 ± 0.010 <sup>a</sup>				
11	PI	0.044 ± 0.002	0.144 ± 0.009 <sup>a</sup>	0.187 ± 0.011	0.607 ± 0.012 <sup>a</sup>	0.012 ± 0.001	0.039 ± 0.004 <sup>a</sup>	3.32 ± 0.11	4.35 ± 0.12 <sup>a</sup>	1.17 ± 0.07	1.23 ± 0.07 <sup>a</sup>
	PS	0.025 ± 0.001	0.075 ± 0.005 <sup>a</sup>	0.107 ± 0.008	0.368 ± 0.010 <sup>a</sup>	0.004 ± 0.001	0.015 ± 0.002 <sup>a</sup>				
	PE	0.381 ± 0.018	0.396 ± 0.011	1.690 ± 0.084	1.760 ± 0.038	0.040 ± 0.005	0.040 ± 0.003				
	PC	0.475 ± 0.020	1.281 ± 0.016 <sup>a</sup>	2.248 ± 0.135	6.020 ± 0.348 <sup>a</sup>	0.115 ± 0.007	0.308 ± 0.009 <sup>a</sup>				
12	PI	0.018 ± 0.001	0.113 ± 0.008 <sup>a</sup>	0.077 ± 0.008	0.479 ± 0.010 <sup>a</sup>	0.005 ± 0.001	0.030 ± 0.004 <sup>a</sup>	2.90 ± 0.09	3.98 ± 0.08 <sup>a</sup>	1.16 ± 0.09	1.68 ± 0.08 <sup>a</sup>
	PS	0.031 ± 0.003	0.110 ± 0.007 <sup>a</sup>	0.149 ± 0.013	0.520 ± 0.013 <sup>a</sup>	0.006 ± 0.001	0.021 ± 0.003 <sup>a</sup>				
	PE	0.551 ± 0.018	0.592 ± 0.013 <sup>a</sup>	2.440 ± 0.149	2.630 ± 0.109 <sup>a</sup>	0.060 ± 0.006	0.070 ± 0.006				
	PC	0.698 ± 0.021	0.933 ± 0.026 <sup>a</sup>	3.270 ± 0.139	4.373 ± 0.658 <sup>a</sup>	0.167 ± 0.015	0.224 ± 0.012 <sup>a</sup>				
13	PI	0.026 ± 0.003	0.039 ± 0.003 <sup>a</sup>	0.113 ± 0.007	0.166 ± 0.009 <sup>a</sup>	0.007 ± 0.001	0.010 ± 0.002	2.66 ± 0.11	3.26 ± 0.14 <sup>a</sup>	0.89 ± 0.05	1.57 ± 0.08 <sup>a</sup>
	PS	0.013 ± 0.001	0.026 ± 0.002 <sup>a</sup>	0.063 ± 0.002	0.123 ± 0.007 <sup>a</sup>	0.002 ± 0.001	0.005 ± 0.001 <sup>a</sup>				
	PE	0.433 ± 0.019	0.546 ± 0.014 <sup>a</sup>	1.920 ± 0.011	2.420 ± 0.105 <sup>a</sup>	0.050 ± 0.005	0.060 ± 0.005				
	PC	0.770 ± 0.030	1.240 ± 0.019 <sup>a</sup>	3.600 ± 0.201	5.800 ± 0.565 <sup>a</sup>	0.184 ± 0.022	0.297 ± 0.015 <sup>a</sup>				

PI: phosphatidylinositol; PS: phosphatidylserine; PE: phosphatidylethanolamine; PC: phosphatidylcholine.

Statistically significant differences for  $p < 0.05$ .

<sup>a</sup> In comparison with control.

**Table I-1. Content of phospholipids and CTA.i CTB of human large intestine of pT3 stage, G3 grade and with metastasis (N+) (c) [11].**

No. of patients	Phospholipids	HPLC method				Electrophoretic method					
		Content of phospholipid of plasmalemma (mg/g tissue)		Surface concentration of phospholipids ( $10^{-7}$ mol/m <sup>2</sup> )		Fraction of surface of occupied by phospholipids		$C_{TA}$ ( $10^{-7}$ mol/m <sup>2</sup> )		$C_{TB}$ ( $10^{-7}$ mol/m <sup>2</sup> )	
		Control	Tumour	Control	Tumour	Control	Tumour	Control	Tumour	Control	Tumour
14	PI	0.200 ± 0.009	0.245 ± 0.010 <sup>a</sup>	0.847 ± 0.030	1.000 ± 0.042 <sup>a</sup>	0.054 ± 0.002	0.064 ± 0.003 <sup>a</sup>	2.62 ± 0.08	4.77 ± 0.31 <sup>a</sup>	1.07 ± 0.06	0.83 ± 0.09 <sup>a</sup>
	PS	0.071 ± 0.005	0.100 ± 0.009 <sup>a</sup>	0.335 ± 0.021	0.463 ± 0.040 <sup>a</sup>	0.014 ± 0.002	0.019 ± 0.003				
	PE	0.462 ± 0.015	0.476 ± 0.019	2.050 ± 0.099	2.110 ± 0.101	0.050 ± 0.003	0.050 ± 0.003				
	PC	0.614 ± 0.018	1.476 ± 0.065 <sup>a</sup>	2.880 ± 0.234	6.920 ± 0.308 <sup>a</sup>	0.147 ± 0.020	0.354 ± 0.022 <sup>a</sup>				
15	PI	0.046 ± 0.007	0.084 ± 0.008 <sup>a</sup>	0.185 ± 0.015	0.379 ± 0.035 <sup>a</sup>	0.012 ± 0.002	0.024 ± 0.004 <sup>a</sup>	2.66 ± 0.14	3.38 ± 0.10 <sup>a</sup>	0.90 ± 0.05	1.23 ± 0.09 <sup>a</sup>
	PS	0.030 ± 0.006	0.034 ± 0.006	0.132 ± 0.011	0.169 ± 0.019 <sup>a</sup>	0.005 ± 0.001	0.007 ± 0.001				
	PE	0.447 ± 0.016	0.456 ± 0.018	1.990 ± 0.096	2.020 ± 0.018	0.050 ± 0.013	0.050 ± 0.012				
	PC	0.677 ± 0.019	1.084 ± 0.050 <sup>a</sup>	3.170 ± 0.301	5.080 ± 0.311 <sup>a</sup>	0.162 ± 0.019	0.260 ± 0.024 <sup>a</sup>				
16	PI	0.043 ± 0.006	0.078 ± 0.007 <sup>a</sup>	0.178 ± 0.011	0.344 ± 0.030 <sup>a</sup>	0.011 ± 0.002	0.022 ± 0.008 <sup>a</sup>	1.86 ± 0.12	2.25 ± 0.12 <sup>a</sup>	0.54 ± 0.06	0.62 ± 0.07
	PS	0.014 ± 0.002	0.057 ± 0.005 <sup>a</sup>	0.066 ± 0.006	0.260 ± 0.018 <sup>a</sup>	0.003 ± 0.001	0.011 ± 0.004 <sup>a</sup>				
	PE	0.443 ± 0.017	0.478 ± 0.016 <sup>a</sup>	1.970 ± 0.122	2.120 ± 0.012 <sup>a</sup>	0.050 ± 0.012	0.050 ± 0.011				
	PC	0.707 ± 0.021	1.386 ± 0.065 <sup>a</sup>	3.320 ± 0.205	6.500 ± 0.405 <sup>a</sup>	0.170 ± 0.020	0.333 ± 0.040 <sup>a</sup>				
17	PI	0.095 ± 0.008	0.245 ± 0.011 <sup>a</sup>	0.414 ± 0.023	1.036 ± 0.055 <sup>a</sup>	0.026 ± 0.005	0.066 ± 0.009 <sup>a</sup>	2.88 ± 0.16	4.15 ± 0.33 <sup>a</sup>	0.98 ± 0.09	1.42 ± 0.08 <sup>a</sup>
	PS	0.115 ± 0.010	0.130 ± 0.010	0.550 ± 0.028	0.603 ± 0.042 <sup>a</sup>	0.023 ± 0.004	0.025 ± 0.004 <sup>a</sup>				
	PE	0.450 ± 0.019	0.620 ± 0.021 <sup>a</sup>	2.000 ± 0.133	2.756 ± 0.119 <sup>a</sup>	0.050 ± 0.006	0.070 ± 0.007 <sup>a</sup>				
	PC	0.650 ± 0.020	0.701 ± 0.023 <sup>a</sup>	3.046 ± 0.199	3.284 ± 0.201	0.156 ± 0.016	0.168 ± 0.020 <sup>a</sup>				
18	PI	0.010 ± 0.002	0.810 ± 0.026 <sup>a</sup>	0.046 ± 0.008	3.419 ± 0.202 <sup>a</sup>	0.003 ± 0.001	0.218 ± 0.015 <sup>a</sup>	2.03 ± 0.11	2.31 ± 0.09 <sup>a</sup>	0.66 ± 0.06	0.75 ± 0.07
	PS	0.019 ± 0.002	0.022 ± 0.003	0.090 ± 0.009	0.104 ± 0.012	0.004 ± 0.001	0.004 ± 0.001				
	PE	0.417 ± 0.022	0.419 ± 0.019	1.850 ± 0.124	3.970 ± 0.320 <sup>a</sup>	0.050 ± 0.006	0.102 ± 0.012 <sup>a</sup>				
	PC	0.770 ± 0.044	1.197 ± 0.055 <sup>a</sup>	3.610 ± 0.202	5.620 ± 0.455 <sup>a</sup>	0.185 ± 0.018	0.288 ± 0.022 <sup>a</sup>				

PI: phosphatidylinositol; PS: phosphatidylserine; PE: phosphatidylethanolamine; PC: phosphatidylcholine.

Statistically significant differences for  $p < 0.05$ .

<sup>a</sup>In comparison with control.

### **1.1.2. Mechanical properties of cell membranes**

Diseases such as cancer or malaria induce mechanical property changes in cells, which may serve as a useful biomarker in the early detection of cancer [19, 20] as well as a test for the efficacy of the cancer treatment. Moreover, investigating the mechanical properties of cancer cells may help to understand the physical mechanisms responsible for cancer metastasis. This can lead to the development of novel strategies for cancer prevention and diagnosis.

Many *in vitro* studies showed that some cancerous cells are softer than their normal counterparts [21-24]. Malignant breast cells have been found to have the apparent Young's modulus significantly lower (1.4–1.8 times) than that of their respective non-malignant counterparts at physiological temperature (37°C) [25]. The cancerous cells are less stiff and easier to deform than non-malignant cells due to the changes in their sub-cellular structures. This reduced stiffness was suggested to be due to a significant reduction in the well-defined F-actin filaments or their bundles (stress fibers) [26]. The reduced F-actin results in a weaker cytoskeleton in cancer cell. This effect was observed in a combination study of AFM (both as an indenter and high resolution imaging tool) and fluorescence microscopy [26]. Hence, these transformed malignant cells possess the ability to migrate easier through surrounding tissue matrixes and small capillaries (metastasis). A study by Cross *et al.* [27], have shown that the cell stiffness of metastatic cancer cells is more than 70% softer, than the normal endothelial cells that line the body cavity. This enhanced softness of cancer cells are contributed by the abnormalities in cytoskeletal materials which could be reduction in the amount of constituent polymers and accessory proteins and a restructuring of the available network [28-32]. Therefore, lower Young's modulus value i.e. lower stiffness, explains the low elasticity and

increases softness properties of the cancerous cells which are mainly due to abnormality in their cytoskeletal materials with respect to their normal counterpart.

### **1.1.3. Modification of Extra-Cellular Matrix (ECM)**

Investigating the composition of the ECM and its stiffness as a risk factor for metastasis or possible target for drug delivery is critical, given the profound changes in the mammary stroma associated with breast cancer and the diversity of diseases associated with changes in collagen deposition, orientation and cross-linking.

Modification of ECM-integrin interactions can profoundly influence expression of the malignant phenotype in culture and *in vivo* [33]. However, the exact molecular mechanisms by which the altered stromal–epithelial interactions regulate tumorigenesis are still to be defined. Although, changes in the ECM composition may induce changes in the epithelial cell integrin expression. For example, altered expression of  $\beta 1$ -,  $\beta 4$ -,  $\alpha 2$ -,  $\alpha 3$ - and  $\alpha 6$ -integrins has been observed in mammary cancer cells [34, 35]. It was observed that matrix stiffness possibly promotes breast tumorigenesis by altering integrins and their adhesion interactions [36]. Paszek *et al.* [36] have shown that blocking integrin-dependent cell contractility reverts the malignant phenotype in culture.

In principle, inhibition of matrix modifying ECM proteins can dramatically reduce tumor progression through effects on invasion and metastasis. Moreover, there is evidence that changes in mammary ECM modifies treatment responsiveness to anti-estrogens in hormone therapy and promotes the progression of the breast carcinoma which eventually decreasing patient survival [36, 37].

## 1.2. Polycations as cancer treatment.

A first attempt to use polycations for cancer treatment was to neutralize the negatively charged surface on the malignant cells, which aim to recover proper immune response and tumor destruction (table 1-2) [38]. The mechanism of action may involve both, a direct effect on tumor cells as well as the nonspecific stimulation of the reticulo-endothelial system (RES) of the patient under treatment.

Table 1-2. The effect of polycations, upon eosin staining, lysis, and clumping of Ehrlich ascites cells, L5178Y cells, and murine erythrocytes treated in vitro. Cells were suspended in Eagle's medium plus 10% calf serum and held for 30mm at 25 °C in a hemocytometer before counting [38].

Polycation (300 µg/ml)	% eosin stained			% lysis			Clumping		
	(3 × 10 <sup>6</sup> /ml)		(5 × 10 <sup>6</sup> /ml)	Ehrlich ascites	L5178Y ascites	Murine erythrocytes	Ehrlich ascites	L5178Y ascites	Murine erythrocytes
	Ehrlich ascites	L5178Y ascites	Murine erythrocytes						
Control	5	0	0	0	0	0	– <sup>a</sup>	–	–
PEI 1000	100	100	100	0	0	20	+	–	–
PEI 600	100	100	100	0	0	35	+	–	–
PEI 18	10	10	10	0	0	0	–	–	–
PEI 6	5	5	0	0	0	0	–	–	–
PPI	95	95	0	20	20	20	+	+	–
Polyamine C3	100	100	0	30	30	30	+	–	–
Polyvinylamine bisulfate C7		100		30	30	100	+	–	–
Poly-L-lysine	100	100		0	0	100	+	+	–

<sup>a</sup> –, none; +, marked.

The polycation polylysine has been shown to bind and have an inhibitory activity against diploid Ehrlich ascites carcinoma [39], human epidermoid cancer cells [40], and polyoma virus-transformed fibroblasts in organ culture [41] and but unfortunately also against normal red blood cells and non-neoplastic cells. Polylysine binds to the lipoprotein surface of tumor cells. This binding causes migration of the nucleus and mitochondria towards the cytoplasmic membrane, which in turn may cause telophase inhibition and unipolar mitosis. The polyelectrolyte character of the polycation most probably causes chromatin clumping [39].

It has also been reported that high-molecular-weight poly-ethyleneimine (PEI), when injected intravenously into tumor-grafted mice at nontoxic doses, is effective in causing regression of tumor and increasing long-term survival [38]. Woodman et al. [42] found that the polycation chitosan aggregated L12 10 leukemia cells and have shown a slight increase (10 to 20%) in the life-span of leukemic mice.

### **1.3. The polycationic approach for diagnostic and therapy**

Previous studies have shown that polycations such as PEI and acidified chitosan, are cytotoxic, and induce apoptosis of cancer cells in hours or even days [43-45]. I hereby propose a novel and selective way to target tumors which may use the difference in physical properties of cancer cells from normal cells. Furthermore, I found that the polyallylamine hydrochloride (PAH), a polycation, could differentiate between normal cells and cancer efficiently causing only minimal adverse effects in healthy cells. It was assumed that this fast recognition of cancer cells could be due to its high negative surface charge of cancer cells. High binding affinity of PAH to cancer cells (sparing the normal cells), shows the potential of PAH to be use as fast diagnostic system. It was also observed that PAH can not only bind to the membrane but it instantly enters the cancer cell and dissociating them into small bead-like structures. This instant entrance of the polycation could be attributed to differences in their physical properties like elasticity [24, 46-48] charge distribution [12] and phospholipid composition [49-51] as compared to normal cells. Whilst further studies are clearly necessary to establish the general validity of our findings, our results strongly support the use of polycations as a novel diagnostic and/or local therapeutic tool for cancer.

## **2. References**

1. Levy-Nissenbaum E, Radovic-Moreno AF, Wang AZ, Langer R, Farokhzad OC. Nanotechnology and aptamers: applications in drug delivery. *Trends Biotechnol* 2008;26(8):442-449.
2. Kim D, Lee ES, Oh KT, Gao ZG, Bae YH. Doxorubicin-loaded polymeric micelle overcomes multidrug resistance of cancer by double-targeting folate receptor and early endosomal pH. *Small* 2008;4(11):2043-2050.
3. Moroson H. Polycation- treated tumor cells in vivo and in vitro. *Cancer Res* 1971;31(3):373-380.
4. Ambrose EJ. The Surface Properties of Tumour Cells. In. E. J. Ambrose and F. J. C. Roe, editors. *The Biology of Cancer*. London: D. Van Nostrand Co. Ltd, 1966. p.65-77.
5. Balner H, Old LJ, Clarke DA. Accelerated Rejection of Male Skin Isografts by Female CS7BL Mice Infected with Bacillus Calmette-Guerin (B.C.G.). *Proc Soc Exptl Biol Med* 1962;169:58-62.
6. Vassar PS. Electrophoretic Mobility of Human Tumour Cells. *Nature* 1963;197:1215-1216.
7. Cook GMW, Heard DH, Seaman GVF. The Electrokinetic Characterization of the Ehrlich Ascites Carcinoma Cell. *Exptl. Cell Res* 1962;28:27-39.
8. Foley GE. Conference on Cell Cultures for Virus Vaccine Production. *Natl. Cancer Inst. Monograph* 1967;29:217-263.
9. Erbil KM, Sen SE, Zincke H, Jones JD: Significance of serum protein and lipid-bound sialic acid as a marker for genitourinary malignancies. *Cancer* 1986;57:1389-1394.
10. Cume GA, Bagshawe KD. The Masking of Antigens on Trophoblast and Cancer Cells. *Lancet* 1967;1:708-710.

11. Dueck DA, Chan M, Tran K, Wong JT, Jay FT, Littman C, Stimpson R, Choy PC: The modulation of choline phosphoglyceride metabolism in human colon cancer. *Mol Cell Biochem* 1996;162(2):97–103.
12. Dobrzyńska I, Szachowicz-Petelska B, Sulkowski S, Figaszewski Z. Changes in electric charge and phospholipids composition in human colorectal cancer cells. *Mol Cell Biochem* 2005;276(1-2):113-9.
13. Szachowicz-Petelska B, Dobrzyńska I, Figaszewski Z, Sulkowski S. Changes in physico-chemical properties of human large intestine tumour cells membrane. *Mol Cell Biochem* 2002;238(1-2):41-7.
14. Monteggia E, Colombo I, Guerra A, Berra B: Phospholipid distribution in murine mammary adenocarcinomas induced by activated neu oncogene. *Cancer Detect Prev* 2000;24:207–211.
15. Mountford CE, Wright LC. Organization of lipids in the plasma membranes of malignant and stimulated cells: a new model. *Trends Biochem Sci* 1988;13:172–177.
16. Podo F. Tumour phospholipids metabolism. *NMR Biomed* 1999;12:413–439.
17. Ran S, Downes A, Thorpe PE: Increased exposure of anionic phospholipids on the surface of tumor blood vessels. *Cancer Res* 2002;62:6132–6140.
18. Mürdter TE, Friedel G, Backman JT, McClellan M, Schick M, Gerken M, *et al.* Dose Optimization of a Doxorubicin Prodrug (HMR 1826) in Isolated Perfused Human Lungs: Low Tumor pH Promotes Prodrug Activation by  $\beta$ -Glucuronidase. *J Pharmacol Exp Ther* 2002;301(1):223-228.
19. Lee GYH, Lim CT. Biomechanics approaches to studying human diseases, *Trends Biotechnol* 2007;25(3):111-118.

20. Lekka M, Laidler P, Gil D, Lekki J, Stachura Z, Hryniewicz AZ. Elasticity of normal and cancerous human bladder cells studied by scanning force microscopy. *Eur Biophys J* 1999;28(4):312–316.
21. Guck J, Schinkinger S, Lincoln B, Wottawah F, Ebert S, Romeyke M, *et al.* Optical deformability as an inherent cell marker for testing malignant transformation and metastatic competence. *Biophys J* 2005;88(5):3689–3698.
22. Lincoln B, Erickson HM, Schinkinger S, Wottawah F, Mitchell D, Ulvick S, *et al.* Deformability-based flow cytometry. *Cytometry A* 2004;59A(2):203–209.
23. Thoumine O, Ott A. Comparison of the mechanical properties of normal and transformed fibroblasts. *Biorheology* 1997;34(4–5):309–326.
24. Suresh S. Biomechanics and biophysics of cancer cells. *Acta Mater* 2007;55(12):3989–4014.
25. Li QS, Lee GY, Ong CN, Lim CT. AFM indentation study of breast cancer cells. *Biochem Biophys Res Commun* 2008;374(4):609-613.
26. Li QS, Lee GYH, Ong CN, Lim CT. AFM interaction study of breast cancer cells. *Biochem Biophys Res Commun* 2008;374(4):609-613.
27. Cross SE, Jin YS, Rao J, Gimzewski JK. Nanomechanical analysis of cells from cancer patients. *Nat Nanotechnol* 2007;2(12):780-783.
28. Ben-Ze'ev A. The cytoskeleton in cancer cells. *Biochim Biophys Acta* 1985;780(3):197-212.
29. Cunningham CC, Gorlin JB, Kwiatkowski DJ, Hartwig JH, Janmey PA, Byers HR, *et al.* Actin-binding protein requirement for cortical stability and efficient locomotion. *Science* 1992;255(5042):325-327.

30. Katsantonis J, Tosca A, Koukouritaki SB, Theodoropoulos PA, Gravanis A, Stournaras C. Differences in the G/total actin ratio and microfilament stability between normal and malignant human keratinocytes. *Cell Biochem Funct* 1994;12(4):267-274.
31. Moustakas A, Stournaras C. Regulation of actin organisation by TGF-beta in H-ras-transformed fibroblasts. *J Cell Sci* 1999;112 ( Pt 8):1169-1179.
32. Rao KM, Cohen HJ. Actin cytoskeletal network in aging and cancer. *Mutat Res* 1991;256(2-6):139-48.
33. Park CC, Zhang H, Pallavicini M, Gray JW, Baehner F, Park CJ, et al. Beta1 integrin inhibitory antibody induces apoptosis of breast cancer cells, inhibits growth, and distinguishes malignant from normal phenotype in three dimensional cultures and in vivo. *Cancer Research* 2006;66:1526–1535.
34. Taddei I, Faraldo MM, Teulière J, Deugnier MA, Thiery JP, Glukhova MA. Integrins in mammary gland development and differentiation of mammary epithelium. *J Mammary Gland Biol Neoplasia* 2003;8(4):383-394.
35. Kass L, Erler JT, Dembo M, Weaver VM. Mammary epithelial cell: influence of extracellular matrix composition and organization during development and tumorigenesis. *Int J Biochem Cell Biol* 2007;39(11):1987-1994.
36. Paszek MJ, Zahir N, Johnson KR, Lakins JN, Rozenberg GI, Gefen A, et al. Tensional homeostasis and the malignant phenotype. *Cancer Cell* 2005;8(3):241-254.
37. Weaver VM, Petersen OW, Wang F, Larabell CA, Briand P, Damsky C, et al. Reversion of the malignant phenotype of human breast cells in three-dimensional culture and in vivo by integrin blocking antibodies. *J Cell Biol* 1997;137(1):231-45.
38. Moroso H. Polycation-treated Tumor Cells in Vivo and in Vitro. *Cancer Research* 1971;31:373-338.

39. Kornguth SE, Stahmann MA, Anderson JW. Effect of Polylysine on the Cytology of Ehrlich Ascites Tumor Cells. *Exptl Cell Res* 1961;24:484-494.
40. Mehrishi JN. Effect of Lysine Polypeptides on the Surface Charge of Normal and Cancer Cells. *Eur J Cancer* 1969;5:427-435.
41. Yarnell MM, Ambrose EJ. Studies of Tumour Invasion in Organ Culture. *Eur J Cancer* 1969;5:255-263.
42. Sirica AE, Woodman RJ. Selective aggregation of L1210 leukemia cells by the polycation chitosan. *J Natl Cancer Inst.* 1971;47(2):377-388.
43. Florea B, Meaney C, Junginger H, Borchard G. Transfection Efficiency and Toxicity of Polyethylenimine in Differentiated Calu-3 and Nondifferentiated COS-1 Cell Cultures. *AAPS PharmSci* 2002;4(2):article 12.
44. Moghimi SM, Symonds P, Murray JC, Hunter AC, Debska G, Szewczyk A. A two-stage poly(ethylenimine)-mediated cytotoxicity: implications for gene transfer/therapy. *Mol Ther* 2005;11(6):990-995.
45. Bullock G, Blazer V, Tsukuda S, Summerfelt S. Toxicity of acidified chitosan for cultured rainbow trout (*Oncorhynchus mykiss*). *Aquaculture* 2000;185(3-4):273–280.
46. Suresh S. Elastic clues in cancer detection. *Nat Nanotechnol* 2007;2:748–749.
47. Cross, S.E., et al. AFM-based analysis of human metastatic cancer cells. *Nanotechnol* 2008;19:384003-384011.
48. Rosenbluth, M.J., Lam, W.A., Fletcher, D.A. Force Microscopy of Nonadherent Cells: A Comparison of Leukemia Cell Deformability. *Biophys J* 2006;90:2994-3003.
49. Gottfried EL. Lipid patterns in human leukocytes maintained in long-term culture. *J Lipid Res* 1971;12:531-537.

50. Liebes LF, Pelle E, Zucker-Franklin D, Silber R. Comparison of Lipid Composition and 1,6-Diphenyl-1,3,5-hexatriene Fluorescence Polarization Measurements of Hairy Cells with Monocytes and Lymphocytes from Normal Subjects and Patients with Chronic Lymphocytic Leukemia. *Cancer Res* 1981;41:4050-4056.
51. Agatha G, Häfer R, Zintl F. Fatty acid composition of lymphocyte membrane phospholipids in children with acute leukemia. *Cancer Lett* 2001;173:139-144.

## CHAPTER 1

*Selective labeling of cancer cells by Poly-allylamine induces rapid cell death.*\*

### 1.1. Aim of the present work

An ideal cancer drug should destroy only tumor cells with high selectivity, and spares the healthy ones. In this work, I show that a specific positively charged polymer (poly-allylamine hydrochloride, PAH) has the ability to fulfill this requirement. I found that PAH enters with high selectivity into leukemic and liver cancer cells. After PAH was internalized, cancer cells are destroyed within minutes while healthy cells remained almost unaffected. It was also evident from the present study that the polycation was more effective in less differentiated cancer types. Cell death could be due to the high affinity of poly-allylamine for phosphate moieties such as PIP<sub>3</sub> and other phosphate bearing cellular moieties, present in higher concentrations in the cytosol of cancer cells. This interaction leads to the disintegration of the cytosol into non-toxic gel beads. Therefore, it would be quite useful to investigate the possible diagnostic and therapeutic use of this polycation for cancer, in particular for the intratumoral administration. More studies ought to be carried out, to investigate whether the phenomenon discovered in the present work, is a general phenomenon for most of the cancer type. It could suggest that, in the case of cancer cells, targeting physical properties may be equally fruitful as the commonly used targeting of biomarkers.

\*

*Manuscript submitted in preparation*

## **CHAPTER 2**

### **2.1. Introduction**

In recent decades, some progress has been made to extend the life span of cancer patients, but, up to date, a definitive treatment that can defeat the disease has not been found. Whilst the origin of cancer is still not completely understood, at present, it is generally accepted that it is a result of mutations that have accumulated in the genome which leads to basic functional alterations in the biology of the cell. Depending on the type of cancer, the treatment may vary from surgery combined with chemotherapy, which are mostly targeted against the DNA synthesis or inhibitors against cell division or radiation therapy. Today, selectively targeting cancer cells is one of the major challenges in nanomedicine. Many approaches are dedicated to finding suitable biomarkers or targets [1], modifying the drug molecules or producing a protective delivery system [2, 3] in order to decrease the collateral effects of chemotherapeutics and increase the tumoral concentration of the drug. The novel approach also includes the use of monoclonal antibodies [4] or tyrosine kinase inhibitors and the improved delivery of standard chemotherapeutic drugs by means of covalent binding to folic acid [5].

In the present study, I propose a novel and selective way to target tumors based on differences in the physical properties of cancer cells in comparison to normal cells. Cancer cells show anomalies in most of their metabolic activities, and as a consequence, in their physical properties. Several studies have underlined that cancer cells have different elasticity [6-10], charge distribution [11] and phospholipid composition [12-14] as compared to normal cells.

In an early attempt to visualize the charge distribution on cells using fluorescence labeled polycations, some specific regions in dividing cells can be seen to have a higher negative charge [15]. As it can be deemed possible that the extra negative charge was concentrated in the regions of new cell growth it was decided to study cancer cells in which cell growth is an ever pervasive feature. Furthermore, two completely different cancer model, leukemia and hepatocarcinomas were considered for the present study. For each cancer model two cell lines were tested, which differs in their stages of differentiation.

The HL-60 cell line was derived from human promyelocytic leukemia [16], immature (undifferentiated) neutrophils); Jurkat cell line, belong to an immortalized mature (differentiated) and T lymphocytes from acute lymphoblastic leukemia (ALL) [17] were all investigated as leukemia model. The corresponding models for hepatocarcinoma were the HuH-7 and JHH-6 cell lines. The HuH-7 cell line was derived from, a well-differentiated type of hepatocellular carcinoma [18]. At the same time JHH-6 cell line, represent a undifferentiated hepatocellular carcinoma [19].

Usually, polycations such as polyethylenimines (PEI) was found to be cytotoxic, and induce apoptosis, a process which leads to cell death in hours or even days [20]. However, my studies with polycation, polyallylamine hydrochloride (PAH) show that the cancer cells began to fragment in less then 5 mins. Furthermore, I found that the strong affinity of PAH to phosphate species most probably leads this fragmentation of the complete cell cytosol in the form of small gel beads. The above observation was supported by the phosphorus peak, as detected with EDS (energy-dispersive X-ray spectroscopy) analysis of the beads, along with ATP assay and PIP<sub>3</sub> antibody binding studies.

Whilst further studies are clearly necessary to establish the general validity of these findings, results strongly support the use of PAH having the potential to become a novel diagnostic and/or local therapeutic tool for cancer.

## **2.2. References**

1. Levy-Nissenbaum E, Radovic-Moreno AF, Wang AZ, Langer R, Farokhzad OC. Nanotechnology and aptamers: applications in drug delivery. *Trends Biotechnol* 2008;26(8):442-449.
2. Kim D, Lee ES, Oh KT, Gao ZG, Bae YH. Doxorubicin-loaded polymeric micelle overcomes multidrug resistance of cancer by double-targeting folate receptor and early endosomal pH. *Small* 2008;4(11):2043-2050.
3. Carter P. Improving the efficacy of antibody-based cancer therapies. *Nat Rev Cancer* 2001;1(2):118-129.
4. Chan JM, Valencia PM, Zhang L, Langer R, Farokhzad OC. Polymeric nanoparticles for drug delivery. *Methods Mol Biol* 2010;624:163-75.
5. Stella B, Arpicco S, Peracchia MT, Desmaële D, Hoebcke J, Renoir M, *et al.* Design of folic acid-conjugated nanoparticles for drug targeting. *J Pharm Sci* 2000;89(11):1452-64.
6. Suresh S. Nanomedicine: elastic clues in cancer detection. *Nat Nanotechnol* 2007;2(12):748-749.
7. Suresh S. Biomechanics and biophysics of cancer cells. *Acta Biomater* 2007;3(4):413-38.
8. Cross SE, Jin YS, Tondre J, Wong R, Roa JY, Gimzewski JK. AFM-based analysis of human metastatic cancer cells. *Nanotechnol* 2008;19(38):384003-384011.
9. Cross SE, Jin YS, Rao J, Gimzewski JK. Nanomechanical analysis of cells from cancer patients. *Nat Nanotechnol*. 2007;2(12):780-783.
10. Rosenbluth MJ, Lam WA, Fletcher DA. Force microscopy of nonadherent cells: a comparison of leukemia cell deformability. *Biophys J* 2006;90(8):2994-3003.

11. Dobrzyńska I, Szachowicz-Petelska B, Sulkowski S, Figaszewski Z. Changes in electric charge and phospholipids composition in human colorectal cancer cells. *Mol Cell Biochem* 2005;276(1-2):113-119.
12. Gottfried EL. Lipid patterns in human leukocytes maintained in long-term culture. *J Lipid Res* 1971;12(5):531-537.
13. Liebes LF, Pelle E, Zucker-Franklin D, Silber R. Comparison of Lipid Composition and 1,6-Diphenyl-1,3,5-hexatriene Fluorescence Polarization Measurements of Hairy Cells with Monocytes and Lymphocytes from Normal Subjects and Patients with Chronic Lymphocytic Leukemia. *Cancer Res* 1981;41(10):4050-4056.
14. Agatha G, Häfer R, Zintl F. Fatty acid composition of lymphocyte membrane phospholipids in children with acute leukemia. *Cancer Lett* 2001;173(2):139-144.
15. Krol S, Diaspro A, Magrassi R, Ballario P, Grimaldi B, Filetici P, *et al.* Nanocapsules: Coating for Living Cells. *IEEE Trans Nanobioscience*. 2004;3(1):32-38.
16. Gallagher R, Collins S, Trujillo J, McCredie K, Ahearn M, Tsai S, *et al.* Characterization of the continuous, differentiating myeloid cell line (HL-60) from a patient with acute promyelocytic leukemia. *Blood* 1979;54(3):713-33.
17. Schneider U, Schwenk H, Bornkamm G. Characterization of EBV-genome negative "null" and "T" cell lines derived from children with acute lymphoblastic leukemia and leukemic transformed non-Hodgkin lymphoma. *Int J Cancer* 1977;19(5):621-626.
18. Nakabayashi H, Taketa T, Miyano K, Yamane T, Sato J. Growth of human hepatoma cell lines with differentiated functions in chemically defined medium. *Cancer Res* 1982;42:3858-3863.

19. Fujise K, Nagamori S, Hasumura S, Homma S, Sujino H, Matsuura T, *et al.*  
Integration of Hepatitis B virus DNA into cells of six established human hepatocellular carcinoma cell lines. *Hepato-gastroenterol* 1990;37:457-460.
20. Moghimi SM, Symonds P, Murray JC, Hunter AC, Debska G, Szewczyk A. A two-stage poly(ethylenimine)-mediated cytotoxicity: implications for gene transfer/therapy. *Mol Ther* 2005;11(6):990-5.

## **CHAPTER 3**

### **Materials and methods**

#### **3.1. Materials**

The polycations, poly-(allylamine hydrochloride) (PAH; MW. 15kDa), and the fluorescent-labeled poly-(fluorescein isothiocyanate polyallylamine hydrochloride) (FITC-PAH; MW. 15kDa;  $\lambda_{exc}=494$  nm,  $\lambda_{em}=520$  nm), 3-(4,5-dimethylthiazol-2-yl)-2,5-diphenyl tetrazolium bromide (MTT),  $MgCl_2$  and dimethylsulfoxide (DMSO), bovine pancreas insulin, dexametasone, Hoechst 33258 ( $\lambda_{exc}=356$  nm,  $\lambda_{em}=465$  nm), spermine and Fetal Bovine Serum (FBS) were purchased from SIGMA-Aldrich (Milan, Italy). Dulbecco's Modified Eagle's Medium (DMEM) were purchased from Lonza (USA), whereas Dulbecco's Modified Eagle's Medium/Nutrient F-12 Ham (DMEM/F12), medium and Williams E medium (WEM) were purchased from Sigma-Aldrich (Missouri, USA), respectively. Dulbecco's modified Eagle's high glucose medium (DMEM-hg), penicillin, streptomycin and L-Glutamine were purchased from Euro-clone (Italy). Anti-phosphatidylinositol-3,4,5-triphosphate-fluorescein-5-isothiocyanate ([Anti-PIP3]-FITC) was purchased from Echelon Bioscience Inc. (Salt Lake City, USA). The plasma membrane specific dye, dialkylaminostyryl (DiA;  $\lambda_{exc}=460$  nm,  $\lambda_{em}=580$  nm), nucleic acid binding dye, Propidium Iodide (PI;  $\lambda_{exc}=537$  nm,  $\lambda_{em}=619$  nm), Hepes buffer and pyridoxine HCl were purchased from Invitrogen (Milan, Italy). All polycation solutions were prepared in DMEM medium immediately before use.

## 3.2. Methods

### 3.2.1. Cell Culture

#### 3.2.1.1. Cell lines

**Leukemia:** Leukemia cell lines (HL60 (ATCC CCL-240™ Human promyelocytic leukemia) and Jurkat (TIB-152™ T lymphocytes from patient with T cell leukemia) cell lines were maintained in DMEM medium supplemented with 10% heat-inactivated FBS, penicillin (100 units/ml), streptomycin (100 µg/ml), gentamicin (10 µg/ml) (DMEM complete medium) at 5% CO<sub>2</sub> and 37°C. The medium was changed every second day and mycoplasma test was performed routinely by fluorescent Hoechst 33258 staining denoting no contamination.

**Hepatocytes:** HuH-7 cell line (JCRB0403 well differentiated Hepatocellular carcinoma (HCC)) and JHH-6 cell line (JCRB1030 undifferentiated HCC) were obtained from Japan Health Science Research Resources Bank (HSRRB, JCRB0403 JCRB1030), respectively. HuH-7 cell culture was performed under standard conditions in Dulbecco's modified Eagle's high glucose medium DMEM with 10% (v/v) FBS, 2mM L-Glutamine, and 1% (v/v) antibiotics (10,000 U/mL penicillin, 10 mg/mL streptomycin). The cells were grown at 37°C in a humidified atmosphere 95% air and 5% CO<sub>2</sub>. JHH-6 was cultured in Williams E medium under the conditions described above.

IHH cell line (hepatic non-tumoral cell line) (a kind gift by Dr. T.H Nguyen [1]) was culture d under standard conditions as described above, using DMEM/F12 1x containing 15 mM Hepes buffer, L-glutamine and pyridoxine HCL, 1 x 10<sup>-6</sup>M dexametasone, 5 µg/mL bovine pancreas insulin, 10,000 U/mL penicillin, and 10 mg/mL streptomycin and 10% (v/v) FBS. Mycoplasma test was performed routinely by fluorescent Hoechst 33258 stain with no contamination ever found.

### **3.2.1.2. Mononuclear Cell Extraction**

Blood samples of healthy volunteers were obtained from the Dermatology Department of Cattinara Hospital and the Liver Research Center, both Trieste, Italy. Leukemic blood samples of patients were obtained from the Hematology Department after direct informed consent that the blood will be used for new experimental diagnostic procedures.

Mononuclear cells (MNCs) were isolated from blood using Ficoll-Paque<sup>TM</sup> PLUS (GE Healthcare) according to manufacture's protocols. The MNC were then washed twice with PBS and once in DMEM complete medium (as explained section 3.2.1.1.). They were then maintained in the same medium during experiment.

## **3.2.2. Polycation as theranostic application**

### **3.2.2.1. PAH, as cancer diagnostic**

#### **3.2.2.1.1. PAH specific binding with cancer cells**

To 5 mL ( $4 \times 10^5$  cells/mL), of HL60, Jurkat, JHH6, HuH7 and IHH cell line as well as MNCs from healthy donors and patients respectively, 400  $\mu\text{g/mL}$  of FITC-PAH was added and incubated for 5min. After washing them twice by repeated centrifugation at  $1000 \times g$  for 5min at RT in case of HL60 and Jurkat cell lines; and simply raising in case of IHH, HuH7 and JHH6 cell lines, with there respective medium without PAH, confocal microscopy was performed to visualize the cells with FITC-PAH. The experiments were repeated at least five times on each cell line.

### 3.2.2.1.2. Possible PAH cell entrance mechanism

In order to understand the mechanism of polycation entrance, I tested two hypotheses (fig. 3-1). The first hypothesis was that the polycation enters via a specific amine channel [2]. This was tested by blocking the channel either with high magnesium ( $50\mu\text{M}$ ) or spermine ( $10\mu\text{M}$ ) concentrations (fig. 3-1a) [2], followed by FITC-PAH ( $13.4\mu\text{M}$ ) treatment on the MDA MB 231 cells. The kinetic of FITC-PAH entrance was studied in the presence and absence of the blocking agents, by time lapse imaging under confocal microscope (supplementary video 1). Each experiment was repeated 4 times.

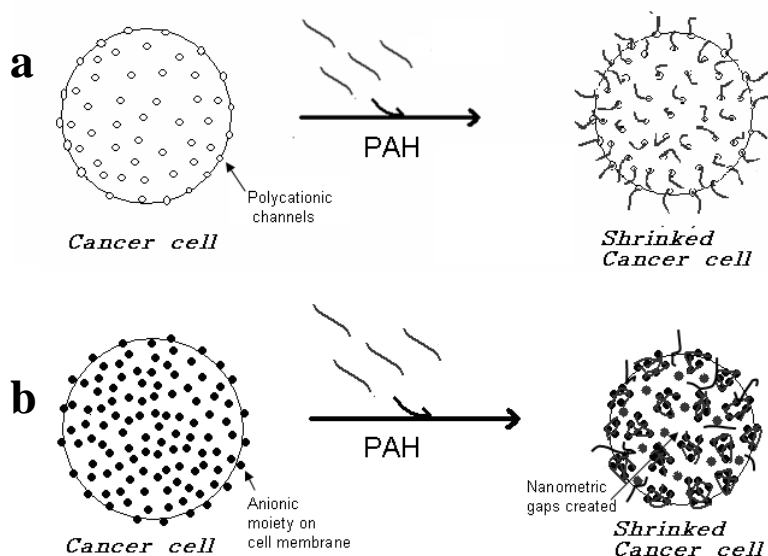


Figure 3-1. Scheme of the hypothetical models for polycation entrance in cancer cells. a) Hypothesis 1: PAH entrance through Polyamine transport channels (e.g. MIC); b) Hypothesis 2: PAH causes cell membrane poration by interaction with negative moieties in the plasma membrane and enters through these nanopores.

The second hypothesis was that the polycation creates nanopores as described for other polycations [3-5]. This was tested by an indirect proof using JHH6 (Fig. 3-1b) and MDA MB 231 cell line. The medium was doped with  $30\mu\text{M}$  Propidium Iodide (PI), a dye which enters into late apoptotic cells when the plasma membrane integrity is lost. Then FITC-PAH

(13.5 $\mu$ M) was added to the cells on a microscopic slide and the entrance of the green and/or the red fluorescence was visualized. The experiment was repeated 4 times.

Imaging was performed with a Nikon C1 laser scanning confocal unit (Nikon D-eclipse C1Si, Japan) attached to an inverted fluorescence microscope with a 100 $\times$ /1.49 oil Apo TIRF objective (Nikon, Japan). The fluorophores were excited with a multiline argon ion laser, FITC-PAH at  $\lambda$ =488 nm, DiA at  $\lambda$ =460 nm and PI at  $\lambda$ =535 nm. Images were acquired and processed using the operation software EZ-C1 for Nikon C1 confocal microscope.

#### **3.2.2.1.3. Caspase assay**

In order to determine if polycation exposure induces apoptosis, Caspase3/7 assay was performed. Caspase-3 is a converging point of these apoptotic pathways [6]. Its activation play a key role in initiation of cellular events involved in the early apoptotic process. The HL60 and Jurkat cells ( $2 \times 10^4$  cells/well) were plated in 96 wells and treated with different concentration of PAH (100, 200 and 400 $\mu$ g/mL) along with respective untreated cells as control. Apoptosis induction was assayed using the Caspase-Glo<sup>®</sup>3/7 assay kit (Promega, USA) according to the manufacture's protocol. Each experiment was repeated 3 times.

#### **3.2.2.1.4. Fluorescence activated cell scanning (FACS) analysis**

To 5mL each of HL60 ( $260 \times 10^4$  cells/mL) and Jurkat ( $645 \times 10^4$ ) cells, different concentrations (50, 100, 200, 400 $\mu$ g/mL) of the polycation (FITC-PAH) was added followed by 5min treatment. The cells were then washed twice by centrifugation (as explained in previous section 2.2.1.1.) to remove the excess of the compound, the pellet was recovered and resuspended in physiologic solution. The respective untreated cells were used as the

negative control. The intracellular green fluorescence from FITC-PAH was collected by Flow Cytometry using a Becton Dickinson FACS Calibur System (Becton Dickinson, Mountain View, CA, USA), equipped with a single argon-ion laser, through a 530 nm band pass filter in combination with a 570nm dichroic mirror. A minimum of 10,000cells was analyzed for each sample.

### **3.2.2.2. PAH as therapeutic**

#### **3.2.2.2.1. Cell viability analysis by MTT assay**

Cell viability after PAH treatment, was determined using the MTT (3-(4,5-dimethylthiazol-2-yl)-2,5-diphenyl-tetrazolium bromide) dye reduction assay as previously described [8]. Briefly, HL60 and Jurkat cells, Mononuclear cells (MNCs) from a healthy donor ( $20 \times 10^4$  cells/per well) were exposed to different final concentrations of PAH (20  $\mu\text{g}/\text{mL}$ , 40 $\mu\text{g}/\text{mL}$ , 80 $\mu\text{g}/\text{mL}$ , 100 $\mu\text{g}/\text{mL}$ , 200  $\mu\text{g}/\text{mL}$  and 400  $\mu\text{g}/\text{mL}$ ) for 5 mins. Untreated cells were considered as a negative control and for the positive control cells they were lysed with 8 $\mu\text{l}$  Lysine. After washing twice with DMEM medium (without serum and antibiotics), the respective cells were incubated with 0.5 mg/mL of MTT for 1 h at 37°C. After removing the medium, cells were lysed and the resulting blue formazan crystals were dissolved in DMSO. Each sample was loaded in triplicates in a 96 well plate. The absorbance of each well was read on a microtiter plate reader (Beckman Coulter LD 400C Luminescence detector) at 570 nm. The absorbance of the untreated controls was taken as 100% survival. The data represents the mean $\pm$ SD of three to five independent experiments. The same procedure was also followed for the hepatic cancer cell lines. Each experiment was repeated at least five times.

### **3.2.3. Toxicology study of the cell-products from PAH treatment**

The idea was to administer the polycation intratumorally and the resulting beads from the cell destruction are released to the blood circulation. As it is well known that PAH usually is highly toxic to endothelial cells [7]. The resulting product obtained due the dissociation of the cells after PAH treatment, was tested for its toxicity. Now on it will be referred as PAH-beads in the present work.

#### **3.2.3.1. PAH-Beads preparation**

The PAH-beads were obtained by incubating 1.6 ml of PAH (400µg/ml) in 3.4 ml of HL 60 and Jurkat cell line (both:  $10^6$  cells/mL) respectively, at 37°C and 5% CO<sub>2</sub>. After 2h of incubation, and in order to obtain as much PAH-beads, cells were washed twice with DMEM by centrifugation/resuspension at 16000×g for 30mins at room temperature. The PAH-beads were resuspended in 5ml medium.

#### **3.2.3.2. SEM (scanning electron microscopy) and EDS (energy-dispersive X-ray spectroscopy) of beads as a product of cell disintegration**

For SEM PAH-beads were prepared as described in section 3.2.3.1. The resulting PAH-beads from the supernatant were washed twice with MQ-water using repeated centrifugation at 16,000×g for 30mins at room temperature and then resuspension in the pure water to exclude the presence of medium components. 100µL of extracted PAH beads were dried on a gold coated mica wafer at 50°C for 6h in order to provide a conductive surface for energy dispersive x-ray spectroscopic (EDS) measurement. .

Morphology of the PAH beads were recorded using a Zeiss SUPRA 40 scanning electron microscope (Gemini, UK), equipped with field emission gun (Field Emission Scanning Electron Microscope (FE-SEM)) which operates between 0.1–30keV providing a lateral resolution of 1nm and an energy dispersive x-ray spectroscope (EDS). The images were acquired with the energy of 1keV. Elementary analysis by EDS was performed with 7keV. This energy generates a 150nm thick measuring volume, as calculated by Monte Carlo simulations [9] and therefore perfectly matches the average diameter of a dried PAH bead of 100-200 nm. The bead diameter was calculated by ImageJ software and the elementary spectra were analyzed for the phosphor (P) to Nitrogen (N) ratio by calculating the peak area with Origin8 statistical software.

### **3.2.3.3. Determination of the content of the PAH beads**

One theory was that the polycation recognizes high concentrations of PIP<sub>3</sub> which are known to be present in the cell membrane of cancer cells. In order to detect PIP<sub>3</sub>, 1ml of the PAH-beads was incubated with 10ul mouse Fluorescein (FITC) conjugated anti-PIP<sub>3</sub> monoclonal antibody ([Anti-PIP<sub>3</sub>]-FITC) diluted 1:50 times (0.1µg/mL) for 1h under the conditions described in section 3.2.1.1. After washing three times with PBS, the FITC were visualised by confocal laser scanning microscopy (CLSM) (as in section 3.2.2.2.). This experiment was repeated three times.

To confirm the presence of PIP<sub>3</sub> in tumor cells, 2ml each of HL60 and Jurkat cells ( $2 \times 10^5$  cells/mL) were seeded on a cover-slip and treated as described before in section 3.2.2.1.1. After washing twice with PBS the cells were fixed with 3.7% para-formaldehyde (PFA) in PBS for 20 min. The respective cell bearing coverslip were then incubated for 1h at RT with saturation solution of PBS Triton-Tween 100× 0.1% containing 5% BSA-5% normal goat

serum (NGS). The fixed slides were then incubated overnight (O/N) at 4°C with Fluorescein (FITC) labeled mouse anti-PIP3 monoclonal antibody at a 1:50 dilution. The next day the cells were washed three times with PBS and the FITC signal coming from the bound PIP<sub>3</sub> mAb was detected by CLSM (as in section 3.2.2.2.).

To determine the presence of ATP, the PAH-beads were assayed with the ATP assay kit (Promaga, Italy) according to manufacturer's protocol. The experiment was repeated three times.

#### **3.2.3.4. PAH-bead toxicity analysis**

The beads for the MTT assay were prepared as described in section 3.2.3.1. but washed twice with medium instead of MQ water. Finally, the beads were resuspended in 5 mL medium. Different volumes (200, 400, 600, 800µL respectively) of bead-containing medium were added to untreated HL60 or Jurkat cell suspensions (both: 10<sup>6</sup> Cells/ml). These were incubated for 2h followed by washing twice with DMEM medium and centrifugation at 1,000×g for 5mins at room temperature. The MTT assay was performed as described in section 3.2.2.2.1. The long term toxicity was investigated by incubating HL60 and Jurkat cells (20×10<sup>4</sup> cells/mL) in the presence of 800µl PAH-bead containing medium for 0, 6, 24, 42, 48h respectively.

#### **3.2.3.5. Fluorescence activated cell scanning (FACS) analysis**

HL60 (260 x 10<sup>4</sup> cells) and Jurkat (645 x 10<sup>4</sup>) cells were treated with different volumes (50, 100, 200, 400µL respectively) of FITC-PAH beads obtained from cells treated for 5 min with FITC-PAH. Cells were centrifuged twice to remove the excess of the compound; the

pellet was recovered and resuspended in physiological salt solution (0.9% w/v of NaCl solution). Untreated cells were used as the negative control. The intracellular green fluorescence from FITC-PAH was collected by Flow Cytometry using a Becton Dickinson FACS Calibur System, equipped with a single argon-ion laser, through a 530 nm band pass filter in combination with a 570 nm dichroic mirror. A minimum of 10,000 cells was analyzed for each sample.

### **3.3. References**

1. Nguyen TH, Mai G, Villiger P, Oberholzer J, Salmon P, Morel P, *et al.* Treatment of acetaminophen-induced acute liver failure in the mouse with conditionally immortalized human hepatocytes. *J Hepatol* 2005;43(6):1031-1037.
2. Kerschbaum HH, Kozak JA, Cahalan MD. Polyvalent Cations as Permeant Probes of MIC and TRPM7 Pores. *Biophys J* 2003;84:2293-2305.
3. Mecke A, Majoros IJ, Patri AK, Baker JRJr, Banaszak Holl MM, Orr BG. Lipid Bilayer Disruption by Polycationic Polymers: The Roles of Size and Chemical Functional Group. *Langmuir* 2005;21:10348–10354.
4. Hong S, Bielinska AU, Mecke A, Keszler B, Beals JL, Shi X, *et al.* Interaction of poly(amidoamine) dendrimers with supported lipid bilayers and cells: hole formation and the relation to transport. *Bioconjug Chem* 2004;15(4):774-7.
5. Chen J, Hessler JA, Putchakayala K, Panama BK, Khan DP, Hong S, *et al.* Cationic nanoparticles induce nanoscale disruption in living cell plasma membranes. *J Phys Chem B* 2009;113(32):11179-11185.
6. Stennicke HR, Salvesen GS. Biochemical characteristics of caspases-3, -6, -7, and -8. *J Biol Chem* 1997;272(41):25719-25723.
7. Chanana M, Gliozzi A, Diaspro A, Chodnevskaja I, Huewel S, Moskalenko V, *et al.* Interaction of polyelectrolytes and their composites with living cells. *Nano Lett* 2005;5(12):2605-2612.
8. Mosmann T. Rapid colorimetric assay for cellular growth and survival: application to proliferation and cytotoxicity assays. *J Immunol Methods* 1983;65(1-2):55-63.

9. Drouin D, Couture AR, Joly D, Tastet X, Aimez V, Gauvin R. CASINO V2.42 - a fast and easy-to-use modeling tool for scanning electron microscopy and microanalysis users. *Scanning* 2007;29(3):92-101.

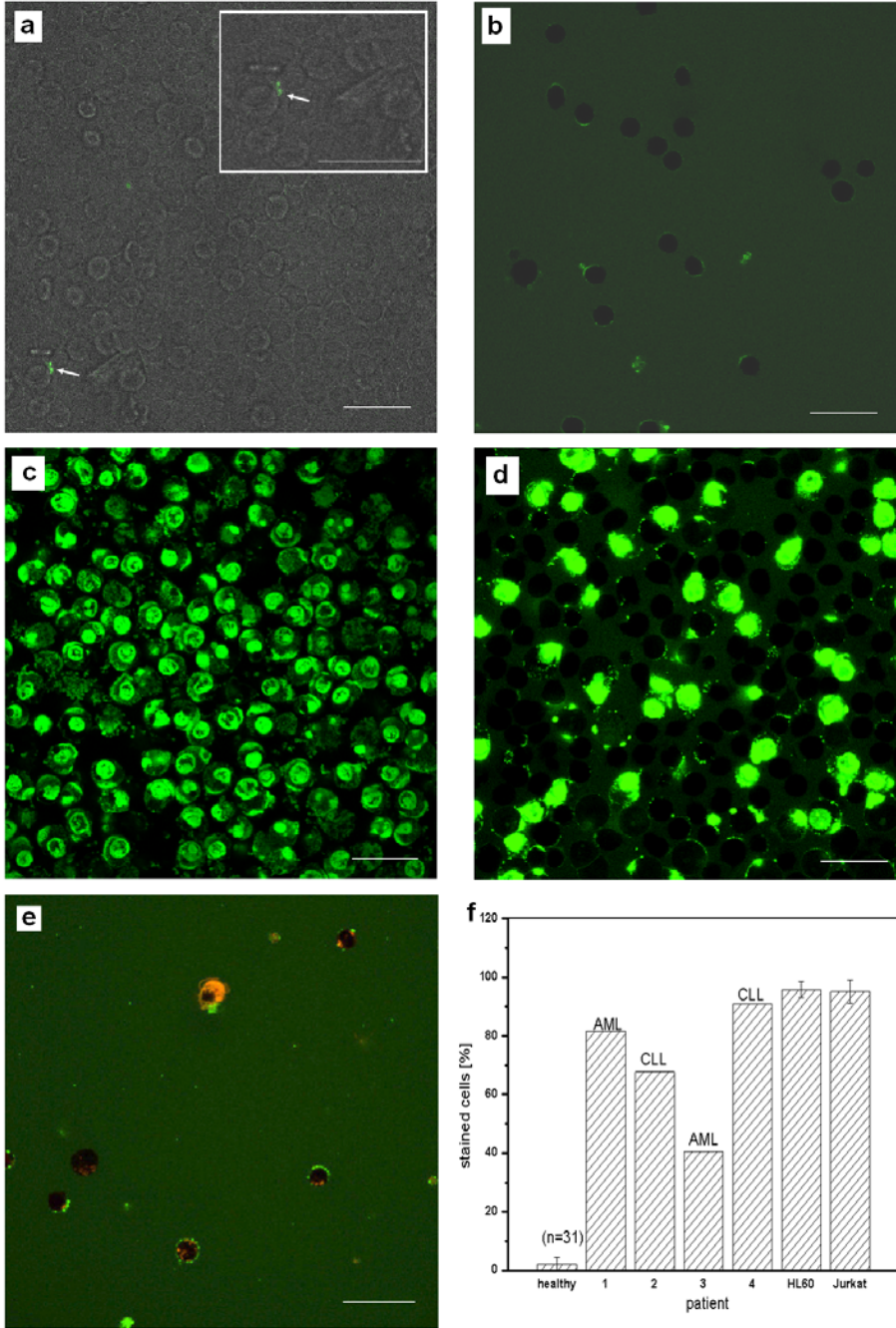
## CHAPTER 4

### Results and Discussions

#### 4.1. PAH, for cancer diagnosis

##### 4.1.1. Selective cancer cell labeling

In an earlier attempt to investigate the charge distribution on budding yeast and germinating *Neurospora crassa* cells, it was noticed that for the growth region a higher level of negative charge was found [1]. In order to understand if the same is true for mammalian cancer cells in comparison with normal healthy cells, I began my study with blood derived cells. Incubation of whole blood samples from healthy donor with the fluorescent labeled polycation PAH (FITC-PAH), showed to no significant staining of the platelets or of the less abundant mononuclear cells (Fig. 4-1a) The same result was observed, when MNCs isolated from the blood of 31 healthy donors were treated with FITC-PAH (fig. 4-1b, & graph 4-1f). After counting the FITC-PAH marked cells in fluorescence micrographs, I found only  $5\pm 2\%$  mononuclear cells (MNC) from healthy donor a fluorescence signal (fig. 4-1f). In fig. 4-1b some of the MNCs of healthy donor showed a low staining of the cell surface, which disappears when the cells are washed with pure medium. Even incubation for 24 h in the polycations did not lead to any cell staining (fig.4-1e).



Next, I investigated leukemic cell lines as models for blood cancer. In the case of HL60 cells, I observed that PAH not only attached to the cell surface but was also able to cross the plasma membrane and enters into the cell interiors. In fig. 4-1d, f, it could be clearly seen that  $97\pm 2\%$  of the cells shows internalized polycation. Finally, the FITC-PAH staining was determined in the MNC fraction of the blood from 4 patients diagnosed with leukemia (2 with chronic lymphoid leukemia (CLL), 2 with acute myeloid leukemia (AML)). The cell staining for a patient with AML is shown in fig. 4-1d. A significantly higher number of cells (40-90%; fig. 4-1f) was found to internalize FITC-PAH as compared to healthy donors (<5%) suggesting that PAH selectively entered the cancerous white blood cells MNCs.

#### 4.1.2. FACS analysis of FITC-PAH internalized cells

FACS is a standard technique, used these days in clinics for cancer detection by immunological phenotype of cancer cells by and screening large amounts of cells which is not possible with fluorescence microscopy [2]. This technique is based on the fluorescently-labeled cell identification. FACS analysis of FITC-PAH (at different concentration) treated HL60 and Jurkat cells (fig. 4-2) confirmed the data observed by confocal microscopy that a high amount of

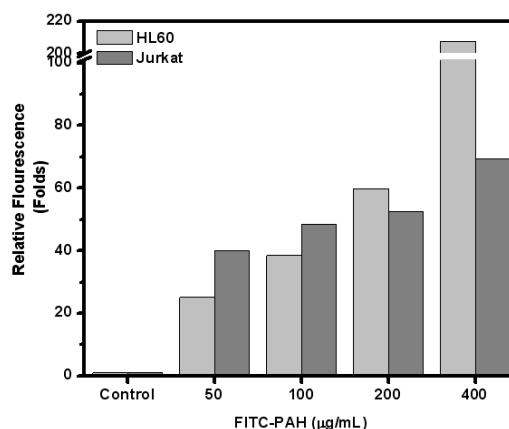


Fig. 4-2. FACS analysis. Graphical presentation of relative fluorescent enhancement of FITC-PAH detected from FITC-PAH internalized cells versus different concentration of FITC-PAH treatment.

the cancer cells internalize the polycation while the healthy cells are unstained. By FACS analysis also it was seen that undifferentiate cancer cell line (i.e. HL60) were more prone to PAH treatment than the more differentiated cancer cell line (i.e., Jurkat).

The above study demonstrates that the PAH treatment can be supported by FACS analysis. The only limitation which encountered was that most of the cells were fragmented in PAH-beads which can falsify the results and lead to higher number of stained cells. A shorter time between exposure to PAH and FACS analysis is required.

### 4.1.3. Possible mechanism of PAH entrance in cancer cells

#### 4.1.3.1. First hypothesis of PAH entrance mechanism

In order to understand the mechanism of polycation entrance, I tested two hypotheses (fig. 3-1). One based on a channel mediated entrance, the other one a forced entrance by nanoporation of the cell membrane as already described for other polycations.

From literature, it is known that at least in the case of Jurkat and basophilic leukemic cells, MIC ( $Mg^{2+}$ -inhibited cation) channels are present in the cell membrane. MIC channel have an internal diameter of 0.6nm (fig. 3-1a, chapter 3) [3]. The hydrodynamic radius of

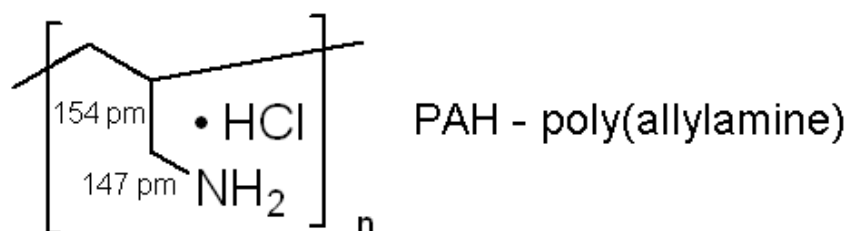
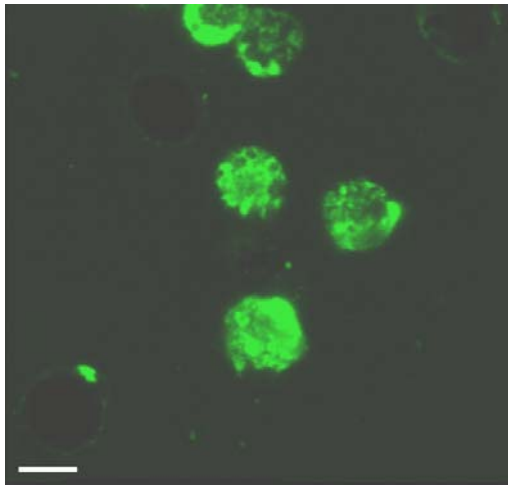


Fig. 4-3. PAH formula structure, with the bond length between C-C: 154pm and C-N: 147pm.

coiled 70kDa PAH was found to be 9.5nm for 2mg/mL [4]. Thus, coiled 70kDa PAH polymer cannot penetrate through these channels. However, in the present study, the PAH used was shorter i.e., 15kDa with 308 pm transversal diameter, calculated on the basis of the binding lengths (fig. 4-3). If we assumed that PAH remains uncoiled while entering in the

channel, it may easily pass through MIC channel. Therefore, the fast entrance of PAH could be mediated through these channels.

Unfortunately, a measurement of the membrane potential with patch clamp as described by Fraser *et al.*[5] was not possible because the cells always disconnected from the pipette



*Fig. 4-4. Confocal micrograph of FITC-PAH internalized HL60 cells after channel blocking by Spermine and  $Mg^{2+}$ . White bar represents  $10\mu m$  scale bar.*

when exposed to the polycation. But the above hypothesis was tested by blocking the channel with either a high magnesium concentration ( $50\mu M$ ) or spermine ( $10\mu M$ ) [5] and the kinetic of a fluorescent-labeled PAH entrance was followed by confocal time series imaging, in the presence and absence of the blocking agents. The

assumption was that if the fast polycation uptake was through these channels, a specific channel-blocker should prevent or prolong the entrance.

Nevertheless, no difference in the kinetics with and without blocking agents was found (fig. 4-4 & supplementary video 1).

#### **4.1.3.2. Second hypothesis of PAH entrance mechanism**

It has been described that cancer cells are usually “softer” than normal cells [6, 7] and have a higher ratio of negative phospholipid in the plasma membrane [8]. Taking this into consideration, the charge of the polycation could interact directly with the phospholipids in the plasma membrane. This can condense the negatively charged phospholipids and, may

induce nanoporation of the cell membrane [9, 10]. This leakage of the cell membrane may lead to instantaneous influx of huge amount of PAH into the cell (fig. 3-1b).

The nanoporation hypothesis due to PAH (polycation) interaction [11-13] was verified by an indirect procedure. Hepato carcinoma cells (JHH-6) (fig. 4-5), as adherent cells allow a long-term visualization and therefore they were treated with FITC-PAH in presence of Propidium Iodide (PI) dye on a microscopic slide. PI enters only in late apoptotic cells when the plasma membrane integrity is decreased. Initially, as expected the PI (red dye) is excluded by the cancer cells because the membrane is still intact. In a time series by confocal microscopy (fig. 4-5a & b) it was observed that 30-60s after the addition of the polycation the PI enters the cell. An exact determination of the kinetic is difficult as it cannot be excluded that the polycation and the cell suspension mix heterogeneously. Similar entrance kinetics was found also for non-adherent HL60 and Jurkat cells. In the case of the HL 60 cells, the complete process from the entrance to the destruction of the cells was followed.

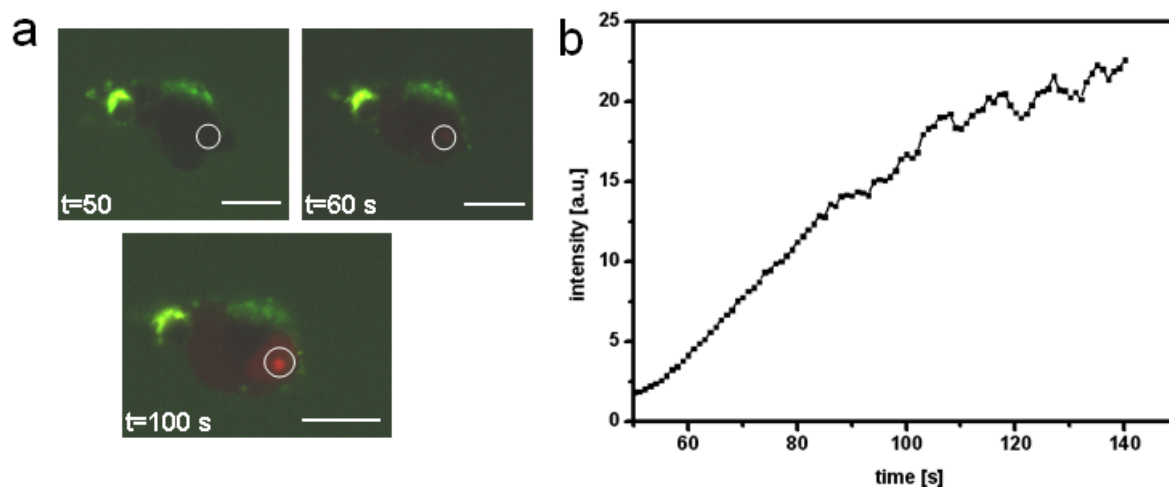


Fig. 4-5. Time-series micrograph of the propidium iodide (PI) influx (red) in JHH6 cell, in the presence of FITC-PAH (green). PI entrance was visualized at different time point,  $t=50$ s,  $t=60$ s, and  $t=100$ s upon PAH exposure in presence of PI. c) Analysis of the fluorescence intensity profile of PI in the white ring of image (a).

The time before cell destruction was too short to conclude that the cells were undergoing apoptosis or necrosis. This was also supported by a negative caspase assay (fig. 4-6). The above studies support the second hypothesis that PAH entrance could be due to nanoporation.

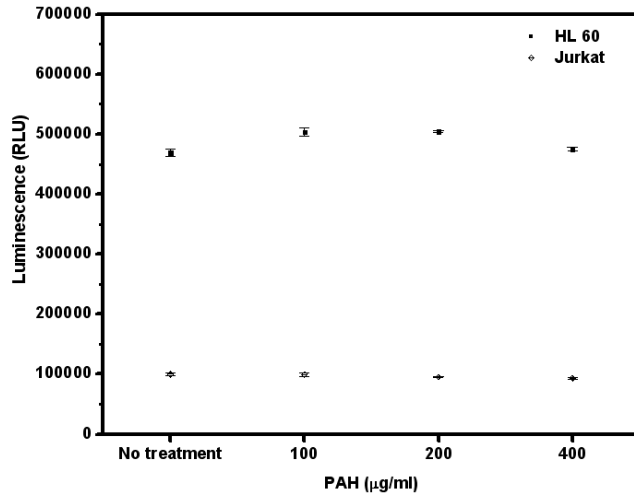


Fig. 4-6. The Caspase-Glo®3/7 assay on the HL60 and Jurkat cells after 5 mins treatment with PAH at different concentrations. The graph presents luminescence intensity vs. PAH concentration. The graph represents the mean±SD value of 3 experiments.

## 4.2. PAH, as cancer therapy

### 4.2.1. PAH reduces cancer cell viability

The well-known cytotoxicity of PAH [14, 15] directed us to postulate its use as a

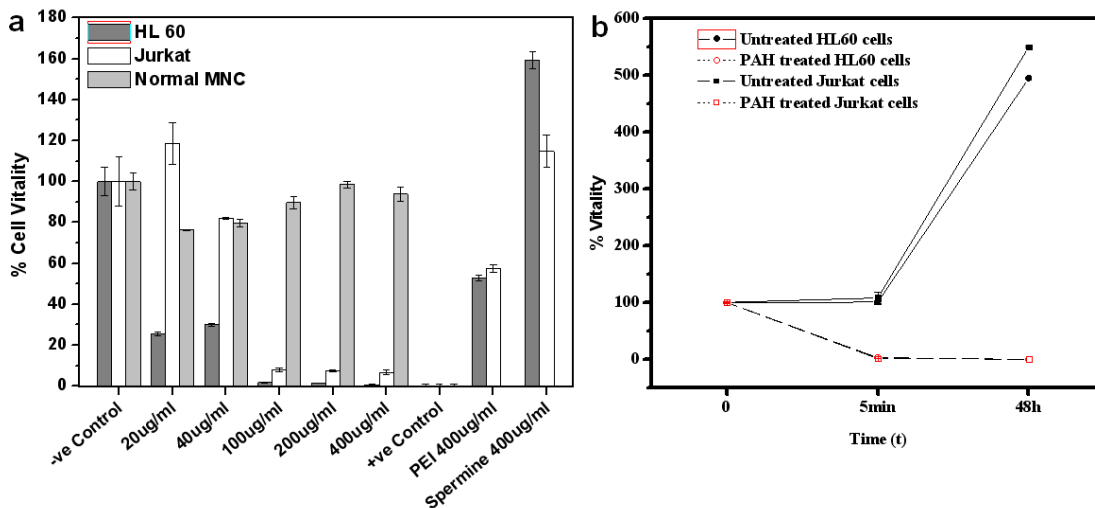


Fig. 4-7. Cell viability assay. (a) Graphical representation of MTT test for cell viability vs. polyamine concentration on leukemic HL 60 and Jurkat cells. Three different polyamines (polyallyamine, poly-ethylenimine, spermine) were tested for their toxicity. (b) The first PAH treatment reveals a fraction of “surviving” cells (t=5 mins). They were re-cultured in fresh medium and the MTT test was repeated after 48h hours.. The graph shows the result of the MTT test at t=0 (before treatment), t=5min (after PAH treatment) and t=48h (after re-culturing) (n=5).

selective drug for cancer cells. Cell survival and the  $LD_{50}$ , as a function of the PAH concentration (for HL60, Jurkat leukemic cell lines and MNC of healthy donors) for short (5mins) exposure to the polycation was determined by MTT assay (fig 4-7a). The healthy MNCs showed almost no toxic effect of PAH (survival: 80-100%). In contrast, in case of both the leukemic cell lines, cell viability decreased rapidly even for PAH concentrations below  $100\mu\text{g}/\text{mL}$ . The  $LC_{50}$  calculated for HL60 cells was  $7.3\pm 0.6\mu\text{g}/\text{mL}$  and for Jurkat cells,  $12.6\pm 1.4\mu\text{g}/\text{mL}$  (fig. 4-8). As the MTT tests were always performed with comparable cell concentrations, the  $LC_{50}$  of both cell lines indicates that the less differentiated cancer cells (HL60) were significantly (about a factor of two) more vulnerable to PAH treatment than the well-differentiated T lymphocytes (Jurkat).

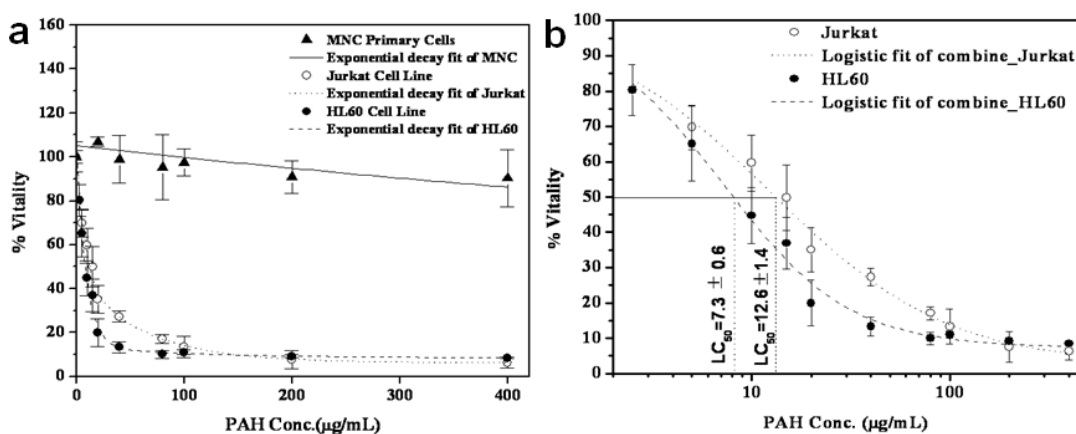


Fig. 4-8. The % cell viability and  $LC_{50}$  analysis after FITC-PAH treatment of the MNCs from healthy donor, HL60 and Jurkat cells. (a) The graph presents the percentage of viable cells after treatment with different PAH concentrations. (b)  $LC_{50}$  determination for HL60 and Jurkat cells for PAH treatment. All experiments represent means  $\pm$  SD of five independent experiments.

The cell viability reaches a minimum value when the cells were exposed to PAH concentrations  $>100\mu\text{g}/\text{mL}$ . In case of HL60 cells, cell viability was found to be  $1.5\pm 0.7\%$  whereas for Jurkat cells, it was estimated to be  $7\pm 1\%$ , suggesting the possible presence of a

small fraction of resistant cells for the PAH treatment. To understand if it was an artifact or this percentage of cell surviving could escape our treatment, eventually causing a relapse of the disease later in the patient; this fraction was re-incubated in fresh medium for 48h. However, the re-culturing experiments suggested that these cells were also dead as no increase of cell numbers was observed (fig. 4-7b).

In order to investigate if the PAH effect on leukemic cells was general, the experiments were repeated with two types of adherent HCC cell lines (fig. 4-9). HuH-7 cells are an

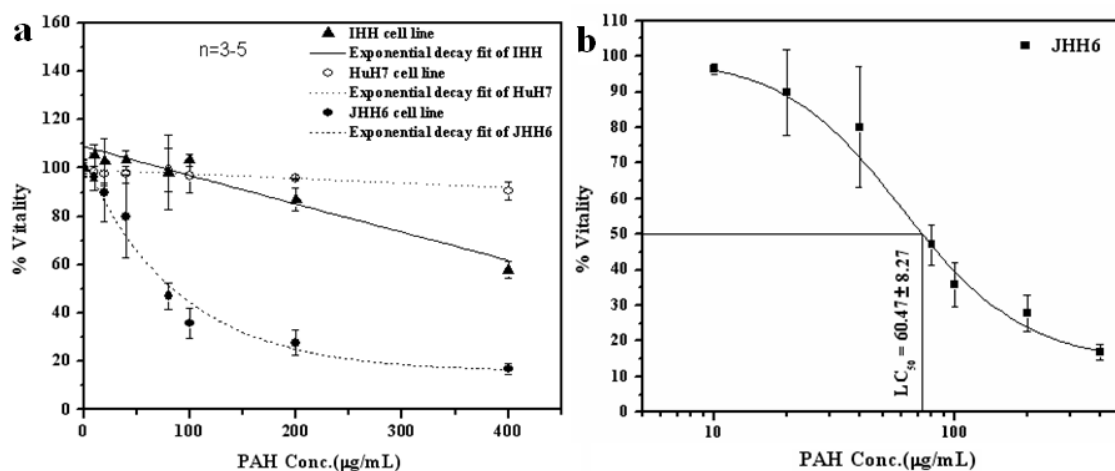


Fig. 4-9. Cell viability and LC<sub>50</sub> analysis of HCC cell line (HuH7, JHH6) and immortalized hepatocyte (IHH) cell lines. (a) Graph presenting % of viable cells after treatment with different PAH concentrations. (b) LC<sub>50</sub> determination for JHH6 cells for PAH treatment. All experiments represent means ± SD of five independent experiments.

example of a well differentiated human HCC cell line, and JHH-6 cells serve as a model for an undifferentiated one. HuH-7 cells are not affected by the PAH while JHH-6 cells are strongly affected leading to immediate cell death (fig 4-9a). The LC<sub>50</sub> value was determined to be 60 ± 8 µg/mL for JHH-6 (fig. 4-9b). In comparison cell survival for HuH-7 cells was still 90%, even at the highest tested concentration of PAH (400 µg/mL). For the immortalized

hepatocytes, the polycation showed no toxicity up to a concentration of 100 $\mu$ g/mL, at which 64% of the IHH cells are dead.

### 4.3. PAH-beads Analysis

Next aim was to analyze the side effect or after effect of PAH treatment. It was observed that after PAH internalization cancer cell dissociates in bead-like structure (fig. 4-10). The hypothesis that the PAH-beads are apoptotic bodies could be neglected because the Caspase assay was negative (fig 4-6) and normally apoptosis takes several hours up to days. Necrosis could be excluded due to the appearance of the cell breakdown in form of vesicle-like structures. Thus, I concluded that the vesicle-like cell disintegration is driven by a novel mechanism.

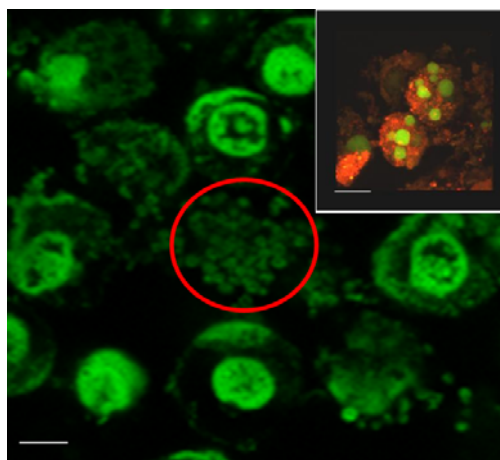
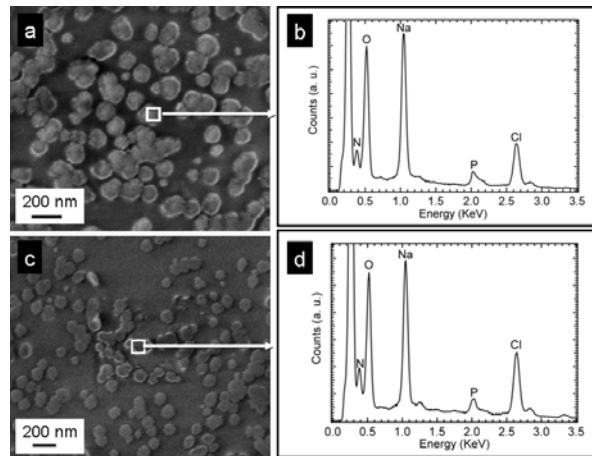


*Fig. 4-10. PAH treated HL60 cells disintegrates in "vesicular" structure (red circle). Inset: 3-D reconstruction of HL60 cells visualized by confocal 3 D optical sectioning. The cells were treated for 10 minutes with FITC-polycation (green) and then stained with DiA (red) for visualization of the membranes. The cell disintegrates very similar fragmentation as typical for apoptosis. The scale bar in both images presents 10 $\mu$ m.*

#### 4.3.1. SEM, EDS and immuno-assays of PAH beads

To further investigate the PAH-bead, the morphology of the beads was investigated by FE-SEM analysis. Representative images of the beads resulting from decomposition of HL60 cells or Jurkat cells are shown in fig 4-11a & c, respectively. The dried single PAH-beads under ultra high vacuum, showed an average diameter of around 100-200nm. Some aggregates are also found.

In order to determine the chemical composition of these PAH-beads an EDS measurement of several beads originated from both leukemic cell types was performed. EDS was performed using the SEM electron beam operated at 7keV. Monte Carlo simulations [16] indicate that the x-ray generation volume at this energy is around 150 nm thick. The areas where EDS spectra corresponding to



the presence of C, O, N, P, Na and Cl signals were taken (Fig 4-11b & d) are highlighted as boxed frames in figures 4-11a & c. The N to P ratio for Jurkat cell derived beads (Fig 4-11c) is ~ 2:1 and for HL60 cells (Fig 4-11d) ~ 3:1. While nitrogen is an element coming from the

cell as well as from the polycation PAH the only possible source for the detected phosphor signal could be the cellular phosphate components.

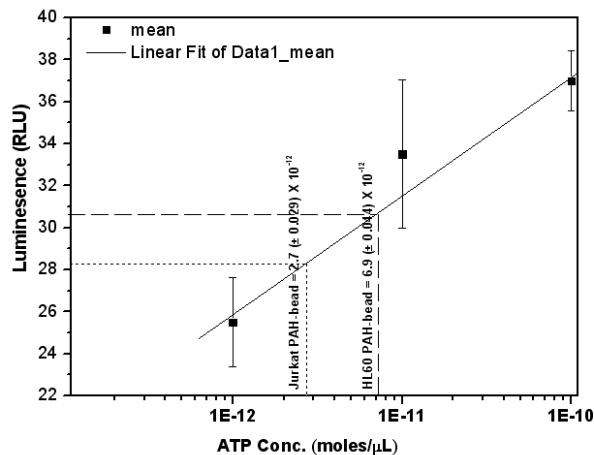


Fig. 4-12. ATP assay on PAH-beads derived from HL60 cells and Jurkat cells. The linear fitting shows the standard curve, whereas the amount of ATP on the HL60 and Jurkat was determined by the respective intersection point with the standard curve. Each point represents mean of 3 experiments.

The origin of the phosphor signal was identified by ATP assay (fig. 4-12) and PIP<sub>3</sub> immuno-fluorescence analysis. As an example, in fig. 4-12, the fluorescence micrograph of beads

derived from HL60 (fig. 4-13a) or Jurkat (Fig. 4-13b) recognized by PIP<sub>3</sub> antibodies labeled with FITC, are shown.

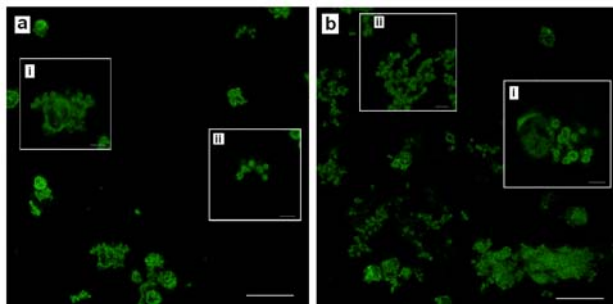


Fig. 4-13. Confocal fluorescence micrographs of FITC-PIP<sub>3</sub> antibodies bound to PAH beads (green) derived from (a) HL60 cells and (b) Jurkat cells. Image (i) presents disintegrating cells, whereas (ii) shows single PAH-beads. The scale bar in (a) and (b) represents 20  $\mu\text{m}$  and in the insets (i) and (ii) 5  $\mu\text{m}$ .

### 4.3.2. PAH-bead toxicity analysis

#### 4.3.2.1. FACS analysis

FACS analysis of the PAH-bead treated cells (fig. 4-14) show that the PAH-bead at its highest volume has no significant uptake as compared to control cells (untreated cells). This results suggested that once the PAH complexes in form of stable PAH-bead they are no longer toxic because they are not able to enter.

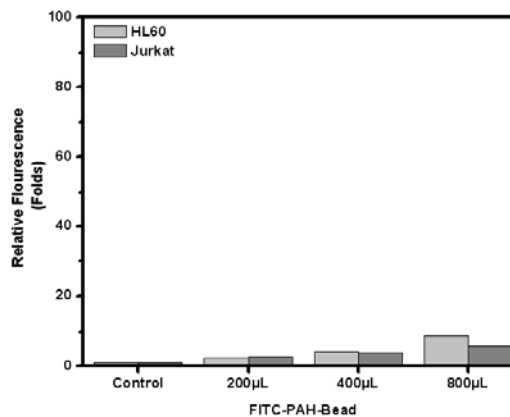


Fig. 4-14. FACS analysis. The graph presents the relative fluorescence intensity due to FITC-PAH-bead internalized cells versus different volumes of FITC-PAH beads.

#### 4.3.2.2. MTT assay

The PAH-beads were studied for a possible toxic effect. HL60 and Jurkat cells were exposed to increasing volumes (200, 600 and 800  $\mu\text{L}$  bead suspension) of the PAH-bead suspension. Cell viability was determined by the MTT assay after 2 h of exposure (fig. 4-15a). The cell

viability shows no significant reduction at any of the tested concentrations. Even incubation

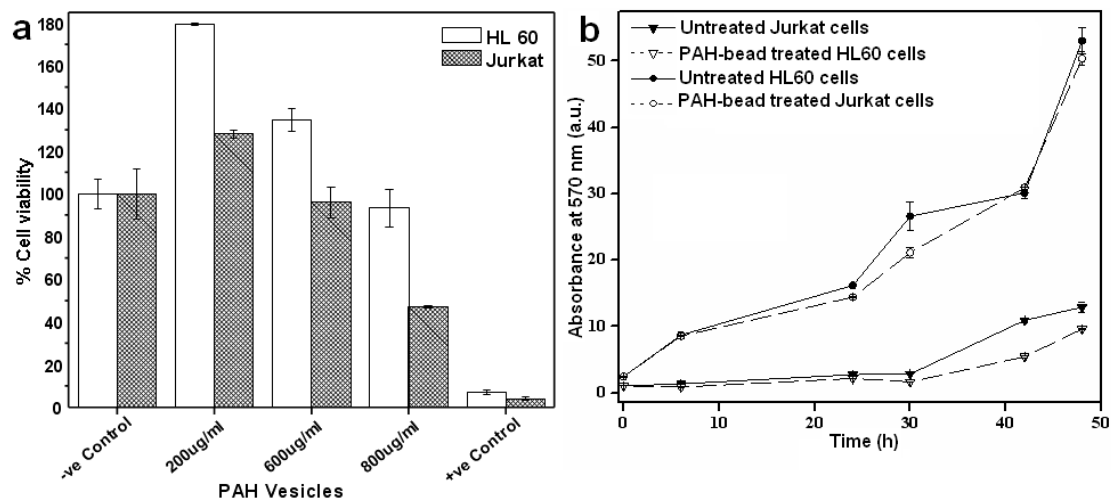


Figure 4-15. MTT assay of HL 60 and Jurkat cells (a) after 30mins of PAH-bead exposure. % cell viability versus the amount of added gel beads. (b) Absorbance at 570nm versus time of exposure to 800 $\mu$ l bead suspension.

of the respective cells with the highest concentration of the PAH-bead for 48h, no significant reduction in cell functionality was observed (fig. 4-15b). Hence, this observation signifies that once PAH are entangled in beaded structure (PAH-bead) they are no more cytotoxic.

#### **4.4. References**

1. Krol S, Diaspro A, Magrassi R, Ballario P, Grimaldi B, Filetici P, *et al.* Nanocapsules: Coating for Living Cells. *IEEE Trans Nanobioscience* 2004;3(1):32-38.
2. Urbanits S, Griesmacher A, Hopfinger G, Stockhammer G, Karimi A, Müller MM, Pittermann E, Grisold W. FACS analysis-a new and accurate tool in the diagnosis of lymphoma in the cerebrospinal fluid. *Clin Chim Acta* 2002;317(1-2):101-107.
3. Kerschbaum HH, Kozak JA, Cahalan MD. Polyvalent Cations as Permeant Probes of MIC and TRPM7 Pores. *Biophys J* 2003;84:2293-2305.
4. Park J, Choi YW, Kim KB, Chung H, Sohn D. Aggregation Processes of a Weak Polyelectrolyte, Poly(allylamine) Hydrochloride. *Bull Korean Chem Soc* 2008;29:104-110.
5. Fraser AV, Woster PM, Wallace HM. Induction of apoptosis in human leukaemic cells by IPENSpm, a novel polyamine analogue and anti-metabolite. *Biochem. J* 2002;367(Pt 1):307-312.
6. Suresh S. Nanomedicine: elastic clues in cancer detection. *Nat Nanotechnol* 2007;2(12):748-749.
7. Suresh S. Biomechanics and biophysics of cancer cells. *Acta Biomater* 2007;3(4):413-38.
8. Dobrzyńska I, Szachowicz-Petelska B, Sulkowski S, Figaszewski Z. Changes in electric charge and phospholipids composition in human colorectal cancer cells. *Mol Cell Biochem* 2005;276(1-2):113-9.
9. Zheliaskova A, Naydenova S, Petrov AG. Interaction of phospholipid bilayers with polyamines of different length. *Eur Biophys J* 2000;29(2):153-157.

10. Morgan DM, Larvin VL, Pearson JD. Biochemical characterisation of polycation-induced cytotoxicity to human vascular endothelial cells. *J Cell Sci.* 1989;94 ( Pt 3):553-559.
11. Mecke A, Majoros IJ, Patri AK, Baker JRJr, Banaszak Holl MM, Orr BG. Lipid Bilayer Disruption by Polycationic Polymers: The Roles of Size and Chemical Functional Group. *Langmuir* 2005;21:10348–10354.
12. Hong S, Bielinska AU, Mecke A, Keszler B, Beals JL, Shi X, *et al.* Interaction of poly(amidoamine) dendrimers with supported lipid bilayers and cells: hole formation and the relation to transport. *Bioconjug Chem* 2004;15(4):774-7.
13. Chen J, Hessler JA, Putchakayala K, Panama BK, Khan DP, Hong S, *et al.* Cationic nanoparticles induce nanoscale disruption in living cell plasma membranes. *J Phys Chem B* 2009;113(32):11179-11185.
14. Sgouras D, Duncan R. Methods for the evaluation of biocompatibility of soluble synthetic polymers which have potential for biomedical use: 1-Use of the tetrazolium-based colorimetric assay (MTT) as a preliminary screen for evaluation of *in vitro* cytotoxicity. *J Mater Sci Mater Med* 1990;1(2):61-68.
15. Boussif O, Delair T, Brua C, Veron L, Pavirani A, Kolbe HV. Synthesis of polyallylamine derivatives and their use as gene transfer vectors *in vitro*. *Bioconjug Chem* 1999;10(5):877-883.
16. Drouin D, Couture AR, Joly D, Tastet X, Aimez V, Gauvin R. CASINO V2.42: a fast and easy-to-use modeling tool for scanning electron microscopy and microanalysis users. *Scanning* 2007;29(3):92-101.

## **CHAPTER 5**

### **5.1. Conclusions**

The selective targeting of cancer cells is one of the major challenges in nano-medicine. Many approaches are dedicated to find suitable biomarkers or targets [1], modifying the drug molecules or producing a protective delivery system [2] in order to decrease the collateral effects of chemotherapeutics and increase the tumoral concentration of the drug. From the present work, I assume that physical properties such as membrane characteristics and cell surface charge could provide us with a new way to target cancer cells. The advantage in targeting physical membrane properties rather than biomarkers is that the probability of change in physical properties in compared to mutational changes in the biomarkers is much less likely. A mutational change in biomarkers will allow the tumor cells to escape marker-targeted cancer treatment.

It is known that the membrane of cancer cells differs from that of normal cells in terms of fluidity, composition and surface charge. Gottfried [3] and Liebes *et al.* [4] provided one of the earliest results of the different phospholipid contents of the membrane of cancerous cells. The special polycation–lipid interaction, which leads to nanoporation permitting the entry of the polymer into the cell, was described in detail by Moghimi *et al.* [5]. They found that polyethylenimine (PEI) cause pores in the cell membrane as well as in the mitochondrial membrane and induce cell death by apoptosis. However, due to the low selectivity and hence the severity of the side-effects, the use of PEI as anti-cancer drug was abandoned.

In the present work I found that PAH has a high selectivity for cancer cells. The leukemic cell lines were treated with the FITC-labeled polycation PAH and the results in terms of

polycation up-take and viability were compared to healthy cells (white blood cells and whole blood). Moreover the blood of four patients diagnosed with leukemia was exposed to PAH and its up-take recorded. The same results were found for real samples. In the present work, I found that the cells from blood cancer and liver cancer can selectively take up polyallylamine with a fast kinetic (<1 min) whilst the polycation is completely excluded from similar healthy cell populations. Once PAH was inside the cells, they disintegrate in less than 5 min to bead like structures. Additionally, I notice that undifferentiated hepatic tumor cells (JHH-6) were stronger affected by PAH than the well-differentiated tumor cells (HuH-7) or the non-cancerous hepatocytes (IHH - immortalized normal hepatocytes).

Two important findings from the present study highlight the potential of PAH to be a possible future diagnostic tool for circulating cancer cells as well as therapeutics for primary tumors. Firstly, the polycation PAH enters rapidly, with a high selectivity, into cancer cells; dedifferentiated cells are even more prone to PAH treatment and once PAH has been internalized, the cells are fragmented. The preferential entry into cancer cells could be due to the difference of cell membrane composition from their normal counterpart. Indirectly, this observation has also been reported by Morgan *et al.* [5]. They found that cancerous cells in vitro that had not yet reached confluence were evidently more liable to the cytotoxic effect of poly-amino acids [5]. Furthermore, an analysis of the phospholipid composition by Gottfried [3] estimated a higher negative surface charge and membrane fluidity of cancer cells in comparison to normal cells. Phosphatidylinositols such as PIP<sub>2</sub> and PIP<sub>3</sub> are known to form transport vesicles, during the late stages of cell division (cytokinesis) and are accumulating in the bridge region of the mother and daughter cell [7]. Cancer cells present a higher division rate and therefore should have high amounts of transport vesicles forming the new cells [8]. It is also known that cancer cells, as differentiating cells, show significantly higher levels of IP<sub>3</sub>

[9, 10] due to up-regulation of two specific kinases and down-regulation of phospholipase C. These inositol polyphosphates contribute significantly to a higher negative charge on the membrane or in close vicinity to it and hence can facilitate the selective entrance of PAH in cancer cells and the untypical destruction in form of gel beads. It was observed that PAH has a high affinity to negatively charged phosphates such as ATP or PIP<sub>3</sub>. Since PAH and phosphates form very stable gels [11], I conclude that the complete cytosol rapidly transformed in gel beads by binding to phosphates or polyphosphates once PAH enters the cell. This conclusion was also supported by the fact that I found a strong phosphorus peak in the beads by EDS analysis. Also, ATP and PIP<sub>3</sub> antibody assays were positive for the gel beads.

Furthermore, the toxicity analysis of the PAH-beads shows that PAH in this form is non-toxic limiting metabolic side-effects after treatment.

By the present studies I show the potential of PAH for fast cancer diagnostics and therapy. Animal experiments to prove the present concept *in vivo*, are in progress.

## **5.2. References**

1. Levy-Nissenbaum E, Radovic-Moreno AF, Wang AZ, Langer R, Farokhzad OC. Nanotechnology and aptamers: applications in drug delivery. *Trends Biotechnol.* 2008;26(8):442-449.
2. Kim D, Lee ES, Oh KT, Gao ZG, Bae YH. Doxorubicin-loaded polymeric micelle overcomes multidrug resistance of cancer by double-targeting folate receptor and early endosomal pH. *Small* 2008;4(11):2043-2050.
3. Gottfried EL. Lipids of human leukocytes: relation to cell type. *J Lipid Res* 1967;8(4):321-327.
4. Liebes LF, Pelle E, Zucker-Franklin D, Silber R. Comparison of Lipid Composition and 1,6-Diphenyl-1,3,5-hexatriene Fluorescence Polarization Measurements of Hairy Cells with Monocytes and Lymphocytes from Normal Subjects and Patients with Chronic Lymphocytic Leukemia. *Cancer Res* 1981;41:4050-4056.
5. Moghimi SM, Symonds P, Murray JC, Hunter AC, Debska G, Szewczyk A. A two-stage poly(ethylenimine)-mediated cytotoxicity: implications for gene transfer/therapy. *Mol Ther* 2005;11(6):990-995.
6. Weber G, Shen F, Prajda N, Yeh YA, Yang H, Herenyiova M, Look KY. Increased signal transduction activity and down-regulation in human cancer cells. *Anticancer Res* 1996;16(6A):3271-82.
7. Echard A. Membrane traffic and polarization of lipid domains during cytokinesis. *Biochem Soc Trans* 2008;36(Pt 3):395-399.
8. Prekeris R, Gould GW. Breaking up is hard to do - membrane traffic in cytokinesis. *J Cell Sci* 2008;121(Pt 10):1569-1576.

9. Santi P, Solimando L, Zini N, Santi S, Riccio M, Guidotti L. Inositol-specific phospholipase C in low and fast proliferating hepatoma cell lines. *Int J Oncol* 2003;22(5):1147-1153.
10. Cocco L, Martelli AM, Capitani S, Maraldi NM, Mazzotti G, Barnabei O, *et al.* Nuclear inositol lipid cycle and differentiation. *Adv Enzyme Regul* 1995;35:23-33.
11. Mazza D, Cella F, Vicidomini G, Krol S, Diaspro A. Role of three-dimensional bleach distribution in confocal and two-photon fluorescence recovery after photobleaching experiments. *Appl Opt* 2007;46(30):7401-7411.

## **Concluding Remark & Future outlook**

The introduction of nanotechnology in healthcare has imposed a vast impact in the fields of drug delivery and diagnostics. The role of nanotechnology in healthcare is becoming very important in terms of eradicating diseases, especially in terms of treating cancer. The unique ability of targeted nanoparticles to preferentially accumulate in and around the tumor mass grants a platform for improved tumor diagnostics and in cancer therapy.

Polymer chemistry is a versatile and adaptable field. Application of polymers as the backbone for nanoparticle formulation has facilitated the advancement in the creation of particles combining multiple functionalities such as protection against immune recognition, targeting against specific diseased cells, the ability to cross barriers, protection of the payload against aggressive environmental conditions, etc. Insertion of tumor-targeting ligands that are directed against markers, such as the folic acid receptor and the Epidermal Growth Factor Receptor-2 (EGFR-2) like Human Epidermal growth factor Receptor 2 (HER2), not only enhances accumulation of the particles in the solid tumor mass, but also allows specific targeting of the nanoparticles to small and early stage tumors, metastatic cancer cells and leukemic cells. Consequently, this will provides a means to greatly improve both the area of targeted drug delivery and visualization of cancerous cells. Especially the targeted delivery will lead to a side-effect free anti cancer treatment which is nowadays still beyond imagination.

The cytotoxicity of the present chemotherapeutics has placed the standard for the development of anticancer therapy; however, their potent toxicity, nonspecific action, and failure in drug-resistant tumors has driven the search for alternative therapies. Polymeric multilayer coated nanoparticles allow the co-encapsulation of several drugs and, therefore

can delivery simultaneous or serial in a time dependent manner multiple drugs. This can offers the possibility to design a treatment which is taking into consideration that the diseased cells change under treatment and the therapy must respond to the modified conditions induced by the treatment.

Moving in the direction of side-effect free treatment are the polymeric CP system presented here, integrating two major natural therapies (anti-sense and gene therapy). This approach has the potential to become a therapy also for genetic disease in which one can block by the siRNA a point-mutation and deliver the wild-type sequence to suppress the expression of modified proteins. Examples could be sickle cell anemia, hemophilia, muscular dystrophy and cystic fibrosis. This strategy may also be on the horizon and applicable for neurological disorders, such as Alzheimer's and Huntington disease, diabetes, Amyotrophic Lateral Sclerosis, Duchenne muscular dystrophy, asthma and arthritis with an inflammatory component, and many others.

Even though cancer therapy can be greatly enhanced by the above mean, the diverse opportunities are available to use polyelectrolytic polymers. One of such application could be polymer coated nanoparticle formulation allows for true multiple functionality of the particles.

The stable polymer coated gold nanoparticles described in this work promises enormous possibilities with further improvements in combining a sophisticated therapy with multi-modal imaging. Even though for cancer treatment, gold nanoparticles offer the possibility to combine tumor imaging with a hyperthermal treatment, or imaging with drug delivery, what is still missing is a formulation that allow effective high contrast image, the delivery of multiple drugs, focus hyperthermal treatment to the tumor, combined with retaining the long circulating and tumor localization properties of the nanoparticulated drug. In a first attempt to

develop a multifunctional nanosystem I have developed the system for BNCT by uploading  $^{10}\text{BPA}$  in the polyelectrolyte multilayers. Similarly, gadolinium can be uploaded along with  $^{10}\text{B}$ , which allows combining cancer imaging by MRI with cancer therapy by NCT. However, in another collaboration work of our group, it was found that these coated particles bear the potential to be used for neurodegenerative disease as well. Therefore, polymer coated nanoparticles pioneer for new strategies not only for a more effective and durable cancer therapy but for other incurable diseases.

An area that also remains unexplored is the properties of polyions as drug itself. The first hint that polymers can be much more than only be a vehicle for a nano-formulated drug, comes from the experiments in which the polymers actively inhibit the expression of proteins related to multidrug resistance, often responsible for tumor evasion of the treatment.

However, I found that polycation can be useful specifically against cancer. Its fast and selective binding and a novel mechanism of cell destruction has proven its potential to be a effective theranostic system. Thus, polycations can help to precisely determine the tumor area which may help during surgery. It can be used in detecting the circulating cancer cells in the onset of metastasis as well as in the follow-up after treatment.

All three approaches developed in this thesis have shown their potential to proceed to *in vivo* studies as they have a promising *in vitro* efficacy.

---

## Epilogue

This thesis is interwoven with the development of effective different strategies based on nano-technological advantages. I have had the great opportunity and the honour of working with four scientific institutions- Scuola Internazionale Superiore di Studi Avanzati/International School for Advance Studies (SISSA/ISAS), Cluster in Bio-Medicine (CBM), Fondazione Italiana Fegato- Liver Research Center and University of Trieste. I found, while working in these establishments, that the best of human beings and the best innovative minds were available in plenty. One thing which I realized while working with these institutions is that we should never be afraid of failures. Failures contain within themselves the seeds of further learning, which can lead to better technology, and eventually, to a high level of success. Another thing which I learnt, is to be a great dreamer, and these dreams finally culminated in all the described achievements in my work. Above all, I have had the opportunity of working with great visionaries; Prof. Giacinto Scoles, Dr. Silke Krol, Prof. Claudio Tiribelli, Prof. Mario Grassi and Prof. Gabriele Grassi, who have all greatly enriched my life.

Future cancer treatment strategies need to be much more patient tailored. Although it is hard to predict how long the “classical” cytotoxic chemotherapy will be in use, now is the time that new improved next-generation multi-functional drugs will hit the market. In order to improve a cancer patient’s life. The next generation medicine will provide the opportunity for doctors to design the treatment plan, according to the needs of the individual patient. The presented thesis work illustrates the different scopes of next-generation medicine with which not only more patients may be truly cured, but others will have their disease converted from a rapidly progressing stage to a more stationary, chronic diseases. I would like to finish my thesis with this thought

*Don't worry and fret, faint hearted,  
The chances have just begun,  
For the Best jobs haven't been started,  
The Best work hasn't been done.*

- Berton Braley

\*\* \*\* \*

